ANALYTICAL AND SIMULATION PERFORMANCE MODELLING OF INDOOR INFRARED WIRELESS DATA COMMUNICATIONS PROTOCOLS

PETER JAY BARKER

A thesis submitted in partial fulfilment of the requirements of Bournemouth University for the degree of Doctor of Philosophy

April 2003

Bournemouth University

Abstract

The Infrared (IR) optical medium provides an alternative to radio frequencies (RF) for low cost, low power and short-range indoor wireless data communications. Low-cost optoelectronic components with an unregulated IR spectrum provide the potential for very high-speed wireless communication with good security. However IR links have a limited range and are susceptible to high noise levels from ambient light sources. The Infrared Data Association (IrDA) has produced a set of communication protocol standards (IrDA 1.x) for directed point-to-point IR wireless links using a HDLC (High-level Data Link Control) based data link layer which have been widely adopted. To address the requirement for multi-point ad-hoc wireless connectivity, IrDA have produced a new standard (Advanced Infrared – AIr) to support multiple-device non-directed IR Wireless Local Area Networks (WLANs). AIr employs an enhanced physical layer and a CSMA/CA (Carrier Sense Multiple Access with Collision Avoidance) based MAC (Media Access Control) layer employing RTS/CTS (Request To Send / Clear To Send) media reservation.

This thesis is concerned with the design of IrDA based IR wireless links at the data link layer, media access sub-layer, and physical layer and presents protocol performance models with the aim of highlighting the critical factors affecting performance and providing recommendations to system designers for parameter settings and protocol enhancements to optimise performance.

An analytical model of the IrDA 1.x data link layer (IrLAP – Infrared Link Access Protocol) using Markov analysis of the transmission window width providing saturation condition throughput in relation to the link bit-error-rate (BER), data rate and protocol parameter settings is presented. Results are presented for simultaneous optimisation of the data packet size and transmission window size. A simulation model of the IrDA 1.x protocol, developed with OPNET™ Modeler, is used for validation of analytical results and to produce non-saturation throughput and delay performance results.

An analytical model of the AIr MAC protocol providing saturation condition utilisation and delay results in relation to the number of contending devices and MAC protocol parameters is presented. Results indicate contention window size values for optimum utilisation. The effectiveness of the AIr contention window linear back-off process is examined through Markov analysis. An OPNET simulation model of the AIr protocol is used for validation of the analytical model results and provides non-reservation throughput and delay results.

An analytical model of the IR link physical layer is presented and derives expressions for signal-to-noise ratio (SNR) and BER in relation to link transmitter and receiver characteristics, link geometry, noise levels and line encoding schemes. The effect of third user interference on BER and resulting link asymmetry is also examined, indicating the minimum separation distance for adjacent links. Expressions for BER are linked to the data link layer analysis to provide optimum throughput results in relation to physical layer properties and link distance.

Table of contents

Acknowledgements

Special thanks to my supervisor Professor Tony Boucouvalas

Thank to Colin Millar, Steve Buttery and Ian Nield at BT labs, Martlesham for initial financial and supervisory support for this project.

To my friends, colleagues, office co-habitants and fellow researchers (in no particular order): Glyn Hadley, Simon Crowle, Jenny Longster, Daniel Vine, Paul and Ruth Nicholson, Carolyn Mair, Tom Teng, David John, Colin Murphy, Periklis Chatzimisios, Vasileios Vitsas, Martin Teal, Tim Orman, Paul Rogers.

To Mum and Ced, Dad and Angelika, Sally and Mark

Accompanying Material

The following papers were published during the course of the research conducted for this thesis.

Journal Publications

[1] Vitsas, V., Barker, P. & Boucouvalas, A.C. (2003), "IrDA Infrared Wireless Communications: Protocol Throughput Optimization", *IEEE Wireless Communications*, Vol. 10, No 2, April 2003, pp. 22 - 29

[2] Barker, P. Vitsas, V. & Boucouvalas, A.C. (2002), "Simulation Analysis of the Advanced Infrared (AIr) MAC Wireless Communications Protocol", *IEE proceedings Circuits and Systems*, Vol. 149, No 3, June 2002, pp. 193 – 197.

[3] Barker, P. & Boucouvalas, A.C. (2000), "Asymmetry in Optical Wireless Links", *IEE Proceedings Optoelectronics*, Vol. 147, No 4 August 2000, pp. 315 - 321.

[4] Barker, P. & Boucouvalas, A.C., (2000) "Performance Modelling of the IrDA Infrared Wireless Communications Protocol", *International Journal of Communications Systems*, Vol. 13, No 7-8, Nov-Dec 2000, pp. 589 - 604.

[5] Barker, P. & Boucouvalas, A.C. (1998), "IrLAP protocol performance analysis of IrDA wireless communications", *IEE Electronics letters*, Vol. 34, No. 25, pp. 2380-2381.

[6] Barker, P. & Boucouvalas, A.C. (1998), "Performance modelling of the IrDA protocol for Infrared Wireless Communications", *IEEE Communications magazine*, Vol. 36, No. 12, December 1998, pp. 113-117.

Conference Publications

[1] Barker, P. & Boucouvalas, A.C. (2002), "Interference Induced Asymmetry in IrDA 4PPM Infrared Wireless Links", *3rd International Symposium on Communication Systems, Networks and Digital Signal Processing (CSNDSP 2002)*, University of Staffordshire, Stafford, 15th - 17th July 2002, pp. 479 - 482.

[2] Barker, P. & Boucouvalas, A.C. (2002), "Directional and Spatial Asymmetry in IrDA 4PPM Infrared Wireless Links with Third User Interference" *3rd Annual postgraduate Symposium on the Convergence of Telecommunications, Networking and Broadcasting (PGNET 2002)*, Liverpool John Moores University, 17th -18th June 2002, pp. 353 - 358.

[3] Barker, P. & Boucouvalas, A.C. (2001), "Performance Comparison of the IEEE 802.11 and AIr Infrared Wireless MAC Protocols", *2nd Annual postgraduate Symposium on the Convergence of Telecommunications, Networking and Broadcasting (PGNET 2001)*, Liverpool John Moores University, 18th-19th June 2001, pp. 113 - 118.

[4] Barker, P. & Boucouvalas, A.C. (2000), "A Simulation Model of the Advanced Infrared (AIr) MAC protocol using OPNET", *2nd International Symposium on Communication Systems, Networks and Digital Signal Processing (CSNDSP 2000),* Bournemouth University, 18th - 20th July 2000, pp. 153 -156.

[5] Barker, P. & Boucouvalas, A.C. (2000), "Modelling of the IrDA and AIr Wireless Infrared Communications Protocols", *1st Annual postgraduate Symposium on the Convergence of Telecommunications, Networking and Broadcasting (PGNET 2000),* Liverpool John Moores University, 19th - 20th June 2000, pp. 137 - 142.

[6] Barker, P. & Boucouvalas, A.C. (1999), "Asymmetric Throughput in Optical Wireless Links", *Second Electronic Circuits and Systems Conference*, Bratislava, Slovakia, September 1999, pp. 129-134.

[7] Barker, P. & Boucouvalas, A.C. (1999), "Asymmetric Throughput in IrDA Links", *IEE Colloquium on Optical Wireless Communications,* Savoy Place, London, 22nd June 1999, pp. 7/1-5.

[8] Barker, P. & Boucouvalas, A.C., (1999), "Effect of Random Alignment Sway on The Performance of IrDA Handheld Device Links", *IEE Colloquium on Optical Wireless Communications,* Savoy Place, London, 22nd June,1999, pp. 9/1-4.

[9] Barker, P. & Boucouvalas, A.C. (1998), "A Simulation Model of IrDA Infrared Communication Protocol", *1st International Symposium on Communication Systems and Digital Signal Processing*, Sheffield Hallam University, 6-8 April 1998, pp. 2-5.

[10] Barker, P. & Boucouvalas, A.C. (1998), "Performance Analysis of the IrDA Protocol in Wireless Communications", *1st International Symposium on Communication Systems and Digital Signal Processing*, Sheffield Hallam University, 6-8 April 1998, pp. 6-9

[11] Barker, P. & Boucouvalas, A.C. (1997), "IrDA Protocol Performance Analysis for Short Range IR Data Communication", *Fourth Communication Network Symposium*, Manchester Metropolitan University, 7 –8 July 1997, pp. 224 – 227.

Abbreviations

ABM	Asynchronous Balanced Mode
ACK	Acknowledgement
AIr	Advanced Infrared
ARM	Asynchronous Response Mode
ARQ	Automatic Repeat-request
BER	Bit Error Rate
BOF	Beginning-Of-Frame
CAS	Collision Avoidance Slot
CDMA	Code Division Multiple Access
CRC	Cyclic Redundancy Check
CSMA/CA	Carrier Sense Multiple Access / Collision Avoidance
CSMA/CD	Carrier Sense Multiple Access / Collision Detection
CTS	Clear-To-Send
CW	Contention Window
DCF	Distributed Co-ordination Function
DIFS	Distributed Interframe Space
EOB	End-Of-Burst
EOBC	End-Of-Burst Confirm
EOF	End-Of-Frame
FCS	Frame Check Sequence
FIR	Fast Infrared
FOV	Field-of-View
FSM	Finite State Machine
FTC	Frame Transmission Complete
FTX	Frame Transmit
HDLC	High-level Data Link Control
IAS	Information Access Service
IEEE	Institute of Electrical and Electronic Engineers
IM/DD	Intensity Modulation / Direct Detection
IR	Infrared
IrDA	Infrared Data Association
IrLAP	Infrared Link Access Protocol
IrLMP	Infrared Link Management Protocol
ISI	Intersymbol Interference
ISR	Interference-to-Signal Ratio
LAN	Local Area Network
LC	Link Controller
LED	Light Emitting Diode
LM	Link Manager
LSAP	Link Service Access Point
MAC	Medium Access Control
MBR	Main Body Received
MUX	Multiplexer
NRM	Normal Response Mode
NRZ	Non Return-to-Zero
OOK	On-Off Keying

PCF	Point Co-ordination Function
PDA	Personal Data Assistant
PHY	Physical Layer
PIN	Positive-Intrinsic-Negative
PPM	Pulse Position Modulation
RF	Radio Frequencies
RHR	Robust Header Received
RR	Repetition Rate or Receive Ready
RTS	Request-To-Send
RZ	Return-to-Zero
RZI	Return-to-Zero Inverted
SIR	Serial Infrared
SNR	Signal-to-Noise Ratio
SOD	Start-Of-Data
SPOLL	Sequenced-Polling
VFIR	Very Fast Infrared
VR	Variable Repetition
VTT	Virtual Transmission Time
WLAN	Wireless Local Area Network
WPAN	Wireless Personal Area Network

List of Figures

List of Tables

1. INTRODUCTION

1.1 Background and Motivation

In recent years there has been a rapid increase in the use of mobile and portable computing devices. Laptop, palmtop and handheld computers have become more popular and increasingly powerful with multimedia capabilities. Mobile phones have also become integrated with computing ability and facilities for e-mail and Internet browsing (Bi et al., 2001). This increase in mobile computing has led to a greater demand for wireless data connectivity with comparable service levels to that of wired networks (DeSimone and Nanda, 1995; Ramiro and Abdallah, 2002). Short-range indoor wireless communications are used in reducing the costs and inconvenience of cabling and to provide local area connectivity for portable computing devices. Such communication can be provided in a number of different configurations. Simple point-to-point wireless connections are used for such applications as file transfer or printing. Wireless network 'hubs' can provide access for multiple wireless devices to a wired local area network. Multiple devices can also connect in an ad-hoc wireless LAN (WLAN), for example around a meeting table (Gummalla and O'Limb, 2000).

Radio frequencies (RF) and Infrared (IR) are competing technologies for short-range wireless data communications. RF is popular because of the high level of mobility provided, but there are limitations. The RF spectrum is heavily congested and tightly controlled by regulation thus limiting the available bandwidth. There are also security and safety concerns as the signals pass through walls and can interfere with sensitive electronics. Radio signals are also susceptible to electrical interference and multipath fading. The IR optical medium provides an attractive alternative to RF for low-cost low-power short-range indoor wireless communications. IR wireless has the benefit of using inexpensive optoelectronic components spawned from the fibre optics industry, with small physical size and low power consumption. IR transceivers can operate at very high data rates and as the IR radiation is confined to the room of operation, there is no requirement for spectral regulation thus providing virtually unlimited bandwidth. Confinement of the radiation also allows separate networks to be established in neighbouring rooms without interference and provides a high level of security against

'eavesdropping'. IR wireless also has good electrical noise immunity and will not cause interference to sensitive electronics. However IR wireless also has limitations. The low power output of IR wireless transmitters (limited by eye safety regulations) and the blocking of the signal by opaque objects provides a limited range and low mobility. IR wireless receivers are also exposed to high background ambient light levels inducing receiver noise, and diffuse link multipath dispersion can limit the available data bandwidth. The signal-to-noise ratio (SNR) of the link depends on the distance and orientation of the receiver in relation to the transmitter and on the ambient light level. The bit-error-rate (BER), derived from the SNR, can therefore vary with movement and positioning of a mobile (e.g. handheld) device communicating in an IR wireless link. Communications protocols used with IR links must therefore contend with a shared wireless medium with a limited range and potentially high and varying error rates (Kahn and Barry, 1997; Street et al., 1997).

The Infrared Data Association (IrDA) was established in 1993 as a 'working group' of research teams from major industrial companies including Hewlett-Packard, Sharp and IBM to establish a set of protocol standards for short-range indoor IR wireless communication. The aim of the standards was to support and promote the use of low-cost mass-produced multi-vendor interoperable IR wireless components. The resultant IrDA 1.0 protocol standard, first released in 1995, specifies point-to-point directed half-duplex links with a data rate up to 115.2 kbits/s and a range not less than 1m using the standard serial port interface. Version 1.1 of the protocol provides data rates up to 4 Mbits/s using additional hardware with a recent extension to 16 Mbits/s. The data link layer of the IrDA 1.x protocol, IrLAP (Infrared Link Access Protocol), is based on the HDLC-NRM (High-level Data Link Control - Normal Response Mode) data link standard and provides framing functions, device discovery and connection, flow control and reliable data transfer between a Primary / Secondary device pair (Millar et al., 1998; Williams, 2000; Yeh and Wang, 1996).

To address a recognised need for multi-point IR wireless connectivity (Ozugur et al., 1999), IrDA have produced a new protocol standard called Advanced Infrared (AIr). The aim of AIr is to support a low-cost non-directed ad-hoc IR wireless LAN

supporting co-existence with IrDA 1.x point-to-point links. With an AIr network, all devices have equal status with no 'master' controller and can join or leave the network at will. AIr has an enhanced physical layer with broad angle transceivers providing a 'broadcast' medium for all devices within range and a robust variable 4PPM symbol repetition modulation scheme at a base data rate of 4 Mbits/s, providing a trade-off between effective data rate and link quality. The AIr MAC (Media Access Control) protocol is based on the CSMA/CA (Carrier Sensing Multiple Access with Collision Avoidance) protocol. Devices only transmit when the medium is detected clear and wait a random number of time slots before transmission to avoid frame collisions. The MAC also uses an RTS/CTS (Request To Send / Clear To Send) media reservation to improve performance. Following establishment of media reservation, a 'burst' of data frame is transmitted within a maximum duration of 500 ms (IrDA, 1999a).

There are different challenges for IR wireless system designers both at the physical layer and upper protocol layers depending on the configuration and application of links. At the physical layer the component cost must be minimised while providing a high data rate, a low bit-error-rate and good power efficiency. At the data link layer, data packet size and transmission window size must be optimised to reduce the effect of acknowledgement delays and frame overheads but limit frame re-transmissions from link bit errors. In a multi-point configuration, effective media access control is required to avoid transmission collisions and ensure fairness of access to the medium. The contention delay must be optimised to effectively avoid collisions but not cause excessive delay in reservation establishment.

Performance modelling of communications systems can be a powerful tool in effective system design and configuration. A communications system can be complex with a large number of inter-related factors and system parameters that can effect the performance. The performance of a communications system at the data link layer is measured by such statistics as throughput, utilisation, packet delay, and packet loss rate in relation to line BER, traffic load and system configuration and parameter settings. Performance modelling can help highlight the critical factors affecting performance and

determine optimum parameter settings and operating conditions before the physical system is implemented (Higginbottom, 1998).

There are two main approaches to performance modelling of communications systems: analytical modelling and computer simulation modelling. Analytical modelling involves the development of a mathematical model based on assumptions of system behaviour leading to a set of expressions or algorithms to provide a numerical measure of performance against input parameter values. Mathematical techniques such as probability theory and stochastic process analysis are used to develop the models. The models often make assumptions and approximations on the system behaviours and its complexity. The use of a computer to perform the required calculations can produce rapid numerical and graphical results. The mathematical expressions developed in an analytical model combined with graphical performance results can provided a physically intuitive understanding of the critical and first-order factors and inter-relations affecting performance. However it may not always be possible or practical to mathematically express the system behaviour of interest.

Computer simulation modelling involves using a software model that mimics a particular part of the system behaviour. Output performance statistics can be produced during and at the completion of a simulation run. Simulation has the advantage of providing much more detail of the system behaviour than an analytical model, such as the dynamic response to a varying system input. Approximations of system behaviour can be avoided and simulation results can be used to validate theoretical model results. Simulation is also powerful in assessing protocol design changes and modifications. However a simulation run may take a number of minutes or even hours to complete depending on the system complexity and output results required. In comparison with analytical modelling, simulation results may not provide as intuitive an understanding to the performance results obtained.

Research into IR wireless communications has so far largely been focused on physical layer issues such as transceiver design (optical and electronic), noise source modelling, diffuse channel modelling and modulation schemes. There has been only limited

published research into the performance of IR wireless protocols above the physical layer. Although the IrDA protocol has been finalised, there is still scope for variation in specific system design issues, parameter settings and optimisation. At the time of writing, the AIr protocol is in a draft status and not fully developed. Performance modelling and analysis of the AIr protocol can help recommend protocol design changes and optimum parameter settings while the protocol is in a development stage. Performance modelling studies, both simulation and analytical, have been published for related HDLC based data link layer protocols (Bux and Kummerle, 1980; Georges and Wybaux, 1981; Marsan et al., 1989; Masunaga, 1978; Schwartz, 1987)and CSMA/CA based MAC protocols (Bianchi et al., 1996; Brewster and Glass, 1987). This therefore provide the opportunity to apply the methods and principles of existing studies of related protocols to the study of the IrDA and AIr protocols.

1.2 Statement of Problem

The BER of an IR wireless link is derived from the signal-to-noise ratio (SNR) seen at the receiver. The received signal strength depends on the transceiver characteristics (e.g. transmitter power, photodiode surface area and responsivity) and link geometry (link distance and orientation of transceivers). The noise power depends on ambient light power levels (the dominant noise source) and the receiver bandwidth. An interfering signal from a third IR wireless device can also result in bit errors.

The IrLAP data link protocol involves transmitting a sequence or 'window' of data frames, following which the transmitting device must wait for an acknowledgement frame from the receiving device. The acknowledgement delay may include turn-around delays to cover hardware latency in addition to the acknowledgement frame transmission time. Data frames are re-transmitted when either lost due to bit errors or if consequently out-of-sequence from subsequent lost frames in the transmission window as indicated by the acknowledgement. Increasing the frame data packet size (bits) will reduce the relative frame overhead contribution and frequency of link turn-around following a transmission window, tending to increase throughput efficiency. However increasing the data packet size will also increase the probability of frame error from a

given bit-error-rate (probability of error per bit) thus increasing the probability of frame re-transmissions and tending to reduce throughput efficiency. Similarly increasing the transmission window size will reduce the frequency of link turn-around but increase frame overhead contributions and the probability of a large re-transmission sequence. By adjusting the data packet size and transmission window size to their optimum values in relation to the BER and link parameter settings, the throughput can be maximised as the link BER varies.

In a multiple-device AIr wireless LAN, once the medium is detected free, a device waits a random number of contention time slots before transmission to avoid frame collision from two or more devices transmitting at the same time. The range from which the random number of contention slots is chosen is referred to as the collision avoidance slot (CAS) window. Increasing the CAS window size reduces the probability of frame collision (from two or more devices choosing overlapping contention slots). However increasing the CAS window also increases the average contention delay before frame transmission. There is therefore an optimum CAS window size for a particular network size (number of contending devices) that will maximum utilisation on the network. A CAS window back-off algorithm has been proposed for AIr that linearly adjusts up or down the window size depending on the success or failure of an RTS/CTS reservation attempt (IrDA, 1999c). Modelling of the AIr protocol can help to highlight the interaction between the network size, CAS window size and other contention parameters, evaluate the effectiveness of the CAS back-off mechanism, and therefore aid the further development of the protocol.

1.3 Outline of Research

The following summarises the main components of the research in the thesis.

Protocol Modelling Methods: Methods used in published literature for the study of related protocols are examined to inform the choice of methods used in the thesis for the study of the IrDA 1.x and AIr IR wireless protocols. Performance studies of HDLC and derived protocols (balanced and unbalanced) using both analytical and simulation modelling are examined for potential modification and application to the study of the

HDLC-NRM based IrDA 1.x IrLAP data link protocol. Similarly performance studies of CSMA/CA protocols including the IEEE 802.11 wireless LAN protocol are examined for potential application to the study of the AIr MAC protocol.

Physical Layer Analysis: The signal-to-noise ratio (SNR) at the receiver of an IR wireless link is dependent on transceiver characteristics such as transmitter power, photodiode area and responsivity, receiver design, link geometry (i.e. link distance and transceiver orientation angles), background ambient light levels and interference levels from other IR wireless devices. The physical layer of IR wireless protocols is analysed with the aim of highlighting the critical factors that effect performance and producing expressions for the SNR and hence bit-error-rate (BER) and packet error rate for standard IrDA based links. The effects of third user interference and resultant link directional and spatial asymmetry are also examined in order to determine the minimum separation distance for independent IR links without cross-interference.

IrDA 1.x Point-to-point Protocol Analysis: Analysis of the IrLAP data link layer of the IrDA 1.x protocol provides throughput and delay performance against link BER and protocol parameter settings of data rate, transmission window size, data packet size and link turn-around delays. An analytical model is produced for saturation throughput using re-transmission probabilities and window width stochastic process modelling. From this, graphical representations of the inter-relationships between parameters are produced. Results are produced showing the improvement of performance using simultaneous optimisation of both data packet size and transmission window size. An OPNET simulation model of the IrDA protocol is presented. A basic model simulating saturation conditions is used to confirm analytical modelling results. An advanced model is used for non-saturation conditions. Linking throughput performance to the physical layer analysis is used to optimise the range of the link.

Advanced Infrared (AIr) IR Wireless LAN Analysis: Analysis of the AIr MAC protocol provides utilisation performance against network size (number of active nodes) and MAC protocol parameters of collision avoidance slot (CAS) window size (the range from which a random CAS delay is chosen), CAS window adjustment parameters, data

packet size and transmission burst size. An analytical model is developed for saturation utilisation and delay in reserved mode using the probability of transmission collision and a Markov process model of the CAS window back-off process is used to examine the effectiveness of the process. An OPNET simulation model is presented and used to confirm the saturation reserved mode analytical results and provide unreserved mode performance results.

1.4 Thesis Format

Chapter 2 presents background information to the thesis including an overview of IR wireless links, data communications protocols and modelling methods for performance analyses of communications protocols.

Chapter 3 presents and overview of the operational details of the IrDA 1.x and AIr IR wireless communications protocols including physical layer specifications and details of the IrLAP and AIr MAC protocols.

Chapter 4 presents an analytical model of the IR wireless physical layer. Expressions are derived for link BER for varying data rates and modulation / encoding schemes. The effects of third user interference and resultant link asymmetry are also examined.

Chapter 5 presents a review of methods that have been used in the modelling, both analytical and simulation, of relevant HDLC based data link protocols and CSMA/CA based media access control protocols.

Chapter 6 presents an analytical performance model and results of the IrDA 1.x IrLAP protocol. Graphical results and analysis are presented for various data rates and parameter configurations. Numerical results are presented for the optimisation of data packet size and transmission window size. Results are also presented from the IrDA 1.x OPNET simulation model for validation of analytical results and non-saturation condition performance.

Chapter 7 presents an analytical performance model and results for the AIr MAC protocol. Results are presented for utilisation against contention window size and network size both with and without the collision avoidance window back-off process. Results are also presented from the OPNET AIr protocol simulation model for validation of analytical results and non-reservation throughput.

Chapter 8 presents thesis conclusions and further work for physical layer, IrDA 1.x and AIr protocol performance modelling.

Appendix A presents an overview of the OPNET simulation software tool and the details of the IrDA 1.x and AIr protocol OPNET simulation models. Appendix B explains the limiting distribution of a Markov chain. Appendix C defines and explains the Q-function.

2. BACKGROUND INFORMATION

This chapter provides background information to the research presented in the thesis. IR wireless communications are introduced with a comparison of radio frequency (RF) and IR optical wireless communications media, the structure and components of a basic IR wireless link, the classification of IR wireless links and the topology of IR wireless link connectivity. Communications protocols are introduced with an overview of data link protocols, media access protocols and their relation in a protocol stack reference model. An overview of current IR wireless protocols is presented: principally the IrDA 1.x protocol, the Advanced Infrared (AIr) protocol and the IEEE 802.11 protocol with IR physical layer. Finally an overview of the benefits and methods for simulation and analytical modelling of communications protocols is provided.

2.1 Wireless Communications Media

Both the IR and RF media have certain strengths and weaknesses which make them more suitable for particular wireless environments and applications. Table 2.1 compares the strengths and weakness of IR and RF media for wireless communications. RF principally benefits from a large range and high level of mobility but is restricted by the high congestion and regulation of the RF spectrum. IR wireless has a limited range, lower mobility and is susceptible high noise levels from ambient light but benefits from low-cost, low-power links with an unregulated spectrum and spatial confinement of the radiation. RF can be seen as favoured for applications where maximum user mobility over long ranges in varying environments (i.e. both indoors and outdoors) is required. Infrared (IR) wireless is seen as favoured for low-cost, low-power, short-range and low mobility, indoor applications with high data rates, high security, safety or electrical sensitivity requirements (Barry, 1994; Heatly et al., 1998; Kahn and Barry, 1997).

	RF	IR Wireless
Strength	• Large range • High level of mobility • High dynamic range • Full duplex communications capability • Frequency division multiplexing, and spread spectrum modulation techniques possible	• No regulation on infrared spectrum • Very high data rates possible • Low power consumption • Low cost • Good security as signal doesn't pass through walls • Good immunity to electrical interference • No interference to electronic equipment • No multipath fading
Weakness	• Frequency spectrum has very high level of congestion • Frequency spectrum use is highly regulated • High level of power consumption. • High component costs • Susceptible to multipath fading and dispersion • Susceptible to electrical interference • Security concerns as signal passes through walls. • Low maximum data rates	• Low mobility • Power output limited by eye safety regulation • Susceptible to noise from ambient light sources • Half-duplex links • Multipath dispersion can limit data rate

Table 2.1: Comparison of radio and IR wireless communications

2.1.2 History of IR Wireless Systems

The use of IR wireless for local-area communication was first proposed in the late 1970s (Gfeller and Bapst, 1979) with initial data rates up to 125 kbits/s. A number of experimental systems were developed during the 1980's (Chu and Gans, 1987; Minami et al., 1983; Nakata et al., 1984; Takahashi and Touge, 1985; Yen and Crawford, 1985) with data rates of 1 Mbits/s. The IrDA SIR (Serial Infrared) standard (v1.0) was first published in 1994 with a data rate up to 115.2 kbits/s. The FIR (Fast Infrared) physical layer at 4 Mbits/s (v1.1) was published in 1995 with the VFIR extension to 16 Mbits/s was published in 1999. The IrDA AIr (Advanced Infrared) MAC protocol was also published in 1999.

2.1.3 IR Wireless Links

The basic configuration of an IR wireless link is shown in Figure 2.1. The transmitter consists of an encoder, an LED driver, and an IR fitted with a beam shaping lens. The LED operates within the 800 to 900 nm wavelength range, where inexpensive silicon photodiodes have a peak spectral response (Figure 2.2).

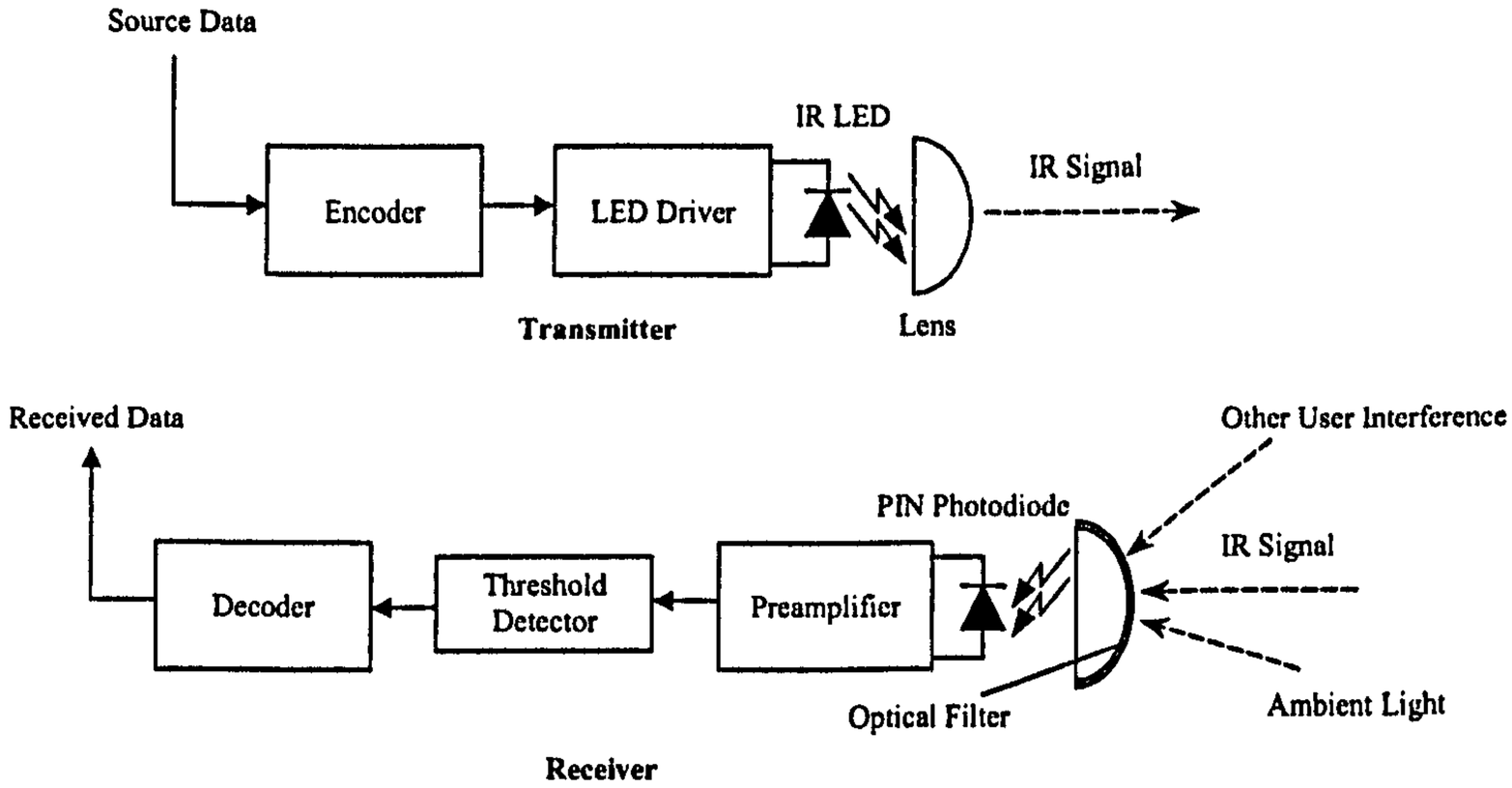

Figure 2.1 Basic wireless infrared link

The output power is restricted by eye safety regulations to give a maximum retina exposure of 10 mW/cm^2 at 900 nm for an LED (IEC, 1993). This typically restricts the transmitter intensity to less than 100 mW/Sr. The receiver consists of a photo-detector (typically a Silicon PIN photodiode) fitted with a collimating lens, a preamplifier (typically a transimpedance preamplifier with high-pass front-end filter), a threshold detector and a decoder. The receiver is also fitted with an optical filter to reduce ambient light levels outside of the IR signal wavelength. For low-cost systems, base-band IM/DD (Intensity Modulation with Direct Detection) in which the waveform is modulated into instantaneous optical power and the photodetector produces a current which is proportional to the received optical power is normally employed (Barry et al., 1991a).

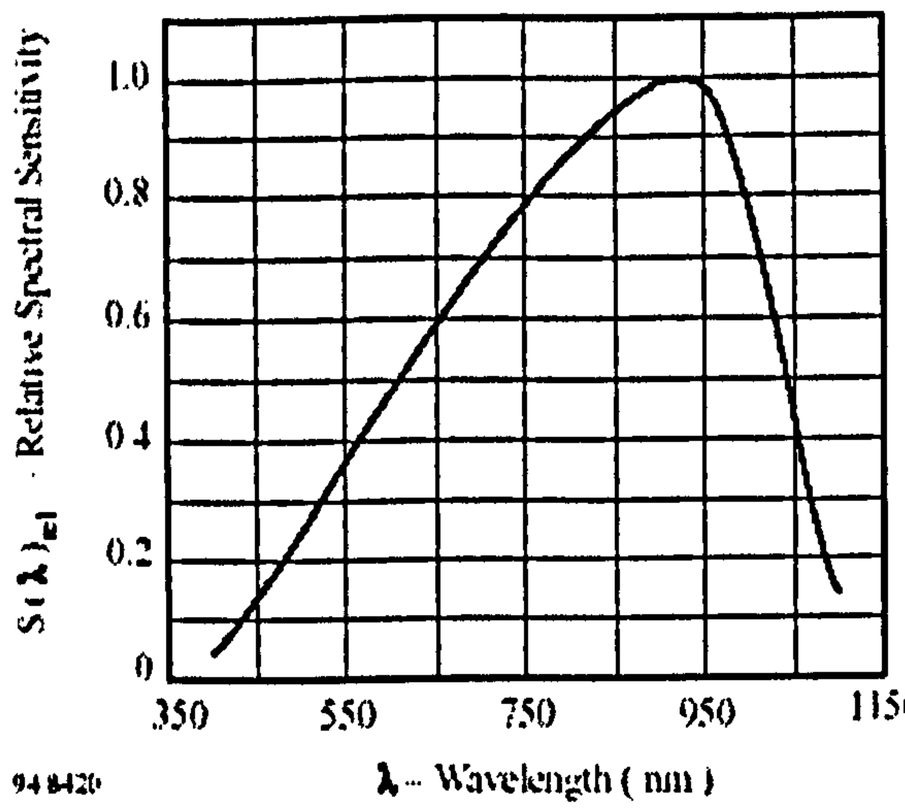

Figure 2.2 Silicon relative spectral sensitivity versus wavelength[1]

2.1.3.1 Binary Modulation and Encoding

The most basic system of binary modulation is NRZ (non-return-to-zero) OOK (on-off keying) which offers simple circuitry and full bandwidth efficiency. However it has poor power efficiency and is particularly susceptible to intersymbol interference from reflections or a third user interferer (Audeh and Kahn, 1995).

By using an RZ (return-to-zero) format, improved power efficiency can be gained. This also stops data loss from a long series of '1s'. However RZ requires a higher receiver bandwidth which makes the link more susceptible to background noise (Garcia-Zambrana and Puerta-Notario, 1999). Higher data rates often use L-PPM (Pulse Position Modulation) encoding in which one pulse in L time slots represents $\log_2 L$ data bits (thus 2, 4, 8 or 16 PPM are used). This provides power efficiency, good noise immunity and facilitates clock extraction, but reduces the bandwidth efficiency (Audeh et al., 1996). However another problem with PPM encoding is the possibility of back-to-back pulses from neighbouring PPM symbols, as with NRZ format.

[1] source: Temic BPW34 Silicon PIN photodiode datasheet

The issue of intersymbol interference has been addressed with more advanced encoding schemes such as Trellis coding (Lee et al., 1997) which removes the possibility of back-to-back pulses, direct-sequence spread-spectrum (Alvarez et al., 1999) and pulse-interval-modulation (Aldibbiat et al., 2001; Ghassemlooy et al., 2001; Ghassemlooy et al., 1998; Hayes et al., 1999; Matsuo et al., 1998; See et al., 2000). Performance has also been shown to improve using advanced modulation schemes with CDMA (Chan et al., 1996; Elmirghani and Cryan, 1994; Shin et al., 1996). However higher performances of advanced modulation and encoding schemes are achieved at the cost of the complexity of the transceiver circuitry required.

2.1.3.2 Noise and Error Detection

For a wireless infrared link, the dominant source of noise is the ambient background light. This can arise from sunlight (both direct and indirect) and artificial lighting including incandescent lamps and fluorescent lights. Optical filters are often used before the photo-detector, to reduce the level of incident light outside the signal wavelength, but the ambient light can still have a high infrared content within the wavelength pass-band of the filter (especially from incandescent lighting and sunlight). The ambient light induces 'shot' noise in the receiver, which is a white Gaussian noise resulting from the random fluctuation of the photocurrent about its mean value (Boucouvalas, 1996; Moreira et al., 1996; Narasimhan et al., 1996). Thermal noise can also be present in the receiver circuitry but can be minimised by suitable receiver design. The total noise power therefore increases with the receiver bandwidth. Interference from other IR wireless users (transmitting in the same IR wavelength band) can also results in bit errors. The effect of noise and interference on an IR wireless link depends on the modulation and encoding scheme used in transmitting the data (Gameiro and Alves, 1999; Georghiades, 1994; Samaras and Street, 1997). Bit errors in a data packet are detected by the use of standard error detection techniques such as the Cyclic Redundancy Check (CRC – both 16 bit and 32 bit are used). This can be implemented in both hardware and software and is often considered part of the physical layer. Corrupted packets are generally discarded and it is the responsibility of upper protocol layers to handle error recovery.

2.1.4 Classification of IR Wireless Links

IR wireless links can be classified according to their beam width, detector field-of-view and directivness. A fitted lens on an LED transmitter will focus the light into a narrower beam. Similarly, the capture angle or field-of-view (FOV) of the receiver can be narrowed with a suitable lens (Gfeller et al., 1996). A link with a narrow transmission beam and narrow FOV is termed '**directed**'. The principal benefit is that links are power efficient as the optical power is concentrated into a narrow beam. It also means that links can be established in close proximity to each other without any cross-talk. Links with a broad transmission beam and wide FOV are termed '**non-directed**'. This provides a greater degree of device mobility but links are less power efficient and more susceptible to third-user interference. '**Line-of-sight**' (LOS) links have a direct optical path between the transmitter and receiver. Links with transmissions reflected of walls and ceiling are termed '**non-line-of-sight**'. These links provide a high level of device mobility but a low level of power efficiency and are susceptible to multi-path dispersion which limits the available data rate. To address the problem of limited power output and multi-path dispersion for diffuse links, multiple narrow beam transmitters with imaging diversity receivers have been investigated (Djahani and Kahn, 2000; Kahn et al., 1998; Tang et al., 1996). Figure 2.3 shows the classification of IR wireless links in terms of line-of-sight (LOS), non line-of-sight, directed, non-directed, and hybrid (Barry and Kahn, 1995).

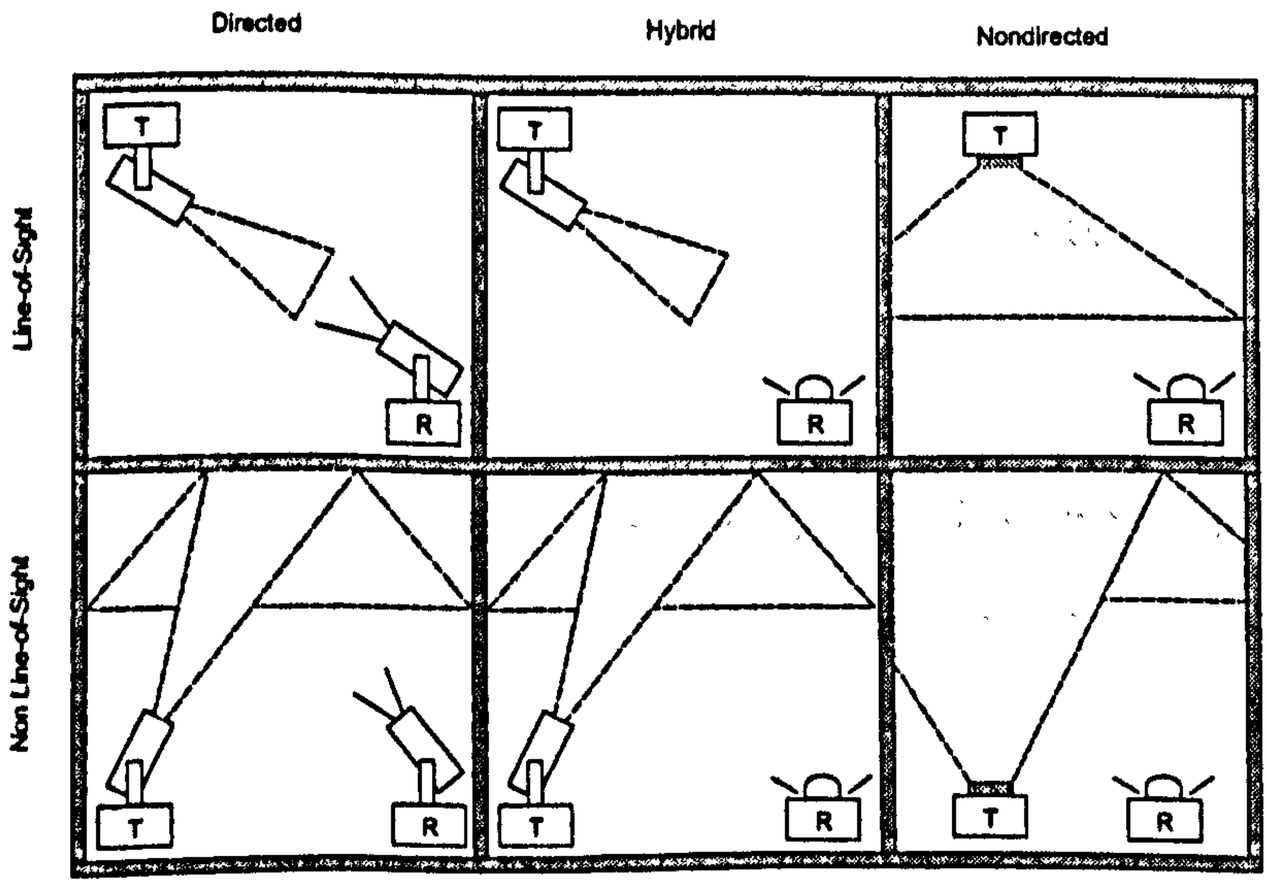

Figure 2.3 Classification of IR links
(after Barry, 1996)

2.1.5 IR Wireless Communication Networks

Individual IR wireless links as described in the previous section can be utilised in a number of different configurations to form wireless communications networks (Stallings, 2000) (Barry, 1994) as illustrated in Figure 2.4.

Point-to-point communication: Two infrared devices communicate with each other exclusively, using point-to-point directed links. Practical examples of this are the transferring of files from a mobile computing device to a desktop computer or wireless printing from a mobile device. One of the devices could also act a network interface port providing wireless access to a standard wired LAN. Media access is relatively simple for point-to-point links where devices simply exchange periods of transmission with one device as a 'master' controller.

Centralised communication: Multiple devices communicate with a central 'hub' node. All data must pass to and from the hub, i.e. other devices cannot communicate directly between themselves. The central hub could be an active participant exchanging data or merely a 'dumb' relay station serving the node devices. A practical example of this would be a ceiling based infrared hub in an office environment to which mobile devices on office desks would communicate. Media access is generally controlled by the hub device and may involve time division access for the node devices.

Infrastructured communication: An extension of the centralised communication concept is that of infrastructured communication where the central node is connected to a network backbone which could also connect additional IR nodes in the same room or in other rooms in the building.

Ad-Hoc communication: Multiple devices are communicating with each other in a 'broadcast' environment in which there is no central co-ordinator. All devices have equal status and can join and leave the network at will. A practical example of this would be the establishment of an ad-hoc network of laptop computers around a meeting table. Media access in the scenario is random and will require the use of a suitable media access control protocol to contend with potential transmission collisions.

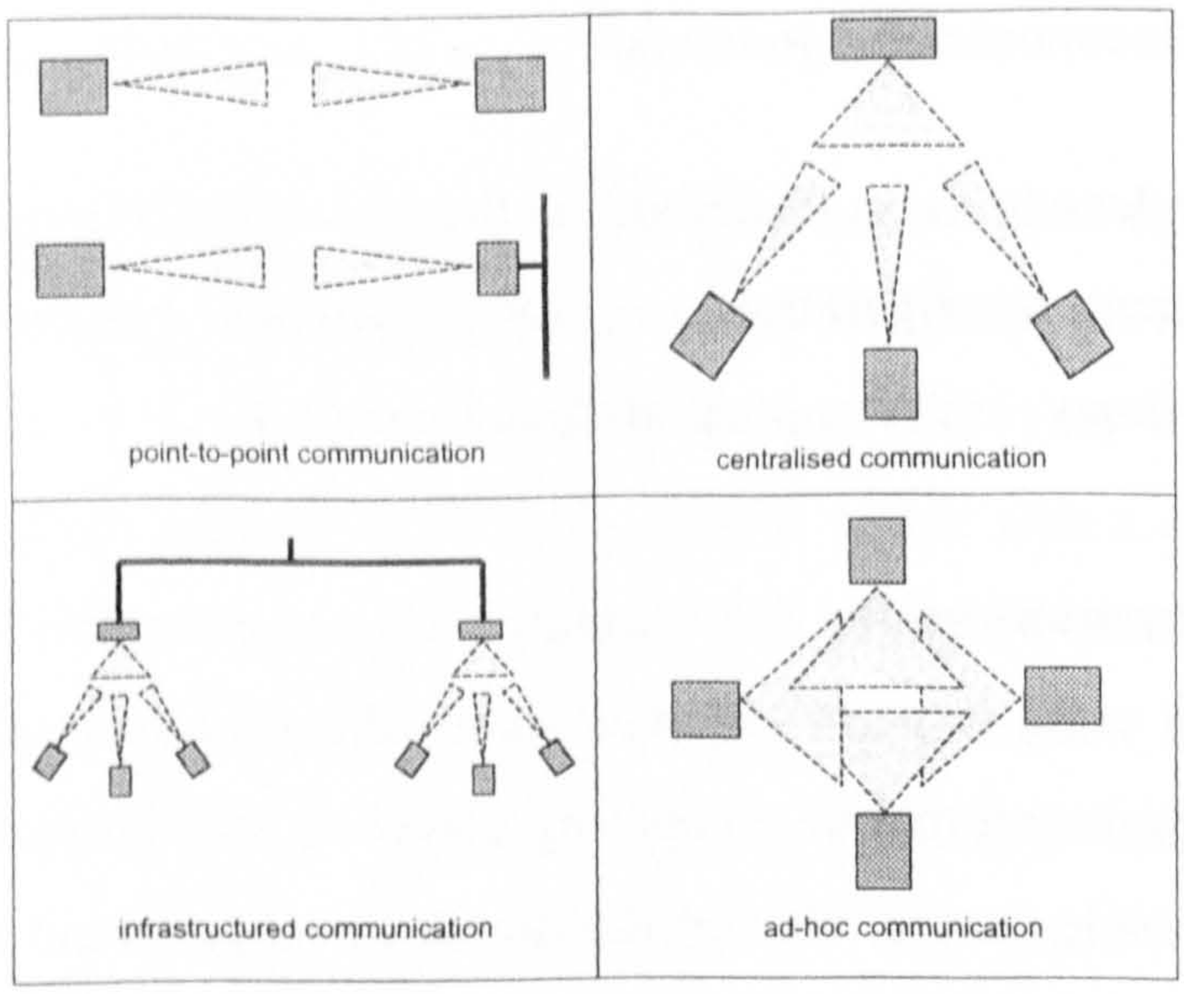

Figure 2.4 Infrared wireless communication networks

2.2 Communications Protocols

The following presents background information on communications protocols relevant to IR wireless communication protocols, including the principles of the communications protocol reference model and the principles of media access and data link protocols.

2.2.1 Protocol Stack Reference Model

The ISO (International Standards Organisation) OSI (Open Systems Interconnection) reference model consists of seven layers: the Physical layer, the Data Link layer, the Network layer, the Transport layer, the Session Layer, the Presentation layer and the Application layer. However when applied to real communications systems, this model is often seen as out-of-data and overly complex with session and presentation layers barely used and the data link and network layers over-full and split into sub-layer functions (Tanenbaum, 2002). In this thesis we are primarily concerned with the physical and data link layers of the reference protocol stack. The data link layer is responsible for packet frame formation functions, reliable transmission of data across the physical medium (error detection and re-transmission), flow control. For multiple access network, medium access control (MAC) functions are contained within the MAC sub-layer of the data link layer (Kurose and Ross, 2001).

2.2.2 Data Link Protocols

The data link layer involves such functions as packet framing, flow control, error detection and correction and link management. Flow control ensures that a device does not transmit more data at a time than a receiving device can handle. Error detection and correction involves the returning of an acknowledgement from the receiving device, the sequential numbering of data frames and re-transmission of corrupted frames. Link management involves controlling the establishment, maintenance and termination of a sustained data communication link. An important data link protocol is HDLC (High-level Data Link Control) which forms the basis of many widely used data link protocols. HDLC uses three station types: primary, secondary and combined. The primary station controls the operation of a link and secondary operates under the control of the primary in a master / slave relationship. A link involving a primary and one or more secondaries is referred to as *unbalanced*. A combined station combines the features of both primary and secondary stations and a link with two combined stations is termed *balanced*. HDLC can operate in three different modes: Normal Response Mode (NRM), Asynchronous Balanced Mode (ABM) and Asynchronous Response Mode (ARM). NRM uses the unbalanced configuration in which the primary initiates communication with a secondary, and the secondary can only transmit in response to a transmission from a primary. ABM uses the balanced configuration in which either combined station can initiate transmission without transmission from the other station. ARM uses the unbalanced configuration in which the primary controls the data flow but the secondary can transmit without explicit permission from the primary (Buchanan, 1996).

There are three frame types used: Information frames (I-frames) which carry the data payload in an established link, Supervisory frames (S-frames) which are short control frames with no data payload used in establishing and controlling the link, and Unnumbered frames which are used in link establishment and for unreliable data transfer. All frames have a control field that contains a frame type identifier and a P/F (Poll/Final) bit used for device polling. I-frames contain a send-sequence-number Ns and a receive-sequence-number Nr. S-frames contain a receive number and command/response codes while U-frames have no sequencing information (hence unnumbered). This is illustrated in figure 2.5.

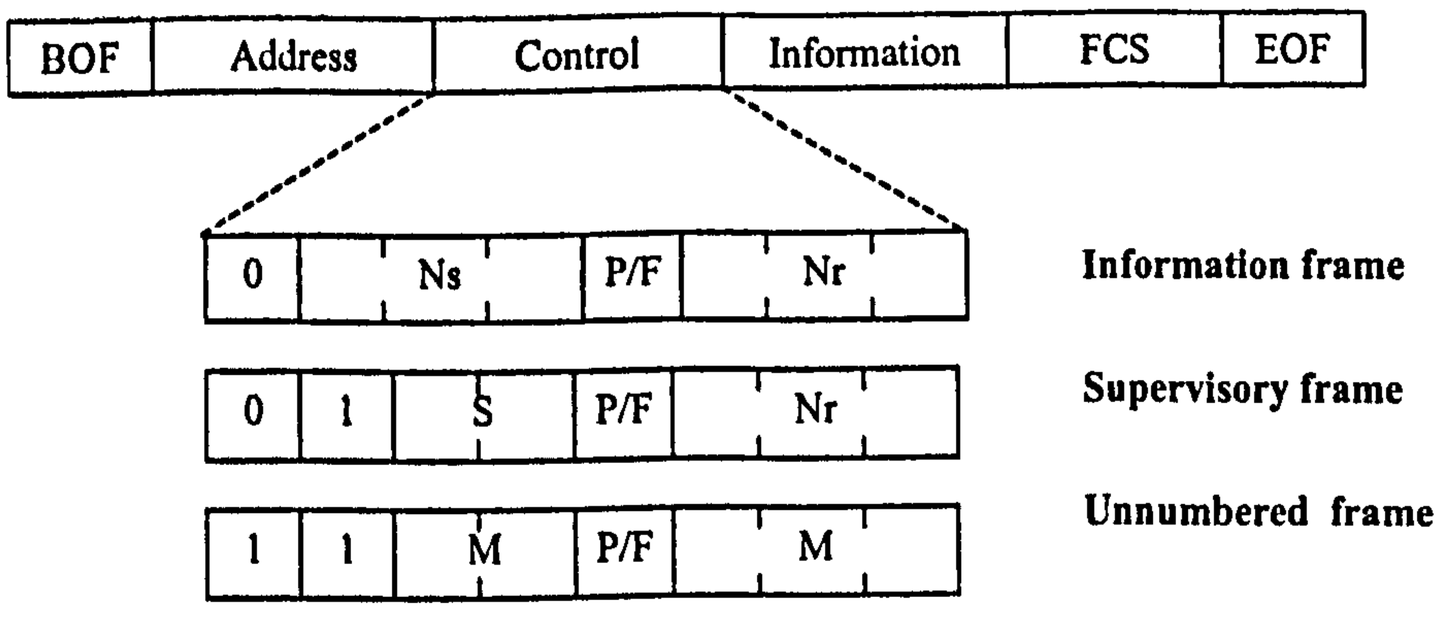

Figure 2.5 Standard HDLC frame structure

Data flow in HDLC involves the use of the send sequence number Ns in I-frames and the received sequence number Nr in I-frames and S-frames. For the 8-bit control field the numbers cycle through 0 to 7 (0 to 127 for the extended 16 bit format). There is therefore a maximum transmission 'window' of 7 frames (or 127 for the extended mode) before a station must wait for acknowledgement. The received sequence number Nr returned in an S-frame acknowledgement or I-frame acknowledges received I-frames with Ns up to and including Nr – 1, thus indicating that Nr is the next expected I-frame. If the received Nr is not as expected, then frames starting from Nr to the last transmitted Ns are re-transmitted. If the re-transmissions do not fill the transmission window, new frames follow the re-transmissions to do so (Carlson, 1980).

HDLC based data link protocols included LAPB (Link Access Procedures Balanced) used in X.25 packet switched networks, LLC (Logical Link Control) used in Ethernet LANs and LAPD (Link Access Procedures D-channel) used in ISDN (Integrated Services Digital Network).

2.2.3 Media Access Protocols

A shared medium such as a LAN or wireless network require some form of access control so that stations are not trying to transmit all at the same time, thus causing frame collisions which will corrupt the transmissions. The simplest type of multiple access is known as ALOHA. With this if a station has a data packet to transmit, then it is simply transmitted. When the receiving station receives the packet, it immediately returns an acknowledgement packet. If the sending station has not received a reply after a period

slightly longer than the maximum round-trip delay, the packet is re-transmitted. However this simplicity is paid for by performance as packet collisions frequently occur, and it can be shown that the maximum throughput achievable is only about 18%. An improvement on basic or pure ALOHA is called 'Slotted ALOHA'. In this packets can only be transmitted within fixed time slots. Collisions can still occur but only when packets are transmitted within the same transmission slot. It can be shown that with slotted ALOHA, the maximum throughput performance improves to around 37% (Schwartz, 1987).

A better system is to 'listen' to the network for traffic and only transmit when the medium is detected free for a short time. This is the basis of Carrier Sense Multiple Access (CSMA). However collisions will still occur when two or more devices attempt to transmit at exactly the same time. This can be addressed by listening to the medium during transmission to detect if a packet collision has occurred. If a collision is detected, the station waits a random period of time before attempting the transmission again. This is called Carrier Sense Multiple Access with Collision Detection (CSMA/CD). This is the basis of standard LAN protocols such as Ethernet (Aimes and Lazowska, 1979; Metcalfe and Boggs, 1976). The performance of ALOHA, S-ALOHA, CSMA and CSMA/CD are plotted in figure 2.6.

With wireless networks, devices generally cannot hear their own transmissions as sending and receiving is either performed asynchronously or on separate channels. Therefore wireless networks must use *collision avoidance* techniques. This generally involves the waiting of a random number of time slots before attempting to transmit. This is therefore termed Carrier Sensing Multiple Access with Collision Avoidance (CSMA/CA). Collisions can still occur but only when devices choose overlapping time slots. Performance can further be improved by using an RTS/CTS (Request To Send / Clear To Send) media reservation before data transmission which also helps contend with 'hidden node' devices (out of range of a transmitting device but within range of the receiving device reply).

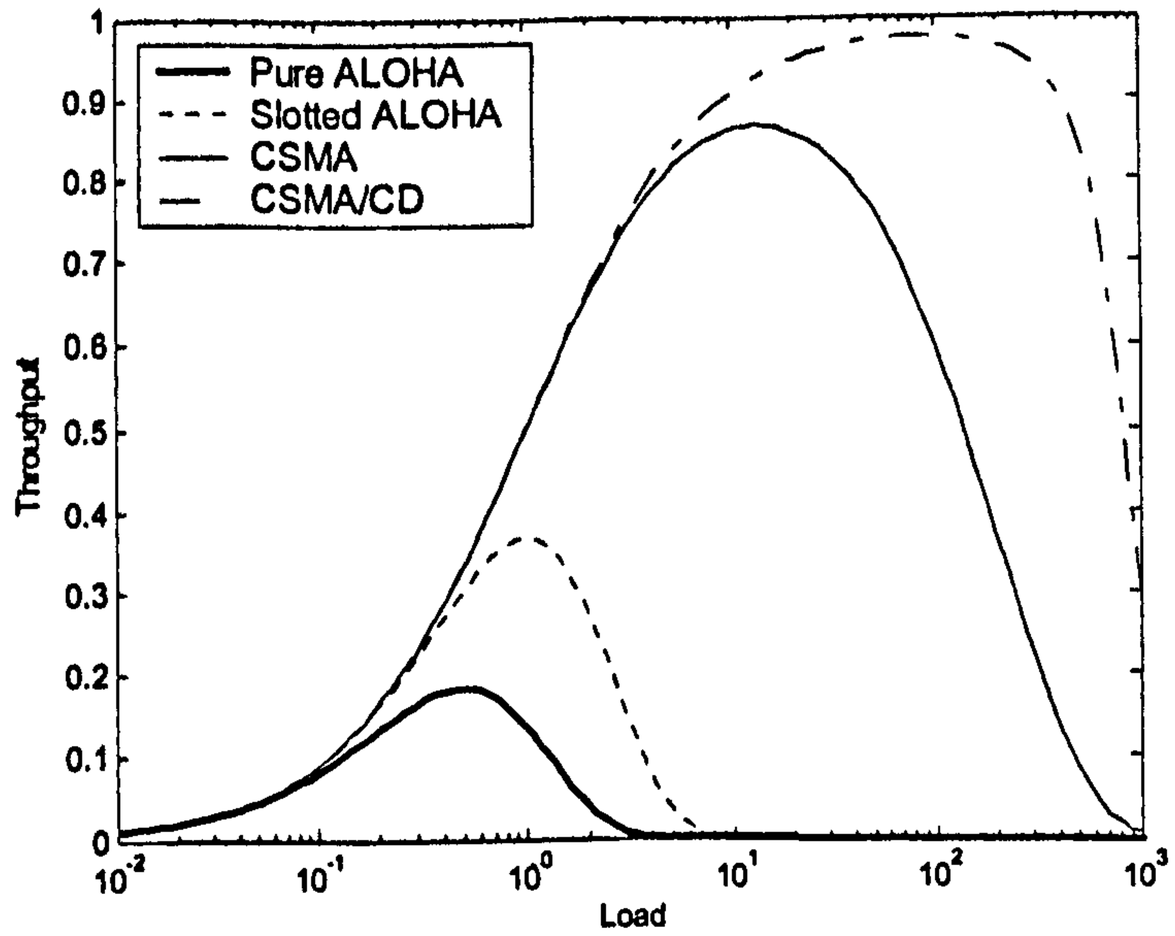

Figure 2.6 Throughput versus load for various media access schemes

2.3 Current IR Wireless Protocols

The principal IR wireless communication protocols used today are the IrDA 1.x protocol, the Advanced Infrared (AIr) protocol and the IEEE 802.11 wireless LAN protocol with IR physical layer. An overview of the protocols follows and the IrDA 1.x and AIr protocols are described in detail in chapter 3.

2.3.1 The IrDA 1.x Protocol

The IrDA 1.x protocol provides point-to-point directed communication with a data rate of up to 115.2 kbits/s through the devices standard serial interface (IrDA SIR – Serial Infrared), or 1.152 Mbits/s and 4 Mbits/s with a high speed hardware extension (FIR – Fast Infrared) , and a recent extension to 16 Mbits/s (VFIR – Very fast Infrared). The main component of the IrDA SIR protocol set is the IrLAP (Infrared Link Access Protocol) data link layer. This is closely based on the HDLC protocol operating in NRM with some additional media access features. The IrLAP protocol is responsible for device discovery, address conflict resolution, and reliable data transfer with error detection and recovery. As with NRM HDLC, IrLAP uses primary and secondary station roles, with station polling and frame sequencing to provide error recovery. The standard IrLAP protocol specifies a maximum transmission window of 7 frames (or 127 frames for 16 Mbits VFIR) and a maximum transmission period of 500ms before 'turn-

around' of the link. The other main component of the IrDA protocol is the IrLMP (Infrared Link Management Protocol) which sits above the IrLAP layer in the protocol stack. This actually consists of two components; IrLMP MUX, an application Multiplexer to the infrared link, and IrLMP IAS (Information Access Services), a database of services that the device supports that can be interrogated by the device requesting connection (Millar et al., 1998). The IrDA 1.x protocol is described in more detail in chapter 3.

2.3.2 The Advanced Infrared (AIr) Protocol

To address a recognised need for multi-point IR wireless connectivity, IrDA in collaboration with IBM developed the Advanced Infrared (AIr) protocol to support a multiple device ad-hoc access IR wireless network. The basis of the AIr protocol is to relax the physical layer restrictions of the IrDA protocol by providing a broad angle transmission and reception 'cone' to provide a 'broadcast' medium. The Physical layer also employs a robust carrier sensing scheme using variable repetition 4 PPM encoding with a base data rate of 4 Mbits/s. This provides a virtual reduction in data rate while increasing the range of the link. This is adjusted in response to the detected packet error rate. The 'header' portion of AIr an frame is always encoded with the maximum 16 RR to give the maximum possible range. For the upper layers of the AIr protocol, the IrLAP layer of the IrDA protocol is effectively split into 3 sub-layers of the AIr MAC, LM (Link Manager) and LC (Link Controller). The AIr MAC is a CSMA/CA protocol using RTS/CTS media reservation. Collision avoidance in the AIr MAC protocol involves detecting the medium free then waiting a randomly chosen set of time slots before transmitting a frame. When the reservation has been established, the MAC can transmit a 'burst' of data packets within a maximum reservation period of 500ms. The MAC can also transmit a single unreliable data packet outside of an established reservation. It is the responsibility of the LM layer to define the set of slot numbers used which are passed to the MAC with a reservation request. A linear back-off algorithm for the slot window size (the range from which the random value is chosen) is utilised for re-transmission attempts when packet collisions occur. The LM specification recommends a minimum slot window of 4 and maximum of 255. The LC layer is a balanced HDLC based data link protocol. This differs from the unbalanced IrLAP data link protocol in

that all stations have equal status (i.e. no primary / secondary roles). The LC provides procedures for discovery, address conflict resolution, reliable data delivery, and error detection and recovery. Further details of the AIr protocol are provided in chapter 3.

2.3.3 The IEEE 802.11 IR-WLAN Standard

The other main IR wireless protocol in use is the IEEE 802.11 standard with an infrared physical layer. The 802.11 specification is a wireless LAN standard using a common MAC layer above different physical layer options, one of which is infrared. The maximum data rate supported by all physical layers is 2 Mbits/s. For the IR physical layer, 1 Mbits/s and 2 Mbits/s data rates are specified. The modulation scheme used is 16 PPM for the 1 Mbits/s and 4 PPM for the 2 Mbits/s. As 16 PPM represents 4 bits per symbol, and 4 PPM represents 2 bits per symbol, the pulse duration is the same for both modulation schemes. The MAC layer of the 802.11 specification can utilise two media access methods. The Point Co-ordination Function (PCF) uses a time-bounded 'polling' method. The Distributed Co-ordination Function (DCF) is a CSMA/CA procedure similar to that of the AIr MAC protocol. The DCF can use either a basic access method or use RTS/CTS media reservation. Before sending a data packet, the DCF must sense the medium free for a period exceeding an average inter-frame time, called the Distributed Interframe Space (DIFS). When the channel is detected free, the DCF waits an additional random back-off period before sending a single data packet. An exponential back-off of the contention window CW is used when collisions occur. This is given by CW_{min}^{i} where $CW_{min} = 7$ and i is the attempt index, with a maximum of $CW_{max} = 255$. The receiving station always acknowledges data packets by returning an acknowledgement (ACK) packet. An optional reservation mechanism using RTS/CTS exchange can also be used (Bianchi et al., 1996; Crow et al., 1997; IEEE, 1997).

2.4 Performance Modelling of Communications Systems

This section provides background information on the methods of modelling communications systems. As stated in chapter 1, a data communications system, including both physical layer and higher protocol layers can be very complex with many factors and system parameters affecting the performance of the system. Modelling and analysis of data communications protocols is useful in determining the processes and

factors that effect the performance of the system and in optimising process parameters to maximise performance.

The principal benefits of modelling are:

- A detailed intuitive understanding of a particular aspect of the system operation and the dominant factors that affect performance can be obtained.
- A performance evaluation of a particular aspect of a system can be made without the need to physically implement or use a real system.
- Values for parameter settings to provide optimum performance under specific conditions can be established.
- Issues of protocol design that effect performance can be highlighted and possible protocol design improvements can be tested and evaluated.
- Recommendations can be made to system designers to obtain optimum system performance.

There are two principal methods for performance modelling of communications systems: mathematical analytical modelling and computer simulation modelling.

Mathematical modelling: This uses a set of mathematical expressions or formulas based on assumptions or approximations of system behaviour that relate a measure of system performance to a number of input parameters. Techniques such a probability theory and stochastic process modelling are used to produce values for a system performance output. The expressions are often evaluated using a computer from which rapid numerical and graphical output results can be obtained. The benefits of using mathematical modelling are that relatively simple formulae can be developed to model the behaviour of a very specific feature of a system and an intuitive understanding of the dominant factor and relationships that affect performance can be obtained. Using assumptions of behaviour and mathematical approximations, first order significant factors can be considered while small insignificant effects can be ignored. However it may not always be possible or practical to model a particular system behaviour (Harrison and Patel, 1993).

Computer simulation modelling: This uses a computer program to accurately mimic a particular feature of a communications systems behaviour. The computer program can simulate the behaviour of an entire network of devices with simultaneous processes. The simulation type considered here is a discrete event simulation where typical events are packet arrivals and timer expirations. Each event in the simulation process has a particular simulation time 'tag' association. This allows events in simultaneous processes in different simulated devices to have the same simulation time although executed sequentially in the computer program. Limitations can arise in simulating some natural process such as traffic load or bit errors. These are generally produced using random outcomes based on a specified distribution function with input parameters. The benefits of simulation modelling are that detailed information and output statistics from the system operation can be examined during simulation execution. The disadvantage is that, depending on the system complexity and the type of output statistics required, the simulation run (or set of simulation runs) can take a considerable period of time. Also the output results may not give the same level of intuitive reasoning to performance as a analytical model as the dominant factors affecting performance are difficult to determine. Simulation modelling presented in this thesis uses the OPNET Modeler simulation package[2]. OPNET uses a set hierarchical graphical domain editors to create models that reflect the structure of actual communications networks. Process models are created using finite-state-machines with C/C++ coded execution blocks using an extensive library of OPNET specific functions in addition to standard C/C++ functions and syntax. Further details are provided in appendix A.

[2] from OPNET technologies, (formerly MIL3 Inc.) – www.opnet.com

2.5 Chapter Summary

This chapter has provided background information on IR wireless communications systems, communications protocols and performance modelling techniques. An overview of IR wireless links was provided including the principal components, modulation and detection schemes, classification of link operational modes, and possible link / network configurations. A review of communications protocol principles for medium access and data link protocols together with descriptions of the IrDA 1.x, AIr and 802.11 IR wireless protocols were given. An overview the performance modelling techniques used in thesis was given. The Following chapter provides a detailed description of the IrDA 1.x and AIr protocols.

3. IR WIRELESS COMMUNICATIONS PROTOCOLS

This chapter describes the specifications and operational details of the two IR wireless communications protocols that are examined in this thesis: namely the IrDA 1.x protocol and the Advanced Infrared (AIr) protocol. Details for the IrDA 1.x protocol, are on the physical layer specification and operation of the IrLAP data link protocol with an overview of other optional components. For the AIr protocol, details of the AIr physical layer, the AIr MAC media access protocol and the AIr LM (Link Management) protocol are presented.

3.1 The IrDA 1.x Protocol

The IrDA 1.x protocol provides directed point-to-point communication between two devices with a data rate of up to 115.2 bits/s using the serial standard interface (IrDA SIR – Serial Infrared), and up to 4 Mbits/s (FIR – Fast Infrared), and a proposed 16 Mbits/s (VFIR – Very Fast Infrared) with additional hardware. The IrDA protocol stack is shown in Figure 3.1.

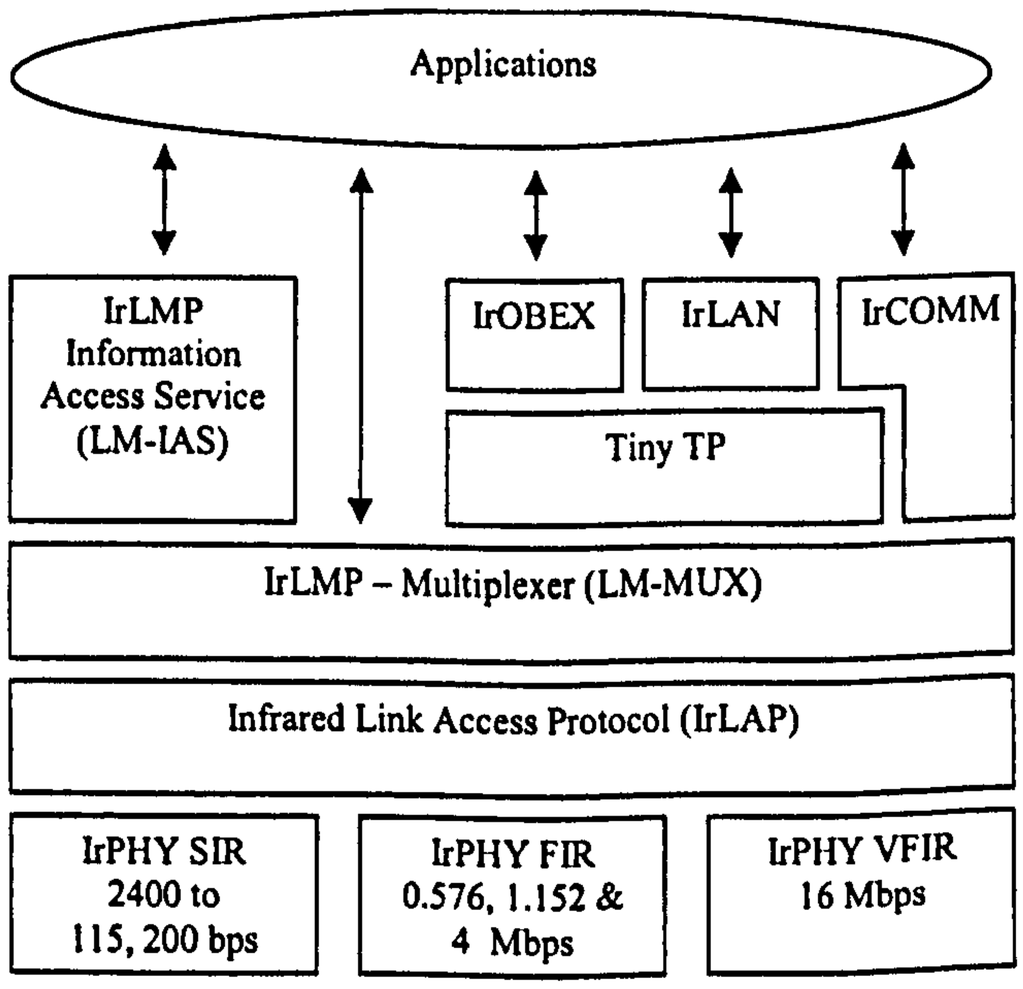

Figure 3.1 The IrDA 1.x protocol stack

The protocol stack consists of 3 mandatory components; the Physical layer (IrPHY), the Data Link layer (IrLAP), and the Link Management layer (IrLMP). The latter consists of two components; an application channel Multiplexer (IrLMP - MUX), and a supported service data base (IrLMP -IAS). Other optional components are Tiny TP - a credit based flow control component, IrCOMM - a serial link emulation component, IrLAN - an IR network point interface component, and IrOBEX - an object exchange component.

3.1.1 The IrDA 1.x Physical Layer

The Physical layer provides the optoelectronic and electronic components to transmit and receive data frames across the IR medium. Packet framing functions and error detection using the CRC are also considered to be part of the physical layer although often implemented as software components. The optical characteristics specification specify that the link should achieve a BER of no-worse than 10^{-8} over a minimum line-of-sight distance of 1m (i.e. a reliable link distance of up to 1m must be guaranteed). The transmitter cone half angle is between 15° and 30°, with a receiver cone half angle of at least 15° (Figure 3.2). The maximum transmitter power output is 500 mW/Sr.

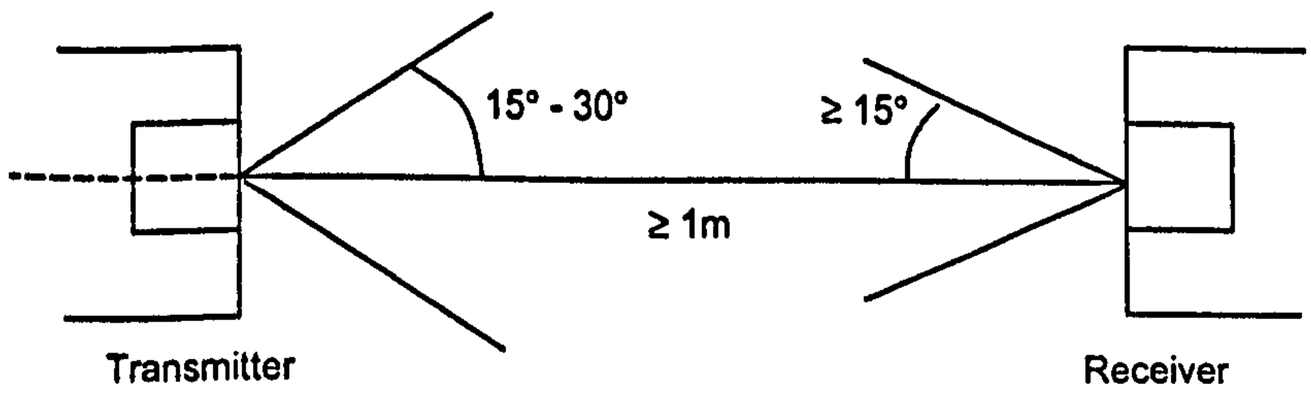

Figure 3.2 IrDA PHY optical interface specification

3.1.1.1 IrDA SIR Physical Layer 2400 to 115,200 bits/s

Version 1.0 of the physical layer is designed to connect directly to a devices serial port interface (either internally or externally). As such the data rate is limited to the maximum data rate of the serial port UART chip, which for modern computing devices is 115,200 bits/s. The schematic for the V 1.0 physical layer is shown in Figure 3.3.

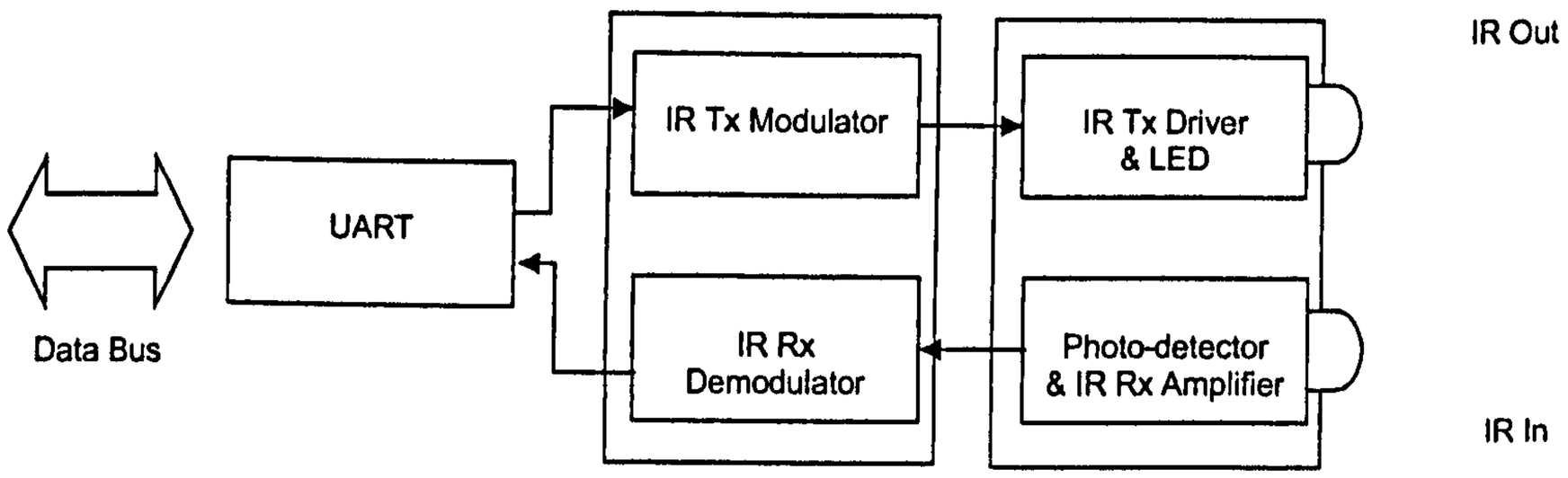

Figure 3.3 IrDA PHY 1.0 schematic

The data formatting used for the V 1.0 physical layer is RZI (Return-to-Zero Inverted) with a 3/16 bit period pulse duration. This uses the 16x clock cycle standard output from the UART chip, with the transmitter counting 3 clock cycles in the centre of the bit period. For 115,200 bits/s, the bit period is 8.7 μs and the IR pulse duration is 1.6 μs. This is shown in Figure 3.4.

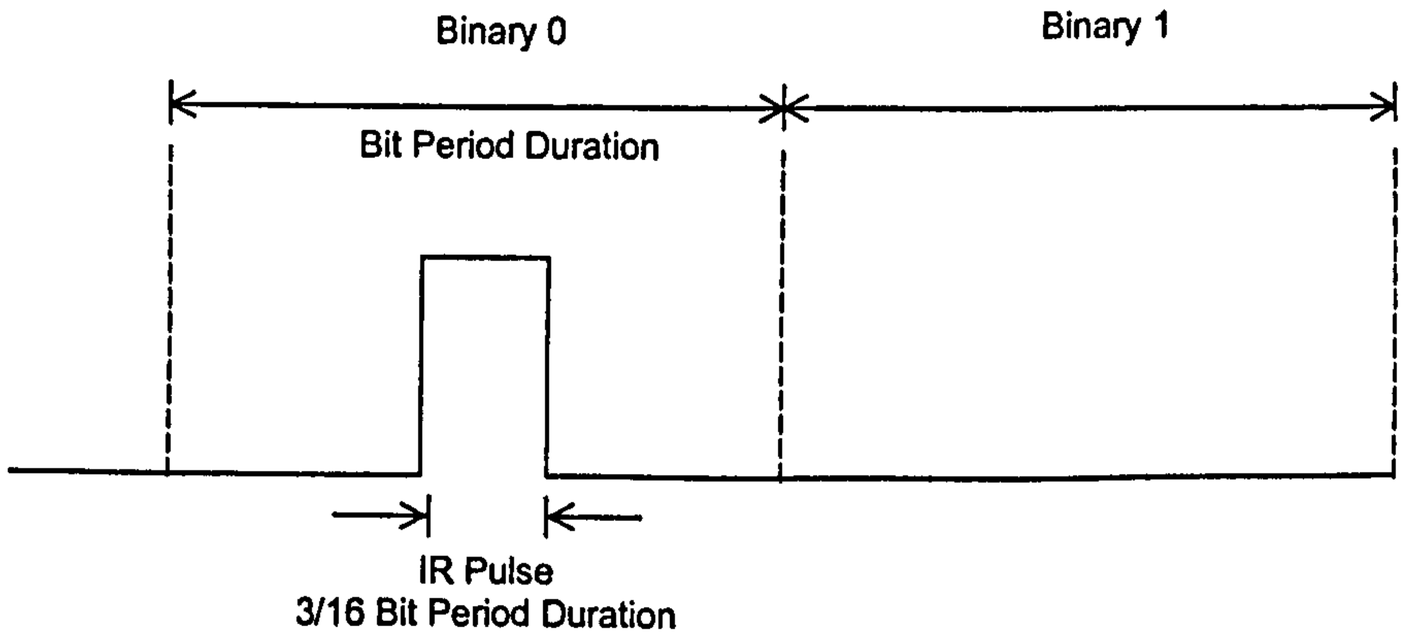

Figure 3.4 IrDA SIR PHY 9600 to 115,200 bits/s 3/16 RZI data format scheme

3.1.1.2 IrDA FIR Physical Layer 0.576, 1.152 and 4 Mbits/s

Version 1.1 of the physical layer supports additional data rates of 0.576 Mbits/s, 1.152 Mbits/s and 4 Mbits/s. For these data rates the link must by-pass the UART and use a dedicated high-speed communications controller which connects into the devices data bus. The higher data rate system is sometimes referred to as FIR (Fast Infrared). The V 1.1 schematic is shown in Figure 3.5.

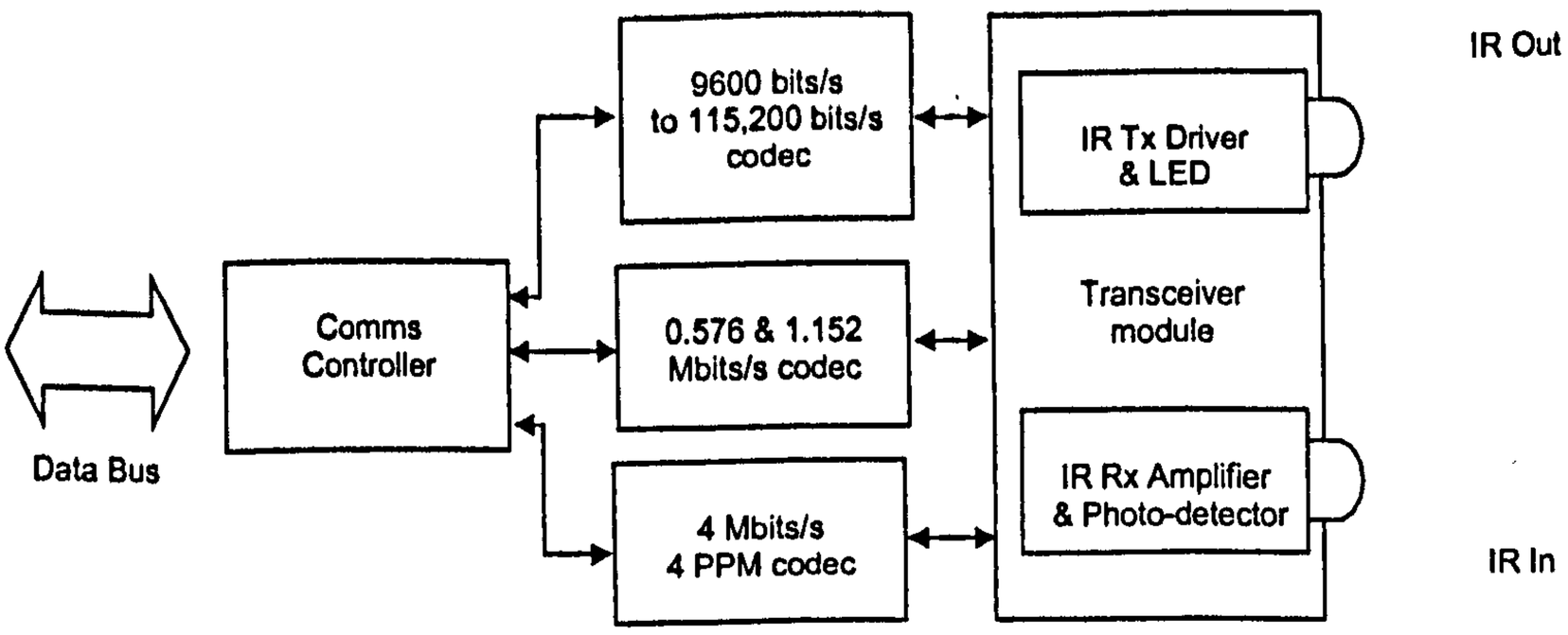

Figure 3.5 IrDA PHY 1.1 schematic

The 0.576 Mbits/s and 1.152 Mbits/s data rates use the same RZI encoding scheme as the V 1.0 physical layer but with a 1/4 bit period pulse duration.

The 4 Mbits/s data rate uses a 4PPM modulation scheme. With 4PPM a bit-pair is represented by a PPM symbol with 4 time slots. A single pulse positioned in each time slot gives each of the 4 possible combinations of the 2 data bits (IrDA, 1995b), as shown in Figure 3.6.

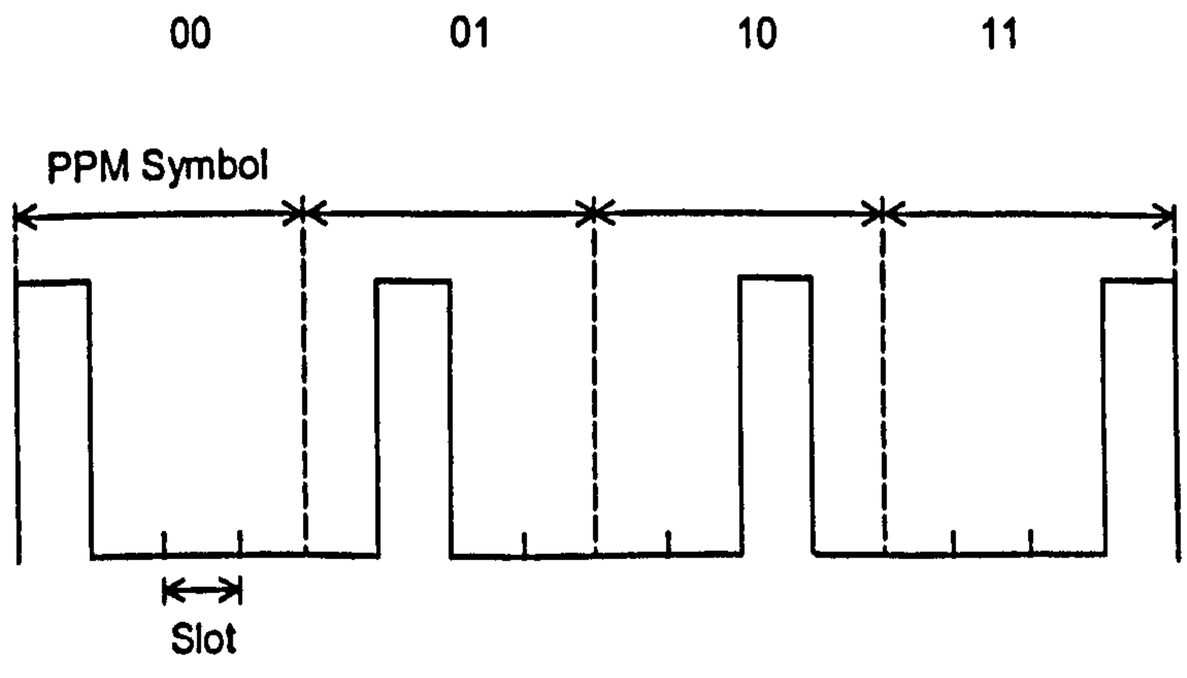

Figure 3.6 IrDA FIR PHY 4 Mbits/s 4PPM modulation scheme

3.1.1.3 IrDA VFIR Physical Layer 16 Mbits/s

A proposal has been made within IrDA to extend the maximum data rate of the IrDA 1.x protocol from 4 Mbits/s to 16 Mbits/s. The 16 Mbits/s VFIR (Very Fast Infrared) extension uses a different modulation scheme to that of the 4 Mbits/s links (Petrilla, 1998). The so called HHH(1,13) modulation code – named after the developers of the code: Walter Hirt, Martin Hassner and Nyles Heise at IBM – is a rate 2/3 (1,13|5) RLL

(run-length limited) code specifically developed for VFIR (Hirt et al., 2001). The encoding provides a minimum pulse separation of 1 empty pulse slot and a maximum of 13 empty pulse slots, with a maximum of 5 consecutive minimum pulse separations. The reason for using an RLL code is to eliminate the possibility of 'back-to-back' pulses, which can lead to intersymbol-interference (ISI) at high data rates from multi-path propagations (Audeh and Kahn, 1995). The rate 2/3 code also has a better bandwidth efficientcy than the 1/2 rate 4PPM encoding (Beale, 1999; Beale, 2000) .

3.1.2 The IrLAP Layer

The IrLAP layer is the data link layer of the IrDA SIR protocol stack. Its operation is closely based on the HDLC NRM (Normal Response Mode) protocol with additional media access functions. As such it is an 'unbalanced' HDLC protocol using Primary and Secondary station roles. Its main functions are:

- Device discovery
- Parameter negotiation
- Link establishment and role assignment
- Data transfer control
- Error recovery
- Link shut-down
- Packet formatting

The IrLAP procedural flow for connection establishment, data transfer and disconnection are shown in Figure 3.7. Before connection can be established, device discovery must complete during which exchange of randomly chosen 32 bit IrLAP addresses takes place. A procedure is also available to resolve any address conflicts. Devices then connect during which negotiation of link parameters takes place (see section 3.1.2.2). After completion of information transfer, the link is disconnected.

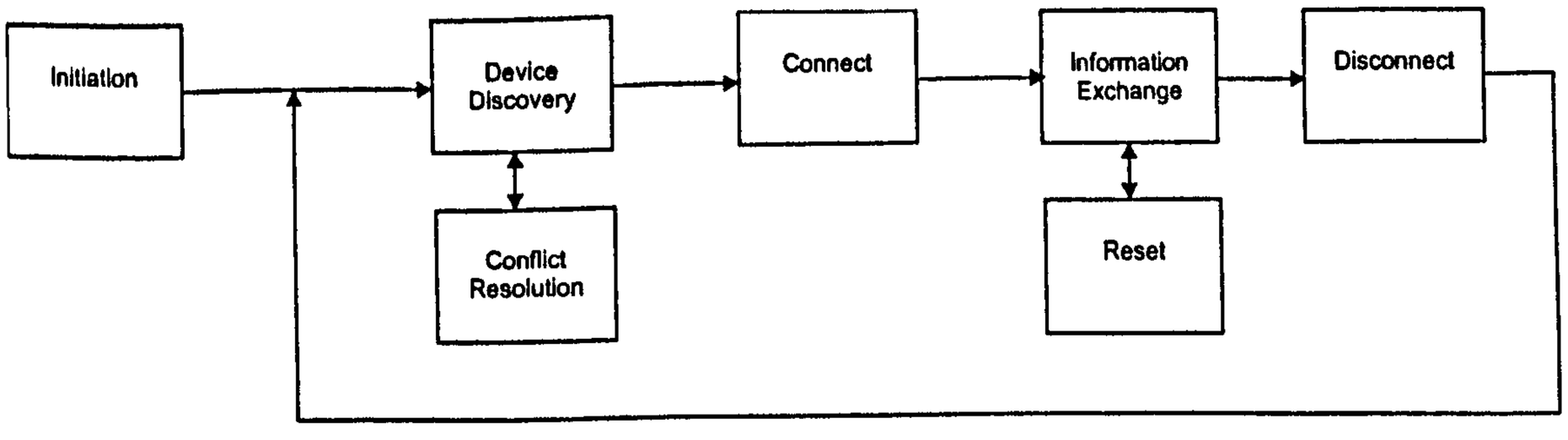

Figure 3.7 IrLAP procedure flow

3.1.2.1 IrLAP Frame Format

The IrLAP packet consists of the Address field, the Control field, and the Information field. The Address field contains a 7 bit connection address and a C/R (Command/Response) flag bit indicating whether the frame represents a command or response. The Control field contains command codes and sequencing information used for information exchange control. The Information field contains the user data packet from the upper layer of the protocol and can have a size from 0 to 2048 bytes (16384 bits). The IrLAP packet is then encapsulated in the physical layer 'wrapper' which consists of a BOF (Beginning Of Frame) field, the FCS (Frame Checking Sequence) for the CRC (16 bit for 9600 bits/s to 1.152 Mbits/s, 32 bit for 4 and 16 Mbits/s) and an EOF (End Of Frame) field. This illustrated in Figure 3.8.

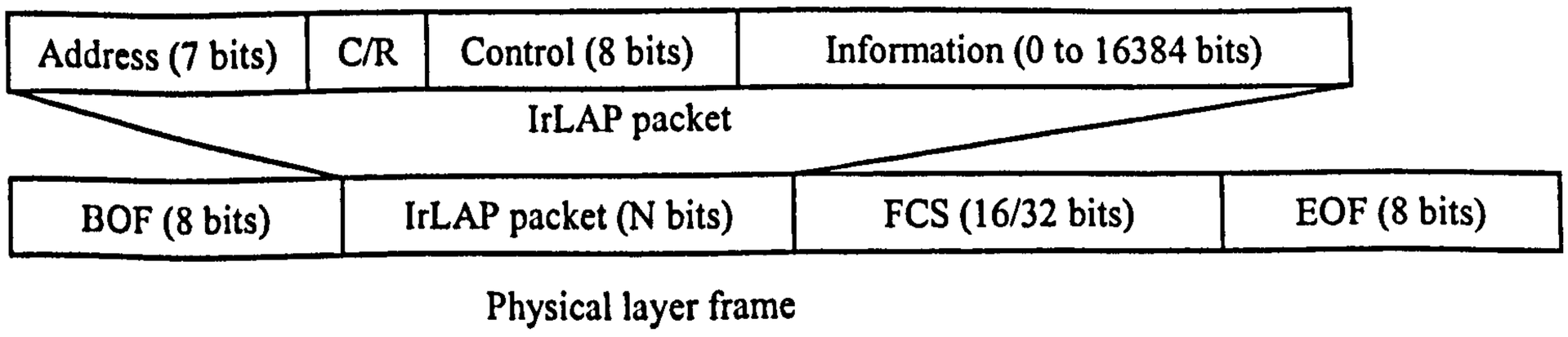

Figure 3.8 IrLAP packet format

The FCS contains the results from a Cyclic Redundancy Check (CRC) operation. The CRC uses the 16 bit CRC-CCITT polynomial ($x^{16} + x^{12} + x^5 + 1$) for the data rates 9600 bits/s to 1.152 Mbits/s, while the 4 and 16 Mbits/s links use the 32 bit IEEE 802 CRC32 polynomial ($x^{32} + x^{26} + x^{23} + x^{22} + x^{16} + x^{12} + x^{11} + x^{10} + x^8 + x^7 + x^5 + x^4 + x^2 + 1$). Frames that fail the CRC are simply discarded and not passed to the IrLAP process.

The Control field identifies the frame type. As with HDLC, there are 3 frame types used; the Unnumbered frame (U-frame), the Supervisory frame (S-frame) and the Information frame (I-frame). The U-frame contains no sequencing information (hence unnumbered) and is used in device discovery and connection procedures (and to exchange data unreliably outside of an established link). The U-frame structure is as shown in Figure 3.9 where X represents command / response code bits which are given in Table 3.1.

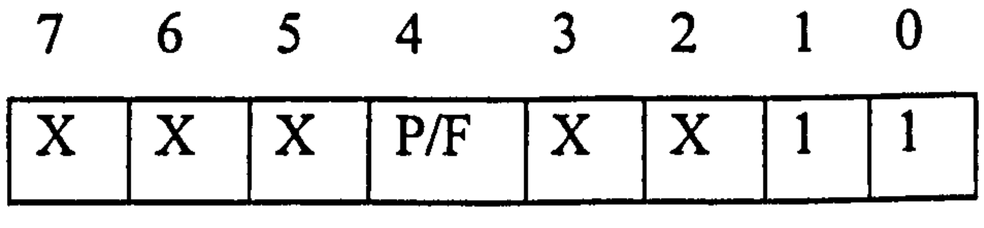

Figure 3.9 IrLAP U-frame control field

Command / Response	Description	Code
SNRM command	Set Normal Response Mode	10000
DISC command	Disconnect	01000
UI command / response	Unnumbered Information	00000
XID command / response	Exchange Identification	00111
TEST command / response	Test	11100
RNRM response	Request Normal Response Mode	10000
UA response	Unnumbered Acknowledgement	01100
FRMR response	Frame Reject	10001
DM response	Disconnected Mode	00011
RD response	Request Disconnect	01000

Table 3.1 IrLAP U-frame command / response codes

S-frames are short control frames, containing no Information field, which are used in controlling the information exchange process. The S-frame structure is shown in a Figure 3.10 with the command / response code bits given in Table 3.2.

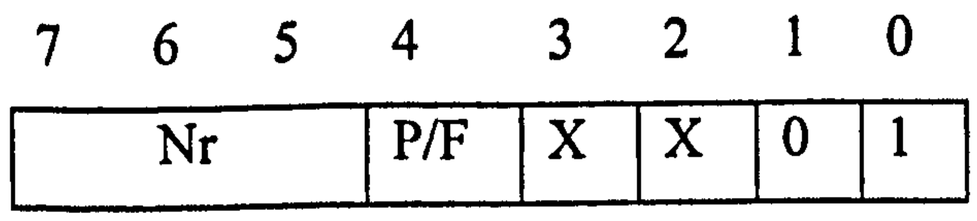

Figure 3.10 IrLAP S-frame control field

Command / Response	Description	Code
RR command / response	Receive Ready	00
RNR command / response	Receive Not Ready	01
REJ command / response	Reject	10
SREJ command / response	Selective Reject	11

Table 3.2 IrLAP S-frame command / response codes

I-frames contain the user data to be exchanged and full sequencing information. The control field structure is shown in Figure 3.11.

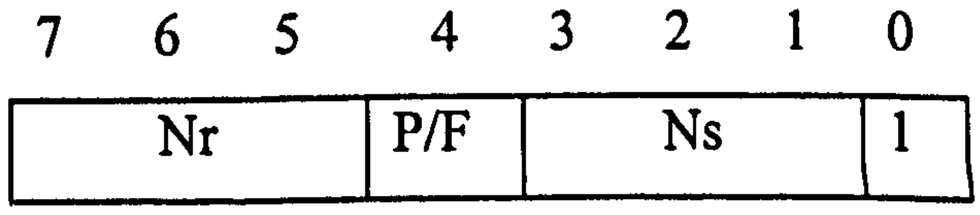

Figure 3.11 IrLAP I-frame control field

All frame types contain the P/F (Poll-Final) bit in the control field which is used for station polling. For the Primary station it is referred to a the Poll bit, and for the Secondary it is the Final bit.

Ns and Nr are send and receive sequence numbers that are contained within 3 bit fields. As such they can represent values 0 to 7. Ns fields are contained in I-frames only and sequence unacknowledged transmitted data frames. Nr fields are contained in both I-frames and S-frames and are used to acknowledge the receipt of I-frames. A returned Nr value indicates that I-frames with Ns values up to and including (Nr –1) have been successfully received (and in order), and that Nr is the next expected Ns value to be received.

3.1.2.2 IrLAP Connection Establishment

Before a link connection can be established, a device must first discover other devices within range that it can connect to. Discovery involves exchanging the 32 bit IrLAP device address which is randomly assigned at IrLAP initiation. In the unlikely event that devices choose the same IrLAP address, the address conflict resolution procedure is invoked which forces the devices to choose new addresses. A device may then connect to one of the devices discovered. During connection establishment, parameter negotiation takes place. All negotiation traffic takes place at the base data rate of 9600 bits/s. The link parameters involved are as follows.

Data Rate: This is the data rate at which information exchange will take place. Connecting devices must agree on the same data rate. This has a maximum value of 115,200 bits/s , 4 Mbits/s or 16 Mbits/s depending on physical layer specification.

Maximum Turnaround Time: This is the maximum time that a station can hold transmission status before it must pass permission to transmit to the other station in the link. This has a maximum duration of 500 ms.

Minimum Turnaround Time: This is the minimum time that the station must wait when transferring from a receiving state to a transmission state. This delay covers for receiver latency. This has a maximum value of 10 ms.

Maximum Data Size: This is the maximum number of data bits that can be sent in each packet. This has a maximum value of 16384 bits (2048 bytes).

Maximum Window Size: This is the requested maximum number of frames that a station can transmit before it must pass permission to transmit to the other station in the link. This has a maximum value of 7 frames or 127 for the VFIR high speed extension. The actual window size used in the link is determined by using the lesser of the requested maximum window size and the window possible to transmit within the maximum turnaround time (which has priority over the requested window size) using the data rate, packet data size and packet overhead size.

3.1.2.3 IrLAP Information Exchange Procedure

There are two principal states, receive (RECV) and transmit (XMIT). The station resides in the XMIT state during the period it has transmission status and accepts data transmission requests from the upper layer. The station resides in the RECV state when the other station in the connection is in the XMIT state and accepts received packets from the physical layer. The minimum turn-around delay must be implemented when moving from the RECV state to the XMIT state. The basic IrLAP information exchange procedure is closely based on the HDLC NRM procedure and is summarised as follows. Each station holds a transmit sequence variable Vs, a receive sequence variable Vr, and a *window* variable. The window variable is initialised to the negotiated maximum window size while Vs and Vr are initialised to 0. When a data packet is to be transmitted, a buffer copy of the data is made with index Vs. The Vs value is then copied to the Ns field of the out-going frame. When the frame has been transmitted the Vs value is incremented by 1, and the *window* value is reduced by 1. If the window value becomes 1, this indicates that the next frame is the last in the sequence. Therefore the P/F bit of the frame is set and station moves to the RECV state on transmitting the frame. The process is illustrated in Figure 3.12.

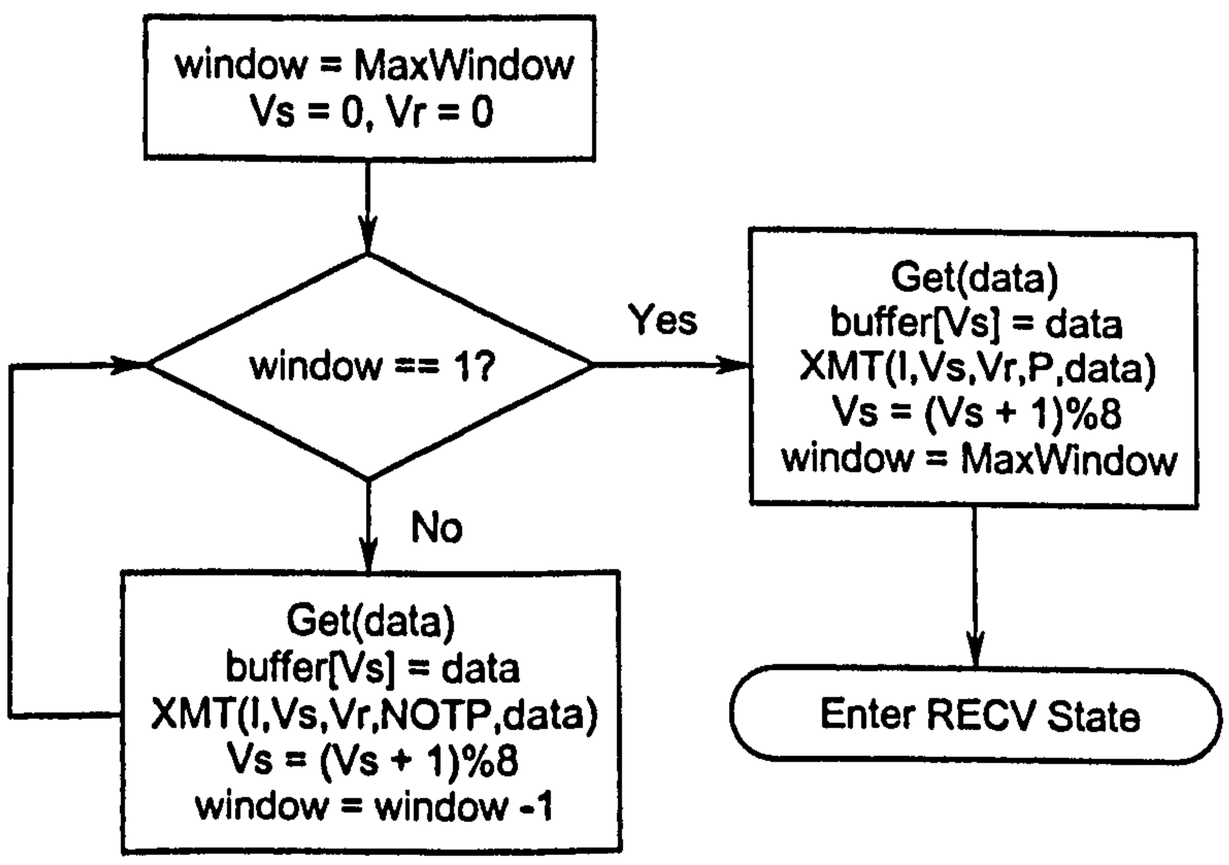

Figure 3.12 Primary station XMIT state frame transmission procedure

When a frame is received, the Ns sequence value is checked against that expected. It should be equal to the current receive sequence variable Vr. If it is as expected, the frame is accepted and the Vr variable is incremented by 1. If it is not as expected, this indicates a lost frame somewhere in the sequence and that the current received frame is out-of-sequence. The frame is then rejected and the Vr value remains unchanged. When transmitting either an S-frame or an I-frame, the current Vr value is copied to the Nr field of the frame. On receiving an S-frame or an I-frame with the P/F bit set the Nr sequence value is also checked against that expected. It should be equal to the current send sequence variable Vs (as Nr indicates the next expected frame number). If it is as expected, the frame sequence has been successfully received and no further action is taken except to clear buffered data that has been acknowledged. If it is not as expected, this indicates a lost transmitted frame. The buffered data must now be re-transmitted beginning with the sequence number indicated by Nr. If the re-transmitted frames do not fill the full sequence window, then new data frames are transmitted to fill the window. Figure 3.13 shows the flow chart for the Primary station frame reception procedure. Figure 3.14 shows the flow chart for the frame re-transmission procedure.

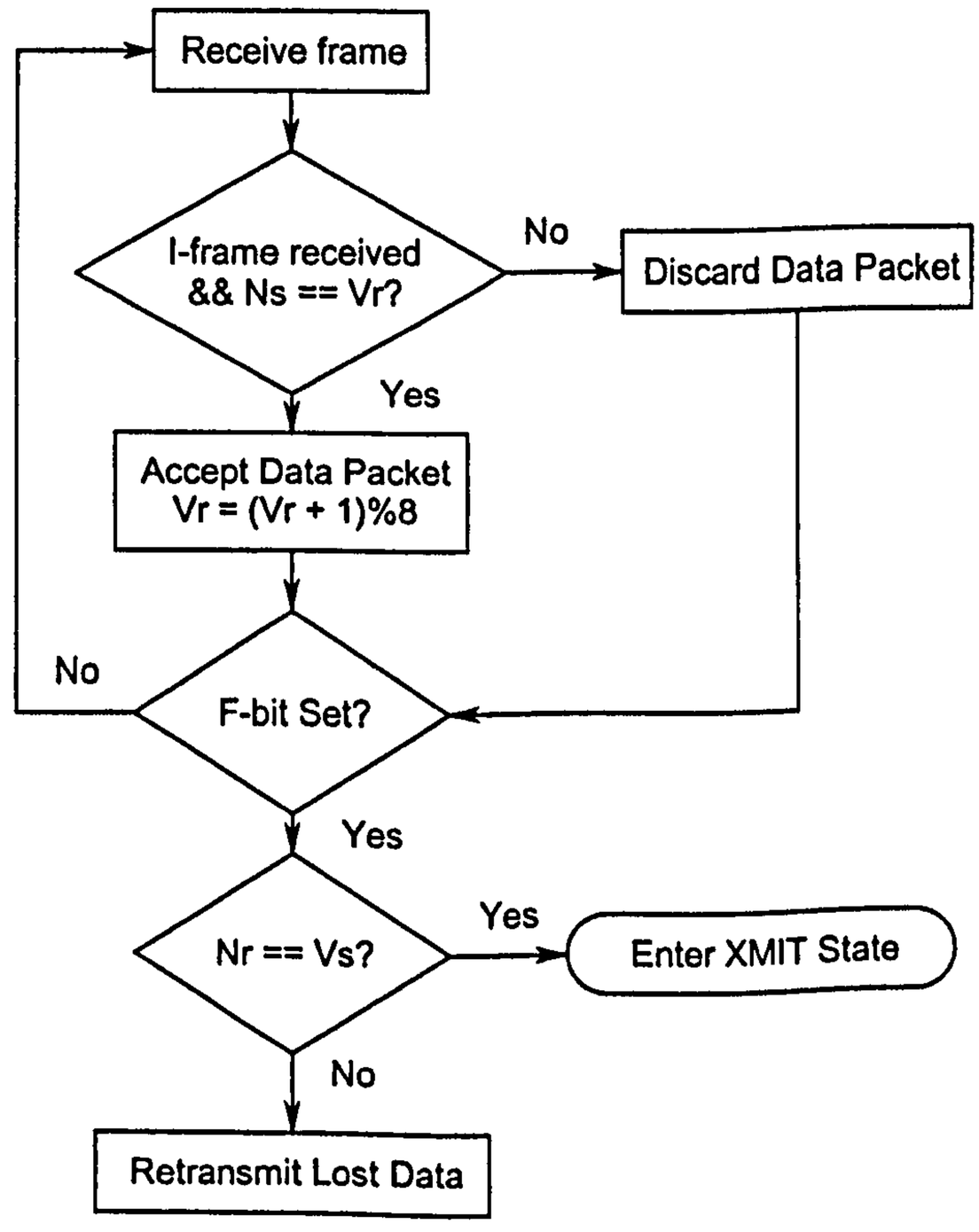

Figure 3.13 Primary station RECV state frame reception procedure

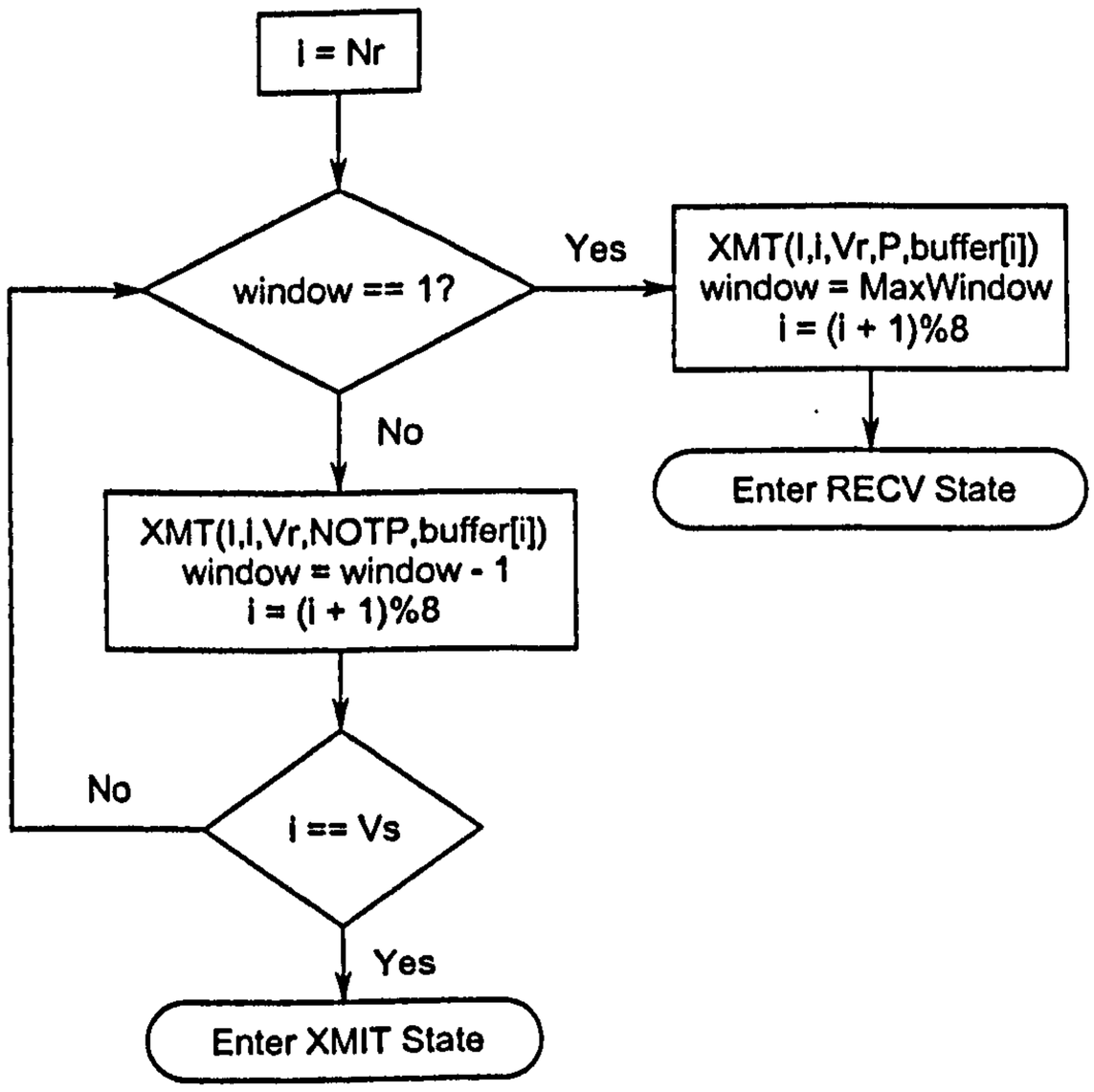

Figure 3.14 Primary station frame re-transmission process

The principal difference between the primary and secondary device in the link is the use of the P-timer and F-timer, held by the primary only. The P-timer is used to set a limit on the time the primary station can hold transmission status when there are limited or sporadic data packet transfer requests from the upper layer. The P-timer is thus started upon entering the XMIT state from the RECV state. If the P-timer expires, the station will transmit a Supervisory RR-CMD frame to poll the secondary station. The F-timer is used to set a limit on the time the primary will wait for a return of a packet with the F-bit set from the secondary. The F-timer is thus started upon entering the RECV state from the XMIT state. If the F-timer expires, the station will transmit a Supervisory RR-CMD to re-poll the secondary. The F-timer can expire if the packet with the P bit set from the primary is lost, or the returning packet with the F-bit set from the secondary is lost, or the secondary has become inactive. The secondary station does not hold P and F timers but must reply with an F bit frame and return to the RECV state if further data packets are not immediately waiting for transmission.

Examples of IrLAP data transfer are illustrated in Figure 3.15. Data transfer from the Primary to Secondary only is shown in sub Figure (a). The Primary transmits a window of 7 frames from I00 (I-frame, Ns = 0, Nr = 0, P-bit not set) to I60. Here frame I30 is lost due to bit errors (marked with an X). The Secondary responds with an S-frame with Nr = 3 acknowledging reception of frames up to and including Ns = 2 (Nr –1). The primary therefore re-transmits with I-frames starting from Ns = 3. When the re-transmission of frames has completed, new frames starting from I70 are transmitted to fill the window.

Two way data transfer from Primary to Secondary and Secondary to Primary is shown sub Figure (b). As before a window of frames is transmitted with frame I30 being lost. The Secondary now replies with its own data packets with Nr indicating acknowledged frames. However frame I13 is also lost due to bit errors. Following the reception of the F bit frame, the Primary re-transmits its data packets with Nr set to acknowledge the received packets from the Secondary. The Secondary will now require to re-transmit its own packets from Ns = 1.

Sub Figure (c) shows data transfer from the Primary to Secondary only but with an F-timer time-out. Here the P bit carrying frame I60P is lost in addition to frame I30. The Secondary therefore does not reply with an S-frame and so the F-timer expires. The Primary then re-polls the Secondary with an S-frame. The Secondary then replies with its own S-frame acknowledging the received frames. The returned Nr is still 3 as this was the first lost frame in the sequence (IrDA, 1996b).

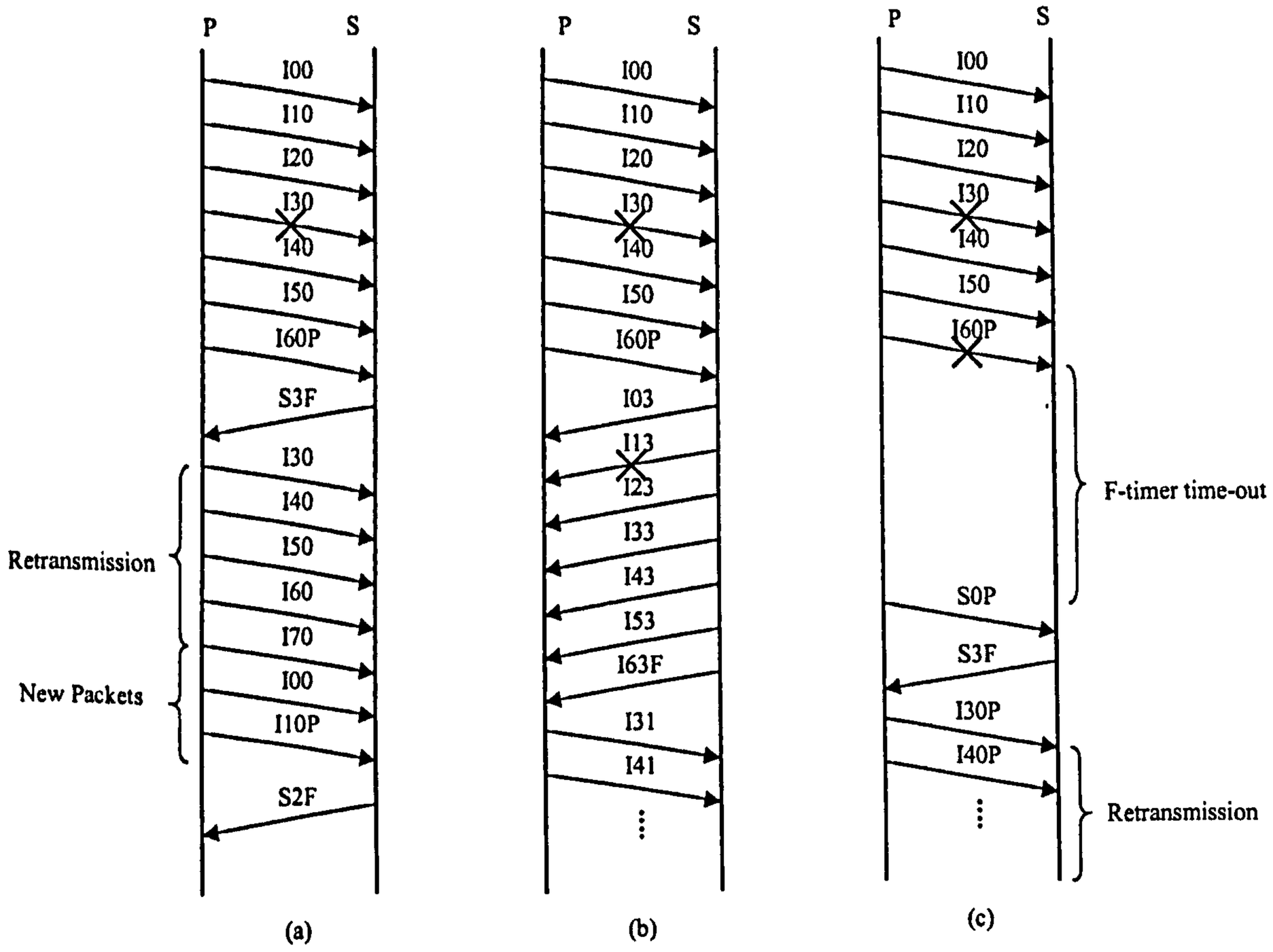

Figure 3.15 Example IrLAP transfers
(a) P to S data transfer (b) P to S and S to P data transfer (c) P to S data transfer with F-timer time out.

3.1.2.4 IrLAP Extension for 16 Mbits/s VFIR

The proposed extension of the maximum IrDA 1.x physical layer data rate to 16 Mbits/s has also required a revision of the IrLAP layer to support the higher data rate. At the 16 Mbits/s rate, the frequency of link turn-around using the standard 7 frame maximum window size and link turn-around delays would impair the efficiency of the link. An extension to the IrLAP protocol was therefore proposed in which the maximum window size was increased from 7 to 127 frames. This required a restructuring of the IrLAP frame control field to increase the Nr and Ns sub-fields from 3 to 7 bits, thus requiring an extension of the control field from 1 to 2 bytes. The additional frame overhead makes negligible difference to the protocol throughput. However the use of the 127 frame maximum window size can have implications for throughput with a poor BER. This is analysed in chapter 6.

3.1.3 Other IrLAP Components

The IrLMP protocol layer sits on top of the IrLAP layer and provides two distinct services: the LM-MUX (Multiplexer) and the LM IAS (Information Access Service). The LM-MUX is a Multiplexer that allows multiple client data applications to communicate independently and simultaneously through a single IrLAP connection. This is achieved through the use of a Link Service Access Point (LSAP) address attached to the user data which will direct the data through the specified Multiplexer channel. The LM-IAS (Information Access Service) is an object based information base that contains information on services made available to a connecting device. Following the claiming of an IrLMP-MUX port, a device advertises itself to the communicating device by placing available service information and related parameters in the database (IrDA, 1996a).

Tiny TP is an optional transport protocol which implements credit-based application-level flow control and data segmentation and re-assembly functions. The credit-based flow control function can overcome possible bottle-neck problems with the IrLMP Multiplexer if a large data set is being transferred over a channel. The flow control will ensure that only a certain amount of application data is released at a time to the Multiplexer (IrDA, 1995c). The IrLAN component is a network interface protocol that provides interaction with Ethernet LANs through an infrared LAN access port (IrDA, 1997a).

The IrCOMM component provides emulation of a serial cable connection between two devices. Legacy serial application can then simply use the virtual COM ports established with IrCOMM to exchange serial data with complete transparency to the underlying IR architecture (IrDA, 1995a). IrCOMM supports both data-terminal-equipment (DTE) and data-communications-equipment (DCE) connections. The IrOBEX component is an object (e.g. business card) exchange protocol that is based upon the HTTP protocol (IrDA, 1997b).

3.2 The Advanced Infrared (AIr) Protocol

The basis of the AIr protocol is to relax the physical layer restrictions of the IrDA physical layer to provide a robust broadcast medium and to split the IrDA protocol IrLAP layer into three sub-layers consisting of the AIr MAC layer, the AIr LM (Link Management) layer and the AIr LC (Link Control Layer). The protocol stack is shown in Figure 3.16.

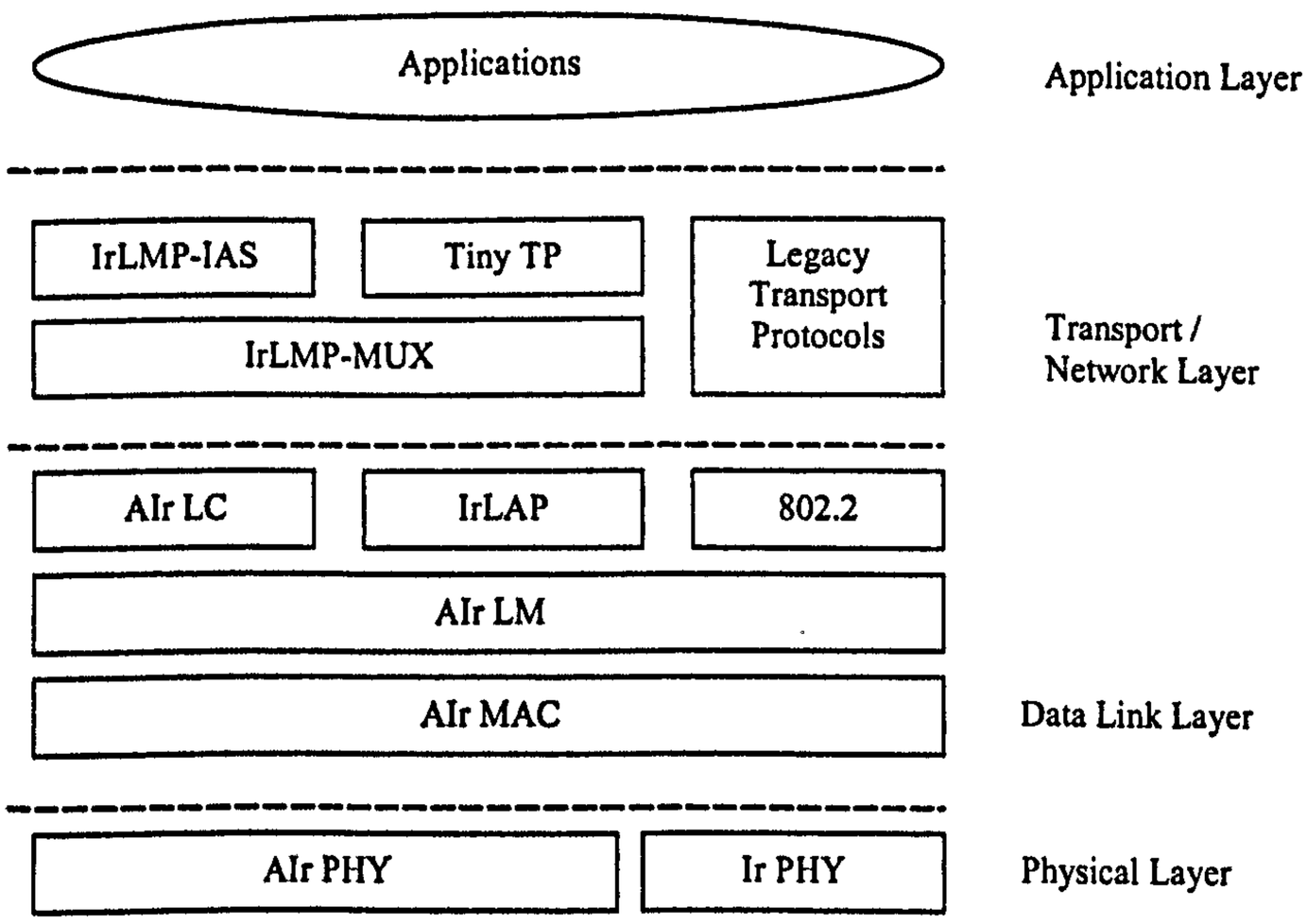

Figure 3.16 The AIr Protocol stack

3.2.1 The AIr Physical Layer

The AIr Physical Layer specifies the transceiver characteristics and modulation scheme to be used by AIr devices. In contrast to the IrDA physical layer (IrPHY) which being used for point-to-point directed links specifies a narrow transmission cone with maximum half angle of ± 15°, the AIr physical layer (AIr PHY) allows for much wider transmission angles and reception angles to provide a 'broadcast' medium in which multiple devices can communicate.

The AIr physical layer specification provides 2 classes of transceiver: standard range (S-Class) and long range (L-Class). S-Class transceivers have a radiant intensity between 60 and 150 mW/Sr which under normal lighting conditions should translate to a range

between 1 and 2.5 m. L-Class transceivers have a radiant intensity of 150 to 360 mW/Sr which gives a range of 2.5 to 6 m.

In addition to the two classes of transceiver power output, there are two classes of transceiver half-power angle: narrow angle and wide angle. Narrow angle transceivers have a half angle between ± 15° and ± 30°. Wide angle transceivers have a half angle between ± 60° and ± 75° (Figure 3.17). The 'half angle' refers to the angle at which the radiant intensity falls to half that of the maximum intensity. Also for AIr transceivers, different half angle values for the horizontal and vertical axes can be used. This allows for a harrow beam in the vertical axis but a wide beam in the horizontal axis in applications where devices are placed in the same horizontal plane (on a meeting table for example) which will help conserve power.

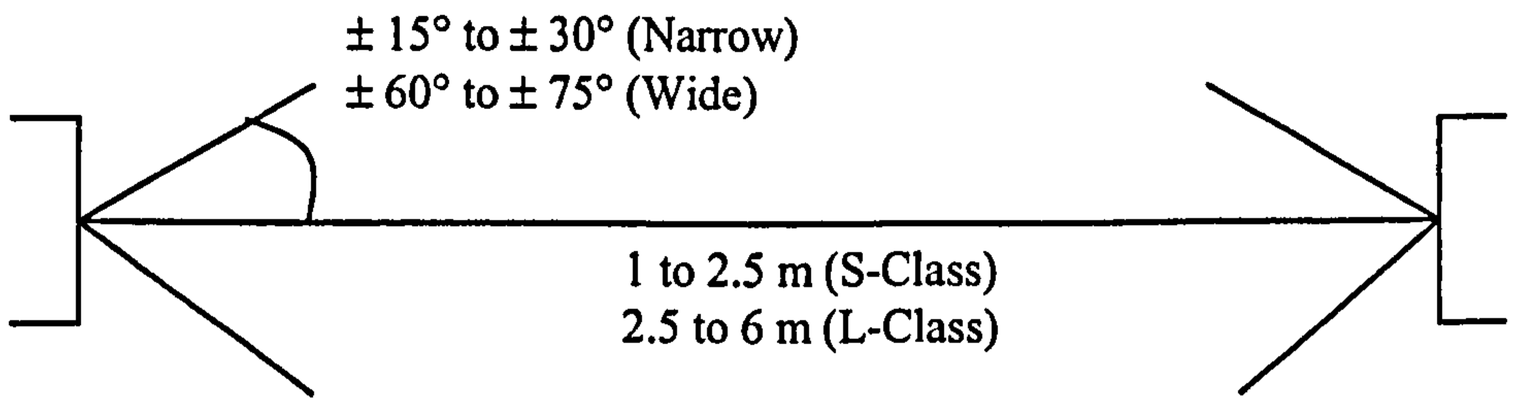

Figure 3.17 AIr optical interface specifications

The modulation scheme used is 4PPM with variable repetition encoding (4PPM VR) with a base data rate of 4 Mbits/s (Figure 3.18). The basis of variable repetition encoding is to use a variable number of repetition of each 4PPM symbol and use majority voting on valid symbols. The principle is to provide a trade-off between effective data rate and link quality. If chip errors occur due to noise in the link it may (depending on the severity of the noise) only cause an error in a minority of the repeated 4PPM symbols in which case the overall symbol (representing 2 data bits) will be accepted. This makes the link highly robust but reduces the effective data rate. In addition, the 4PPM/VR scheme provides a variable data rate and virtual receiver bandwidth reduction (B/RR) without any physical change to the receiver circuitry (Gfeller and Hirt, 1998).

RR	Effective Data Rate	SNR Gain (wrt RR =1)
1	4 Mbits/s	0 dB
2	2 Mbits/s	3 dB
4	1 Mbits/s	6 dB
8	500 kbits/s	9 dB
16	250 kbits/s	12 dB

Table 3.3 Variable repetition rates with effective data rate and SNR gain

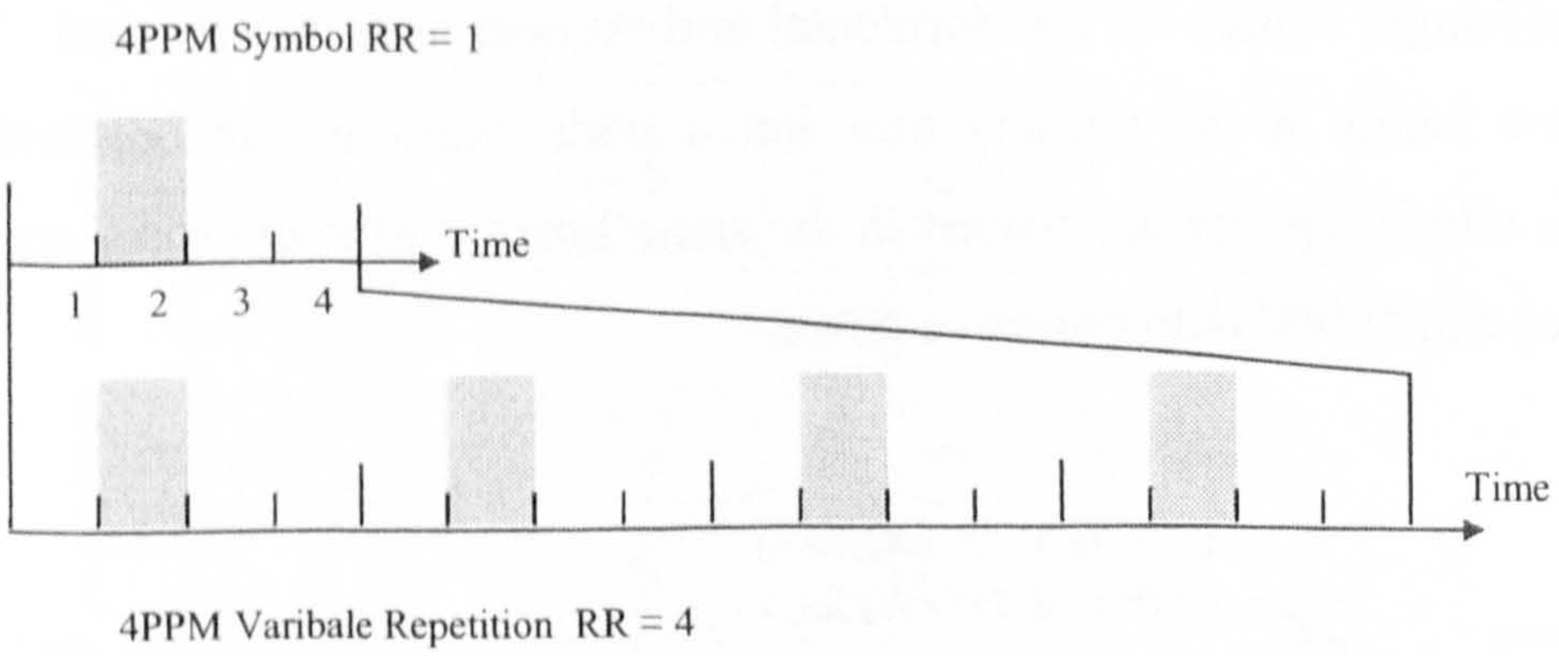

Figure 3.18 Example variable repetition 4PPM encoding

3.2.2 The AIr MAC Protocol

The AIr MAC protocol is a CSMA/CA (Carrier Sensing Multiple Access with Collision Avoidance) medium access protocol with RTS/CTS medium reservation. Although the AIr MAC specification provides a range of data delivery services, including unreserved and proxy, the following principally describes the reserved mode data transfer.

3.2.2.1 The AIr MAC Frame Structure

The AIr frame structure is given in Figure 3.19. The Preamble (PA) and Synchronisation (Sync) fields are used in carrier sensing, receiver synchronisation and identifying the exact start of the actual frame. The robust header identifies the frame type and carries other essential information for MAC operation. The Robust Header has just 32 bits but is always encoded with the maximum 16 RR repetition. The Main Body field is not always present and can be of a variable length and with variable RR encoding. It is primarily used to carry the payload data but can also carry addressing

information in certain frames. If the Main Body is present, it is protected by a 32 bit CRC field. The CRC used is the IEEE 802 CRC32 polynomial. If the CRC fails, the Main Body only is discarded while the Robust Header is still passed to the MAC procedure.

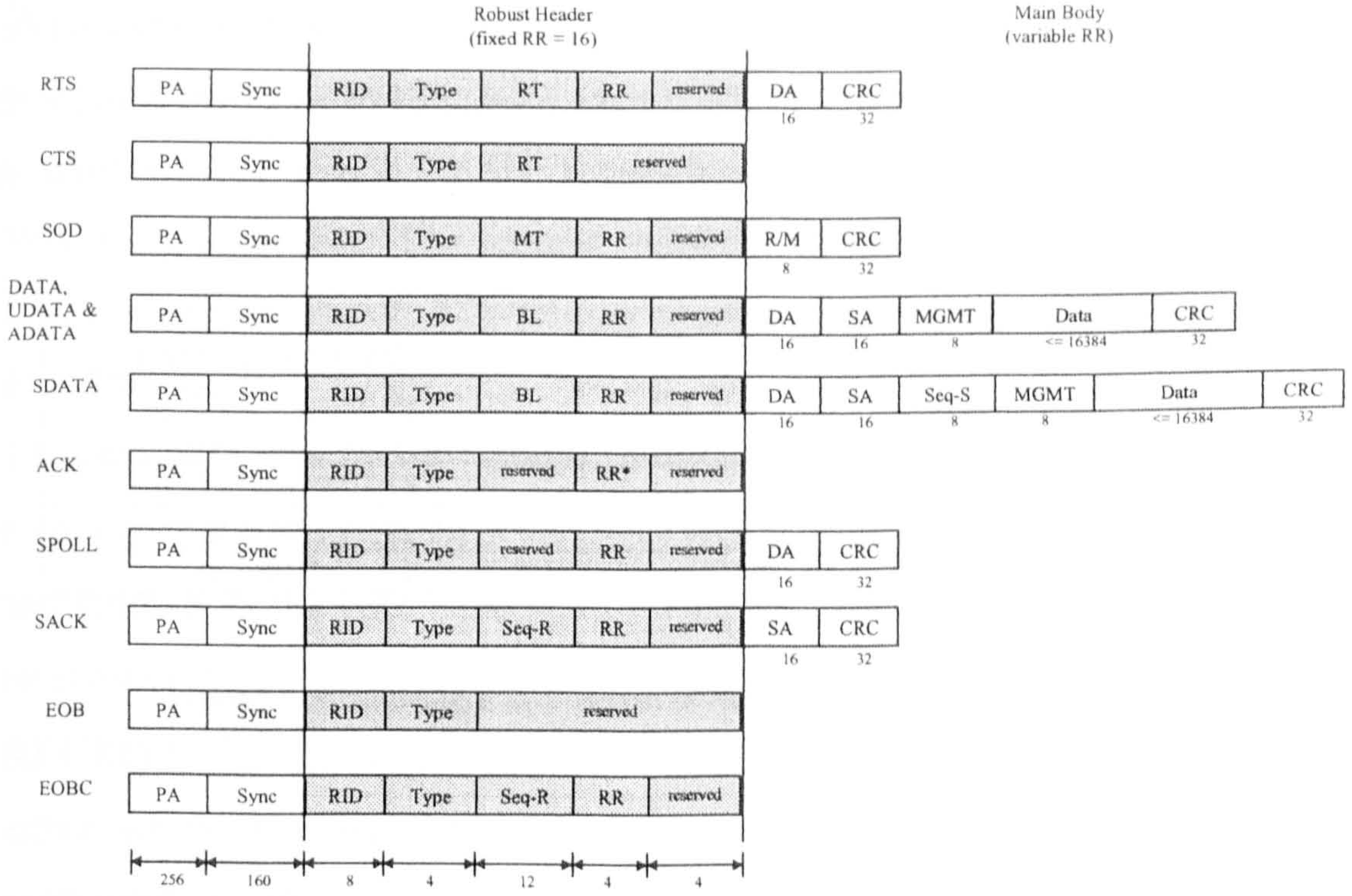

Figure 3.19 Air MAC frame structure

There are 12 frame types specified which are given in Table 3.4.

Type	Description
RTS	Request To Send
CTS	Clear To Send
SOD	Start of Data
EOB	End of Burst
EOBC	End of Burst Confirm
DATA	Reserved Data
ADATA	Acknowledged Reserved Data
SDATA	Sequenced Reserved Data
UDATA	Unreserved Data
ACK	Acknowledgement
SACK	Sequenced Acknowledgement
SPOLL	Sequenced Poll

Table 3.4 Air MAC frame types

The RTS, CTS, DATA, EOB and EOBC frames are used in reserved mode data transfer. ACK frames are used where an acknowledgement is required for each transmitted data frame. SDATA frames are used for sequencing data frames with SACK frames used for their acknowledgement. The SPOLL frame can be used to poll the receiving station for a SACK frame after transmitting a certain number of SDATA frames. UDATA frames are used for unreliable data transfer outside of a reservation.
The SOD frame is used to 'announce' the transmission of Non-AIr modulation frames (i.e. IrDA frames) used for coexistence purposes. Table 3.5 gives the AIr frame section lengths and transmission times.

Frame Section	Length (bits)	Transmission Time
Preamble (PA)	256	64 µs
Synchronisation (Sync)	160	40 µs
Robust Header	32	128 µs (RR = 16)
RTS Main Body	48	12 µs (RR = 1)
DATA Main Body	16456 (Data = 16384 bits)	4.1 ms (RR = 1)

Table 3.5 AIr frame section sizes and transmission times

3.2.2.2 AIr MAC Finite State Machine

The Finite State Machine for the AIr MAC process is shown in Figure 3.20. This has 7 states with transition conditions between the states.

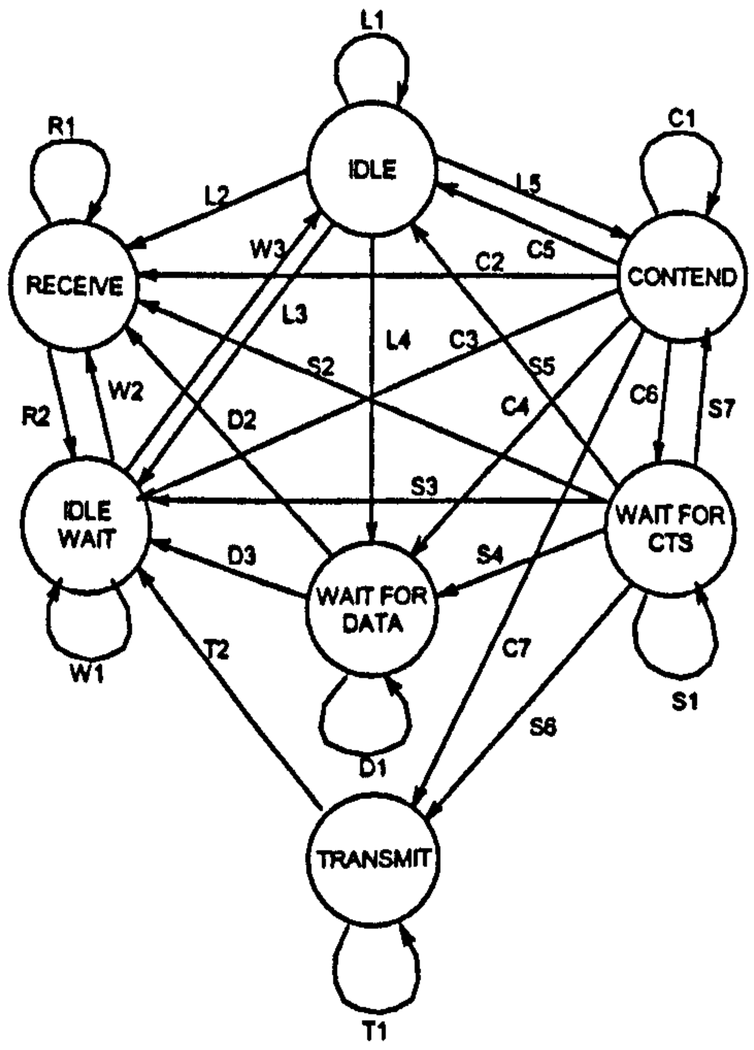

Figure 3.20 AIr MAC finite state diagram

The function of each state is described as follows.

- **IDLE:** The process remains in this state when there is no detected activity on the medium.
- **CONTEND:** The process moves to this state when contending for the medium and remains in this state while waiting for collision avoidance slots to expire.
- **WAIT FOR CTS:** The process moves to this state after transmitting an RTS frame and remains in the state while waiting for a CTS reply or for the Wait-for-CTS timer to expire.
- **WAIT FOR DATA:** The process moves to this state having transmitted a CTS frame in response to an RTS frame and remains in the state while waiting for the first data packet or for the Wait-for-Data timer to expire.
- **TRANSMIT:** The process moves to this state having received a CTS frame in response to transmitting an RTS frame and after transmitting the first data frame, and remains in the state while transmitting further data to the target station in the reservation.
- **RECEIVE:** The process moves to this state after receiving the first data frame either when receiving data in a reservation or when 'standing by' as a non-participant in a reservation.
- **IDLE WAIT:** This acts as a synchronisation state by all stations upon termination of a reservation before returning to the IDLE state

3.2.2.3 Alr MAC Reserved Mode Data Transfer

The basic process for sending **Reserved** data can be summarised as follows. When reserving the medium for data transmission, three main station roles are assigned. The *Requestor* is the initiator of the reservation who transmits data to the *Target* station. Any other station in the network is a *Non-participant*. When in the IDLE state, if a station 'hears' an RTS/CTS exchange from another station pair, the station will move to the RECEIVE state to wait for the media to become free again. Any request for data transmission from the upper layer should be queued until the media is free. Upon receiving a request from the upper LM layer to reserve the medium for data transmission, the requestor station moves to the CONTEND state and waits a number of

Collision Avoidance (CA) time slots before transmitting an RTS frame addressed to the target station. The number of Collision Avoidance Slots (CAS) used is chosen by the LM layer and sent with a set of CAS values as part of the reservation request. If the start of a frame from any other contending station is received before the collision avoidance timer has expired, the timer is paused and resumed (from the beginning of the next time slot) when the medium becomes free again. Having transmitted the RTS frame, the station starts the Wait-For-CTS (WF-CTS) timer moves to the WAIT-FOR-CTS state and waits for a CTS reply from the target station. If the CTS frame is not received before expiration of the WF-CTS timer (if a frame collision has occurred or the device has become unavailable, for example) a new CAS value is chosen and the collision avoidance timer is started again. If the reservation attempt fails for a number of successive tries, a failure is returned to the upper LM layer.

Once the medium has been successfully reserved a burst of data packets can be transmitted. The number must be such that the maximum reservation time of 500ms is not exceeded. After the first data frame has been transmitted, the requestor moves to the XMIT state to continue transmitting data. Following the final data frame an EOB (End Of Burst) frame is transmitted. Upon receiving an RTS frame, the target station replies with a CTS frame, starts the Wait-For-DATA (WF-DATA) timer and moves to the WAIT-FOR-DATA state to wait for the first data packet. On receiving a CTS frame, non-participating stations start the Wait-For-DATA-Non-participating (WF-DATAN) timer. When the first data packet has been received both the target and non-participating stations move to the RECV state. Received data packets are ignored by the non-participating station but are passed to the upper LM layer by the target station. On sending an EOB frame, the requestor station starts the EXIT1 timer and moves to the IDLE-WAIT state to synchronise with other stations before returning to the IDLE state. On receiving the EOB the target station replies with an EOBC frame, starts the EXIT2 timer and moves to the IDLE-WAIT state. A reservation time (RT) timer (duration specified by the LM data request) is also used to terminate the reservation if an EOB frame is not received within an acceptable period. A Turn-Around (TA) delay is also implemented at each station when moving from a transmission mode to a receiving

mode to cover receiver latency. Default timer durations for the AIr MAC process are given in Table 3.6.

Timer	Description	Duration
CA Slot	Single Collision Avoidance slot time	800 μs
Guard Timer	Overlapping reservations detected	400 μs
TA Timer	Receive / Transmit turn-around delay to cover receiver latency	200 μs
WF-CTS	Time-out duration for CTS reply	556 μs
WF-DATA	Time-out duration for first data frame (Target station)	632 μs
WF-DATAN	Time-out duration for first data frame (Non-participant station)	864 μs
EXIT1	Requestor station end-of-reservation synchronisation delay	632 μs
EXIT2	Target / Non-participant station end-of-reservation synchronisation delay	200 μs

Table 3.6 AIr MAC default timer durations

The reserved mode data transfer is illustrated in Figure 3.21. The other contending station here pauses the CA timer on receiving the start of a valid RTS frame. The CA timer is resumed on receiving a valid EOBC frame and expiration of the EXIT2 timer to synchronise beginning of contention with other stations

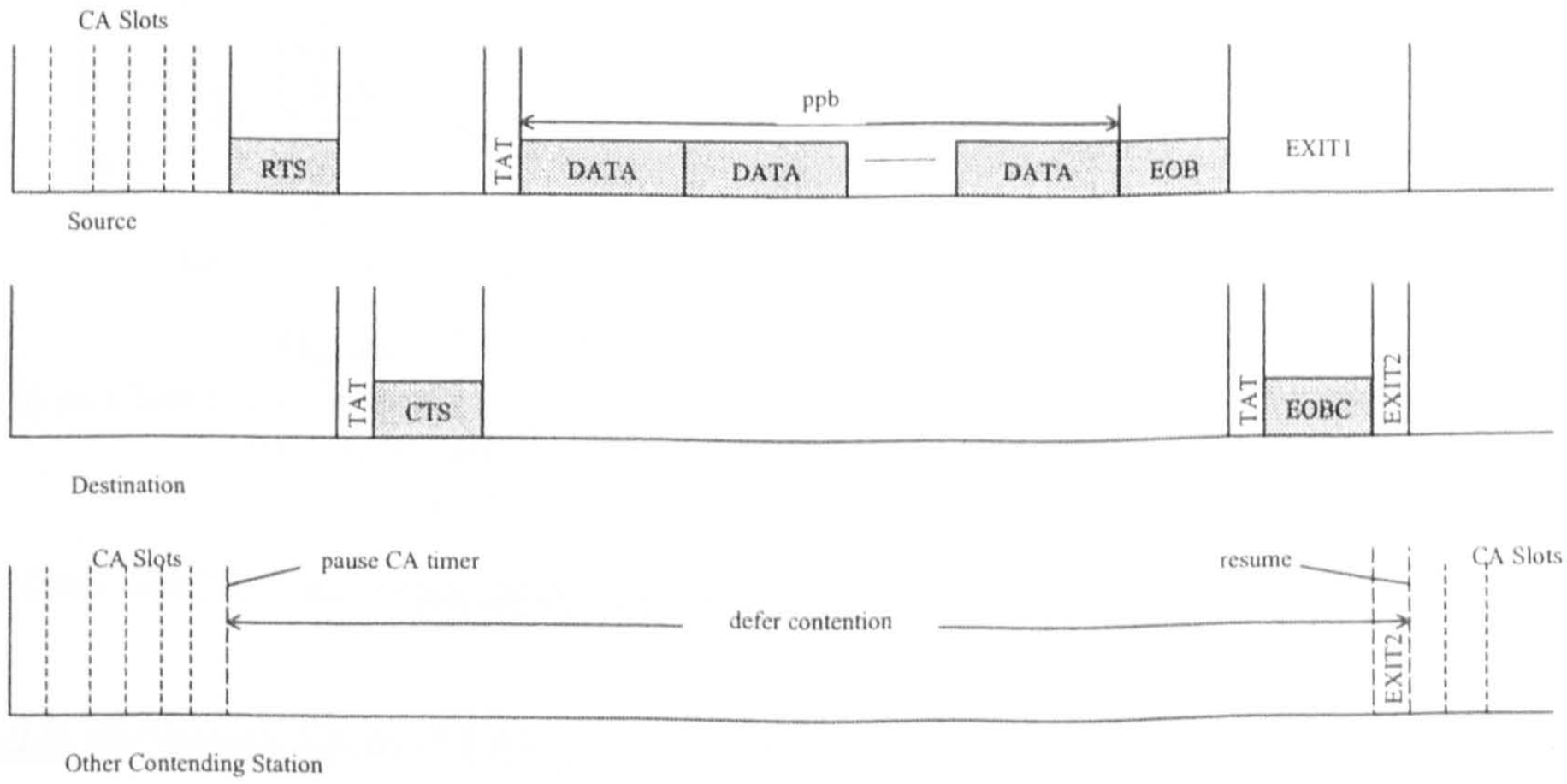

Figure 3.21 AIr MAC reserved mode data transfer process

The RTS/CTS exchange involved in establishing the reservation effectively deals with the 'hidden node' problem. A hidden node *C* is one which is out of range of a transmitting station *A* but which is within range of a receiving station *B*. By using the RTS/CTS exchange the station *C* will not receive the RTS transmission from station *A* but will receive the CTS reply from station *B* (Figure 3.22). As the CTS reply also contains the requested reservation time, station *C* will know to defer any transmission until the reservation time has completed or the EOBC reply from station *B* is received. The CA slot time employed, specified as 800 μs, is chosen to deal with hidden nodes as it is long enough to cover an RTS transmission, a turn-around delay and the beginning (PA + SYNC) of a CTS reply. If the RTS initiator is hidden from a receiving station, it can still receive start of the CTS reply and pause its own CA timer before possible transmission in the next slot. The slot time is thus constrained by:

$$T_{slot} > T_{RTS} + T_{ta} + T_{PA} + T_{SYNC}$$

$$= 424^{*}\ \mu s + 200\ \mu s + 64\ \mu s + 40\ \mu s = 728\ \mu s$$

* using the maximum 16 RR for the RTS main body.

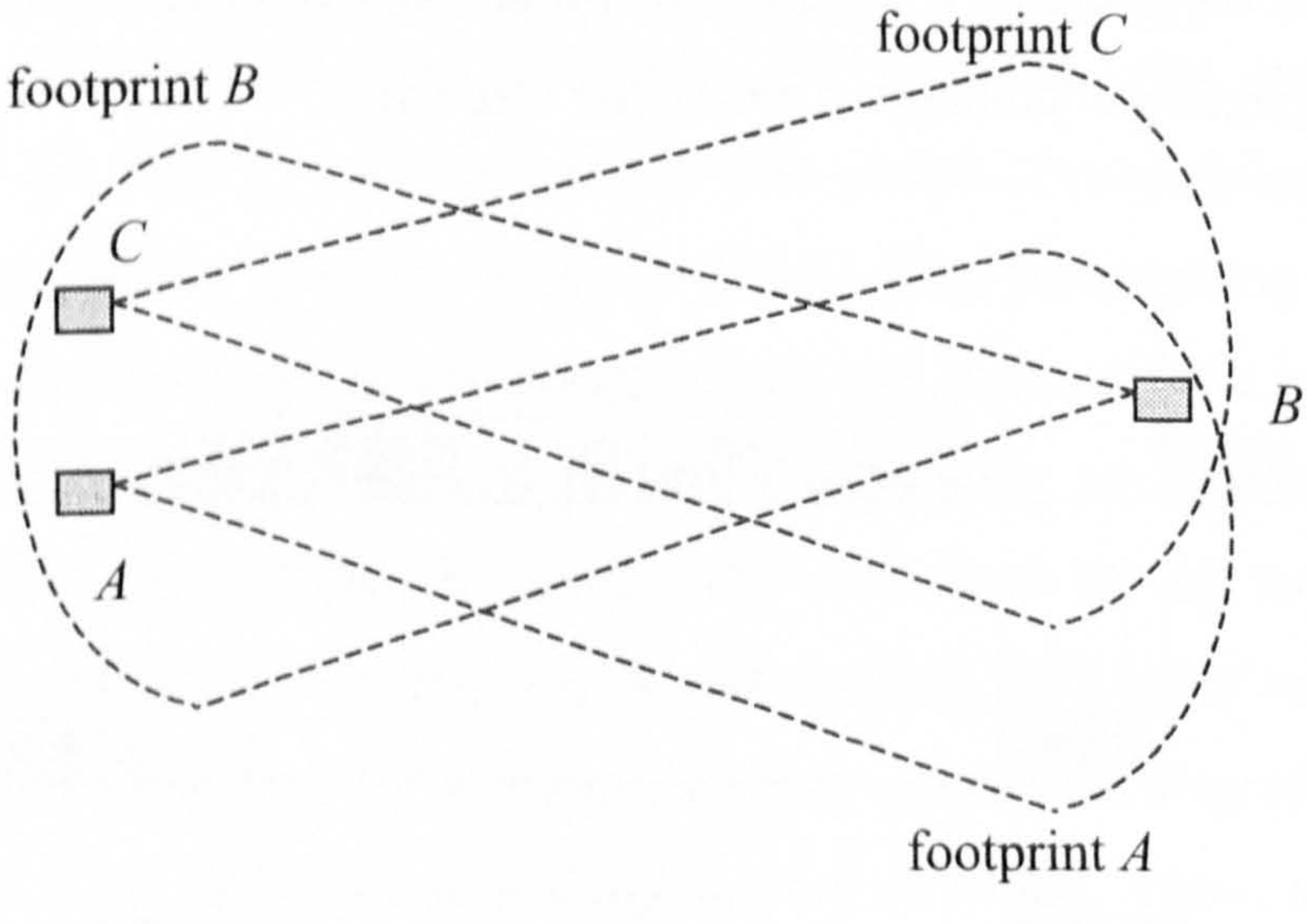

Figure 3.22 The hidden node problem

It is also possible to transmit in Reserved mode using acknowledgements. In this case ADATA (Acknowledgement DATA) frames are transmitted and each frame must be acknowledged with an ACK frame returned from the destination station (Figure 3.23 b). If the ACK is not returned within an acceptable period, determined by the WFACK

(Wait For ACK) timer the reservation is terminated by sending an EOB frame. Sequenced data can also be transmitted using SDATA (Sequenced DATA) frames. These contain sequence numbers contained in the Seq-S field. The frames are acknowledged by the returned EOBC frame from the destination station with a received sequenced number in the Seq-R field. As with the IrLAP protocol the receive sequenced number indicates the next expected send sequence number (Figure 3.23 c). Another method of data transfer in the reserved mode is sequenced polling for reliable multicast. With this, a sequence of SDATA frames is transmitted with a multicast address (i.e. the frames are received by all stations). The station then polls each station in turn using the SPOLL (Sequenced Poll) frame and waits for each station to return a sequenced acknowledgement (SACK) frame that acknowledges the received sequence frames (Figure 3.23 d). The transmitting of sequenced frames allows a certain level of reliable data transmission at the MAC layer but the exact process for error recovery is not fully developed in the specification.

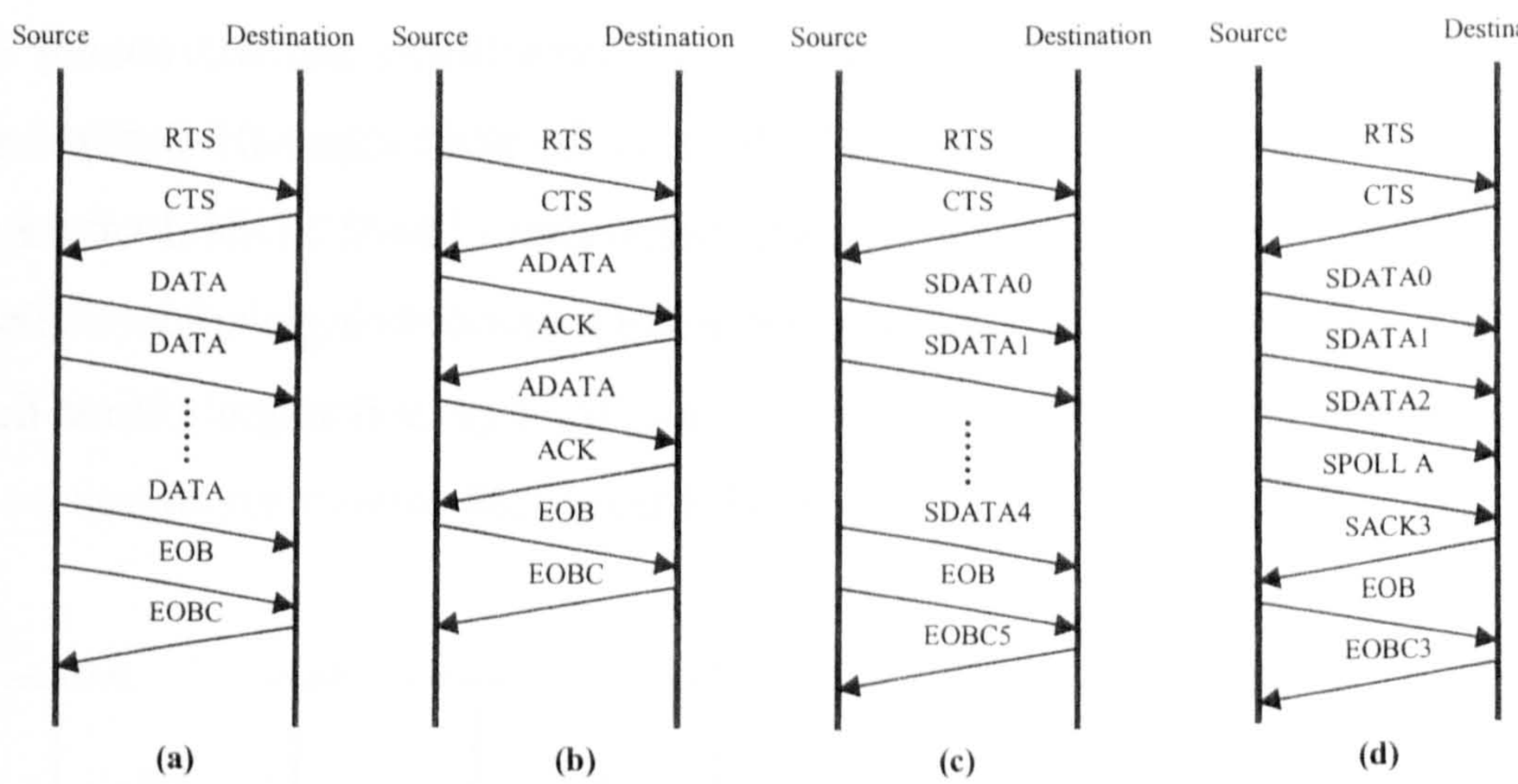

Figure 3.23 AIr MAC reserved mode transfer methods
(a) standard reserved data transfer (b) reserved data transfer with acknowledgement (c) reserved sequenced data transfer (d) reserved reliable multicast data transfer

3.2.2.4 AIr MAC Unreserved, Announced and Proxy Modes

The AIr MAC can also operate in **Unreserved** mode. Here the station will still carry out carrier sensing and collision avoidance procedures as before but when contention is won will transmit a single UDATA frame with no acknowledgement from the receiver. If a packet collision occurs due to two or more stations choosing the same time slot, it will

be the responsibility of upper protocol layers to instigate error recovery. This is obviously a more unreliable method of data transfer than using the RTS/CTS media reservation. It should also be noted that as there is no acknowledgement of a transmitted UDATA packet and it is therefore not possible for the transmitting station to determine if a collision has occurred (Figure 3.24 a).

Other possible modes of operation for the AIr MAC are the Announced and Proxy modes. With the **Announced** mode, an RTS frame is transmitted prior to transmitting a burst of data packets which is terminated by transmitting an EOB frame. However there is no acknowledgement (CTS or EOBC) from the receiving station. This provides less of an overhead than the full reserved mode but is less reliable as there is no confirmation of the receipt of data and the hidden node problem is not addressed (Figure 3.24 c).

The **Proxy** mode is used to transmit data using non-AIr modulation. This is used to support coexistence with other IR Wireless modulation schemes and is primarily aimed at supporting AIr - IrDA interaction. In both cases the SOD (Start Of Data) frame is used to initiate transfer of the non-AIr modulation data. The R/M field of the SOD frame is used to indicate the modulation scheme and data rate being employed. The MT (Modulation time) field in the SOD header indicates the expected length of time that the indicated modulation scheme will be employed (Figure 3.24 d).

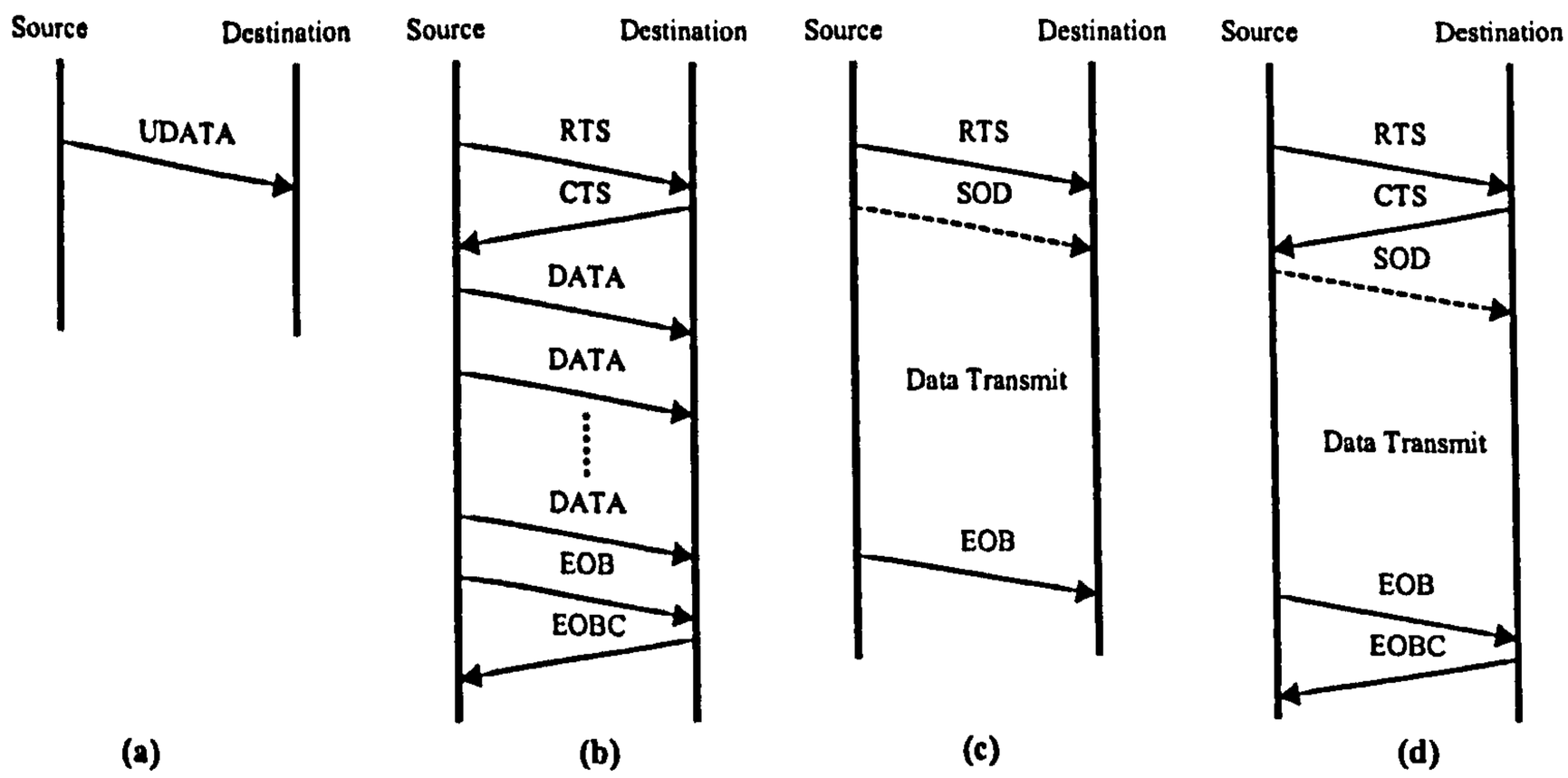

Figure 3.24 AIr MAC data transfer modes.
(a) Unreserved, (b) Reserved, (c) Announced, (d) Proxy.

3.2.3 The AIr LM Layer

The AIr LM (Link Management) layer is the upper layer client for the AIr MAC. The LM provides multiplexing for different LC (Link Control) clients in addition to providing support for GroupWare services, reliable, unreliable and priority data delivery, coexistence services (with the IrDA protocol) and adaptive data rates. In requesting a reservation from the AIr MAC it is the responsibility of the LM to define the set of CAS (Collision Avoidance Slot) values to be used by the MAC. The values are sent to the MAC as a CAS vector where the index is the current reservation retry-count. The CAS values are chosen randomly from a range of possible values called the 'CAS window' (i.e. from 0 to *W*-1) which becomes a input parameter to the system. A minimum CAS window value of 8 slots is specified. It can be seen that the larger the CAS window the less likely that 2 or more stations will choose the same CAS value and cause an RTS collision. However a large CAS value will cause an excessive time overhead in reserving the medium. Therefore a linear CAS back-off algorithm is provided in the specification in which the CAS window size is increased (with an upper limit) for the next retry following a failed reservation attempt, and decreased (with a lower limit) following a successful reservation (Figure 3.25). The specification advises an minimum CAS window increment of 4 slots, and a maximum CAS window decrement of 4 slots with a lower CAS limit of 8 slots and an upper CAS limit of 256 slots. This is illustrated in figure 3.25 where *a* is the CAS window increase adjustment for a successful reservation and *b* is the CAS window decrease for a reservation failure.

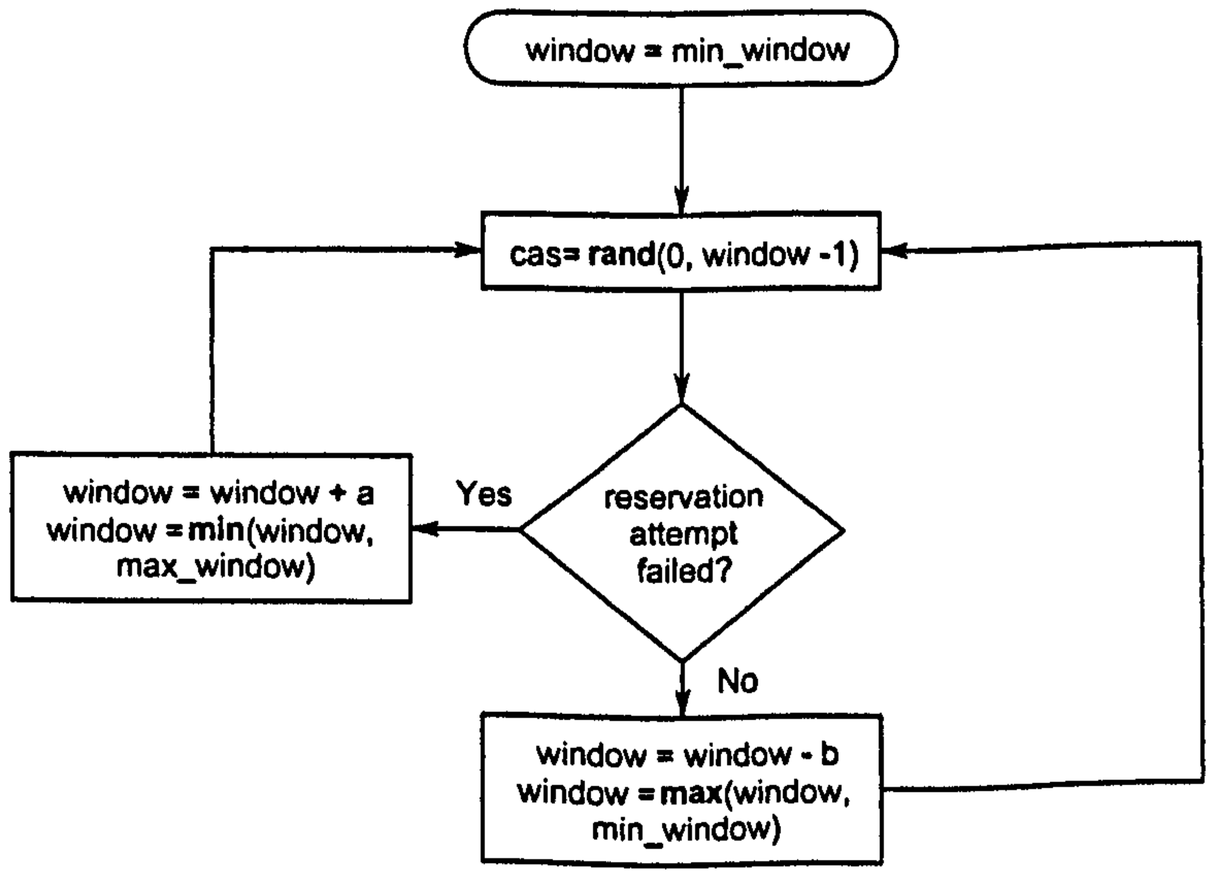

Figure 3.25 AIr LM CAS back-off process

The LM is also responsible for supplying other reservation parameters to the MAC layer such as the Repetition Rate (RR) to be used, the required reservation time, and the retry limit (IrDA, 1999c).

3.2.4 The AIr LC Layer

The AIr LC (Link Control) layer is a HDLC based data link protocol. As such it can be seen as replacement for the reliable data delivery functions of the IrLAP protocol. However the AIr LC protocol uses balanced stations (i.e. there are no primary / secondary roles) and as such is based on HDLC ABM (Asynchronous Balanced Mode) as opposed to the NRM based IrLAP protocol. However the error recovery procedure uses Ns and Ns sequence fields and operates in the same manner as described for the IrLAP protocol. The specification for the LC protocol is currently in a draft state and the exact method of interaction with the lower protocols is not yet fully developed (IrDA, 1999b).

3.3 Chapter Summary

This chapter has described in detail the two IR wireless protocol standards whose performance is investigated in this thesis. The IrDA 1.x protocol is described with emphasis on the IR PHY layer, and the IrLAP data link layer information exchange procedure. The functions of the upper layer in the protocol set and the proposed high speed (16 Mbits/s) extension are also summarised. The Advanced Infrared (AIr) protocol which is a development of the IrDA protocol to provide a multiple access IR 'network' is described with emphasis on the AIr PHY layer and AIr MAC layer. The following chapter provides and analytical model of the IR wireless physical layer relating bit-error-rate (BER) to transceiver characteristics, link geometry and noise source levels. Third user interference and resulting asymmetry effects are also examined.

4. PHYSICAL LAYER ANALYSIS

This chapter examines physical layer properties of IR wireless links to highlight the critical physical layer factors affecting performance and provides expressions for the bit-error-rate (BER) and packet error probabilities of links. The BER at the receiver is derived from the receiver electrical signal-to-noise ratio (SNR) and the line encoding and detection scheme employed. The SNR is dependent on the transceiver characteristics, link geometry and receiver noise levels. The effects of third user interference and resultant link asymmetry are also examined.

4.1 IR Channel Model

We assume in this model a directed LOS link with no multipath propagation. The characteristics of non-directed channels have been modelled elsewhere (Barry et al., 1991b; Carruthers and Kahn, 1997; Florez et al., 1997; Jungnickel et al., 2002; Samaras et al., 1998). Other assumptions are made during the course of the analysis. We assume that an IR wireless link employing an LED transmitter and PIN photodiode receiver uses intensity modulation with direct detection (IM/DD). Figure 4.1 shows the IR wireless IM/DD transmission and reception model. The LED output power P_T (Watts) is modulated by the signal waveform $u(t)$ giving the transmitted signal $X(t)$. This is convoluted with the channel impulse response $h(t)$ and the receiver responsivity R (Amps / Watts) and is added to the receiver noise signal $N(t)$ to produce the output photocurrent signal $Y(t)$.

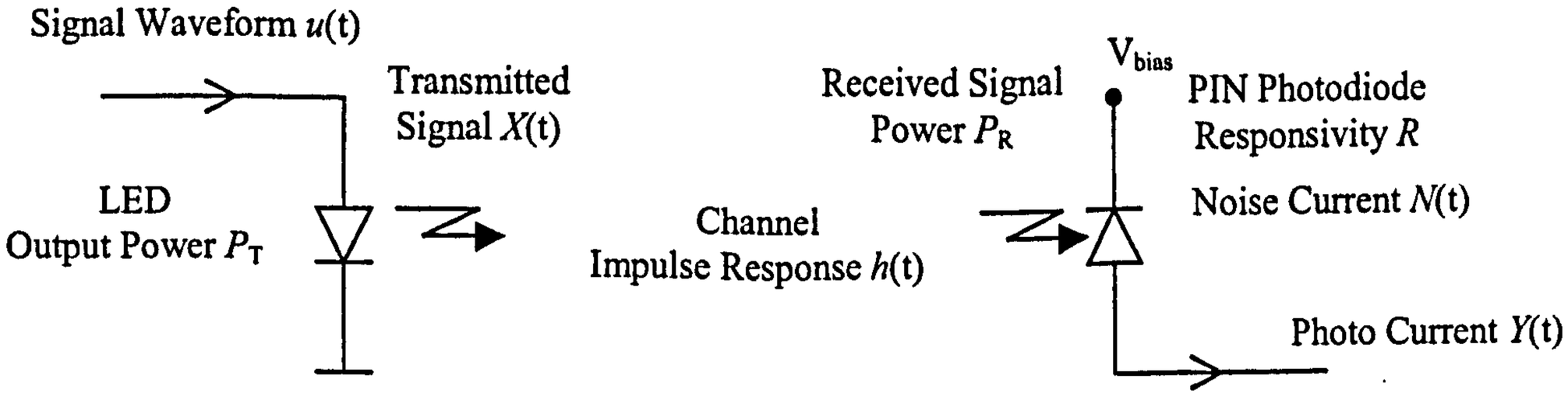

Figure 4.1 IM/DD transmission and reception model

The channel model can be represented by the schematic in Figure 4.2.

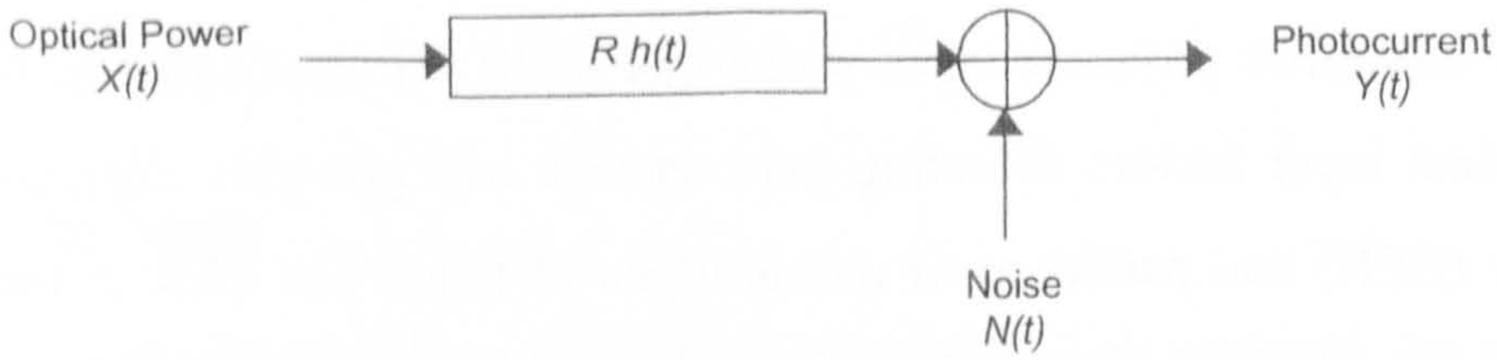

Figure 4.2 IR Wireless channel model

Thus the system output photocurrent $Y(t)$ can be given by:

$$Y(t) = RX(t) \otimes h(t) + N(t) \tag{4.1}$$

where $\otimes$ denotes 'convolution' and $X(t) = P_T u(t)$.

The frequency response $H(f)$ of the channel can be given by the Fourier transform of the channel impulse response $h(t)$.

$$H(f) = \int_{-\infty}^{\infty} h(t) e^{-i2\pi ft} dt \tag{4.2}$$

The received optical power P_R is determined from the channel dc response $H(0)$ by:

$$P_R = H(0) P_T \tag{4.3}$$

The electrical peak signal-to-noise ratio (SNR) is then given by:

$$SNR = \frac{(P_R R)^2}{N_o B} = \frac{(RH(0)P_T)^2}{N_0 B} \tag{4.4}$$

where N_0 is the double-sided noise power spectral density (A^2/Hz), assuming an independent white Gaussian dominated noise signal $N(t)$, and B is the receiver electrical bandwidth (Hz).

4.1.1 Transmitted Optical Power

Power output from an LED emitter can either be specified as total output power in Watts (W) or specified as *Radiant Intensity* (within an angular range) in Watts per Steradian (W/Sr). The Steradian is the unit of solid angle defined as the angle ω subtended from the centre of a sphere of radius **R** to a sphere surface element of area $\mathbf{A} = \mathbf{R}^2$ (Figure 4.3).

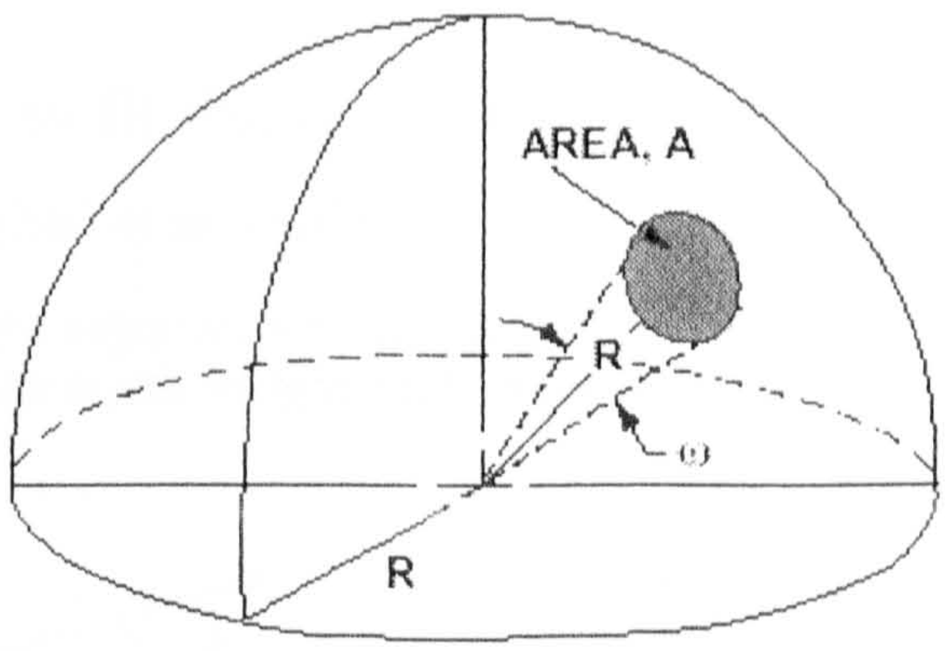

Figure 4.3 Solid angle geometry

The radiant intensity $I(\theta, \phi)$, where θ is the azimuth ($-\pi/2$ to $\pi/2$) angle and ϕ is the polar angle (0 to 2π), is given by:

$$I(\theta,\phi) = \frac{dP_T}{d\omega} \tag{4.5}$$

where the total output power P_T is given by the integral of the radiant intensity over all angles.

$$P_T = \int_{-\pi/2}^{\pi/2} \int_{0}^{2\pi} I(\theta,\phi) d\theta d\phi \tag{4.6}$$

Typical LEDs have a symmetrical iradiance about the optical axis. Therefore we can simplify the model to plane geometry and consider $I(\theta)$ only.

Modelling the LED using the general Lambert cosine law (Gfeller and Bapst, 1979) gives:

$$I_n(\theta) = \begin{cases} I_0 \cos^n \theta & -\pi/2 \le \theta \le \pi/2 \\ 0 & \pi/2 < \theta < -\pi/2 \end{cases} \tag{4.7}$$

where I_0 is the axial radiant intensity (at $\theta = 0$) given by:

$$I_0 = \frac{(n+1)}{2\pi} P_T \tag{4.8}$$

and n is the *mode index* of the radiation lobe. The higher the n value, the 'narrower' the radiation lobe becomes (Figure 4.4).

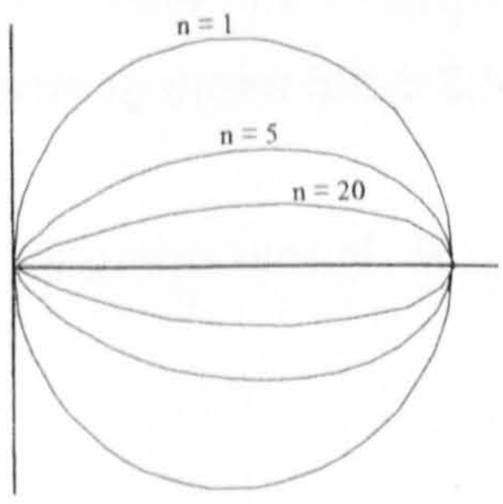

Figure 4.4 Radiant intensity pattern for increasing n

The extent of the 'narrowness' of the radiation beam can also be indicated by the half-power angle, which is the angle at which the beam intensity drops to half the maximum intensity, given by:

$$\theta_{0.5} = \cos^{-1}(0.5^{1/n}) \tag{4.9}$$

Table 4.1 shows the required mode index values for typical IR LED half-power angles.

Half Power Angle (degrees)	Mode Index – n
60	1
30	5
15	20

Table 4.1 Mode index values for typical LEDs

4.1.2 Received Optical Power

The optical geometry of an IR link is shown in Figure 4.5, where the transmitter of radiant intensity $I(\theta)$, aligned at an angle θ_T, and the receiver of effective detection area A_{eff}, aligned at angle θ_R, are separated by a distance d.

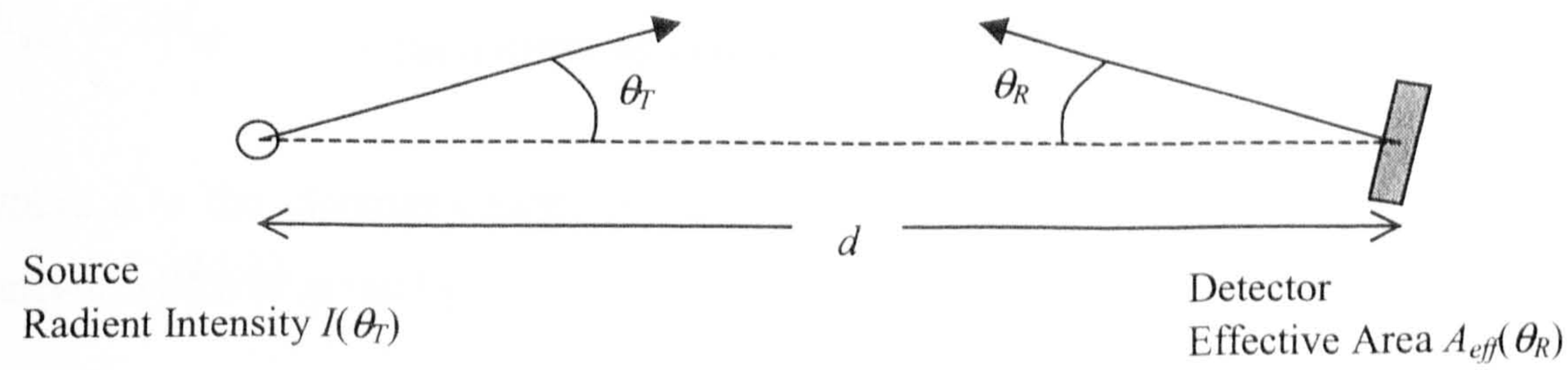

Figure 4.5 Optical link geometry

Using the inverse square law of radiation, the received optical power P_R, assuming isotropic radiation ($n = 1$), is given by:

$$P_R = \frac{I(\theta_T) A_{eff}(\theta_R)}{d^2} \tag{4.10}$$

It is assumed that any optical filter fitted has 100% transmittance at the signal wavelength. For a bare (i.e. unlensed) detector of area A, the effective area is given by the cosine of the incident angle.

$$A_{eff}{}^{bare}(\theta_R) = A\cos(\theta_R) \tag{4.11}$$

The same generalised Lambert cosine law can be applied to a detector if a lens is applied to determine the field-of-view (FOV). Therefore the effective area, where m is the mode index for the receiver lens, given by:

$$A_{eff}^{lensed}(\theta_R) = A\cos^m(\theta_R) \tag{4.12}$$

The received optical power is therefore:

$$P_R = \frac{I(\theta_T)A\cos^m(\theta_R)}{d^2} \tag{4.13}$$

4.1.3 Signal-to-Noise Ratio

The electrical signal-to-noise ratio (SNR) can therefore be written as:

$$SNR = \frac{\left[I_0 AR\cos^n(\theta_T)\cos^m(\theta_R)\right]^2}{d^4 N_0 B} \tag{4.14}$$

This provides the electrical peak signal-to-noise ratio in terms of the transceiver characteristics and link geometry. Analysis of the dominant noise sources can provide an expression for the noise power spectral density N_0.

4.2 Modelling Noise Sources

Unlike fibre optic links, the IR wireless receiver is exposed to ambient background light and interference from other transmitting IR devices. These sources decrease the signal to noise ratio and thus increase the bit-error-rate of the link. In the absence of any external interfering signal, the noise in an optical receiver is dominated by two sources: detector 'shot noise' and preamplifier 'thermal noise'. Shot noise is defined as the random fluctuation of the photodetector current about its mean value caused by the statistical nature of the quantum photon detection process. Shot noise is therefore a white Gaussian noise with a peak level proportional to that of the photodetector current,

and therefore to the level of the incident optical power. Shot noise is produced as a result of both the optical signal and the background ambient light but is normally dominated by the from ambient light. Thermal noise is caused by the thermal agitation of electrons in the carrier. This can also be considered as a white Gaussian noise. The total double-sided power spectral density N_0 is therefore given by:

$$N_0 = N_{shot} + N_{thermal} \tag{4.15}$$

4.2.1 Ambient Light Induced Shot Noise

From Gaussian statistics, the double-sided power spectral density N_{shot} (A^2/Hz) for shot noise is given by

$$N_{shot} = 2qI_{dc} \tag{4.16}$$

where q is the electron charge (~ 1.6 x 10^{-19} C) and I_{dc} is the total photodetector dc current which is given by:

$$I_{dc} = R(P_R + P_B) \tag{4.17}$$

where P_R is the average received optical power from the IR signal and P_B is the received background ambient light optical power. If we assume that the ambient light power is much greater than the signal power ($P_B >> P_R$), then the dc current can be given by:

$$I_{dc} = RP_B = RAE_B \tag{4.18}$$

where A is the receiver area and E_B is the background ambient *iradiance* (W/m^2). This assumes that the ambient light power is constant. This is the case with natural sunlight (direct and indirect). For artificial light, possible interference from modulation of the source (e.g. from electronic ballast or the AC mains frequency) may need to be taken into consideration (Moreira et al., 1996). The spatial distribution of ambient light is assumed to be uniform although this may often not be true for real environments

(Bakalidis et al., 1996). Typical sources of ambient light in an office or home environment are:

- Direct sunlight
- Indirect sunlight
- Incandescent lamps (i.e. filament bulbs)
- Halogen lamps
- Fluorescent light with conventional ballast (CB)
- Fluorescent light with electronic ballast (EB)

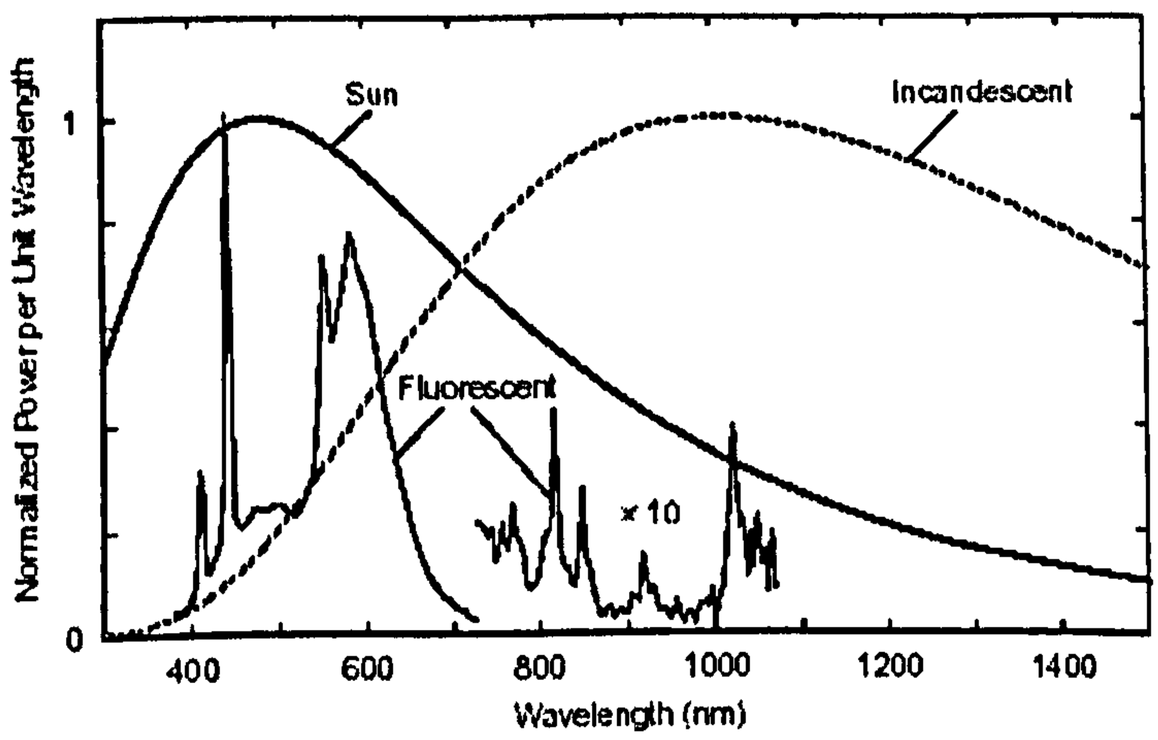

Figure 4.6 Normalised power spectra for ambient light sources
(after Kahn & Barry, 1997)

Figure 4.6 shows normalised power spectra of typical ambient light sources. It should be noted that the powers are normalised so that each has the same maximum power. In reality, sunlight power will greatly exceed other sources. Low cost silicon photodiodes have a maximum response in the 800 to 900 nm range (see Figure 2.2). It can be seen from Figure 4.6 that incandescent lamps have a peak presence in this region. Experimental ambient iradiance values for different light sources including sunlight, incandescent lamps, and florescent lighting both with and without optical filters, are provided by Moreira (1997). The values vary from 10 mW/cm^2 for direct sunlight, to 4.3 $\mu W/cm^2$ for a 13 W fluorescent lamp with conventional ballast. The IrDA test guidelines specify a background iradiance no greater than 490 $\mu W/cm^2$ for correct operation of links.

4.2.2 Thermal Noise

In an optical receiver, the photodiode is typically followed by a transimpedance preamplifier which converts the input current into an output voltage. These are used as they provide a wide bandwidth and large dynamic range. Figure 4.7 shows a basic transimpedance preamplifier receiver design.

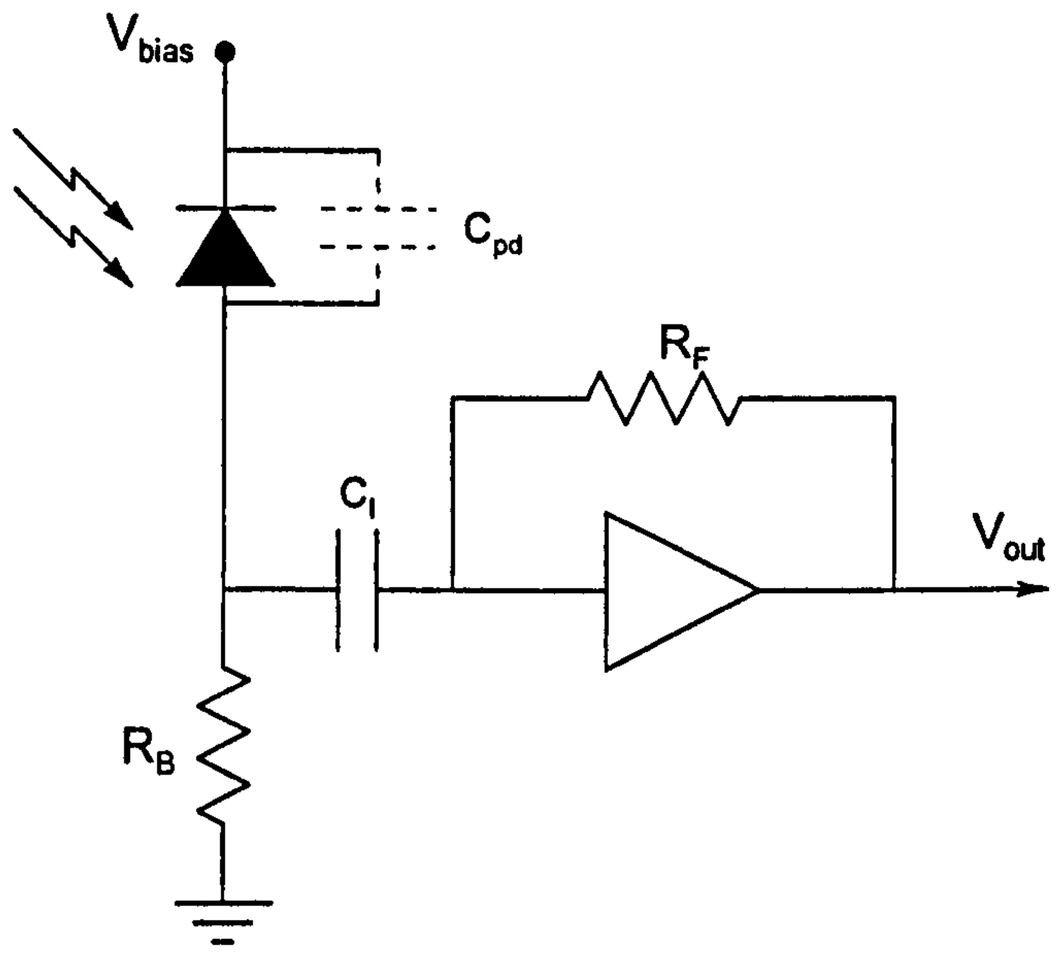

Figure 4.7 Basic transimpedance receiver preamplifier design

The use of a high pass input filter (capacitor C_I) reduces the dc level in the receiver from ambient light (the shot noise is from the white Gaussian random fluctuations about the mean value).

The dominant current in the receiver is that in the feedback resistor R_F. The double-sided power spectral density $N_{thermal}$ (A^2/Hz) for thermal noise is therefore given by:

$$N_{thermal} = \frac{2kT_K}{R_F} \tag{4.19}$$

where k is the Boltzman constant (~1.38 x 10^{-23} J/K), and T_K is the absolute temperature. It can be seen that the noise power is inversely proportional to the feedback resistance

of the amplifier. Thus the noise is easily reduced by increasing the resistance. However this can reduce the bandwidth of the amplifier, given by:

$$B \approx \frac{1+A_g}{R_F C_T} \tag{4.20}$$

where A_g is the amplifier voltage gain, and C_T (= C_{pd} + C_I) is the total input capacitance (Phang and Johns, 1999). The resistance R_F must therefore be set such that the thermal noise is minimised but with sufficient amplifier bandwidth for the intended bit rate. It can be seen that the bandwidth is inversely proportional to the input capacitance. The photodiode capacitance C_{pd} is proportional to the detector area A. This should therefore be minimised while obtaining sufficient optical power to maintain a required SNR. Minimising A also reduces the level of incident ambient light power.

The careful design of IR receivers normally makes thermal noise negligible. The total noise can be assumed to be dominated by that from the ambient light induced shot noise. Therefore the total double sided noise power spectral density N_0 is given by:

$$N_0 = 2qI_{dc} = 2qRAE_B \tag{4.21}$$

The total expression for SNR can then be written as:

$$SNR = \frac{RA\left[I_0 \cos^n(\theta_T)\cos^m(\theta_R)\right]^2}{2d^4 qE_B B} \tag{4.22}$$

This provides the electrical peak signal-to-noise ratio in terms of the transceiver characteristics (transmitter radiant intensity I_0 and lens mode index n, receiver area A, responsivity R, lens mode index m and bandwidth B), link geometry (transmitter alignment θ_T, receiver alignment θ_R and link LOS distance d) and ambient light iradiance E_B.

4.3 BER and Packet Errors

To determine the bit-error-rate (BER) and packet-error-probability from the SNR, we need to make assumptions about the modulation and encoding scheme used and the demodulation and decoding process.

For an on-off-keying non-return-to-zero (OOK NRZ) modulation scheme, considering a threshold voltage v_T, an error will occur when the receiver output voltage $v < v_T$ for a '1' transmitted, or $v > v_T$ for a '0' transmitted (Gagliardi and Sherman, 1995).

The average BER or probability of bit error p_e, assuming and equal probability of a '1' and '0' bit being in error is thus given by:

$$p_e = \frac{1}{2}\Pr[v < v_T \mid 1] + \frac{1}{2}\Pr[v > v_T \mid 0] \tag{4.23}$$

This can be written as:

$$p_e = \frac{1}{2}Q\left(\frac{v_1 - v_T}{\sigma_1}\right) + \frac{1}{2}Q\left(\frac{v_T}{\sigma_0}\right) \tag{4.24}$$

where $Q(z)$, is the Gaussian tail integral function (see Appendix C) given by :

$$Q(z) = \frac{1}{\sqrt{2\pi}}\int_z^\infty e^{-y^2/2}dy \tag{4.25}$$

The values σ_0 and σ_1 are the noise variance for a transmitted '0' and '1'. If we assume that the noise power is dominated the ambient light induced shot noise, this gives:

$$\sigma_0 = \sigma_1 = \sqrt{N_0 B} \tag{4.26}$$

The BER is minimised by choosing the threshold v_T to be half the received signal level (i.e. $v_T = v_1/2$). Applying this to equation (4.24) gives

$$p_e = Q\left(\frac{v_1}{2\sqrt{N_0 B}}\right) \tag{4.27}$$

If the voltage v_1 is produced from a signal current RP_R, this provides p_e in relation to the electrical peak SNR of:

$$p_e = Q(\sqrt{SNR}/2) \tag{4.28}$$

The packet capture probability p_{pc} and packet error probability p_{pe} for a data length l bits are then:

$$p_{pc} = (1 - p_e)^l \tag{4.29}$$

$$p_{pe} = 1 - (1 - p_e)^l \tag{4.30}$$

By using an adaptive threshold where the comparator reference input is set to half the maximum received signal voltage level the bit-error-rate can minimised (Ananth et al., 1997; Otte et al., 1999).

4.3.1 Required Bandwidth

The electrical bandwidth B of the receiver needs to be sufficiently large to correctly receive transmitted pulses at the maximum link data rate and encoding scheme employed. However, increasing the bandwidth increases the total noise power (from the dominant 'white' shot noise) and hence reduces the signal-to-noise ratio and so should be no larger than required. An approximate upper limited on the bandwidth is obtained from the inverse of the transmitted pulse duration T_P.

$$B_{req} \approx \frac{1}{T_P} \tag{4.31}$$

However depending on the data rate, modulation or encoding scheme employed and the receiver design, the bandwidth can be made smaller than that calculated and still correctly receive transmitted pulses. The recommended bandwidth can be obtained from the transfer function $G(f)$ of the receiver filter and amplifier circuitry (Hirt et al., 2001).

4.3.2 IrDA SIR RZI Modulation

IrDA links up to 1.152 Mbits/s do not use NRZ modulation but RZI (Return-to-Zero Inverted) modulation with a 3/16 bit period pulse width for up to 115.2 kbits/s and 1/4 bit period pulse width for 1.152 Mbits/s. Using a shorter pulse duration reduces the average power requirement for the link. This also insures that a long string of zeros is not lost in the transmission. However this also increases the bandwidth requirement which will increase the noise power level at the receiver. The transmitted pulse is counted for 3 clock cycles (4 for 1/4 RZI) and transmitted in the middle of the bit period. The rising edge of the received pulse (above receiver threshold) triggers the receiver to count 16 clock cycles during which a zero level output is produced. If no following rising edge is detected, a '1' output is produced for a count of 16 clock cycles. This is demonstrated in Figure 4.9 (Agilent, 2000).

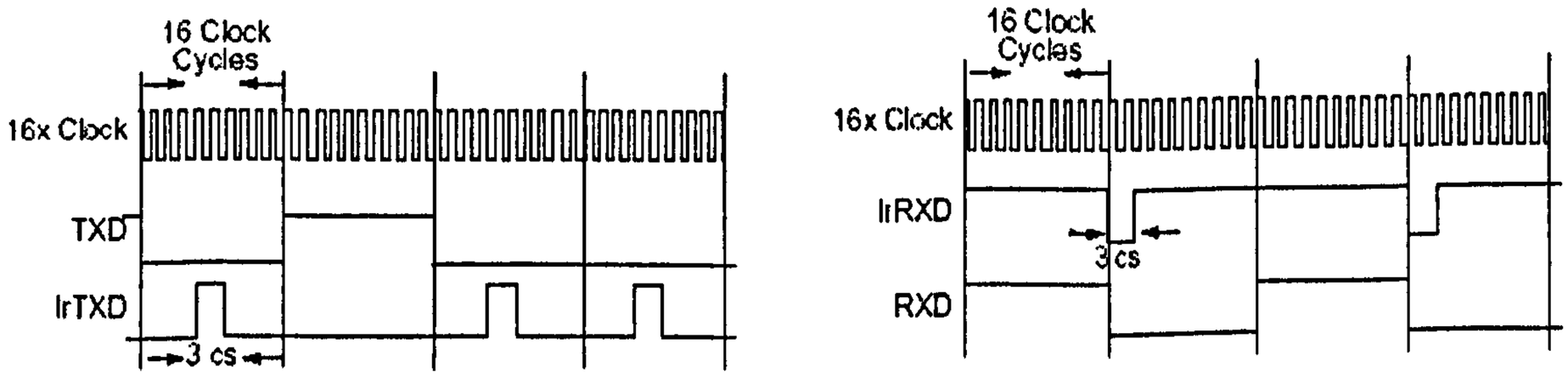

Figure 4.8 IrDA SIR 3/16 RZI transmission and detection

The same BER analysis for NRZ OOK using the peak electrical SNR can be used for RZI. The difference is in the average power requirement P_{req} and bandwidth requirement B_{req}. There are given by (4.33) and (4.34) for 3/16 and 1/4 RZI respectively where R_b is the line data rate (Barry, 1994).

$$P_{e(RZI)} = Q(\sqrt{SNR}/2) \tag{4.32}$$

$$P_{req(3/16RZI)} = \frac{3}{32}P_T \text{ and } P_{req(1/4RZI)} = \frac{1}{8}P_T \tag{4.33}$$

$$B_{req(3/16RZI)} = \frac{16}{3}R_b \text{ and } B_{req(1/4RZI)} = 4R_b \tag{4.34}$$

4.3.3 FIR 4Mbits/s 4PPM Modulation

For PPM modulation, determination of the actual data bit-error-rate is a bit more difficult as for 4PPM, each symbol represents 2 data bits. Therefore it is generally easier to determine the error probability of an individual pulse or 'chip', the chip-error-probability.

$$p_{c1} = Q\left(\frac{v_1 - v_T}{\sqrt{N_0 B}}\right) \tag{4.35}$$

$$p_{c0} = Q\left(\frac{v_T}{\sqrt{N_0 B}}\right) \tag{4.36}$$

Assuming $v_T = v_1/2$, for 4PPM this gives:

$$p_{c1} = p_{c0} = Q(\sqrt{SNR}/2) \tag{4.37}$$

For 4PPM, the symbol capture probability, assuming $p_{c1} = p_{c0} = p_c$, is:

$$p_{sc} = (1 - p_{c1})(1 - p_{c0})^3 = (1 - p_c)^4 \tag{4.38}$$

which gives a packet error probability (for l data bits) of:

$$p_{pe} = 1 - p_{sc}^{\,l/2} = 1 - (1 - p_c)^{2l} \tag{4.39}$$

This provides a derived bit-error-rate p_e of:

$$p_{e(4ppm)} = 1 - \sqrt{p_{sc}} = 1 - (1 - p_c)^2 \tag{4.40}$$

The average power requirement and bandwidth requirement for 4 PPM are given by:

$$P_{req(4ppm)} = \frac{1}{4} P_T \tag{4.41}$$

$$B_{req(4ppm)} = 2R_b \tag{4.42}$$

4.3.4 VFIR 16 Mbits/s Rate 2/3 (1, 13 | 5) RLL HHH Encoding

From the complexity of the rate 2/3 (1, 13 | 5) HHH encoding used for the 16 Mbits/s VFIR physical layer (see section 3.1.1.3), it can be difficult to accurately determine the bit-error-probability. However if we assume an equal error probability for pulse and non pulse slots, again assuming $v_T = v_1/2$, the chip error probability is:

$$p_c = Q(\sqrt{SNR}/2) \tag{4.43}$$

As the coding rate produces 3 chips for every 2 data bits, the packet-error probability can be given as:

$$p_{pe} = 1 - (1 - p_c)^{3l/2} \tag{4.44}$$

providing a derived bit-error-rate

$$p_{e(HHH)} = 1 - (1 - p_c)^{3/2} \tag{4.45}$$

The average duty cycle for HHH encoding is given by Hirt et. al. (Hirt et al., 2001) as 0.258, giving an average power requirement of:

$$P_{req(HHH)} = (0.258)P_T \tag{4.46}$$

The required bandwidth for the 3/2 rate encoding is:

$$B_{req(HHH)} = \frac{3}{2}R_b \tag{4.47}$$

Table 4.2 provides the BER expressions, power requirements, calculated bandwidth and recommended bandwidth for IrDA 1.x data rates and modulation / encoding schemes.

Data Rate Range	Modulation / Encoding	Average Power Requirement	BER	Calculated Bandwidth	Recommended Bandwidth
9600 – 115,200 bits/s	3/16 RZI	(3/32) P_T	$Q(\sqrt{SNR}/2)$	615 KHz	250 KHz
0.576 & 1.152 Mbits/s	1/4 RZI	(1/8) P_T	$Q(\sqrt{SNR}/2)$	4.6 MHz	2.48 MHz
4 Mbit/s	4 PPM	(1/4) P_T	$1-(1-Q(\sqrt{SNR}/2))^2$	8 MHz	6.1 MHz
16 Mbit/s	HHH	(0.258) P_T	$1-(1-Q(\sqrt{SNR}/2))^{3/2}$	24 MHz	14.5 MHz

Table 4.2 BER expressions power requirements and bandwidth requirements for IrDA modulation / encoding schemes

Figure 4.10 shows BER versus SNR (electrical – dB) for RZI, 4PPM and HHH modulation schemes. It can be seen that performance depends on the coding efficiency of the modulation code with RZI having an efficiency of 1, 4PPM an efficiency of ½ and HHH an efficiency of 2/3. It is seen that an SNR of around 21 dB is required to achieve the minimum specified BER of 10^{-8} over 1m. Figure 4.11 shows packet capture probability, from (4.29), for l = 2 Kbytes (16384 bits) versus SNR. It can be seen that there is an effective zero probability of packet capture below an SNR of 16.5 dB.

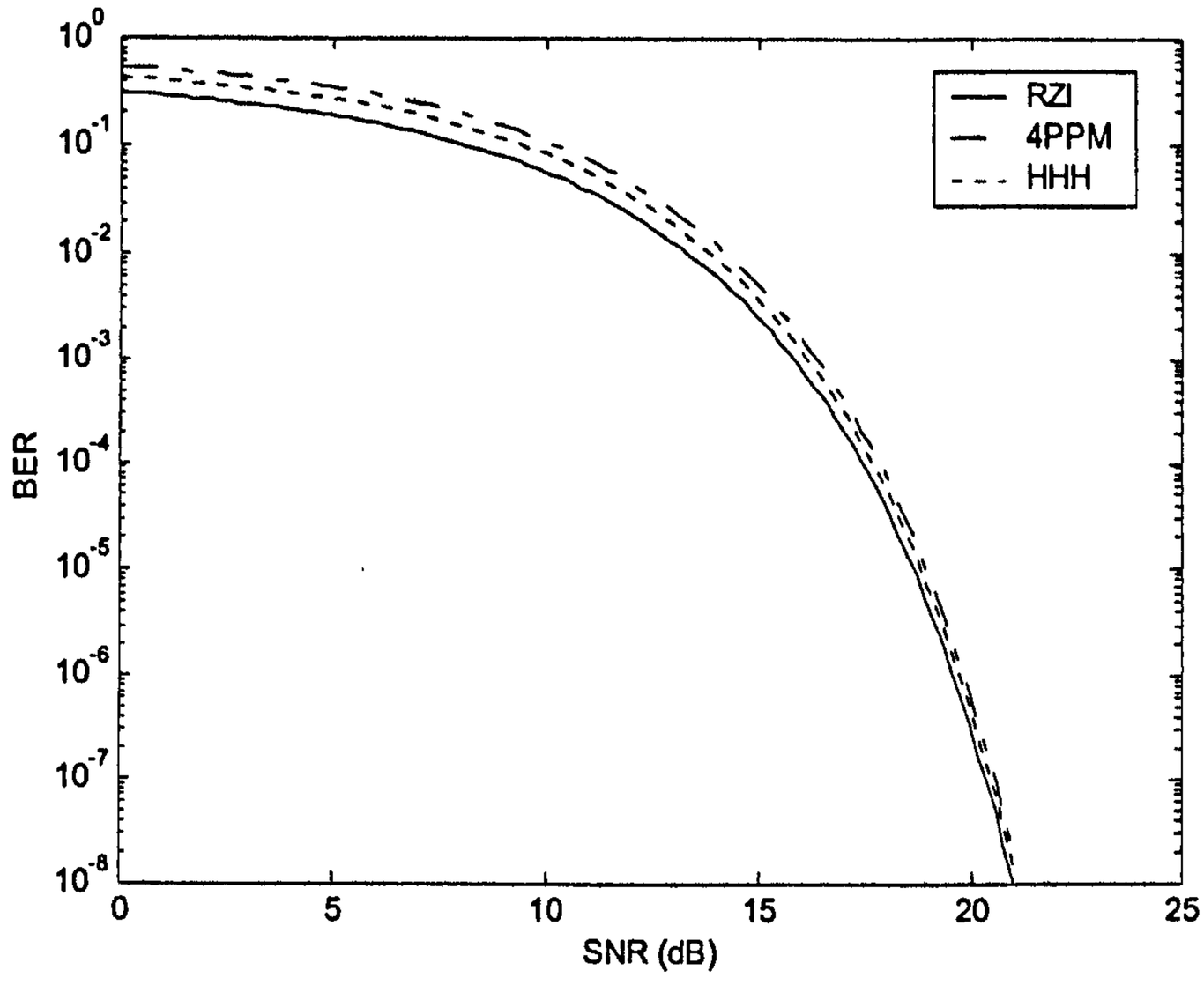

Figure 4.8 BER versus SNR for IrDA modulation schemes

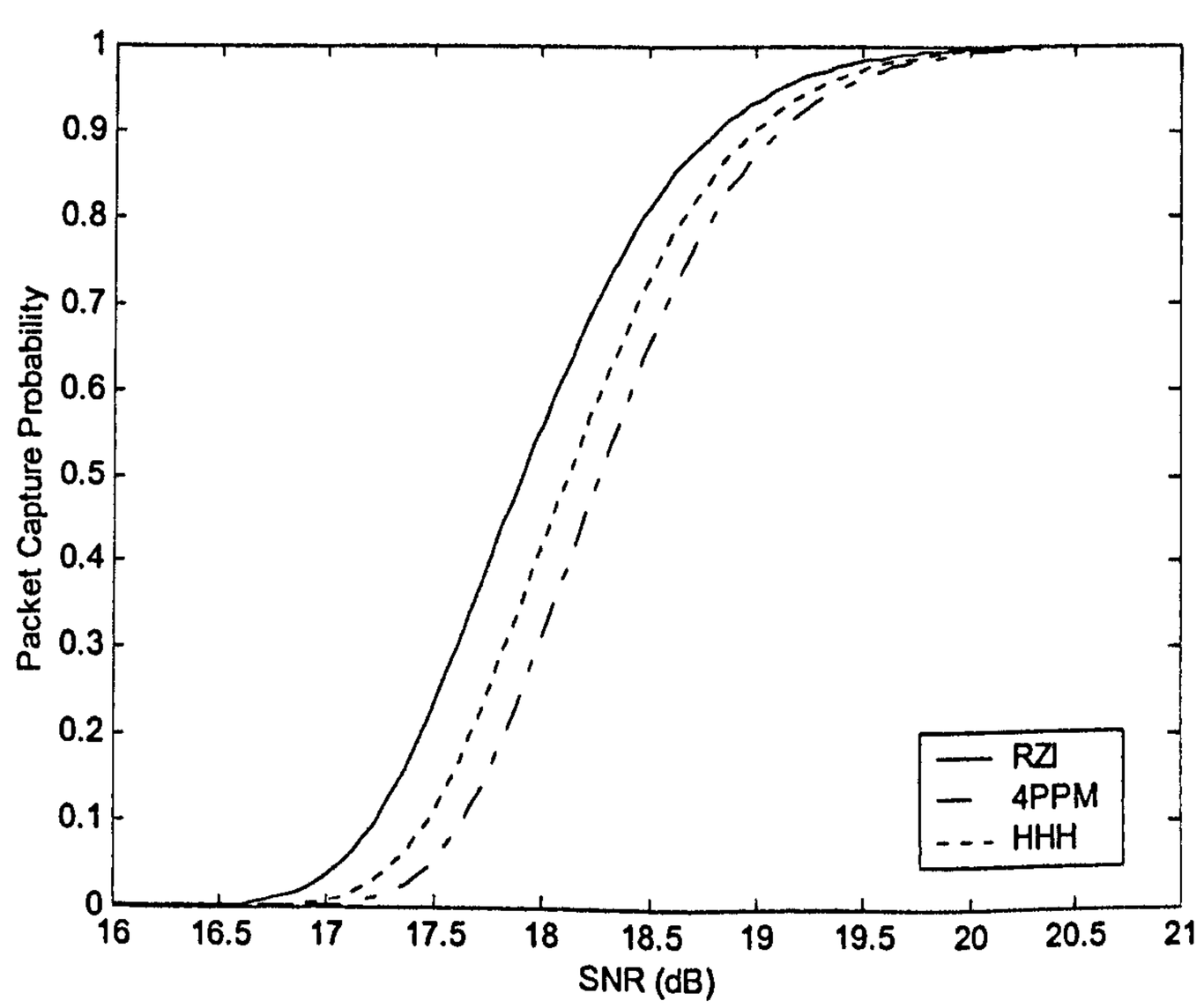

Figure 4.9 Packet capture probability versus SNR for IrDA modulation schemes

4.3.5 Example Implementation and Performance Calculation

Example implementation parameters are provided in the specification documentation (IrDA, 1995b) and summarised in Table 4.3.

Parameter	Value	Units
Detector Area	0.16	cm^2
Detector Responsivity	44	$\mu A/(mW/cm^2)$
Transmitter Intensity	109	mW/Sr
Ambient Intensity	490	$\mu W/cm^2$

Table 4.3 example parameter setting for IrDA links

Figure 4.12 shows the bit-error-rate (BER) versus LOS distance for IrDA 1.x data rates and modulation schemes using the parameters in Table 4.3 and recommended bandwidth values as given in Table 4.2. It can be seen that the higher data rates suffer from reduced performance from the higher bandwidth requirement causing a higher total noise level in the receiver. A higher transmitter output power is therefore required for higher data rate transmissions to achieve the same range. It can be seen that using the specified transmitter radiant intensity of 109 mW/Sr, the 16 Mbits/s link just achieves the minimum required performance of a BER of 10^{-8} at 1 meter. Figure 4.13 shows the packet capture probability versus LOS distance using the same values with data packet size l = 2 Kbytes. It can be seen that there is a very sharp cut-off distance for the performance of the links.

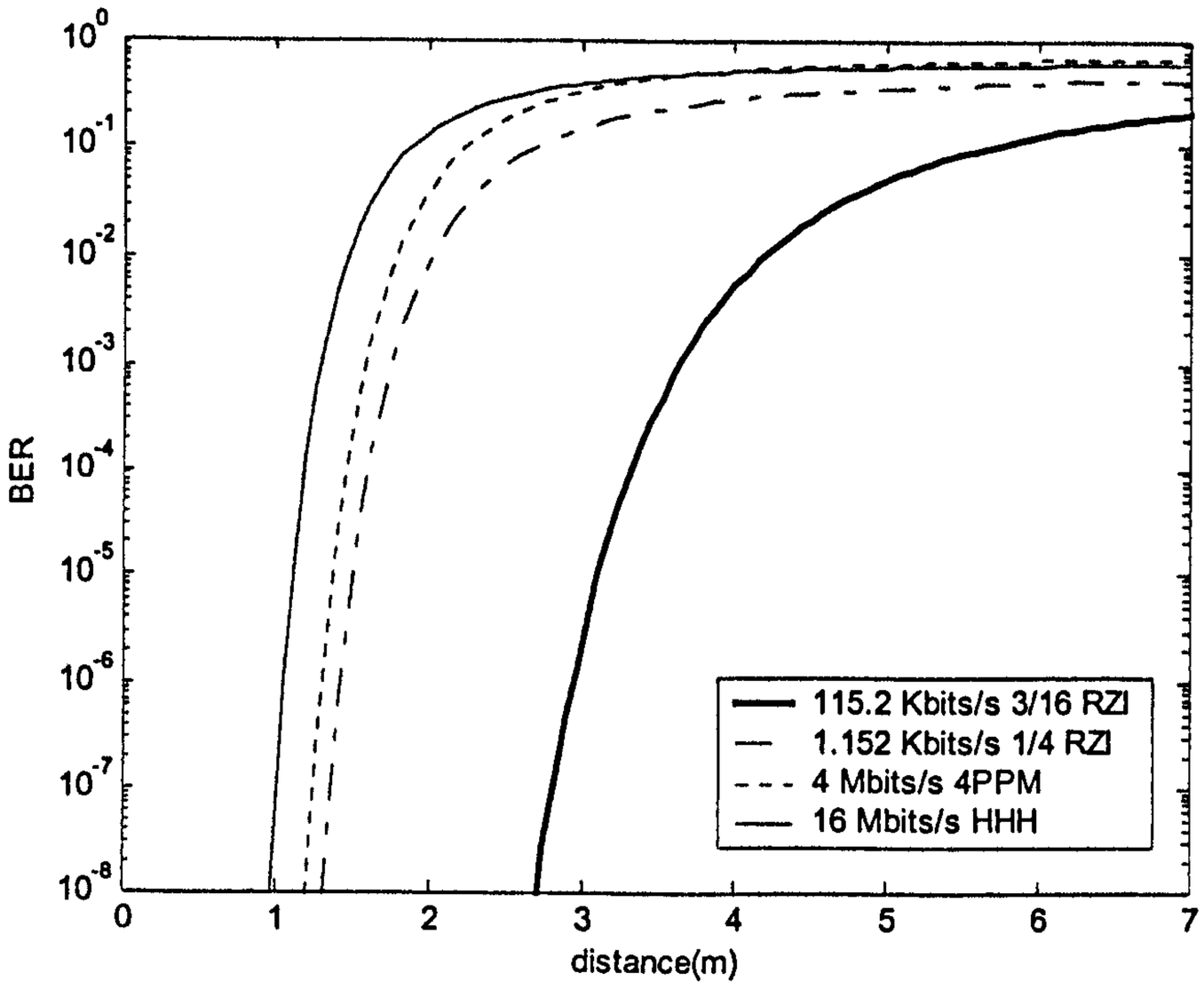

$A = 0.16\ \text{cm}^2$ $R/A = 44\ \mu\text{A}/(\text{mW}/\text{cm}^2)$ $I_0 = 109\ \text{mW/Sr}$
$E_B = 490\ \mu\text{W}/\text{cm}^2$ $\theta_T = 0$ $\theta_R = 0$

Figure 4.10 Bit error rate versus link LOS distance for IrDA links

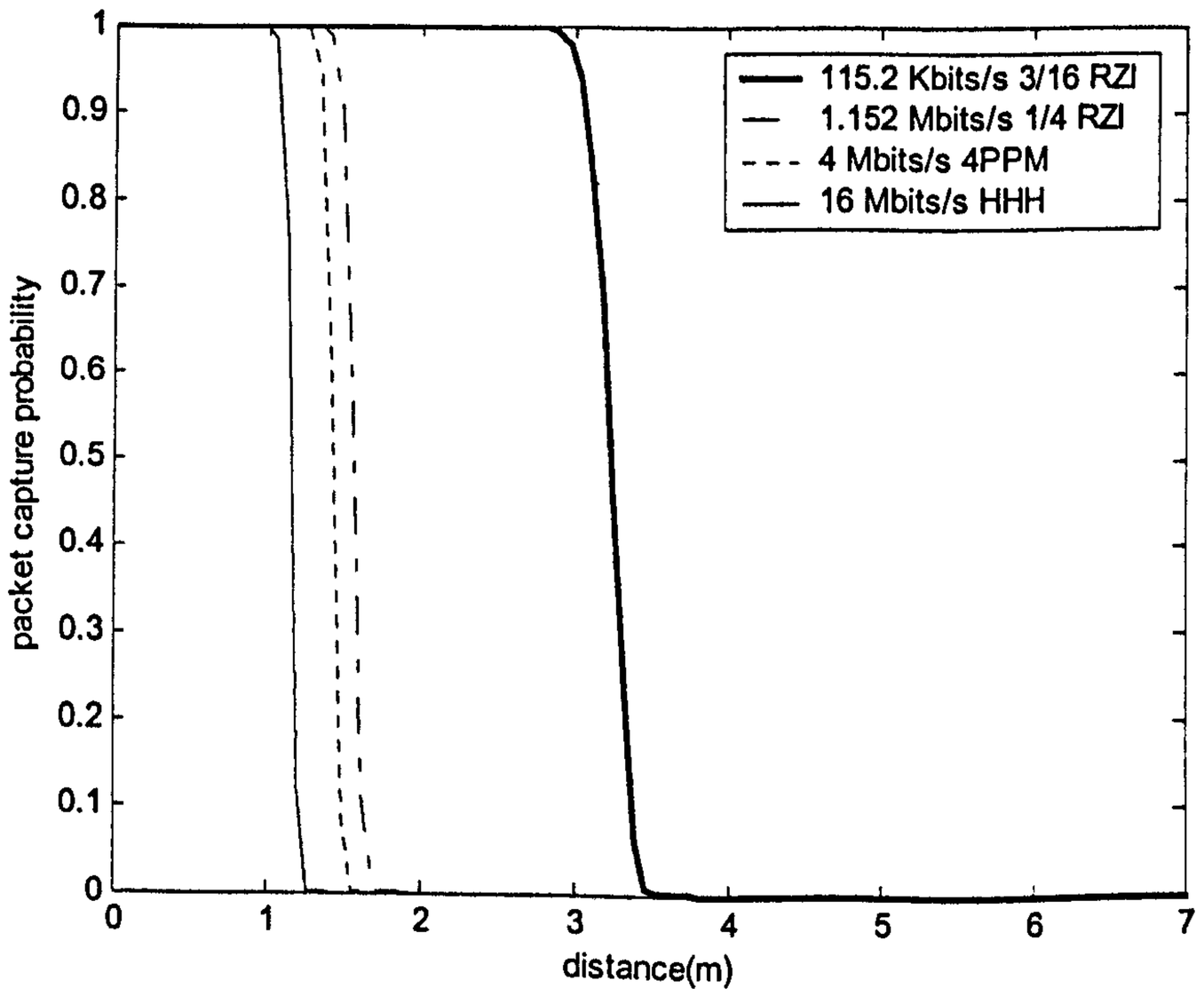

$A = 0.16\ \text{cm}^2$ $R/A = 44\ \mu\text{A}/(\text{mW}/\text{cm}^2)$ $I_0 = 109\ \text{mW/Sr}$
$E_B = 490\ \mu\text{W}/\text{cm}^2$ $\theta_T = \theta_R = 0$ $l = 2\text{Kbytes}$

Figure 4.11 Packet capture probability versus LOS distance for IrDA links

4.3.6 Approximation of BER

Approximations of the bit error rate value can be made by assuming adherence of physical layer properties to meet the minimum link specifications. If we take an LOS link ($\theta_T = \theta_R = 0$) to have a BER of 10^{-9} over a distance of 1m, thus approximating the minimum IrDA physical layer specification (actually 10^{-8} over 1m), using the fact that $Q(6) \approx 10^{-9}$, gives the approximation for BER of:

$$BER = Q\left\{\frac{6\cos^n \theta_T \cos^m \theta_R}{d^2}\right\} \tag{4.48}$$

For an LOS link, this reduces to the expression:

$$BER(d) = Q(6/d^2) \tag{4.49}$$

Figure 4.14 shows BER versus LOS distance for the approximation expression in 4.45. This can be seen to closely agree with the 16 Mbits/s HHH performance result in Figure 4.12.

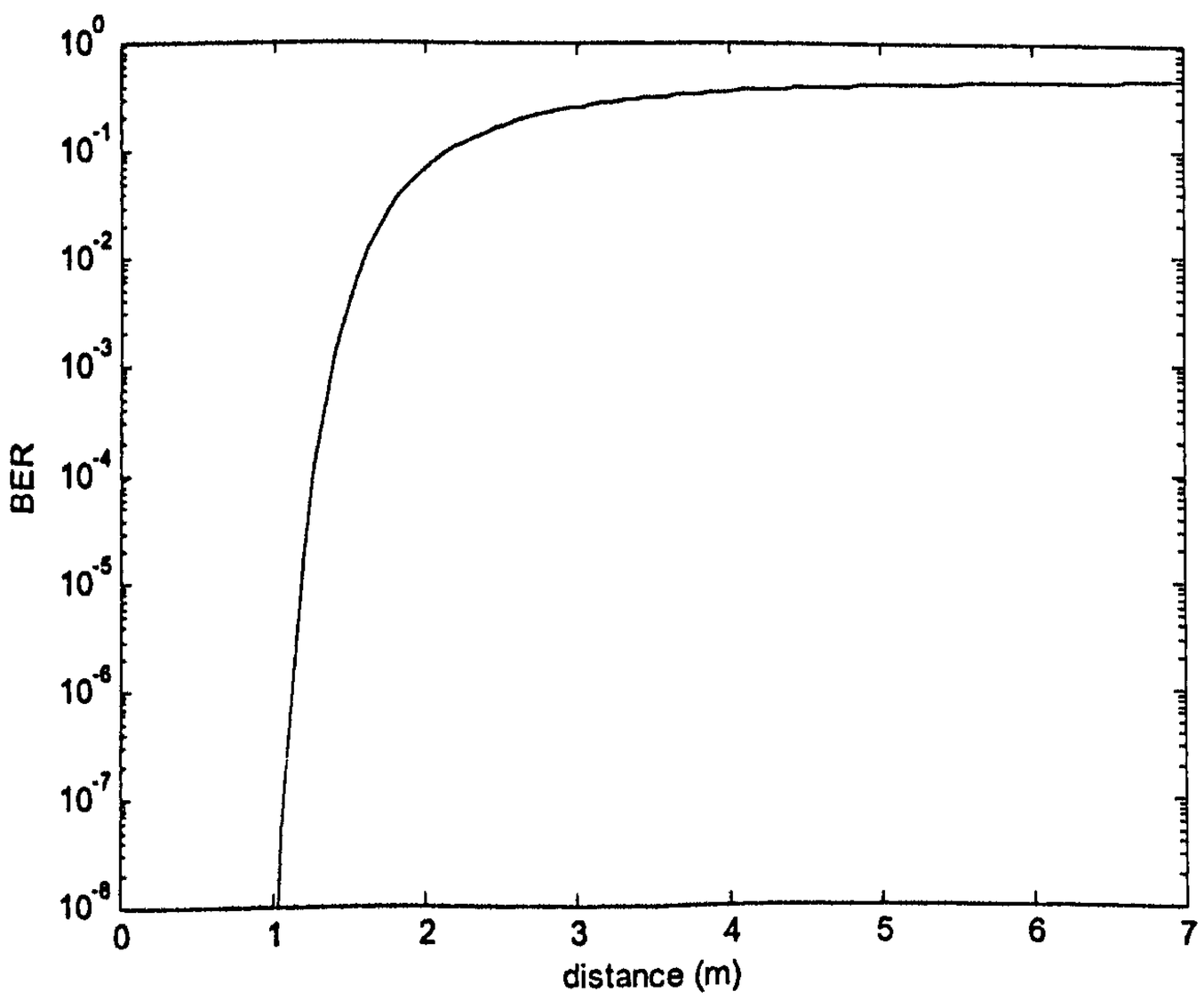

$$\theta_T = \theta_R = 0$$

Figure 4.12 BER versus LOS distance with IrDA BER approximation

4.3.7 4PPM –Variable Symbol Repetition

For variable repetition PPM encoding as used in the Advanced Infrared (AIr) protocol (see chapter 3), where each PPM symbol is multiplied a number of times and majority voting takes place on valid symbols, determination of the packet error and capture probability is more complex. Using a single chip-error-probability p_c, Chow and Kahn (1999) give the 4PPM/VR symbol capture probability p_{sc} as:

$$p_{sc} = \sum_{k=0}^{4RR} h_k {p_c}^k (1-p_c)^{4RR-k} \tag{4.50}$$

where RR is the repetition rate and the h_k is the number of correctable error patterns for k chip errors. However h_k is difficult to determine exactly (particularly for large RR) and has to be approximated.

The analysis provided by Ozugar (Ozugur et al., 1998) varies from that of Chow and Kahn in that it uses separate chip-error-probabilities p_{c1} and p_{c0} and assumes a symbol is captured when the PPM slot with the original pulse has the maximum number of pulses of all slot positions counted. This produces a successful symbol capture probability p_{sc} of:

$$p_{sc} = \sum_{i=0}^{RR-1} \left[\Phi_i^1 \left(1 - \sum_{j=0}^{i} \Phi_j^0 \right)^3 \right] \tag{4.51}$$

where $\Phi^1{}_i$ is the probability of the counter having RR – i pulses given by:

$$\Phi_i^1 = \binom{RR}{i} (1-p_{c1})^{RR-i} {p_{c1}}^i \tag{4.52}$$

and Φ^0_j is probability of any of the remaining 3 slot counter having RR $-j$ pulses, given by:

$$\Phi^0_j = \binom{RR}{j}(1-p_{c0})^j p_{c0}^{RR-j} \tag{4.53}$$

The packet capture probability p_{pc} for a packet length l bits is then given by:

$$p_{pc} = p_{sc}^{l/2} \tag{4.54}$$

Figure 4.15 shows the packet capture probability versus SNR (dB) for 4 PPM-VR with repetition rates of 1, 2, 4, 8 and 16, with a packet size of 2 Kbytes (16384 bits). Figure 4.16 shows the packet capture probability versus the LOS link distance (meters) using the physical parameters in table 4.4. It can be seen that increasing the RR increases the link range but at the expense of a lower data rate. This is effectively the equivalent of a virtual reduction in the receiver bandwidth while maintaining the same physical bandwidth.

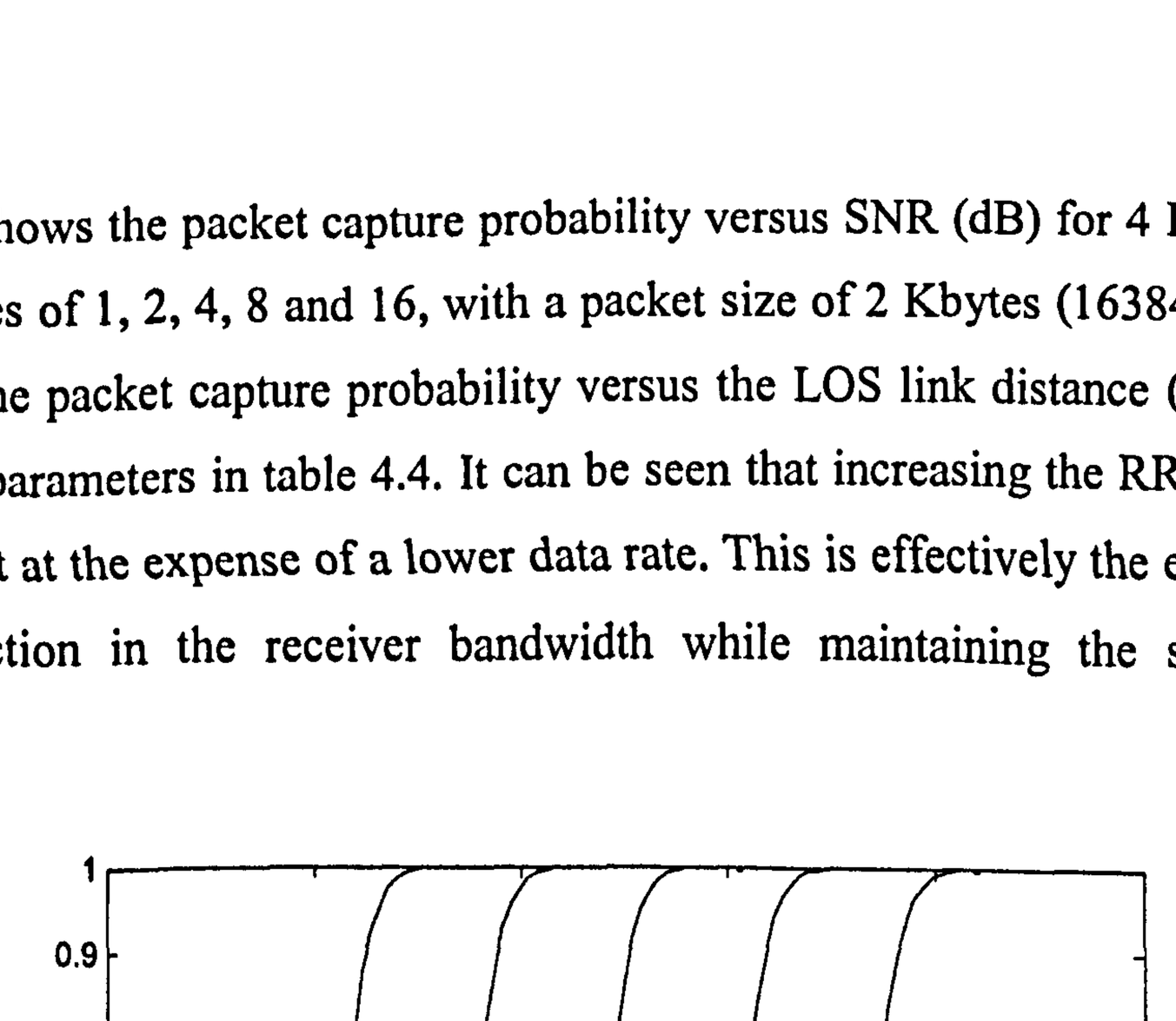

Figure 4.13 Packet capture probability versus SNR for 4PPM/VR

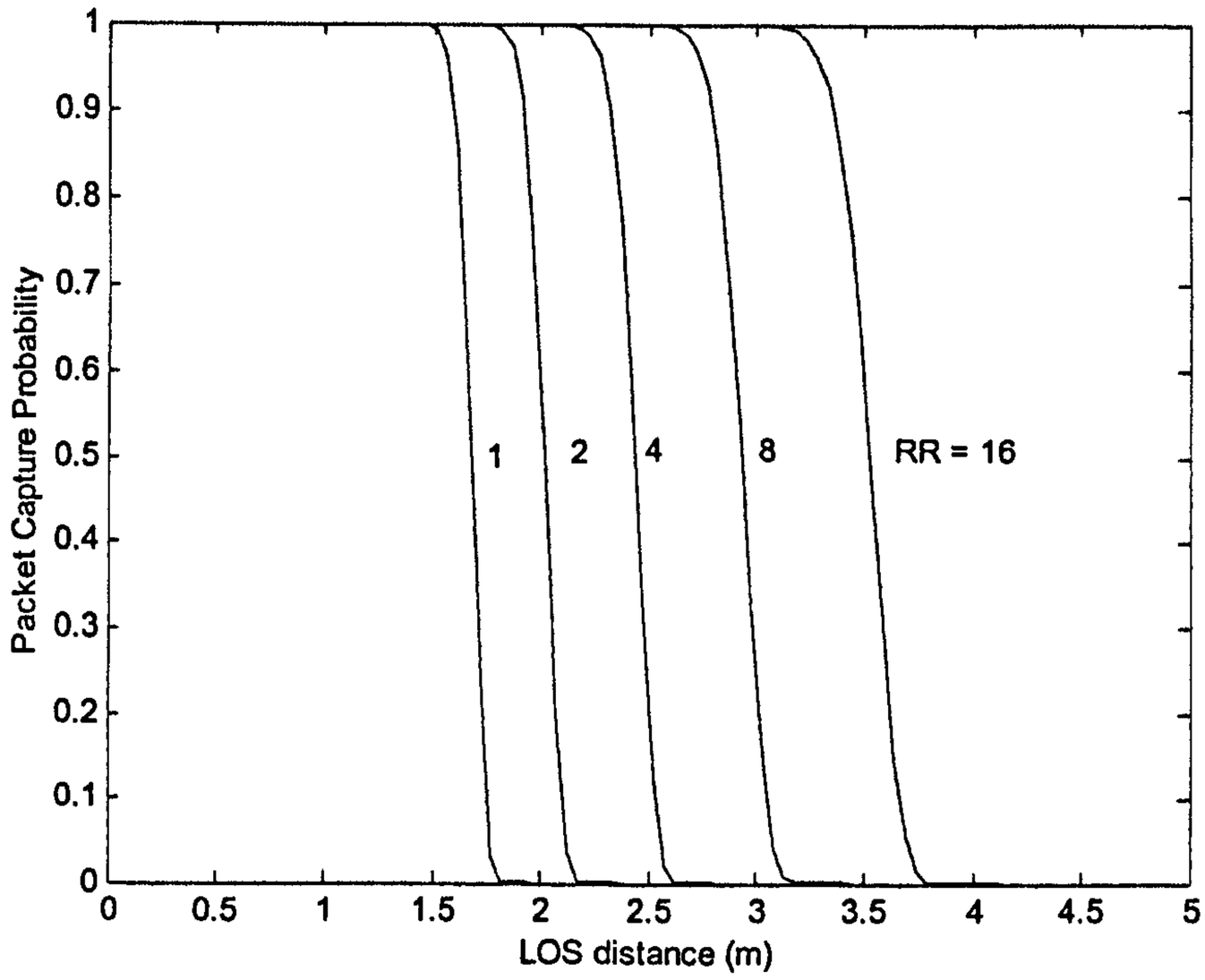

Figure 4.14 Packet error probability versus link LOS distance for 4 Mbits/s 4PPM/VR modulation

4.4 Third User Interference

In addition to noise from ambient light sources, third user interference can also degrade a link quality. Third user interference is where an unintended IR signal from a device outside of an established IR link coincides with the intended signal at the receiver thus causing potential bit errors. IrDA 1.x links are particularly susceptible to third-user interference as there is no inherent mechanism in the protocol to contend with it (i.e. carrier sensing). Determining the effect of the interference can be difficult if a different modulation scheme and/or different data rate to the signal is employed by the interferer.

In the simplest case, we can assume a basic NRZ modulation with an interferer transmitting at the same data rate and synchronised with the transmitted data signal. In the presence of an interfering signal the BER of a link is then given by (Boucouvalas et al., 1996):

$$BER = Q\left\{\frac{R(P_R - P_I)}{2\sqrt{N_0 B}}\right\} \tag{4.55}$$

where P_R is the received optical signal power and P_I is the interference optical signal power. Equation (4.58) can also be written as:

$$BER = Q\left\{\frac{RP_R}{2\sqrt{N_0 B}}\left(1-\frac{P_I}{P_R}\right)\right\} = Q\left\{\sqrt{SNR}(1-ISR)/2\right\} \qquad (4.56)$$

where *SNR* is the electrical Signal-to-Noise Ratio and *ISR* is the Interference-to-Signal Ratio.

A more realistic analysis can be provided for PPM interference by modelling the interfering signal $y(t)$ as a raised cosine pulse with roll-off factor α and amplitude y_{max} (Ozugur, 2000).

$$y(t) = \left|\frac{y_{max}\sin(\pi t)\cos(\pi\alpha t)}{\pi(1-4\alpha^2 t^2)}\right| \qquad (4.57)$$

We assume in this case that the phase of the interfering pulse is random within the pulse period T. The probability of strength of the interferer is determined by splitting the signal into M quantisation levels that result in an interference-signal ratio (ISR) for level i (Figure 4.17).

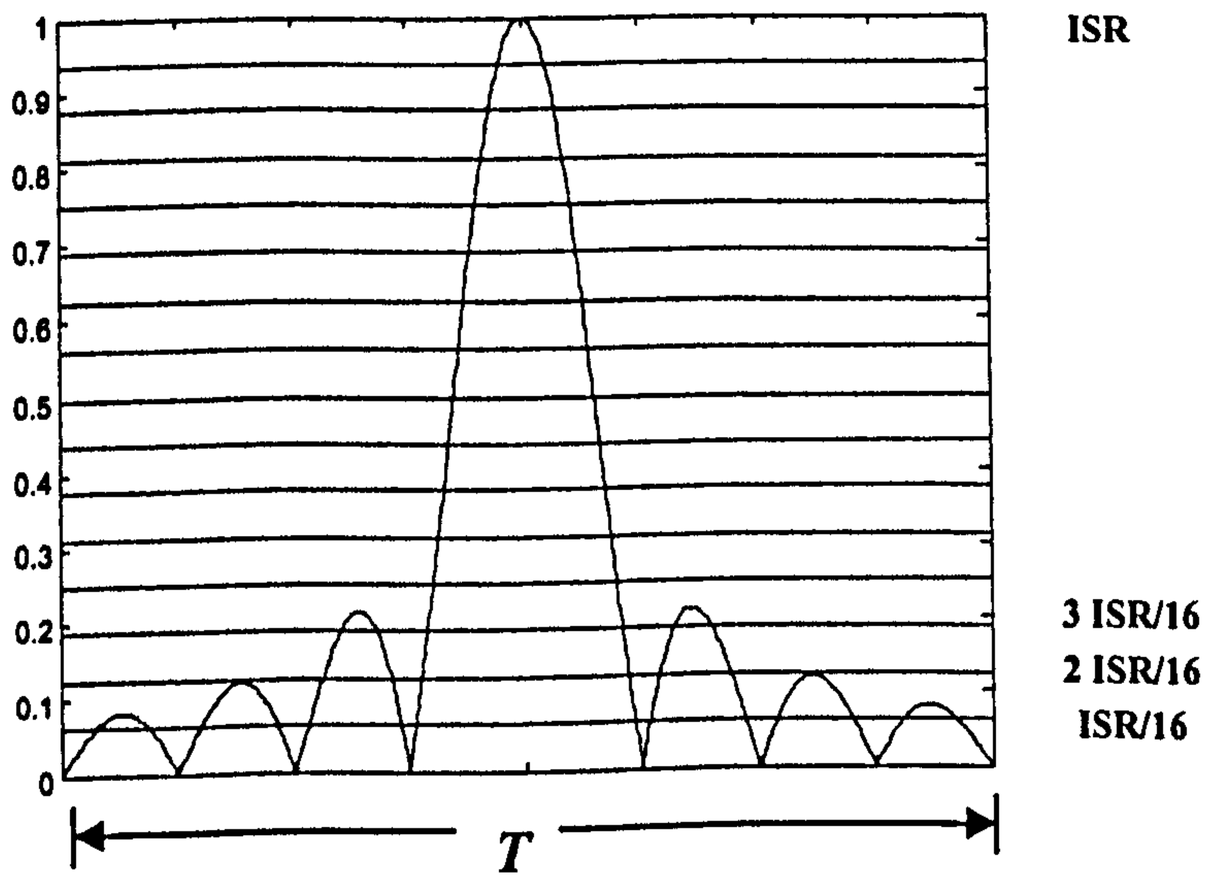

Figure 4.15 Raised cosine interference pulse with quantisation ISR levels

The quantisation level of the interference-to-signal ratio, ISR_i is therefore given by:

$$ISR_i = ISR\left(\frac{(i-1)}{16}+\frac{1}{32}\right) \quad i=1,2,3\cdots M \tag{4.58}$$

The probability p_i of the interference signal $y(t)$ being between the quantisation levels i and $i+1$, using k samples per period, is defined as:

$$p_i = \sum_k \frac{|t_k - t_{k+1}|}{T} \tag{4.59}$$

where t_k is the time where the signal passes from quantisation level i to $i+1$ and is determined numerically. The chip error probabilities for pulse and non-pulse slots, p_{c1} and p_{c0}, are then given by:

$$p_{c1} = \sum_{i=1}^{M} p_i Q((1-(Th+ISR_i))\sqrt{SNR}) \tag{4.60}$$

$$p_{c0} = \sum_{i=1}^{M} p_i Q((Th-ISR_i)\sqrt{SNR}) \tag{4.61}$$

where Th is the normalised threshold level (e.g. 0.5). The PPM symbol capture probability p_{sc} is then given by:

$$p_{sc} = (1-p_{e1})(1-p_{e0})^3 \tag{4.62}$$

The bit-error-rate p_e, is then given by:

$$p_e = 1-\sqrt{p_{sc}} \tag{4.63}$$

Figure 4.18 show BER versus *SNR* for 4 PPM with *ISR* values of 0, 10% and 20%. A raised cosine 'roll-off' factor α of 0.75 is used with normalised receiver threshold of

0.5. The effect of the third user interferer is to increase the SNR required to achieve the same level of BER.

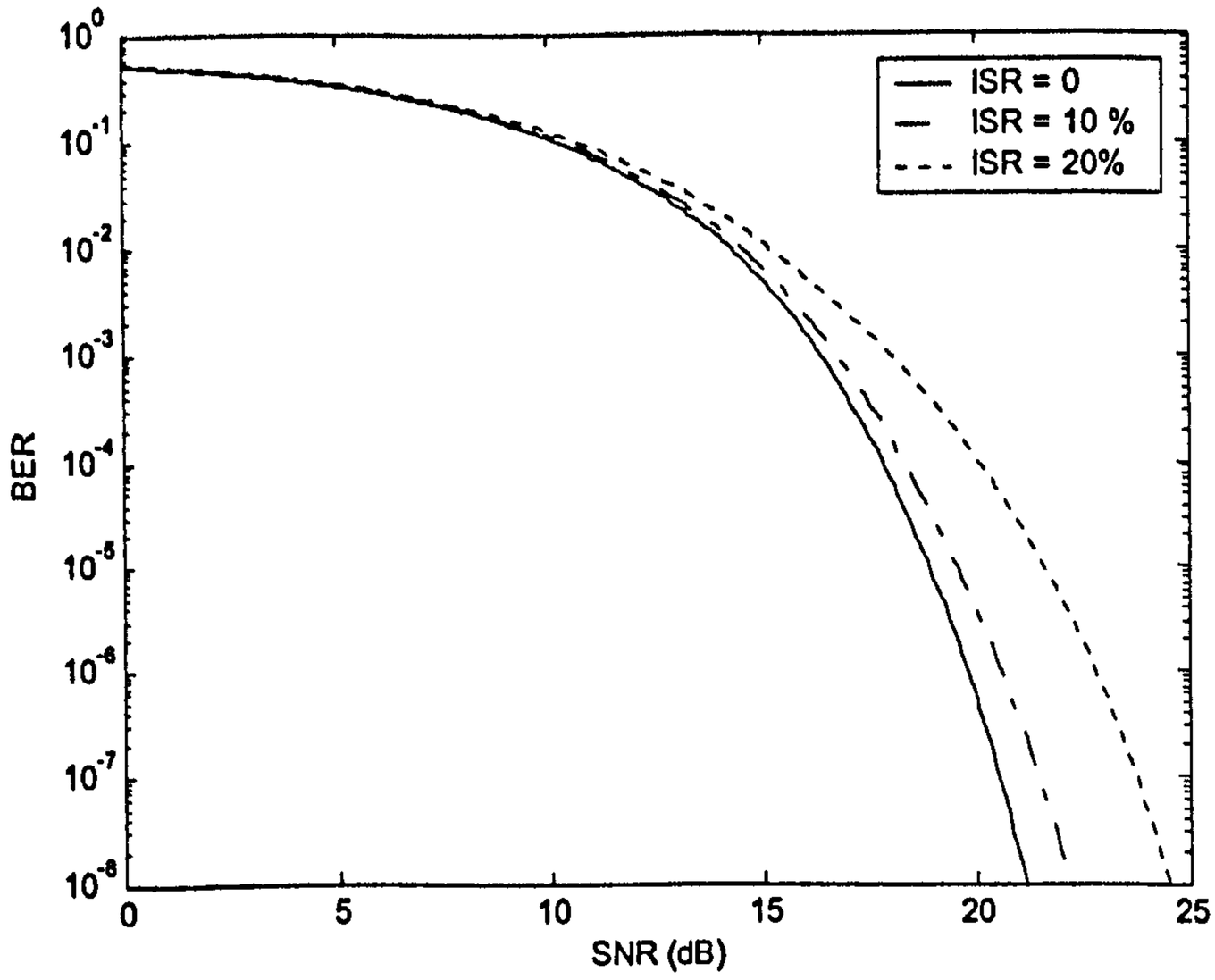

Figure 4.16 4PPM packer error probability versus SNR for varying ISR levels

4.4.1 Directional Asymmetry from Third User Interference

Directional asymmetry in an IR wireless link is here defined as a difference in the BER between each direction in the link (i.e. from user A to user B and user B to user A). Asymmetry can be caused by interference from a third IR wireless user, ambient light spatial distribution, and link component differences (Boucouvalas and Barker, 2000). Asymmetry can cause instability in the link and is therefore usually undesirable. In this section we examine directional asymmetry from a third user interferer. In the example situation below, users A and B are in an established link, and user C is interfering with the receiver of user A only. This causes a degradation in the link BA while link AB is unaffected. Figure 4.19 shows the geometry involved.

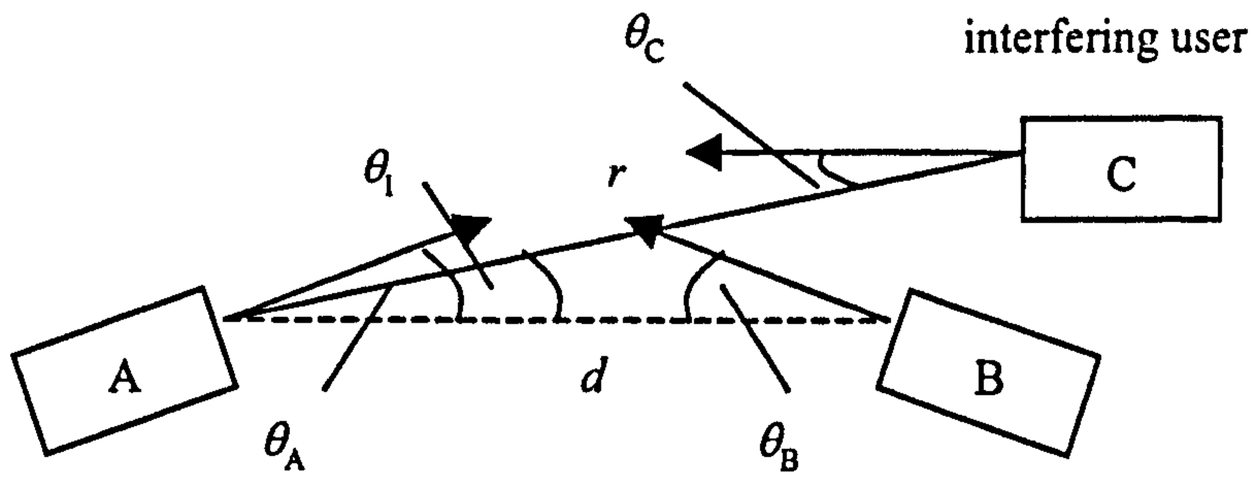

Figure 4.17 Directional asymmetry model geometry

Users A and B are in an established link of distance d and aligned at angles θ_A and θ_B as shown. Interfering user C is at a distance r from user A, moving towards A along AC, and aligned at angle θ_C. The angle made between user C and the line-of-sight path between users A and B is the interference angle θ_I. The received signal power at A from B, P_R and the interference signal power at A from C, P_I are given by:

$$P_R = \frac{I(\theta_B) A_A R_A \cos^n \theta_A}{d^2} \tag{4.64}$$

$$P_I = \frac{I(\theta_C) A_A R_A \cos^m (\theta_A - \theta_I)}{r^2} \tag{4.65}$$

Assuming that devices B and C have the same power output and the device angles are aligned such that $\theta_A = \theta_B = \theta_C = 0$, the interference-signal-ratio (ISR) is therefore given by:

$$ISR = \frac{d^2 \cos^m \theta_I}{r^2} \tag{4.66}$$

The BER for the links AB and the link BA are therefore different and given by:

$$BER_{AB} = Q(\sqrt{SNR_0}/2)$$
$$BER_{BA} = Q(\sqrt{SNR_0}((1/2) - ISR)) \tag{4.67}$$

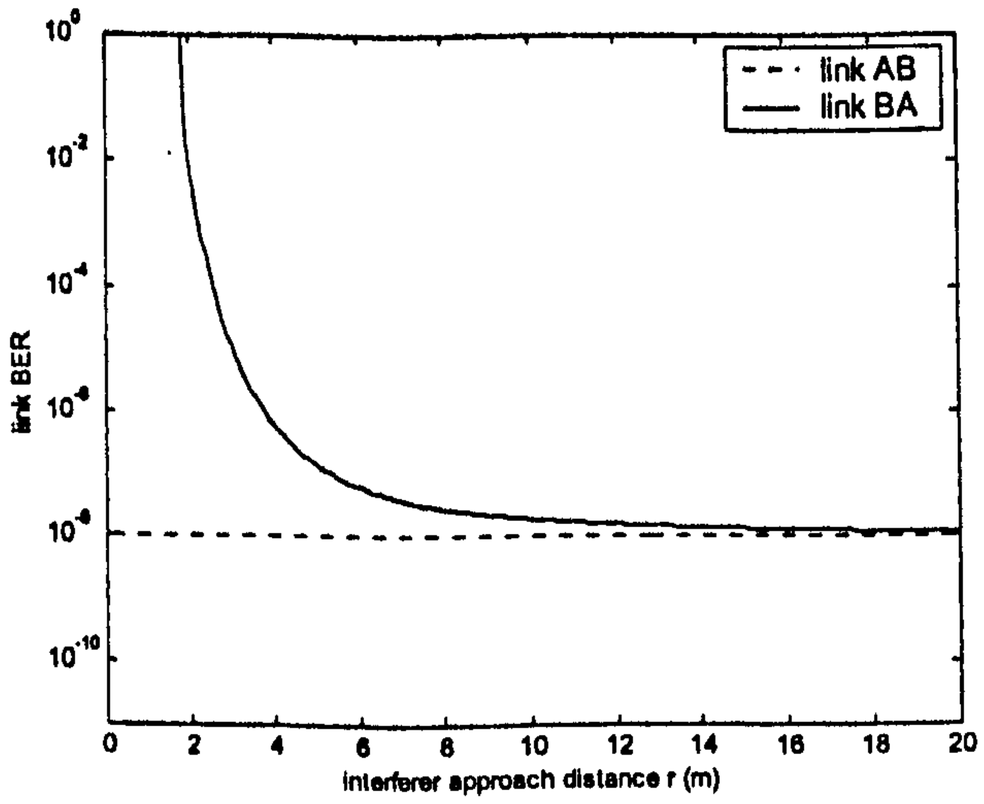

Figure 4.18 Directional BER asymmetry versus interferer approach distance

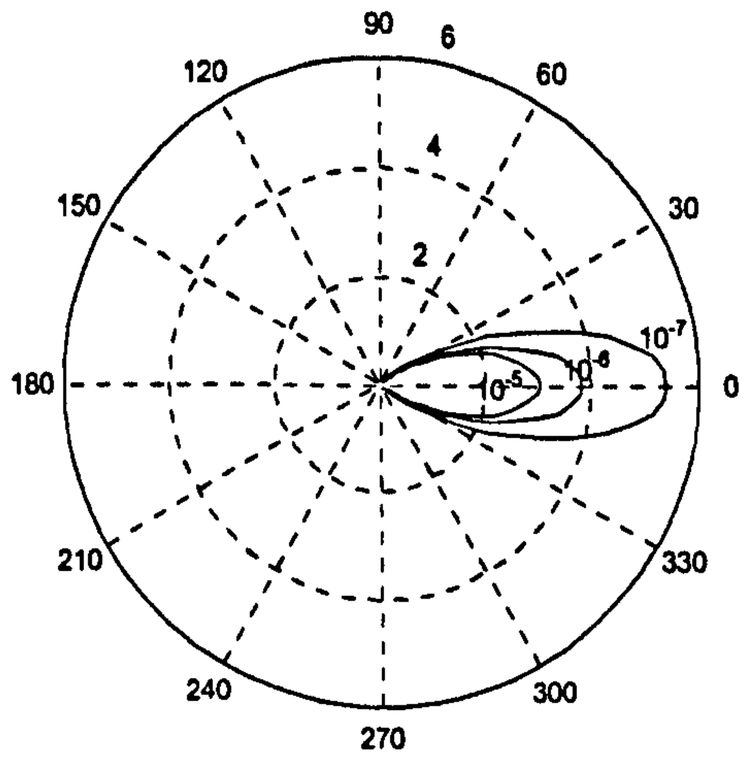

Figure 4.19 Interferer loci for constant BER values with narrow angle transceivers

Figure 4.20 shows the BER of link AB and link BA versus the approach distance of interferer C with the link AB distance *d* set to 1m. SNR_0 is the SNR from ambient light only and is set to give a BER without interference of 10^{-8} (dotted line). It can be seen that the BER of link BA (solid line) begins to significantly degrade at an interferer distance of 3m. Figure 4.21 shows the position loci of the interferer (angle θ_1 and distance *r*, Figure 4.19) to achieve BER values in the link AB of 10^{-5}, 10^{-6} and 10^{-7} using narrow angle transceivers (m = 20). This shows that if the interferer approaches from an angle greater than 30°, the approach distance can be less than 2 meters before the BER is significantly degraded.

4.4.2 Spatial Asymmetry from Moveable Link with Fixed Interferer

In addition to directional asymmetry, spatial asymmetry can also occur in a link where the BER varies with the spatial orientation of a receiver in relation to a fixed interferer. This scenario can arise where two independent IR links are operating in close proximity. In the example situation, users A and C are in an established link and interfered with by user B transmitting to unseen user D. User C is movable with respect to A, but interfering user B is fixed and transmitting parallel to A with a separation distance *d*. This is shown in Figure 4.22.

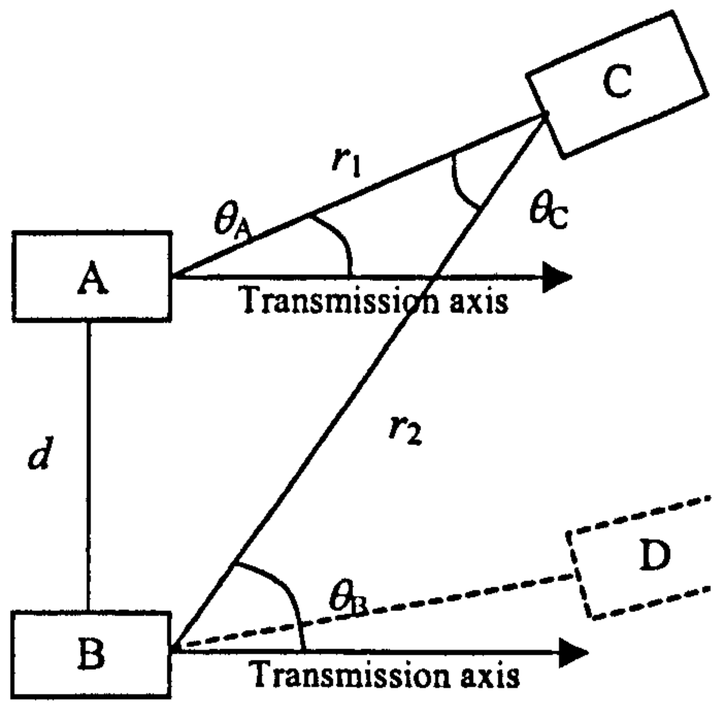

Figure 4.20 Geometry of spatial asymmetry scenario

The received power at device C from A and at C from B are given by :

$$P_r(C,A) = \frac{P_A A_C (n+1)\cos^n \theta_A}{2\pi r_1^{\,2}} \tag{4.68}$$

$$P_r(C,B) = \frac{P_B A_C (n+1)\cos^n \theta_B \cos^m \theta_C}{2\pi r_2^{\,2}}$$

If we assume that all devices have identical transmitter and receiver characteristics, the interference-to-signal ratio is then given by:

$$ISR = \frac{\cos^n \theta_B \cos^m \theta_C r_1^{\,2}}{\cos^n \theta_A r_2^{\,2}} \tag{4.69}$$

Using trigonometry it can be established that:

$$r_2 = \sqrt{d^2 + r_1^{\,2} - 2dr_1 \cos(\theta_A + \pi/2)} \tag{4.70}$$

$$\theta_C = \sin^{-1}\left[\frac{d\sin(\theta_A + \pi/2)}{r_2}\right] \tag{4.71}$$

$$\theta_B = \theta_A + \theta_C \tag{4.72}$$

In this case the SNR (without interference) will also vary with the geometry of the link AC. The SNR, can therefore be given by:

$$SNR = SNR_0 \left[\frac{\cos^m \theta_A}{r_1^2} \right] \tag{4.73}$$

where SNR_0 is the SNR to achieve a LOS BER of 10^{-8} with $\theta_A = 0$ and $d = 1$m. Figure 4.23 shows the polar plot of the loci of user C in relation to A (angle θ_A and distance r_1) to provide a BER better than or equal to 10^{-8} (shaded areas) (Barker and Boucouvalas, 2002a; Barker and Boucouvalas, 2002b) with varying separation d of devices A and B and with narrow and wide angle transceivers. This demonstrates how the separation distance between two independent IR wireless links affects the spatial BER and throughput of the links. It can be seen that there is a significant spatial asymmetry effect using wide angle transceivers. For narrow angle transceivers, the effect only becomes significant when the separation distance d is less than 0.4 meters. This therefore shows that two independent links adhering to the minimum IrDA specification can be as close as 0.4 m apart without mutual interference.

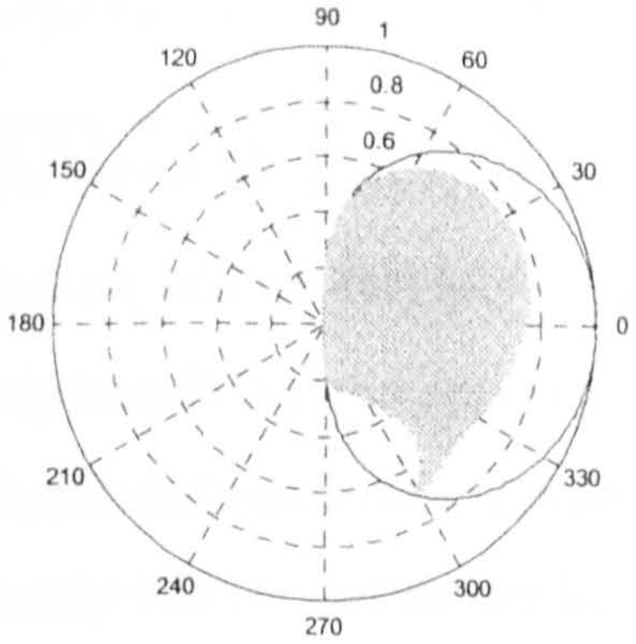

wide angle transceivers, d = 0.8 m

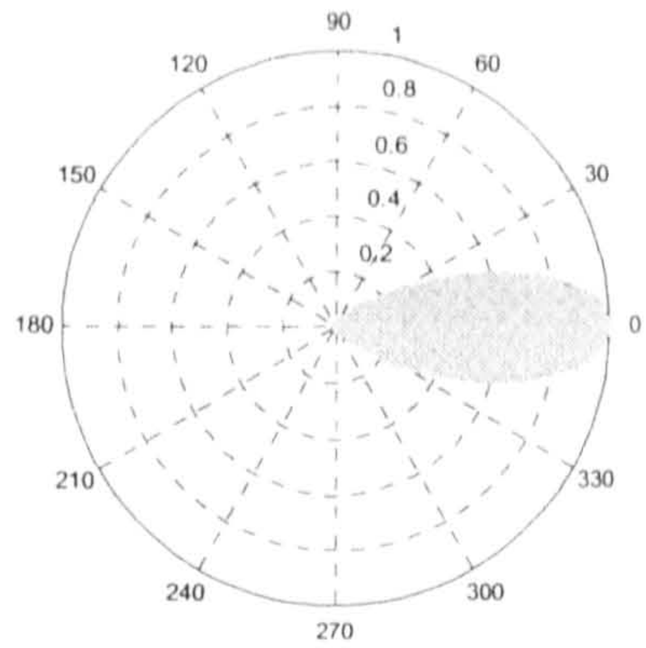

narrow angle transceivers, d = 0.8 m

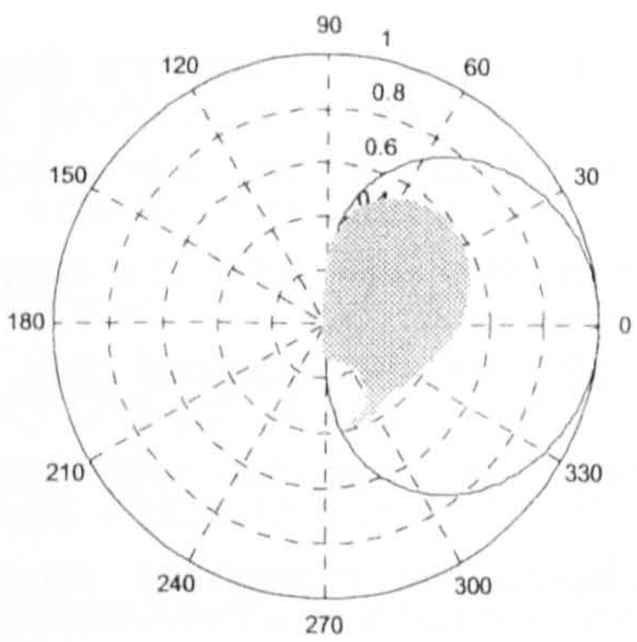

wide angle transceivers, d = 0.4 m

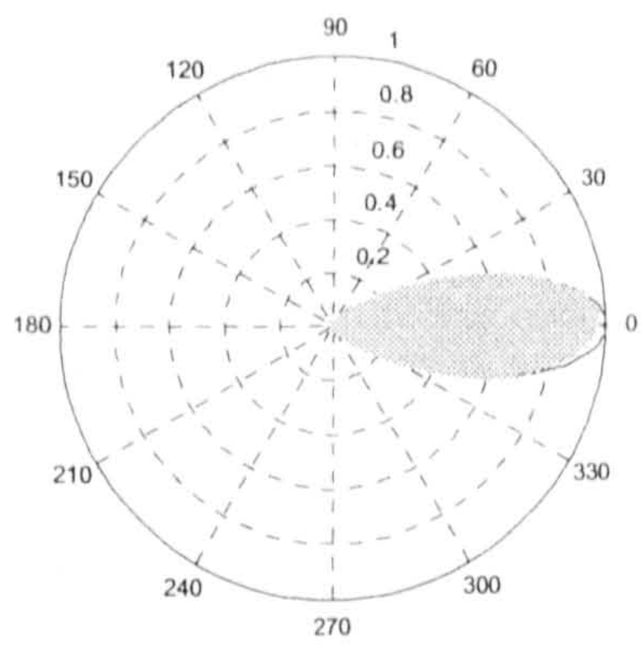

narrow angle transceivers, d = 0.4 m

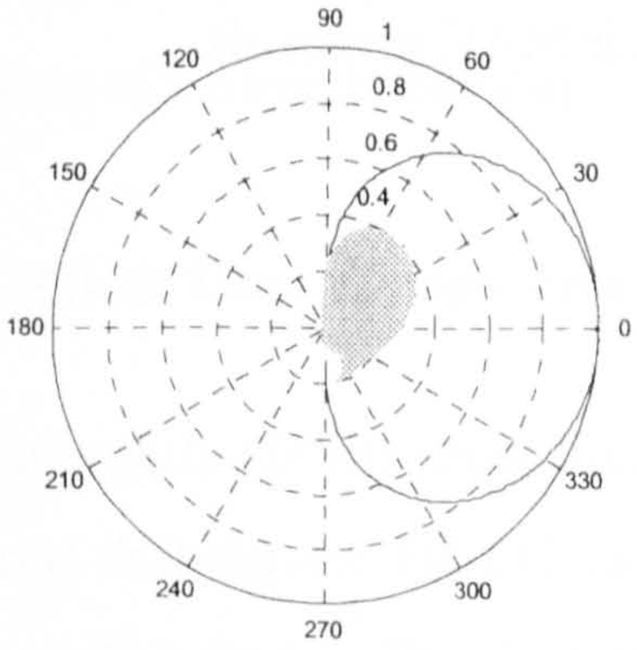

wide angle transceivers, d = 0.2 m

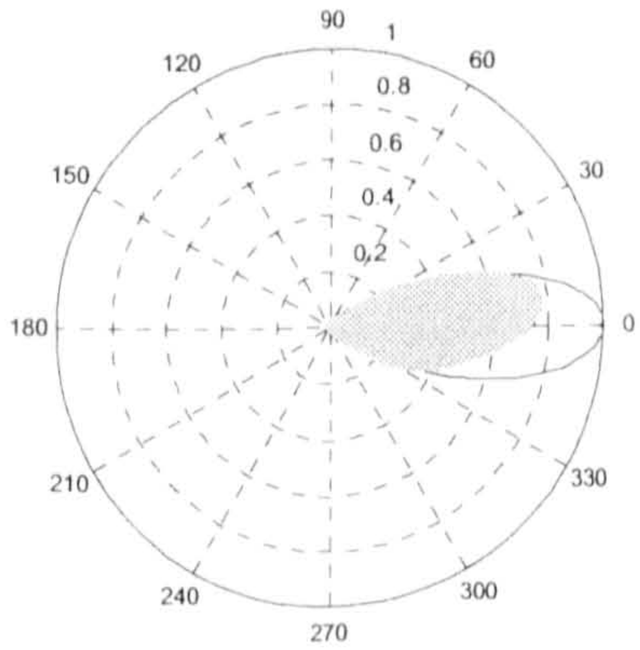

narrow angle transceivers, d = 0.2 m

Figure 4.21 Spatial asymmetry for user C loci and AB separation distance *d* to provide BER < 10^{-8}

4.5 Chapter Summary

In this chapter we have examined the physical layer characteristics of an IR wireless data link in order to establish expressions for the bit-error-rate (BER) and packet error probabilities for specific data rates, modulation and encoding schemes. Expressions for BER can be linked to the throughput analysis (Chapter 6) to provided throughput performance in relation to physical layer characteristics. Expressions for the transmitted optical power in terms of transmitter characteristics and modulation scheme are derived and expressions for the received optical power are derived in terms of detector characteristics and system geometry. Noise sources are examined to determine the noise power from ambient background light induced shot noise. From these, expressions for the SNR and hence BER of an IR link were derived. It is shown that there is a sharp cut-off distance for link quality and that the receiver bandwidth for the required data rate is a significant factor in performance. Third user interference is examined with resulting directional and spatial asymmetry effects. These indicate the minimum separation distance for independent links. The following chapter examines existing studies of data link and media access protocols with the aim of choosing suitable methods for the application to performance analyses of the IrLAP and AIr MAC protocols.

5. MODELLING OF COMMUNICATIONS PROTOCOLS

This chapter examines methods that have been used in modelling general communications protocols that are of relevance to the current study. In particular it looks at analytical modelling of data link protocols and multiple access protocols.

5.1 Modelling HDLC Based Data Link Protocols

Data link protocols are primarily concerned with frame error detection and correction and flow control regulation. Therefore in performance modelling of data link protocols we are looking at the dependence of the end-to-end throughput on frame-error-probability (simply related to the bit-error-rate) and the interaction with link parameter settings and characteristics. Throughput is determined by calculating the proportion of time spent successfully transmitting data to the total active time. This can be determined in a number of ways depending on nature of the system being investigated (e.g. balanced or unbalanced, full or half-duplex, saturated or unsaturated) and on other assumptions of system behaviour.

5.1.1 The Virtual Transmission Time Method

Bux & Kummerle (1980) presented a method for determining the saturation throughput of balanced full-duplex HDLC using the concept of the 'virtual transmission time' (VTT) for a data frame. This is defined as the time from the start of frame transmission at the transmitter to the completion of successful frame reception (including possible frame re-transmissions) at the receiver. The VTT for the last frame in a transmission window also includes the time for the acknowledgement from the receiving station before transmission can resume. The maximum frame throughput is then the reciprocal of the average frame VTT.

The model assumes a saturation data condition where data packets are continuously available for transmission. It is also assumed that data traffic is passed in one direction only and that S-frame acknowledgements are small enough to be considered error free. The VTT for a particular frame is dependent on the window size (w) seen by the frame, defined as the number of frames remaining to be transmitted before transmission must stop due to $M-1$ unacknowledged frames where M is the modulus of the transmission sequence count (8 for standard HDLC, 128 for extended HDLC). The average virtual transmission time t_v is then given by:

$$t_v = \sum_{w=0}^{M-2} \phi(w) t_v(w) \qquad (5.1)$$

where $\phi(w)$ is the probability of the frame having window width w, and $t_v(w)$ is the window width dependent virtual transmission time.

The window width process for HDLC is modelled as the finite state machine shown in Figure 5.1 where w is the variable window width and p is the probability of frame error. This is related to the link bit-error-rate p_e by:

$$p = 1-(1-p_e)^{l+l'} \qquad (5.2)$$

where l is the frame data size (bits) and l' is the frame overhead size (bits). Taking a maximum transmission window size of $M-1$ frames, the window width w is the number of frames remaining to be transmitted following a transmission and thus has values 0 to $M-2$. Following a successful transmission the window size is reduced by 1. However following a transmission failure (frame in error) the frame and following frames in the transmission window will be re-transmitted from the start of the next transmission window. Thus the window width returns to the maximum $M-2$. This is illustrated in the finite state machine diagram in Figure 5.1.

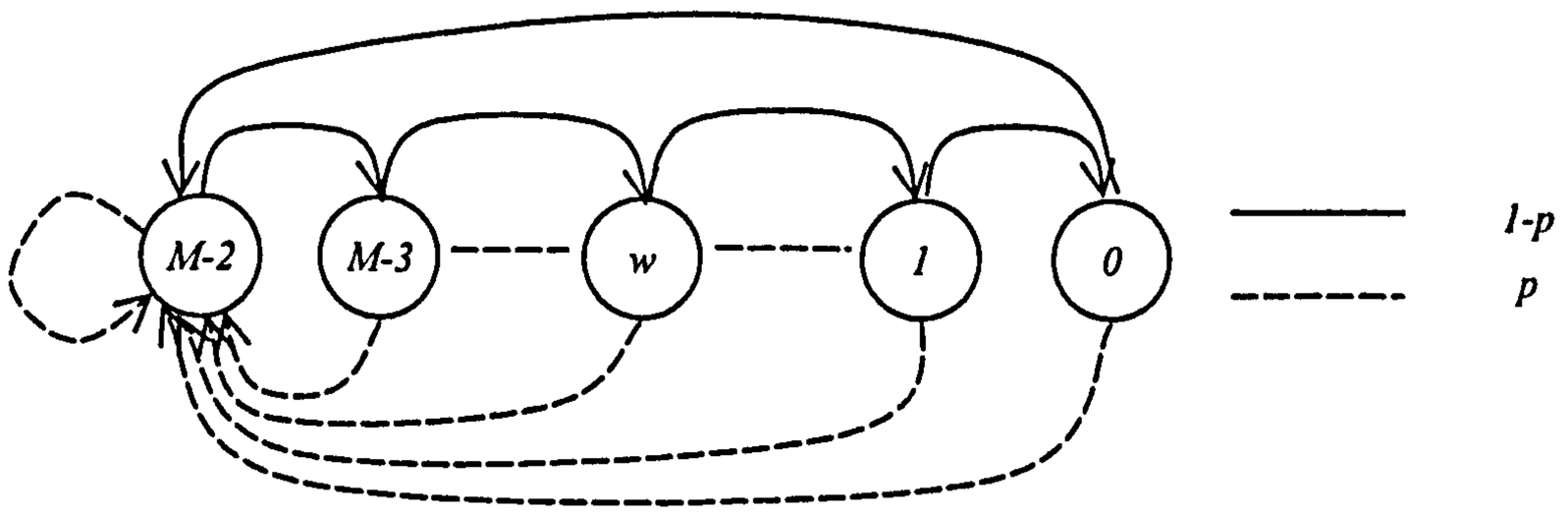

Figure 5.1 HDLC window width process finite state diagram

Using Markov analysis it can be shown that the probability $\phi(w)$ of a frame seeing a window width w is given by:

$$\phi(w) = \frac{p(1-p)^{M-2-w}}{1-(1-p)^{M-1}} \qquad w \in \{0,1,\cdots,M-2\} \tag{5.3}$$

Calculation of the window width dependent VTT $t_v(w)$ depends on whether the acknowledgement delay (t_{ack}) is greater than the window transmission time (where N is the maximum window size and t_I is the I-frame transmission time) or not. This takes into account possible propagation delays with long distance links (e.g. satellite). The expressions for $t_v(w)$ are given by:

$$t_v(w) = E[T_0(w)] + pE[T_1(w)] + \frac{p^2}{1-p}T_2 \qquad t_{ack} > Nt_I \tag{5.4}$$

$$t_v(w) = t_I + pE[T_1] + \frac{p^2}{1-p}T_2 \qquad t_{ack} \le Nt_I \tag{5.5}$$

where $T_0(w)$ is the time for the initial frame transmission, $T_1(w)$ is time for the first re-transmission ($E[T_1(w)]$ and $E[T_0(w)]$ are the average or expected values) and T_2 is the time for subsequent re-transmissions. The value for T_2 is independent of w because for subsequent re-transmissions the frame considered will be the first in the re-transmission window. These elements are expressed in terms of conditional time components and the probabilities of the conditions occurring. The use of the virtual transmission time provides a mechanism for determining throughput in relation to all operational

parameters (bit-error-rate, data packet length, frame overhead, window size, data rate, propagation delay) and provides a clear explanation of the individual processes that effect the performance (Schwartz, 1987). The model analyses full-duplex balanced HDLC procedures but the method can be applied to all HDLC procedures with suitable modifications.

The model by Bux was modified by Burakowski (1986) to model HDLC-ABM with dependent error channels in which the probability of a bit error is not assumed to be independent but is dependent on the preceding bit success. This is assumed to be a more realistic evaluation of bit-errors for real communications channels. The bit transmission process is modelled as a Markov process. This results in a modification to the window width probability distribution given in equation 5.3

$$\phi(w) = \frac{p(E \mid C)[p(C \mid C)]^{M-2-w}}{1-[p(C \mid C)]^{M-1}} \tag{5.6}$$

where $p(E \mid C)$ is the probability of a bit error given a preceding correct bit and $p(C \mid C)$ is the probability of a correct bit given a preceding correct bit. The window width dependent VTT $t_v(w)$ formulae are also modified to include the above probability and $p(E)$, $p(C)$ the probability of a independent error bit and correct bit respectively. This analysis may be suitable for wired data links with low error rates or noise-burst error conditions, but may not be suitable to IR wireless links.

5.1.2 Queuing Analysis Method

Queuing analysis is a common method for performance evaluation of communications networks (Chan, 2000) where data packet service queues are a major bottleneck in the network performance. Labetoulle and Pujolle (1981) determine the maximum throughput for bi-directional error-free saturated HDLC-ARM links with non-uniform packet sizes using queuing analysis. The model uses a system of N parallel servers corresponding to the maximum window size. Packets arrive at service rate μ_1 and each server has mean service time S. The model is an *M/G/N/N* queue with loss and the throughput T is therefore given by:

$$T = \mu_1 \left(1 - \frac{\frac{\rho^N}{N!}}{\sum_{n=0}^{N} \frac{\rho^n}{n!}} \right) \tag{5.7}$$

where $\rho = \mu_1 \cdot S$

Such an analysis may be beneficial for land based or satellite HDLC links where the bit-error-rate is very low but not suitable for wireless links with potentially high error rates.

5.1.3 Probabilistic Automaton

Masunaga (1978) developed a throughput expression for NRM half-duplex HDLC from a probabilistic automaton (finite state machine). The point-to-point throughput was derived by reducing a four-state automaton of the two-way data transfer procedure between a primary (P) and secondary (S) station to a two state goal process. The principal assumption made in this analysis is that either all frames in the window are transmitted correctly or one or more frames including the final frame are in error and the entire window re-transmitted. The four state finite state diagram is given in Figure 5.2.

The process flow is as follows.

$S_0 \rightarrow S_1$: P transmits window to S, P-bit frame not lost, probability P_{01}, time T_{01}

$S_0 \rightarrow S_2$: P transmits window to S, P-bit frame lost, probability P_{02}, time T_{02}

$S_2 \rightarrow S_2$: P re-transmits window to S, P-bit frame lost, probability P_{22}, time T_{22}

$S_2 \rightarrow S_1$: P re-transmits window to S, P-bit frame lost, probability P_{21}, time T_{21}

$S_1 \rightarrow S_0$: S transmits window to P, F-bit frame lost, probability P_{10}, time T_{10}

$S_1 \rightarrow S_3$: S transmits window to P, F-bit frame not lost, probability P_{13}, time T_{13}

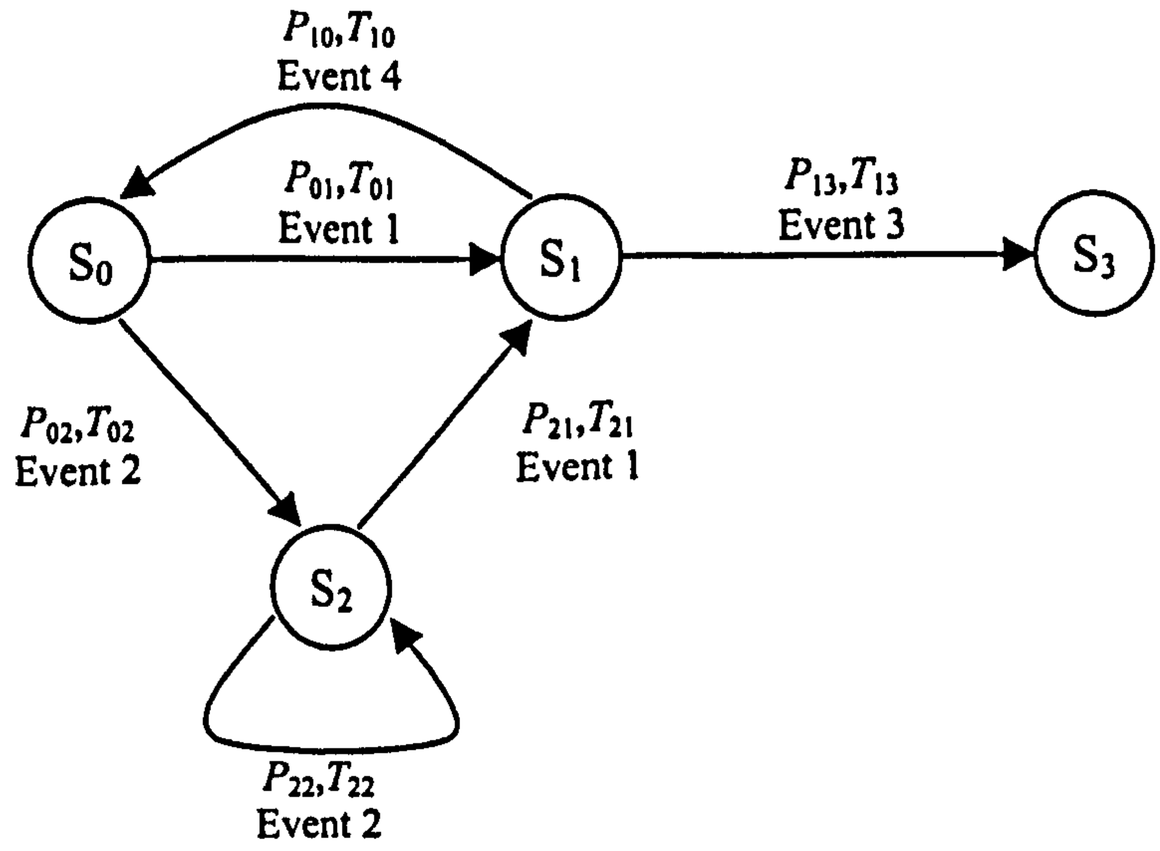

a) Four state HDLC process

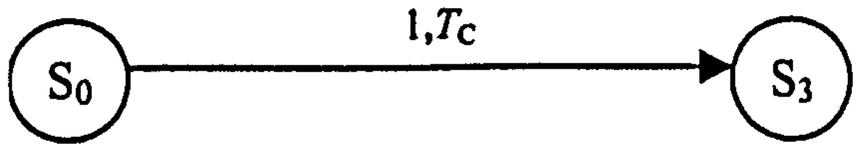

b) Two state goal process

Figure 5.2 HDLC half-duplex NRM finite state process and goal process

In reducing the four state machine to a two state machine from state S_0 to S_3 with time T_C and probability of 1, the time T_C (the average time to transmit a frame window from P to S and S to P) is given by:

$$T_C = T_{13} + \frac{P_{10}}{P_{13}}T_{10} + \left(1 + \frac{P_{10}}{P_{13}}\right)\left[P_{01}T_{01} + P_{02}T_{02} + P_{02}T_{01} + \frac{P_{02}P_{22}}{P_{21}}T_{22}\right] \qquad (5.8)$$

The time T_{ij} and probability P_{ij} (from state i to state j) are calculated from the HDLC operational parameters and line bit-error-rate. The focus of the model is the impact of the time-out period when the P or F bit is lost. The assumption that the entire window is either accepted or rejected may be acceptable for a small window size but not as the window size becomes larger. It will certainly not be acceptable for the 127 frame window size used with 16 Mbits/s VFIR.

From the above studies it can be seen that the analysis by Bux although based on balanced full-duplex HDLC procedures provides a very accurate analytical model with minimal simplification assumptions for saturation throughput which may be applied to

the unbalanced half-duplex HDLC based IrLAP protocol. Other studies have unacceptable assumptions or approximations (e.g. a low bit-error rate) for the analysis IR wireless links.

5.1.4 Simulation Studies of HDLC

A simulation study of HDLC links was presented by Georges and Wybaux (1981). The study examined both saturated and non-saturated balanced HDLC links. For both cases the data packet lengths are random with an independent three phase distribution. This is intended to simulate random network data traffic consisting of 1) short network control packets, 2) maximum length data packets, and 3) varying length data packets less than the maximum. In the saturated condition, the input queue has just one place which is occupied by a waiting data packet. This is immediately replaced by another when the packet is transmitted. In the non-saturated case, data packets arrive at the input queue according to a Poisson process with specified Mean Interarrival Time parameter ($1 / \lambda$). As the input queue in the saturated case is unbounded, $1 / \lambda$ should remain greater than the mean packet transfer time determined from the saturated case. The generation of packet errors is also modelled on a Poisson process where the probability P_r of one or more errors in frame of data length l is given by:

$$P_r = 1 - e^{l \cdot BER} \tag{5.9}$$

Results of the saturation case help decisions on the transmission window size parameter and acknowledgement timer duration parameter.

A simulation model of balanced HDLC using a Petri Net description and PROTOB simulation environment was given by Marsan and Barbetta (Marsan et al., 1989). Petri Nets are a formal description of dynamic systems that can be used for the specification of communications protocols. The PROTOB simulation environment is based on a class of Petri Net called Prot-nets that allows an object oriented development of a discrete event simulation model with a graphical and textual environment.

Larue and Frost (1990) presented a technique for extrapolating the performance of HDLC links. The basis of their technique was to take the results from a single simulation run for the HDLC protocol with a single error rate parameter and extrapolate results for a range of error rates. This was aimed at reducing the computational load for a simulation study at a time when computing processor speed was still limited. The technique used involves the weighting of packet end-to-end delay values by the probability that they would be observed under different operating conditions. This is a form of the 'importance sampling' technique.

Such studies are useful in highlighting the important issues in the simulation of data link protocols that can be of benefit in the design of a simulation model for the IrDA 1.x protocol (see Appendix A).

5.2 Modelling CSMA/CA Medium Access Protocols

With multiple access schemes for a shared medium we are primarily interested in the efficiency of network utilisation and end-to-end packet delays where collisions on the medium force frame retransmissions.

5.2.1 Performance Models of CSMA/CA

An analysis (Brewster and Glass, 1987) and simulation (Glass et al., 1988) of non-persistent CSMA/CA was first presented by Glass and Brewster. The analysis examined both slotted and non-slotted CSMA/CA with Poisson distributed traffic load. The throughput for the non-slotted case was given as:

$$S = \frac{e^{-aG}}{[1/G + 3a + (1+a)e^{-aG} + a(1-e^{-aG})\{3 + (1/aG) - e^{-aG}/(1-e^{-aG})\}]} \qquad (5.10)$$

where as with the CSMA/CD analysis, G is the channel load and a is the normalised propagation time.

The simulation model was developed using the SLAM II (Simulation Language for Alternative Modelling) language.

Further analyses of CSMA/CA have largely concentrated on the IEEE 802.11 MAC protocol. As described in chapter 1, the IEEE 802.11 is a standard for wireless local area networks (W-LANs) using a common CSMA/CA based MAC protocol for a number of physical layer options.

A major study of the performance of the IEEE 802.11 protocol has been produced by Chhaya and Gupta (Chhaya and Gupta, 1997). This examined both the 'basic' access and RTS/CTS methods with non-saturated load using a mathematical analytical model verified with simulations using OPNET. They also examined the effects of non uniform frame sizes and spatial analysis. In the analysis for the 'basic' access method the throughput *S(i, j)* from station *i* to *j* is given by:

$$S(i,j) \approx \frac{p_S(i,j)}{T_S}\left(\frac{G(i,j)}{G} + (1-e^{-\beta G(i,j)})\sum_{m,n} G(m,n)\right) \qquad (5.11)$$

where $p_S(i, j)$ is the probability of a successful transmission from station *i* to *j*. $G(i, j)$ is the offered load from *i* to *j* and *G* is the total load. The set *(m, n)* denotes all other station pairs excluding *(i, j)*. T_S is the average length the 'renewal period' following a successful transmission. This is the length of time between the medium being detected free and is given by:

$$T_S = 1/G + DIFS + l + \beta + l_{ack} \qquad (5.12)$$

where *l* is the frame transmission time and β is the propagation delay.

Crow (Crow et al., 1996) produced a bespoke simulation model of the 802.11 MAC protocol. The model investigated the performance of both the Distributed Co-ordination Function (DCF) used for ad-hoc network configurations and the Point Co-ordination

Function (PCF) used for an infrastructured network configuration. With the latter there is a central co-ordinating station that polls the other stations in sequence.

Bianchi (Bianchi, 1998; Bianchi, 2000) produced a mathematical model for the saturated throughput of the 802.11 MAC DCF protocol using both the 'basic' and RTS/CTS access methods. The analysis uses a Markov model of the exponential back-off collision avoidance process.

The derived throughput is given by:

$$S = \frac{P_S P_{tr} E[P]}{(1-P_{tr})\sigma + P_{tr} P_S T_S + P_{tr}(1-P_S)T_C} \tag{5.13}$$

where P_{tr} is the probability of at least one transmission in a particular time slot, given by:

$$P_{tr} = 1-(1-\tau)^n \tag{5.14}$$

where τ is the probability of transmitting in a chosen time slot and n is the number of stations in the network. P_S is the probability that a transmission is successful and is given by:

$$P_S = \frac{n\tau(1-\tau)^{n-1}}{P_{tr}} \tag{5.15}$$

The component $E[P]$ represents the expected transmission time for the packet size and σ is the collision avoidance slot duration. The periods T_S and T_C are the time sensed on the medium for a successful transmission and when a collision occurs respectively. These are illustrated in figure 5.3.

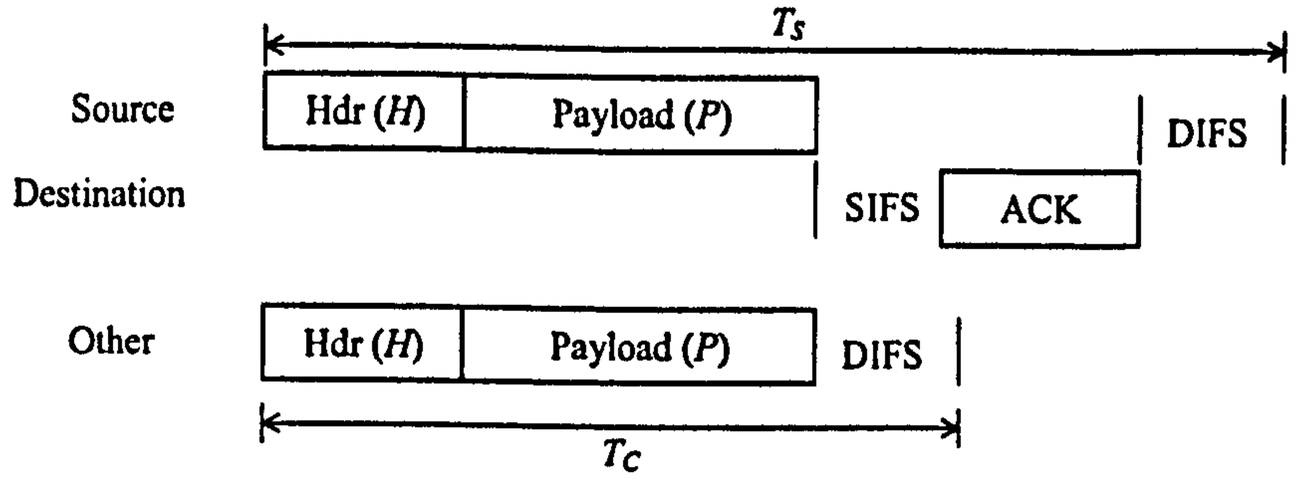

a) Basic Access

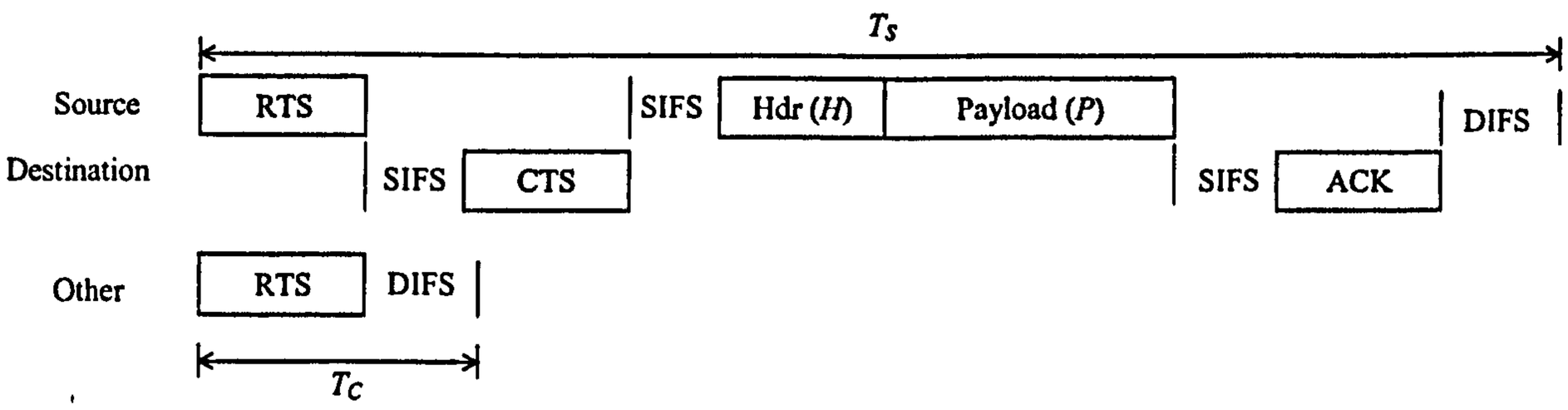

B) RTS/CTS Access

Figure 5.3 Basic and RTS/CTS access times for 802.11 DCF

These depend on the access method used. For the basic and RTS/CTS methods, the successful transmission media time T_S and collision transmission media time T_C respectively are:

$$T_S^{bas} = H + E[P] + SIFS + \beta + ACK + DIFS + \beta$$
$$T_C^{bas} = H + E[P^*] + DIFS + \beta \quad (5.16)$$

$$T_S^{rts} = RTS + SIFS + \beta + CTS + SIFS + \beta + H$$
$$+ E[P] + SIFS + \beta + ACK + DIFS + \beta \quad (5.17)$$
$$T_C^{bas} = RTS + DIFS + \beta$$

where each element is a time component. H is the packet header duration and β as before is the propagation delay. The value $E[P^*]$ is the average length of the longest packet in a collision. If a fixed data packet size is used then we simply have $E[P] = E[P^*] = P$.

The probability τ of transmitting in a particular time slot is provided by the Markov model analysis of the exponential back-off process and gives:

$$\tau = \frac{2(1-2p)}{(1-2p)(W+1)+pW(1-(2p)^m)} \tag{5.18}$$

where W is the initial contention window size CW_{min} and m is the maximum exponential back-off stage such that $CW_{max} = 2^m CW_{min}$. The value p is the probability of collision and is given by:

$$p = 1-(1-\tau)^{n-1} \tag{5.19}$$

This results in a non-linear system in p and τ which must be solved numerically.

This model is based on the exponential contention window back-off process used in the 802.11 DCF protocol but can equally be applied to the linear contention window back-off process of the AIr MAC protocol with suitable modifications.

5.3 Chapter Summary

This chapter has provided a review from published literature of methods used for performance modelling of communications protocols that are relevant to the present study. This involves data link layer protocols and shared media access protocols using both mathematical analytical and simulation methods. The methods used for maximum throughput in saturated data conditions and for non-persistent data with variable packet sizes is also examined. The following chapter presents an analytical model of the IrDA IrLAP protocol with performance results and optimisation analysis. The model is based on the HDLC performance model of Bux, described in this chapter.

6. IrDA 1.x PROTOCOL PERFORMANCE MODELLING

This chapter presents an analytical model of the IrDA 1.x IrLAP data link protocol information transfer process. The model provides saturation throughput in relation tó the link BER and other protocol parameter settings. Graphical results are presented for theoretical maximum link throughput and in relation to varying BER and link parameter values. This leads to optimum values for the data packet size and transmission window size.

6.1 IrDA IrLAP Analytical Model

The model presented here is an evolution of the model given by Bux and Kummerle (1980) which analysed balanced full-duplex circuit HDLC procedures, to the analysis of the un-balanced half-duplex HDLC based IrLAP protocol. The basis of the model is to calculate the average 'virtual transmission time' (VTT) for a frame being transmitted in an IrLAP link. The VTT is the total time taken for the reliable end-to-end transmission of an I-frame between peer IrLAP layers. The VTT of a specific frame begins at the start of the frame transmission and ends with the successful reception of the frame (or frame re-transmission) in-sequence and without error at the receiving station. The VTT for the first frame in a transmission window must also include the time for the acknowledgement reply (including link turnaround delays) from the receiving station for the previous window.

The VTT is calculated using the probability of packet error based on a specified BER and on the re-transmission times required for a particular packet position within the transmission window. The probability of the packet being in a particular window slot is determined by a Markov model of the window width process. The average saturation throughput is therefore given by the reciprocal of the average virtual transmission time multiplied by the packet data size. The model thus provides the theoretical maximum IrLAP link throughput in terms of the link BER and link parameter settings of link data rate, data packet length, maximum window size, maximum turn-around time (window transmission time) and minimum turn-around delay.

6.1.1 Model Assumptions and Parameters

The model assumes a primary and secondary station pair operating in the data exchange phase of the IrLAP procedure. All user data packets (i.e. I-frames) are transmitted from the primary to the secondary only. The link is assumed to be saturated, i.e. there is data continually waiting transmission at the primary (thus the P-timer is not of relevance). The secondary responds with RR (Receive Ready) S-frames only. It is assumed that an S-frame, whether from the primary or secondary, is small enough to be considered error free. The action of the F-timer is incorporated when the primary forces a reply from the secondary if there is corruption of a P bit frame. As link distances are very small, the propagation delay is negligible.

The following input parameters are used in the analysis:

Parameter	Description	Unit
C	Link data baud rate	bits /sec
p_b	Link bit error rate	-
l_{data}	I-frame data packet length	bits
l_{oh}	S-frame length / I-frame overhead	bits
t_{ta}	Minimum turn-around time	sec
T_{max}	Maximum turn-around time	sec
W_{max}	Maximum window size	frames

Table 6.1 IrDA analytical model input parameters

The S-frame transmission time t_S and I-frame transmission times t_I are calculated by:

$$t_S = \frac{l_{oh}}{C} \tag{6.1}$$

$$t_I = \frac{l_{data} + l_{oh}}{C} \tag{6.2}$$

The acknowledgement time t_{ack} is the time following the completion of transmission from the primary, for an acknowledgement S-frame to be returned from the secondary and the primary to resume transmission. This therefore requires a turn-around delay at the secondary, the transmission time of the S-frame and a turn-around delay at the primary.

$$t_{ack} = 2t_{ta} + t_S \tag{6.3}$$

The frame error probability p is the probability that there is at least one bit in an I-frame in error, and is therefore related to the link bit error rate p_e by:

$$p = 1 - (1 - p_e)^{l_{oh} + l_{data}} \tag{6.4}$$

The variable window width w is defined as the number of remaining frames (from the start of the current frame) that can be sent before transmission control is passed. With IrDA, the maximum window width is determined by the 'maximum window size' parameter, here denoted W_{max}, negotiated during the link establishment, and the maximum turn-around time combined with the data rate and packet data size which may limit the number of frames that can be sent to below W_{max}. We therefore use a value N to indicate the number of frames that can be sent before transmission is passed to the other station.

$$N = min\left\{W_{\max}, floor\left(\frac{T_{\max}}{t_I}\right)\right\} \tag{6.5}$$

where *min* is 'the lesser of', and *floor* is the rounded down integer.

The F-timer timeout period t_{Fout} could be set to the maximum turn-around time T_{max}, however this could cause an unnecessary delay when the full window is returned well within this period. Therefore we can set the F-timer period to the maximum time (assuming the same packet size) that would be required to return an F-bit packet from the Secondary. This is therefore:

$$t_{Fout} = Nt_I + 2t_{ta} \tag{6.6}$$

6.1.2 Calculation of the Virtual Transmission Time

The average virtual transmission time is determined by summing the frame virtual transmission times for all values of w, multiplied by the probability of the frame having each value of w. This is therefore given by:

$$t_V = \sum_{w=1}^{N} \phi(w) t_v(w) \tag{6.7}$$

where $t_v(w)$ is the virtual transmission time for a frame seeing a window width w, and $\phi(w)$ is the probability that the window width has a specific value of w. The average data throughput D (bits/s) is then given by:

$$D = \frac{l_{data}}{t_V} \tag{6.8}$$

6.1.2.1 Window Width Probability

Each time a frame is transmitted error free (with probability $1 - p$), the window width reduces by 1 (Figure 6.1a). When it reaches 1, the window width returns to its maximum value of N. However if a frame is in error (with probability p) then it and all the following frames in the window will need to be re-transmitted. The next transmission window will therefore begin with re-transmission of the errored frame (Figure 6.1b). Therefore following the successful transmission of the errored frame the window width is $N - 1$. This is demonstrated in Figure 6.1 where sub-Figure (a) represents an error free situation and sub-Figure (b) has frame I30 (I-frame, Ns = 3, Nr = 0) in error.

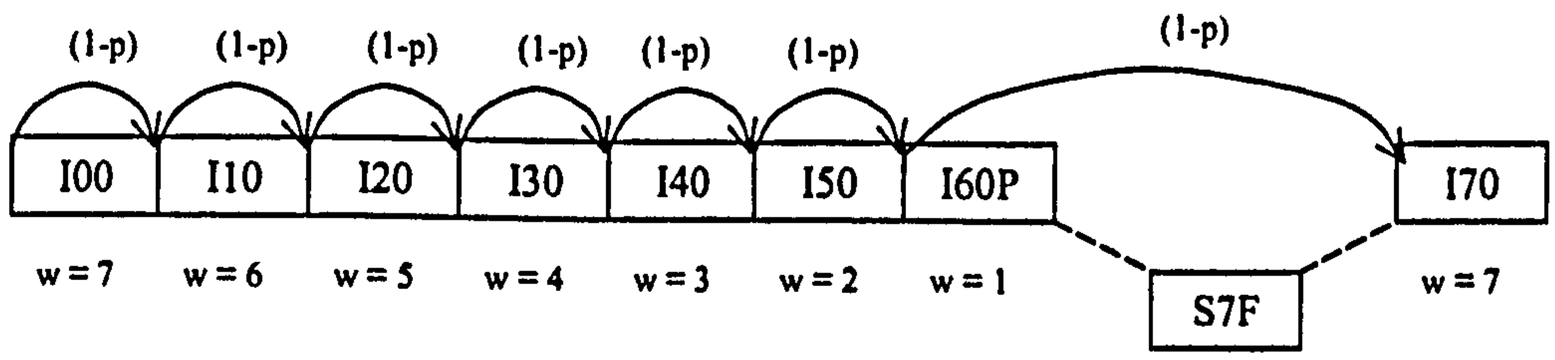

Figure 6.1 Window width states for N = 7
(a) error free, (b) frame I30 in error

The overall process can be considered as a Markov chain with N states representing the widow width values. This can be presented as the state transition diagram shown in Figure 6.2 where the solid line represents an error free frame transmission (with probability 1-p) and the dashed line represents frame error transmission (with probability p).

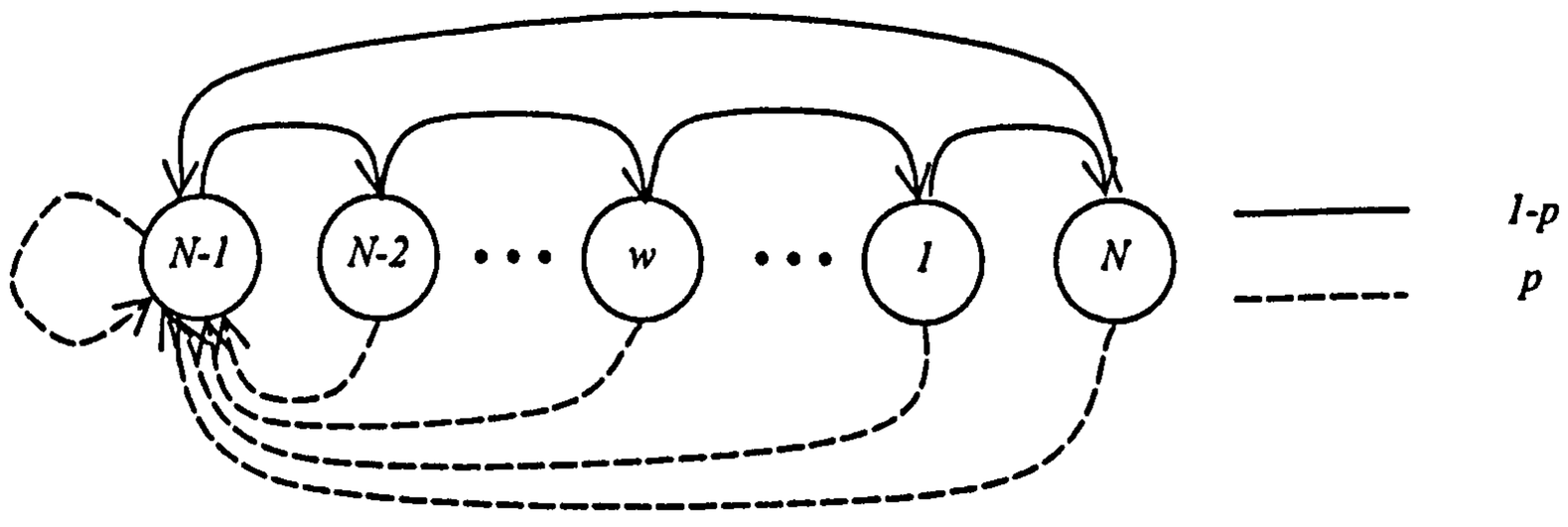

Figure 6.2 Markov process diagram for IrLAP window width process

The value for $\phi(w)$ in (6.7) can then be determined by calculating the 'limiting (i.e. steady-state) probability distribution' for the window width state set in Figure 6.2. The state transition diagram can be represented by the state transition matrix R, where the probability of going from a state i to a state j is given by the element r_{ij}.

$$R = \begin{array}{c|ccccccc} & (N-1) & (N-2) & \cdots & (w) & \cdots & (1) & (N) \\ \hline (N-1) & p & 1-p & 0 & 0 & 0 & 0 & 0 \\ (N-2) & p & 0 & 1-p & 0 & 0 & 0 & 0 \\ \vdots & p & 0 & 0 & 1-p & 0 & 0 & 0 \\ (w) & p & 0 & 0 & 0 & 1-p & 0 & 0 \\ \vdots & p & 0 & 0 & 0 & 0 & 1-p & 0 \\ (1) & p & 0 & 0 & 0 & 0 & 0 & 1-p \\ (N) & 1 & 0 & 0 & 0 & 0 & 0 & 0 \end{array} \tag{6.9}$$

If we define the limiting probability distribution vector Q such that

$$Q = [\phi(N) \quad \cdots \quad \phi(w) \quad \cdots \quad \phi(1)] \tag{6.10}$$

using matrix multiplication we can determine Q by using the Markov equality (see Appendix B):

$$Q = R.Q \tag{6.11}$$

This gives the set of simultaneous equations

$$p\sum_{w=1}^{N-1}\phi(w) + \phi(N) = \phi(N-1) \tag{6.12}$$

$$(1-p)\phi(i) = \phi(i-1) \quad i \in (2, N-1) \tag{6.13}$$

$$(1-p)\phi(1) = \phi(N) \tag{6.14}$$

and

$$\sum_{w=1}^{N}\phi(w) = 1 \tag{6.15}$$

therefore equation (6.12) becomes

$$p(1-\phi(N)) + \phi(N) = \phi(N-1) \tag{6.16}$$

which can be re-arranged as

$$(1-p)\phi(N) + p = \phi(N-1) \tag{6.17}$$

we also get

$$\phi(N) = (1-p)^{N-1}\phi(N-1) \tag{6.18}$$

combining the above we get

$$\phi(N-1) = \frac{p}{1-(1-p)^{N}} \tag{6.19}$$

and since

$$\phi(w) = (1-p)\phi(w+1) \quad w = 1,2\cdots N-1 \tag{6.20}$$

this gives us

$$\phi(w) = \begin{cases} \dfrac{p(1-p)^{N-w-1}}{1-(1-p)^{N}} & w = 1,2\cdots N-1 \\ \dfrac{p(1-p)^{N-1}}{1-(1-p)^{N}} & w = N \end{cases} \tag{6.21}$$

This provides an expression for $\phi(w)$ for equation (6.7) in terms of the packet error probability p and maximum window width W.

6.1.2.2 Window Width Dependent Virtual Transmission Time

The window width dependent VTT $t_v(w)$ is calculated by the addition of the time to transmit the initial frame and the time required for subsequent re-transmissions of the frame multiplied by the probabilities that these re-transmissions are required.

$$t_v(w) = T_0(w) + \sum_{n=1}^{\infty} P_n E[T_n(w)] \tag{6.22}$$

where T_0 is the time to transmit the frame initially P_n is the probability that the n_{th} re-transmission is required, and $E[T_n(w)]$ is the expectation value of the time required for the n_{th} re-transmission.

In calculating the virtual transmission time we need to examine a number of different cases involving whether an error occurred, in what position in the window the error is located, whether there are additional errors in the sequence and in what positions, and whether the re-transmissions of frames are themselves in error.

A. Initial frame transmission time

The transmission time in this situation is simply the transmission time for the I-frame unless the frame is the first frame of a window (i.e. $w = N$) in which case the primary station must wait to receive an acknowledgement from the receiving station for the previously transmitted window before continuing to transmit. This is shown in Figure 6.3.

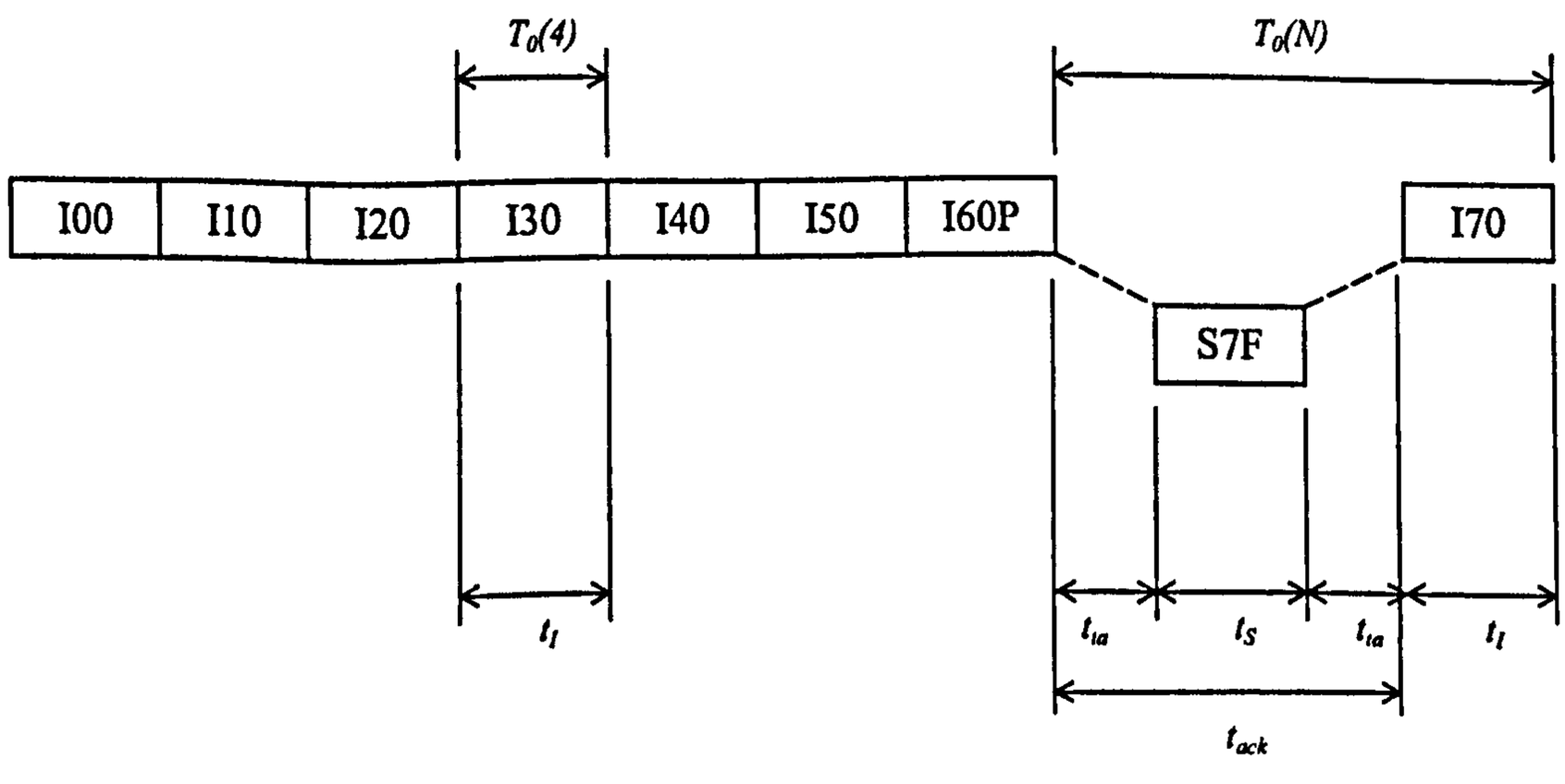

Figure 6.3 Case A transmission times

The initial frame transmission time T_0 is therefore given by:

$$T_0(w) = \begin{cases} t_I & w \neq N \\ t_I + t_{ack} & w = N \end{cases} \qquad (6.23)$$

B. Re-transmission of a frame in error

This case examines the situation where a frame transmitted needs to be re-transmitted because it has been in error. This case has the probability of a single error, i.e. p. The time $T_1(w)$ denotes the time taken from the end of the initial errored frame transmission to the end of the first frame re-transmission. We need to examine whether we have additional errors following the initial error frame, and whether this includes the last frame in the window.

B(i) Single error, not last in window

This is illustrated in Figure 6.4. Here the frame is simply re-transmitted at the end of the sequence and after the S-frame has been returned. The re-transmission time $T_1(w)$ includes the transmission time for any following frames in the window, the acknowledgement time from the secondary and the frame re-transmission time.

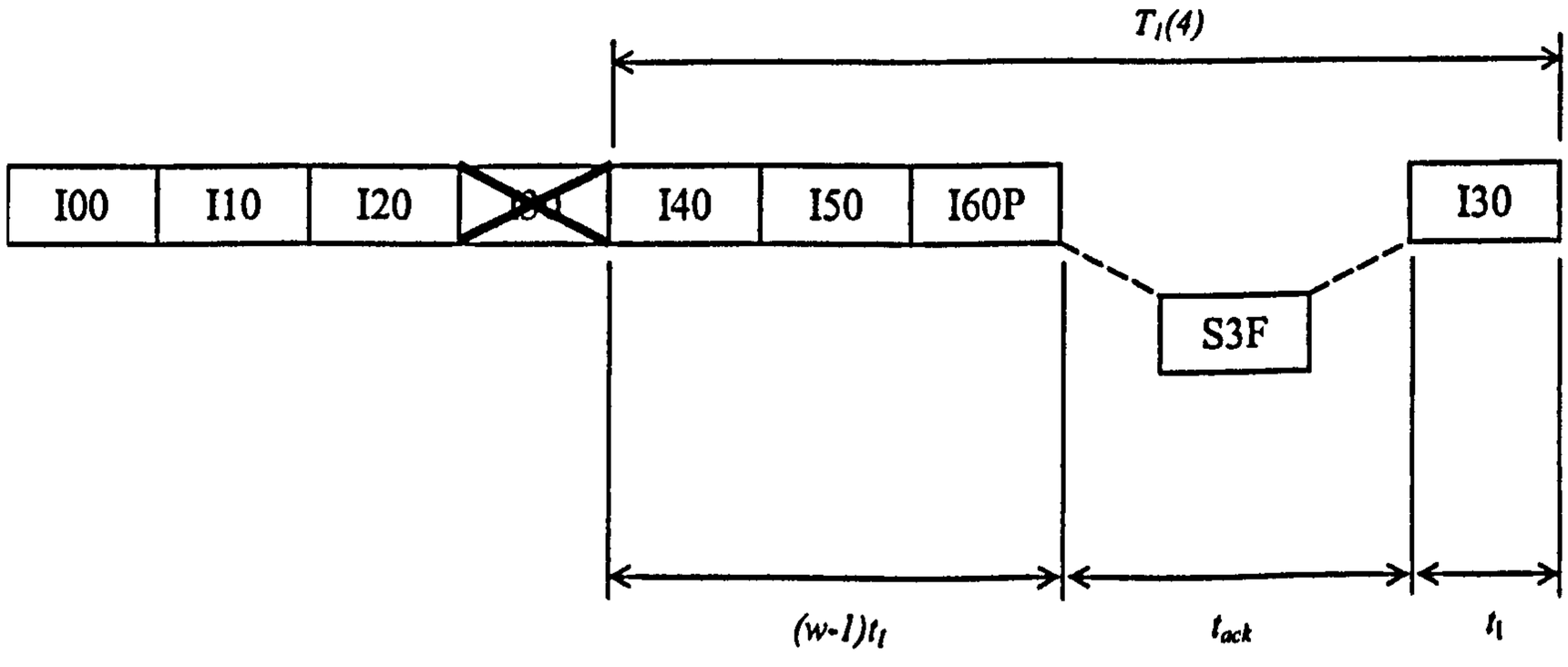

Figure 6.4 Case B(i) re-transmission time

$$T_1(w) = wt_f + t_{ack} \tag{6.24}$$

B(ii) Errors including last in window

This is illustrated in Figure 6.5. In this case the P-bit is lost, therefore the secondary will not know that it can now transmit. If the primary has not received a response when the F-timer has expired a P bit will be sent with an RR S-frame. This situation has an

additional probability of p, i.e. the probability of a specific frame (the last) following the first corrupted frame being in error. Note that additional frame errors within the window not including the P-bit frame will not effect the throughput as all frames from the initial errored frame within the window are retransmitted.

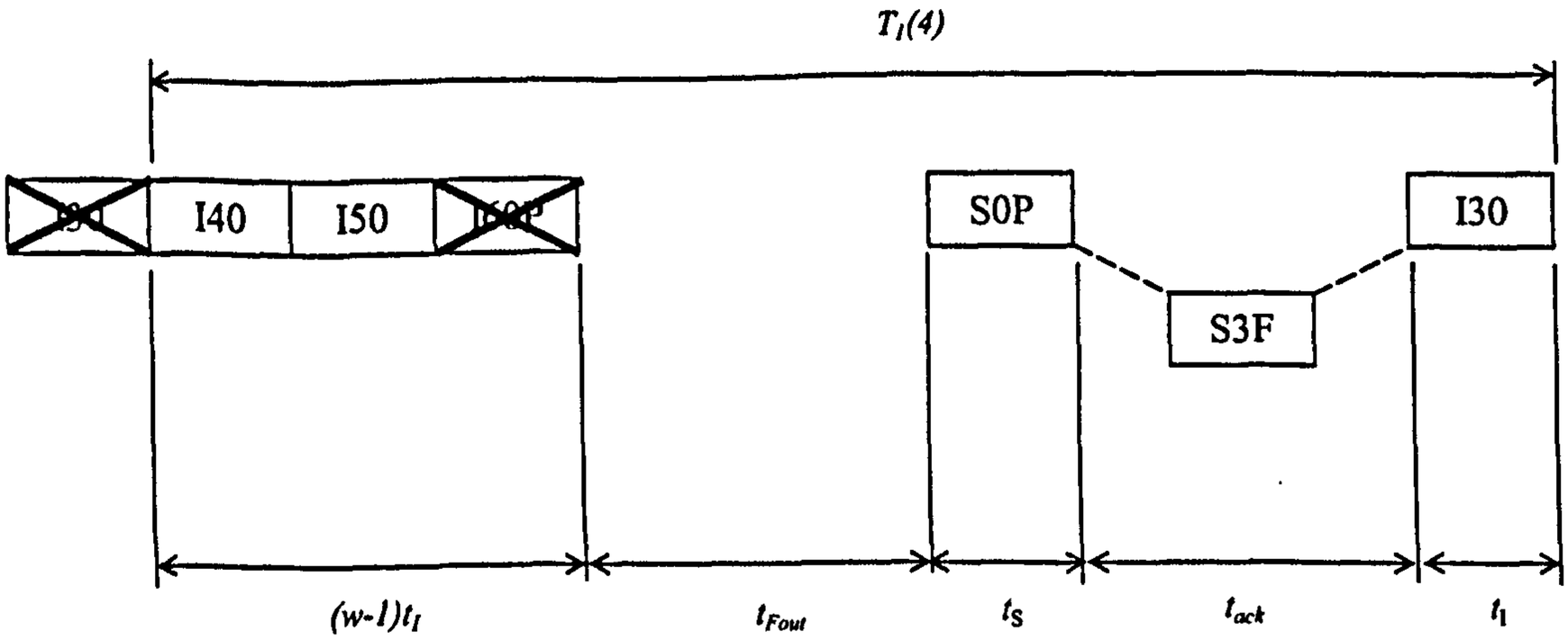

Figure 6.5 Case B(ii) re-transmission time

$$T_1(w) = wt_I + t_{Fout} + t_S + t_{ack} \tag{6.25}$$

B(iii) Single error being the last in the series

This case is the same as case B(ii) above with w = 1 except that there is only one error in the sequence, thus there is only the single error probability.

Therefore by combining equations (6.24) and (6.25), with the stated additional probabilities the overall expectation value of $T_1(w)$ and the probability P_1 can be given by:

$$P_1 = p \tag{6.26}$$

$$E[T_1(w)] = \begin{cases} wt_I + p(t_{Fout} + t_S) + t_{ack} & w \neq 1 \\ t_I + t_{Fout} + t_S + t_{ack} & w = 1 \end{cases} \tag{6.27}$$

C. Secondary re-transmissions due to subsequent frame errors

As the initial resent frame will be the first in the window, all N frames will be re-transmitted. Therefore the re-transmitted frame will always be the first in the window. However as before if the last frame of the sequence is also in error, the P bit will not be received so the recovery only begins when the F-timer expires. The probability of n successive transmissions of the same frame being in error is p^n. Thus we have:

$$P_n = p^n \quad n \geq 2 \tag{6.28}$$

and by using:

$$\sum_{n=2}^{\infty} p^n = \frac{p^2}{(1-p)} \tag{6.29}$$

gives:

$$\sum_{n=2}^{\infty} P_n E[T_n(w)] = \frac{p^2}{(1-p)} T_2 \tag{6.30}$$

where T_2 is the time for each successive re-transmission of the frame and is now independent of the window width w, given by:

$$T_2 = \begin{cases} Nt_I + p(t_{Fout} + t_S) + t_{ack} & N \neq 1 \\ t_I + t_{Fout} + t_S + t_{ack} & N = 1 \end{cases} \tag{6.31}$$

The overall virtual transmission time for a specific value of w can therefore be determined by using the expression in equation (6.22) and applying the derived expressions for the expectations of the individual cases as shown above, combined with the stated probabilities of each case arising.

$$t_v(w) = T_0(w) + pE[T_1(w)] + \frac{p^2}{(1-p)} T_2 \tag{6.32}$$

In summary the saturation condition throughput D (bits/s) is given by:

Throughput

$$D = l_{data} / t_V$$

Average virtual transmission time

$$t_V = \sum_{w=1}^{N} \phi(w) t_v(w)$$

Window width probability

$$\phi(w) = \begin{cases} \dfrac{p(1-p)^{N-w-1}}{1-(1-p)^N} & w = 1,2 \cdots N-1 \\ \dfrac{p(1-p)^{N-1}}{1-(1-p)^N} & w = N \end{cases}$$

Window width dependent virtual transmission time

$$t_v(w) = T_0(w) + pE[T_1(w)] + \frac{p^2}{(1-p)} T_2$$

Packet error probability

$$p = 1-(1-p_b)^{l_{oh}+l_{data}}$$

Calculated window size

$$N = min\left\{W_{\max}, floor\left(\frac{T_{\max}}{t_I}\right)\right\}$$

Initial frame transmission time

$$T_0(w) = \begin{cases} t_I & w \neq N \\ t_I + t_{ack} & w = N \end{cases}$$

First re-transmission expectation time

$$E[T_1(w)] = \begin{cases} wt_I + p(t_{Fout} + t_S) + t_{ack} & w \neq 1 \\ t_I + t_{Fout} + t_S + t_{ack} & w = 1 \end{cases}$$

Second and above re-transmission time

$$T_2 = \begin{cases} Nt_I + p(t_{Fout} + t_S) + t_{ack} & N \neq 1 \\ t_I + t_{Fout} + t_S + t_{ack} & N = 1 \end{cases}$$

S-frame and I-frame transmission times

$$t_S = \frac{l_{oh}}{C} \qquad t_I = \frac{l_{data} + l_{oh}}{C}$$

Acknowledgement time

$$t_{ack} = 2t_{ta} + t_S$$

F-timer duration

$$t_{Fout} = Nt_I + 2t_{ta}$$

These expressions therefore provide the saturation throughput in relation to the data rate, link BER and IrLAP parameter settings of data packet size, window size, maximum turn-around time and minimum turn-around time (Barker and Boucouvalas, 1998a; Barker and Boucouvalas, 1998b; Barker and Boucouvalas, 1998c; Barker et al., 2000).

6.1.2.3 Bi-directional Data Flow Throughput

The model has so far assumed that the secondary returns error-free S-frame acknowledgements only. However, if both the primary and secondary are transmitting saturated data, the acknowledgement time seen at the primary would be extended to cover the return of a full I-frame window from the secondary.

$$t_{ack} = Nt_I + 2t_{ta} \tag{6.33}$$

The throughput from the primary to the secondary will not concern errors in the returned I-frames from the secondary unless the last frame in the window (with F-bit set) is lost causing expiration of the F-timer. There is therefore an additional probability that the F-timer will expire (i.e. if either the last frame in the transmitted window or the last frame in the returned window are in error). Following expiration of the F-timer an S-frame is transmitted to the secondary (assumed error free). The secondary will then transmit the next window of I-frames (with re-transmissions if errors occurred) with the F-bit on the final frame. There is therefore a probability of further F-timer expirations if the last returned frame is again in error. Assuming the same frame error rate in both directions, the window width dependent virtual transmission time $t_v(w)$ is now given by:

$$t_v(w) = T_0(w) + pE[T_1(w)] + \frac{p^2}{(1-p)}T_2 + \frac{p}{(1-p)}(t_{Fout} + t_S) \tag{6.34}$$

6.1.2.4 F-timer Duration

If the P-bit frame or returned F-bit frame from the secondary is lost, the primary must wait for the expiration of the F-timer before sending an S-frame to re-poll the secondary. This delay can significantly affect the link throughput. The secondary station will only return data frames if it immediately has data available to transmit. The F-timer period may then be set to the maximum duration that may be required to return the F-bit in a sequence of data frames. The F-timer duration has therefore been given as:

$$T_{F-timer} = t_{ta} + Nt_I \tag{6.35}$$

However this duration can still be excessive in respect to the acknowledgement time if the secondary is not returning data but only returning an S-frame. Generally the primary cannot know if the secondary has data to transmit or not and thus must set the F-timer to the duration as given. However there may be some applications where the secondary will only reply with S-frames (e.g. a printing application) in which case the F-timer may be set to cover this acknowledgement timer only:

$$T_{F-timer} = t_{ta} + t_S \tag{6.36}$$

In practice an additional small delay may also be required for processing of the received F-bit frame or the timer 'latched' until any frame reception and processing is complete.

6.1.3 Optimum Packet Length and Window Size

The throughput of a link for a particular BER is affected by the packet length and window size parameter settings such that optimum values can be determined to maximise the throughput. This is achieved by finding the value for which the first order derivative of the throughput with respect to the parameter is at zero, i.e.:

$$l_{data} \text{ such that } \frac{dD_b(l_{data})}{dl_{data}} = 0 \tag{6.37}$$

$$\text{and } W_{max} \text{ such that } \frac{dD_b(W_{\max})}{dW_{\max}} = 0 \tag{6.38}$$

It is possible to find the exact analytical first order derivative of the throughput with respect to l_{data} and W_{max}, but this would be mathematically complex. By using suitable approximations (Vitsas and Boucouvalas, 2000; Vitsas and Boucouvalas, 2001a; Vitsas and Boucouvalas, 2001c) expressions for the optimum window and packet size have been obtained.

Using the approximations $l_{\text{data}} \approx l_{\text{data}} + l_{\text{oh}}$ and $p \approx l_{\text{data}} p_{\text{e}}$ the optimum window size is given as:

$$N(Opt) \approx \sqrt{\frac{2t_{ack}C}{l_{data}{}^{2} p_{e}}} \tag{6.39}$$

and using the approximations and $p \approx (l_{\text{data}} + l_{\text{oh}})p_{\text{e}}$ and $(1 - p)/p \approx 1/p$ the optimum packet size is given as:

$$l_{data}(Opt) \approx \sqrt{\frac{2(Nl_{oh} + t_{ack}C)}{N^{2} p_{e}}} \tag{6.40}$$

A more accurate solution can be obtained using a numerical method. This determines the numerical first order derivative by calculating the change in throughput for a unit change in window size and packet length.

$$\frac{dD_{b}(N)}{dN} \approx D_{b}(N) - D_{b}(N+1) \tag{6.41}$$

$$\frac{dD_{b}(l_{data})}{dl_{data}} \approx D_{b}(l_{data}) - D_{b}(l_{data}+1) \tag{6.42}$$

The value for which the derivatives equate to zero is determined by a successive approximation algorithm. This is demonstrated with the following pseudo code for the window size where WMAX is the maximum range of the window size and N is the number of iterations for the algorithm (Gerald and Wheatley, 1999).

```
N = 1
for i = 1:k
        diff = thrpt(N) – thrpt(N+1);
        if (diff > 0)
                N = floor(N + WMAX / 2^i);
        else
                N = floor(N – WMAX / 2^i);
        end
end
```

The larger the value of k, the higher the degree of accuracy. It can be seen from equations (6.37) and (6.38) that the optimum window size is dependent on the packet size and the optimum packet size dependent on the window size. It would therefore be advantageous to obtain the simultaneous optimisation of the both the packet size and window size (Boucouvalas and Vitsas, 2001).

This can be obtained by solving for the partial simultaneous differential equation.

$$\frac{\partial D_b(N)}{\partial N} = \frac{\partial D_b(l_{data})}{\partial l_{data}} = 0 \tag{6.43}$$

This produces the approximate results (Vitsas and Boucouvalas, 2001b)

$$N(Opt)^* = \sqrt{\frac{2t_{ack}C}{l_{oh}}} \tag{6.44}$$

$$l_{data}(Opt)^* = \sqrt{\frac{l_{oh}}{p_e}} \tag{6.45}$$

* = only optimum when both parameters are simultaneously optimised.

It can be seen that the optimum window size is dependent on the minimum turn-around delay and the link data rate but is independent of the bit-error-rate. Conversely the optimum packet size is dependent on the bit-error-rate but is independent of the data rate and minimum turn-around delay. These results can also more accurately be obtained as before with numerical optimisation.

6.1.4 Validation of IrLAP Analytical model

The graph in Figure 6.6 shows a comparison of results for a 4 Mbits/s link from the analytical model and the OPNET simulation described in appendix A The graph demonstrates a good agreement between the two results. Table 6.2 shows comparison numerical results from the analytical and simulation models for the 4 Mbits/s link with a turn-around time of 0.1 ms and using a simulation time of 100 seconds. Differences are principally due to the simulation time taken for the simulation run. For the simulations for BER values of 10^{-9} and $2x10^{-9}$, no errors occurred during the simulation time. For the BER values of $4.8x10^{-4}$ and 10^{-3}, all packets were in error during the simulation time.

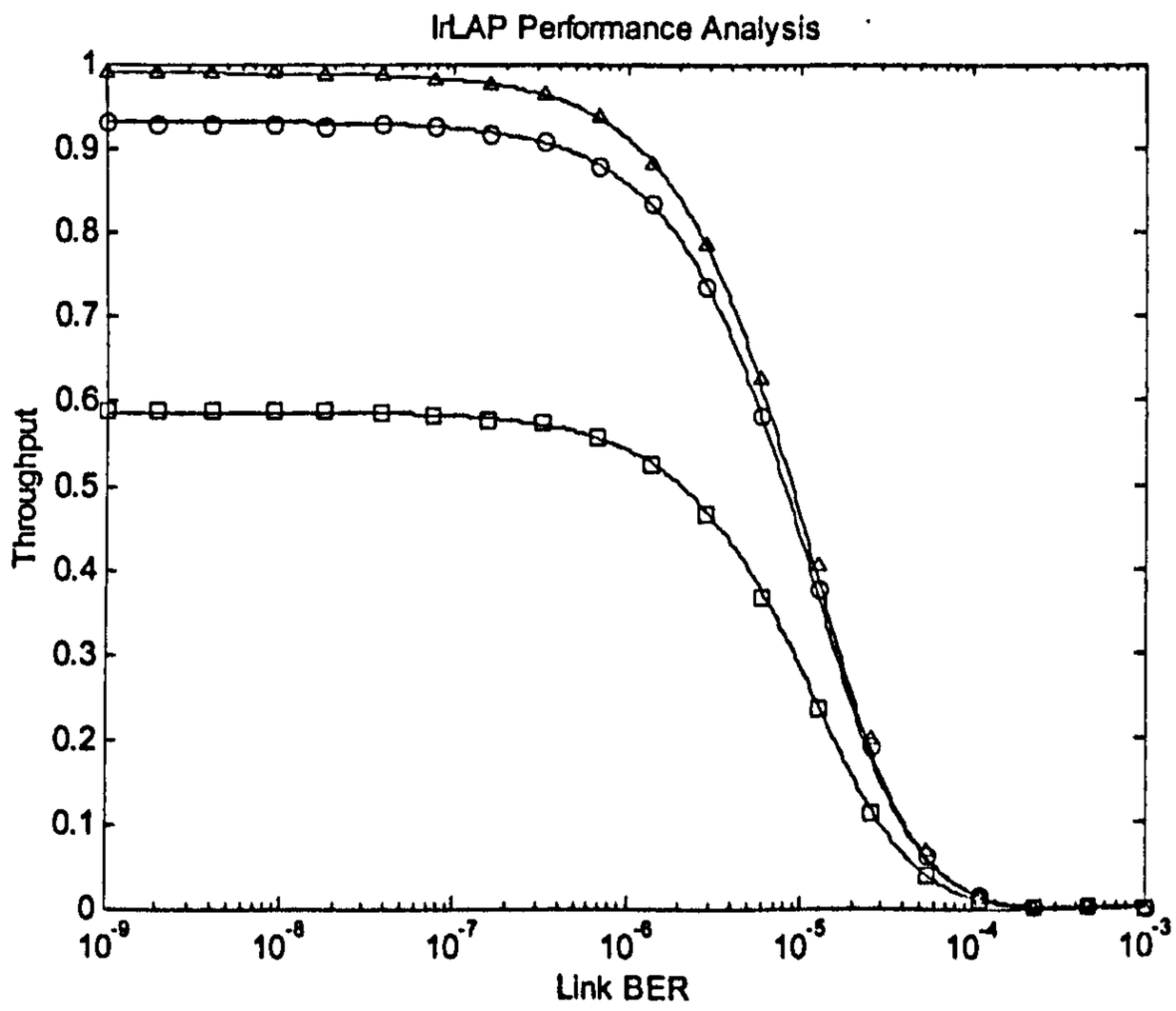

Figure 6.6 Simulation and analysis model results comparison for 4 Mbits/s IrDA link

BER	Throughput Efficiency (Analysis)	Throughput Efficiency (Simulation)
1e-9	0.988608404	0.988652
2e-9	0.988527163	0.988652
4e-9	0.988364704	0.988324
9e-9	0.987958701	0.988201
1.8e-8	0.987228417	0.98689
3.8e-8	0.985607960	0.984433
7.8e-8	0.982376928	0.981647
1.6e-7	0.975794286	0.974602
3.3e-7	0.962320818	0.962724
6.9e-7	0.934543253	0.937165
1.4e-6	0.882623745	0.886866
2.9e-6	0.784270692	0.789996
6.1e-6	0.616598022	0.621036
1.3e-5	0.385803960	0.383427
2.6e-5	0.186672727	0.190792
5.4e-5	0.062094262	0.062587
1.1e-4	0.015085827	0.014377
2.3e-4	0.001665257	0.001393
4.8e-4	2.632210195e-5	0
1e-3	5.044571374e-9	0

Table 6.2 Numerical comparison of 4 Mbits/s IrDA 1.x simulation and analysis results

6.2 IrLAP Analysis Results

The following performance results are produced using the IrLAP throughput expressions derived in the previous section. Numerical optimisation results are presented for data packet size and transmission window size.

6.2.1 IrDA SIR 115.2 kbits/s Analysis

Figure 6.7a shows throughput efficiency versus data packet size for a 115.2 kbits/s link with a BER of 10^{-9} and minimum turn-around times of 10, 1 and 0.1 ms. This also uses the maximum requested window size for IrDA SIR of 7 frames. It can be seen that the throughput increases with packet size as the relative size of the overhead from the frames and minimum turn-around time is reduced. The 'jerky' nature of the analysis plot at the higher packet sizes is due to the quantised reduction in the calculated window size that can be transmitted within the maximum turn-around time of 500 ms. Note that at the maximum specified packet size of 16384 bits (2 Kbytes) at 115.2 kbits/s, the maximum window size that can be transmitted within 500 ms is only 3 frames. Figure

6.7b shows the performance for the same configuration but with a BER of 10^{-5}. It can be seen that the throughput initially rises, peaks (at around 10^3 bits for a turn-around time of 0.1 ms) and then falls as the probability of packet error increases. This demonstrates the requirement for optimisation of the data packet size to maximise throughput. It is also seen that the optimum packet size is higher (although the maximum throughput is lower) for a higher minimum turn-around time.

Figure 6.8a shows throughput efficiency versus requested window size for 115.2 kbits/s with a BER of 10^{-9} and maximum data packet size of 16384 bits. This shows how the throughput improves as the window size increases from 1 to the maximum of 3. Figure 6.8b shows the performance for the same configuration but with a BER of 10^{-5}. For this error rate the performance reduces as the window size increases. However the change in throughput, particularly for a small turn-around time, is minor and only significantly affected by a change in the packet size.

Figure 6.9 shows the optimum packet size for the 115.2 kbits/s link with the maximum requested window size of 7 frames. The nature of the plots at low BER values is due to the quantised reduction in the frames that can be transmitted within the 500 ms maximum transmission time. The data packet size maximises at the maximum size that can be send within 1 frame within the maximum transmission time of 500 ms, calculated as 57551 bits. Note that this exceeds the maximum specification packet size of 16384 bits. Figure 6.10 shows the optimum window size for the 115.2 kbits/s link with a data packet size of 16384 bits. It can be seen that the optimum window size changes from 2 frames to 1 frame but at a BER value that increases with the minimum turn-around time.

Figure 6.11 shows the optimised data packet size for the 115.2 kbits/s link with simultaneously optimised transmission window size. This shows an effective independence of the optimum packet size from minimum turn-around delay until the reduction of the window size. Figure 6.12 shows the optimised window size for the 115.2 kbits/s link with simultaneously optimised data packet size. The window size increases with decreasing BER until the increasing packet size causes a reduction in the

window size that can be transmitted within the maximum transmission time of 500ms. For the 10 ms minimum turn-around delay, the optimum window size increases beyond the maximum 7 frames.

Figure 6.13 shows throughput efficiency versus BER using maximum, optimum and simultaneous optimum packet sizes and window sizes. It can be seen that simultaneous optimisation improves the performance over using maximum values. At a BER of 10^{-4}, the throughput efficiency improves by approximately 75% with optimisation. It can also be seen that the greater effect is from optimisation of the data packet size. At a BER of 10^{-4}, the throughput efficiency improvement from packet size optimisation alone is approximately 65%. Figure 6.14 shows throughput against link distance using the derived BER expression for 115.2 kbits/s with transmitter radiant intensity of 109 mW/Sr, receiver bandwidth of 250 KHz and link parameters from Tables 4.3. This shows that optimisation provides a more gradual 'fall off' in throughput with link distance than with maximum values which is quite abrupt. The 'cut-off' distance at this data rate can be seen to increase by approximately 1 meter.

In summary, simultaneous optimum values are found for the data packet size and transmission window size that maximise throughput for a given BER value and minimum turn-around delay time. The effect of optimisation is to increase the throughput for a given BER over fixed values. The dominant effect is that from optimisation of the data packet size.

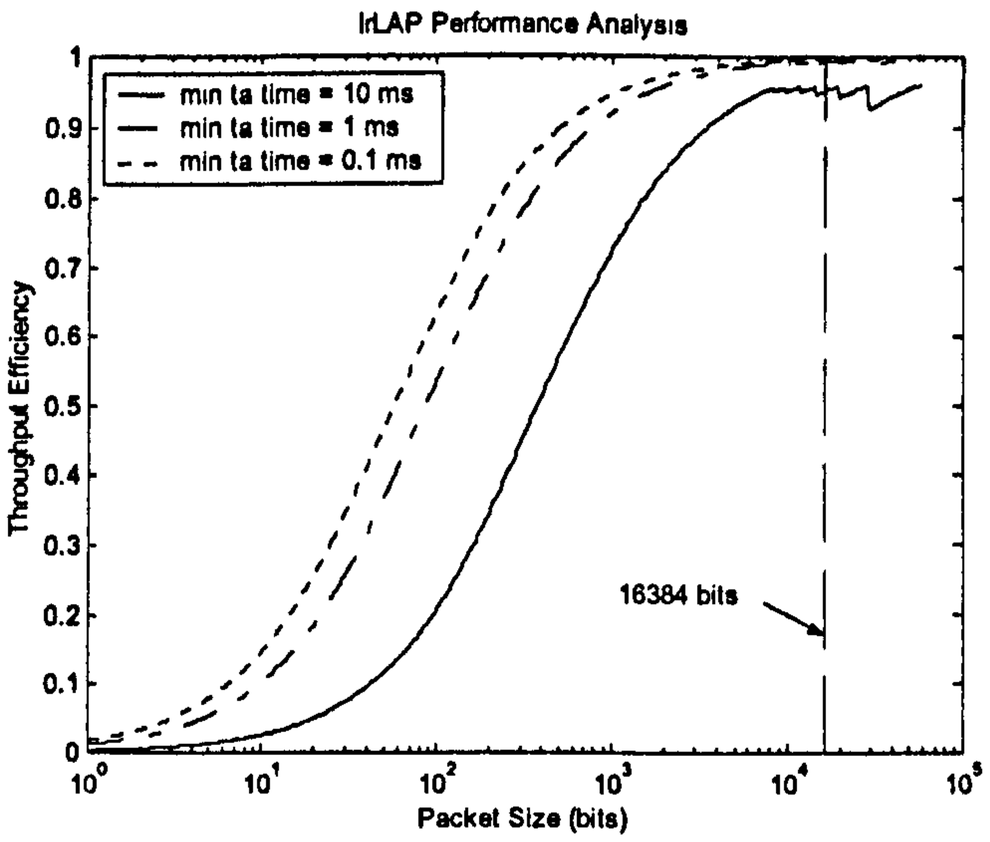

a) BER = 10^{-9}

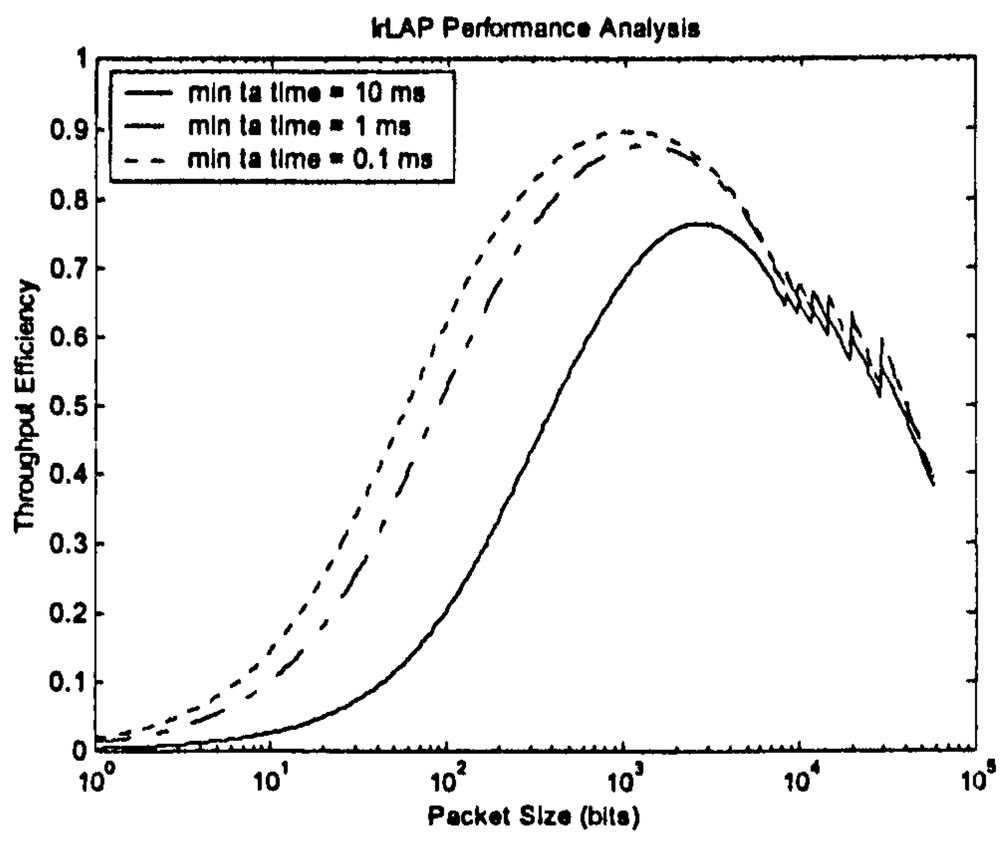

b) BER = 10^{-5}

data rate = 115.2 kbits/s
max ta time = 500 ms
window size = 7 frames
overhead = 48 bits

Figure 6.7 Throughput versus packet size for 115.2 kbits/s IrDA SIR link

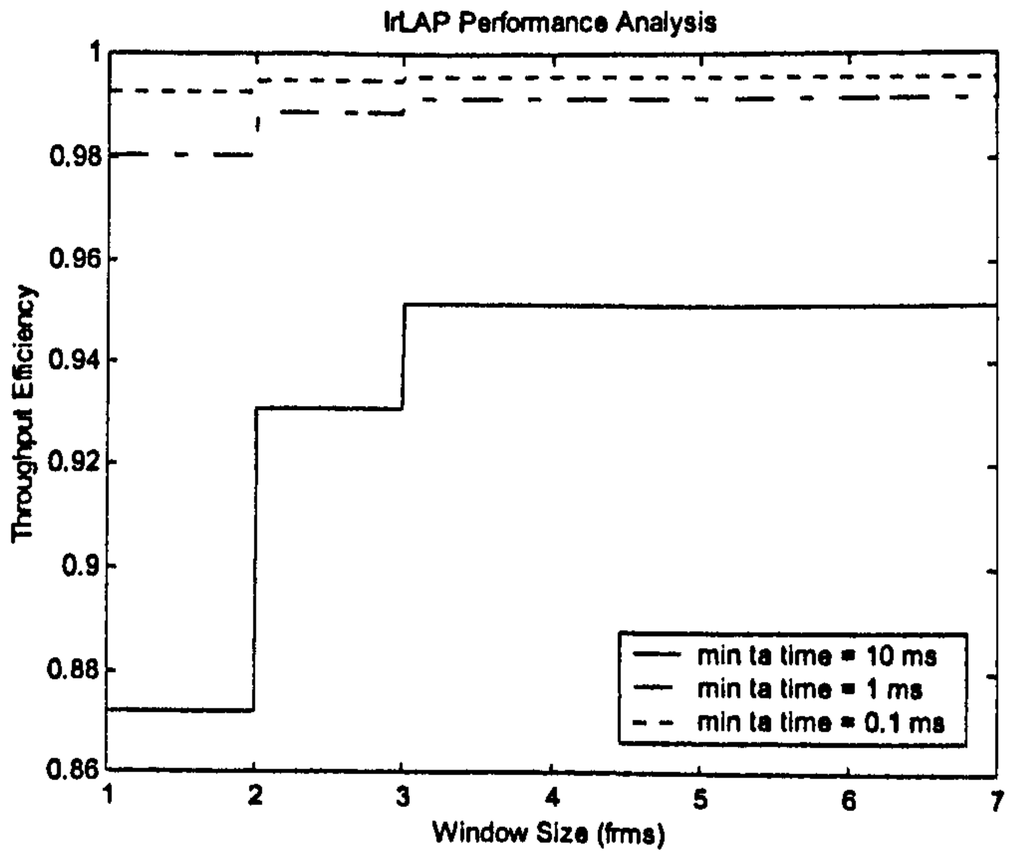

a) BER = 10^{-9}

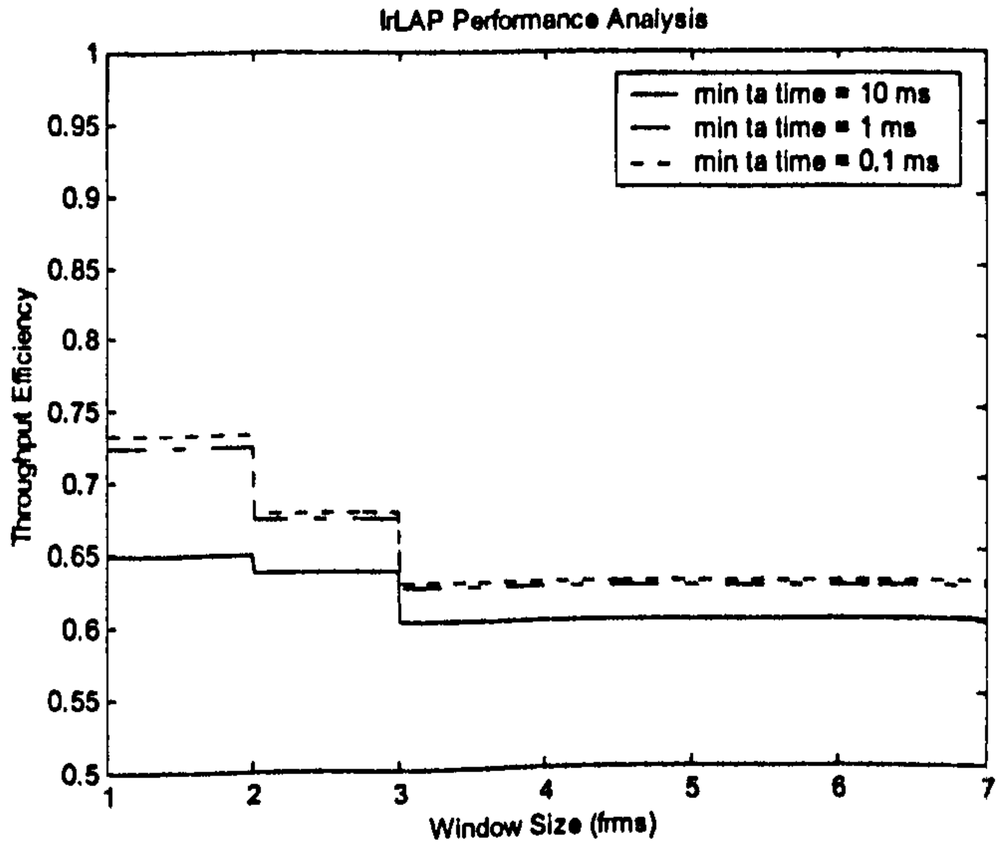

b) BER = 10^{-5}

data rate = 115.2 kbits/s
max ta time = 500 ms
packet size = 16384 bits
overhead = 48 bits

Figure 6.8 Throughput versus window size for 115.2 kbits/s IrDA SIR link

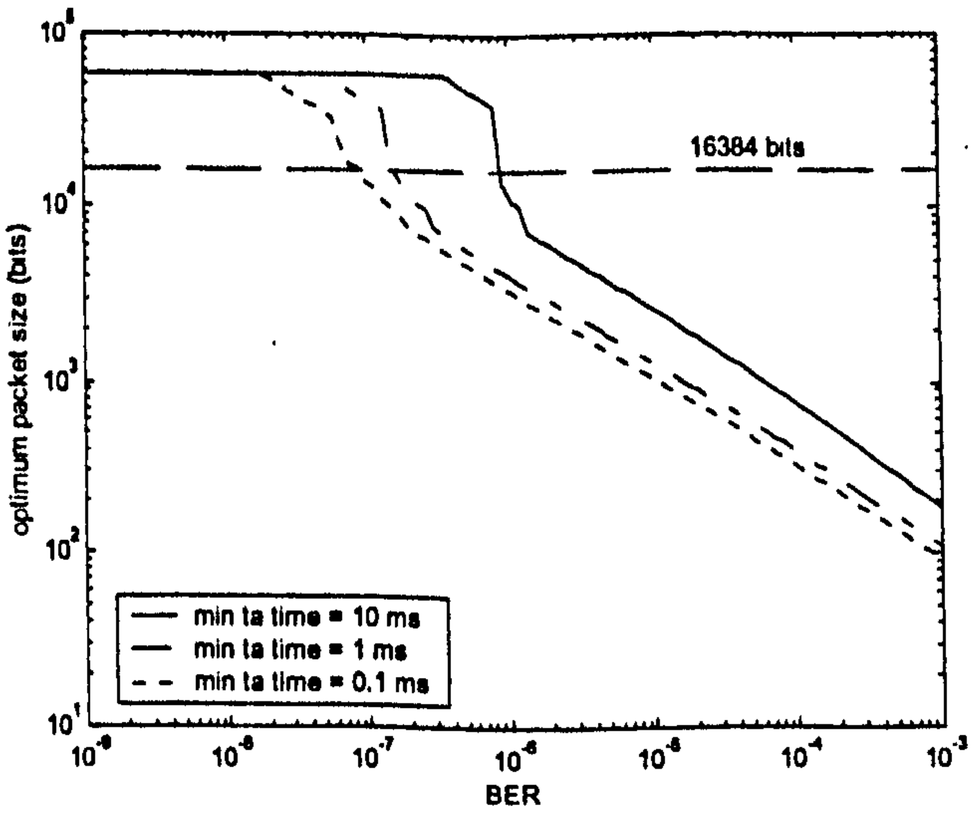

data rate = 115.2 kbits/s window size = 7 frames
max ta time = 500 ms overhead = 48 bits

Figure 6.9 Optimum packet size versus link BER for 115.2 kbits/s

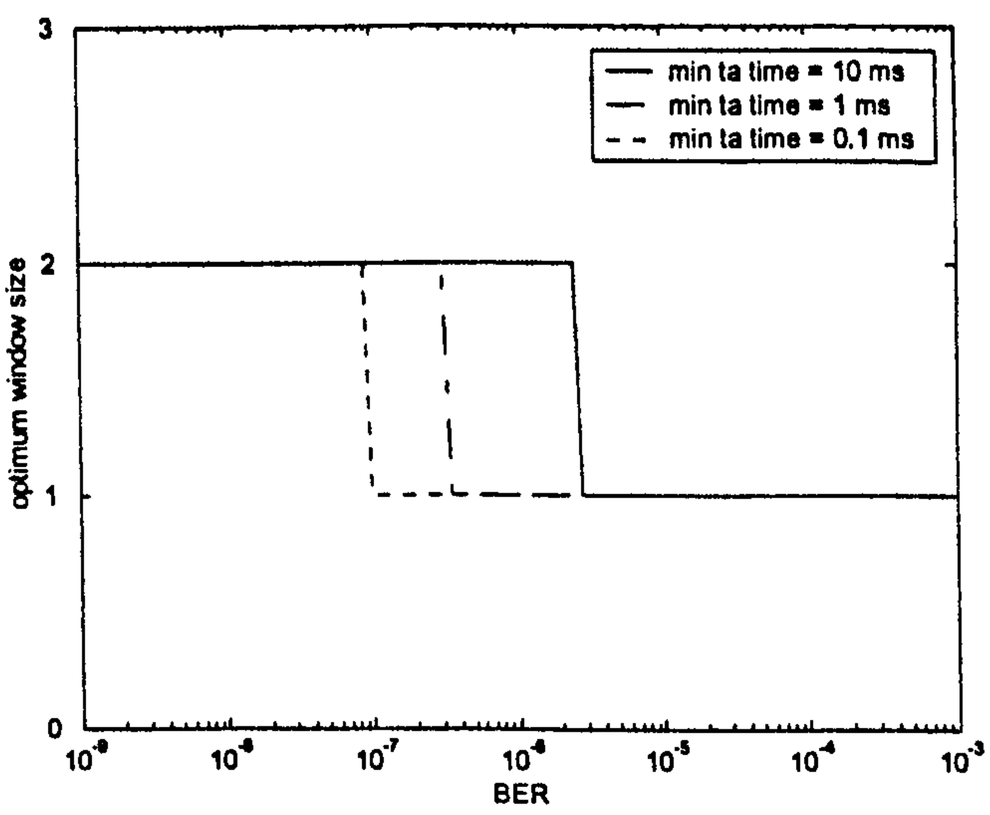

data rate = 115.2 kbits/s packet size = 16384 bits
max ta time = 500 ms overhead = 48 bits

Figure 6.10 Optimum window size versus BER for 115.2 kbits/s

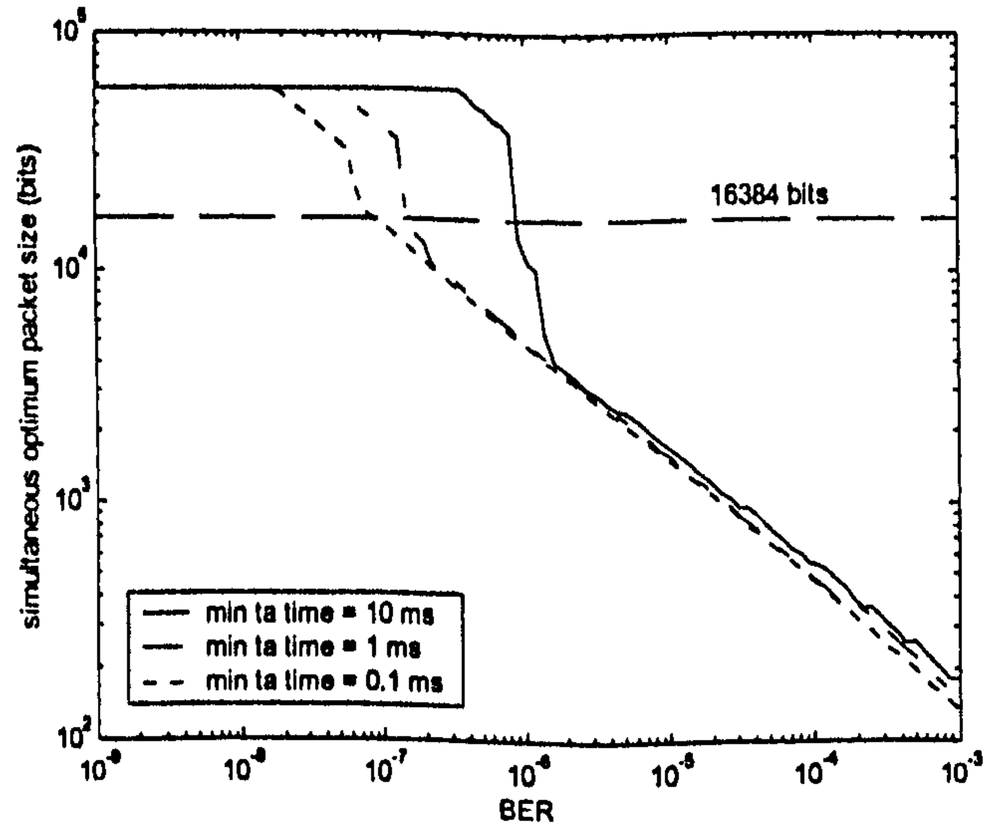

data rate = 115.2 kbits/s window size = optimum
max ta time = 500 ms overhead = 48 bits

Figure 6.11 Simultaneous optimum packet size versus link BER for 115.2 kbits/s

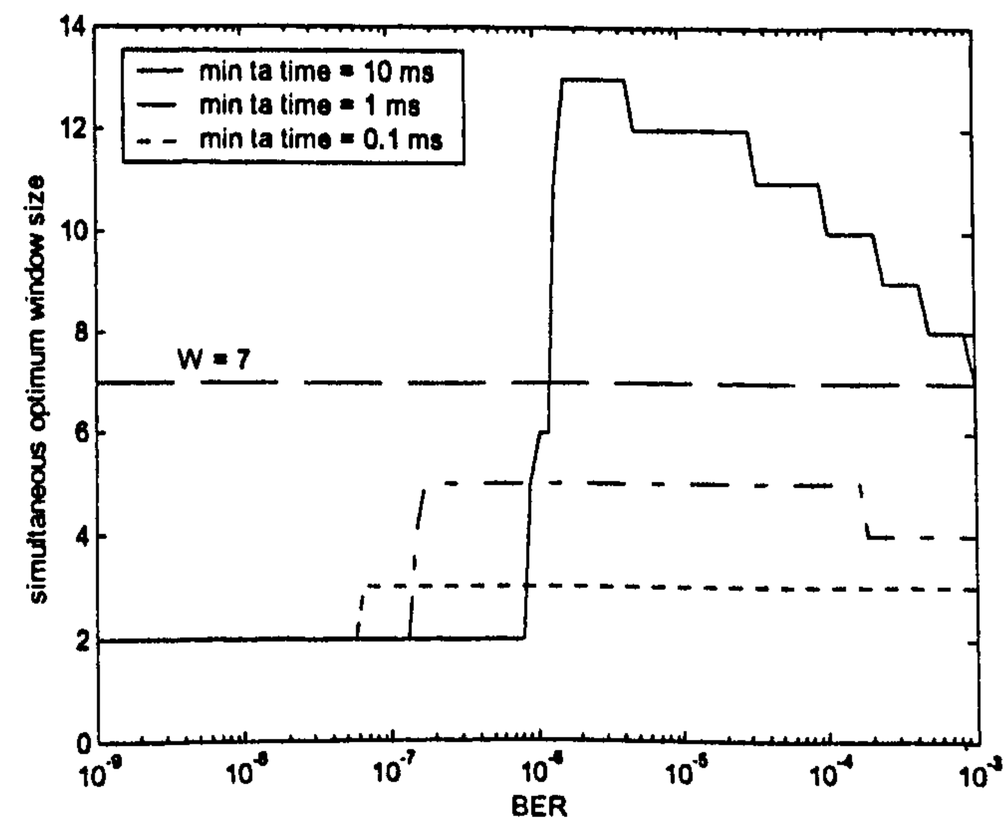

data rate = 115.2 kbits/s packet size = optimum
max ta time = 500 ms overhead = 48 bits

Figure 6.12 Simultaneous optimum window size versus BER for 115.2 kbits/s

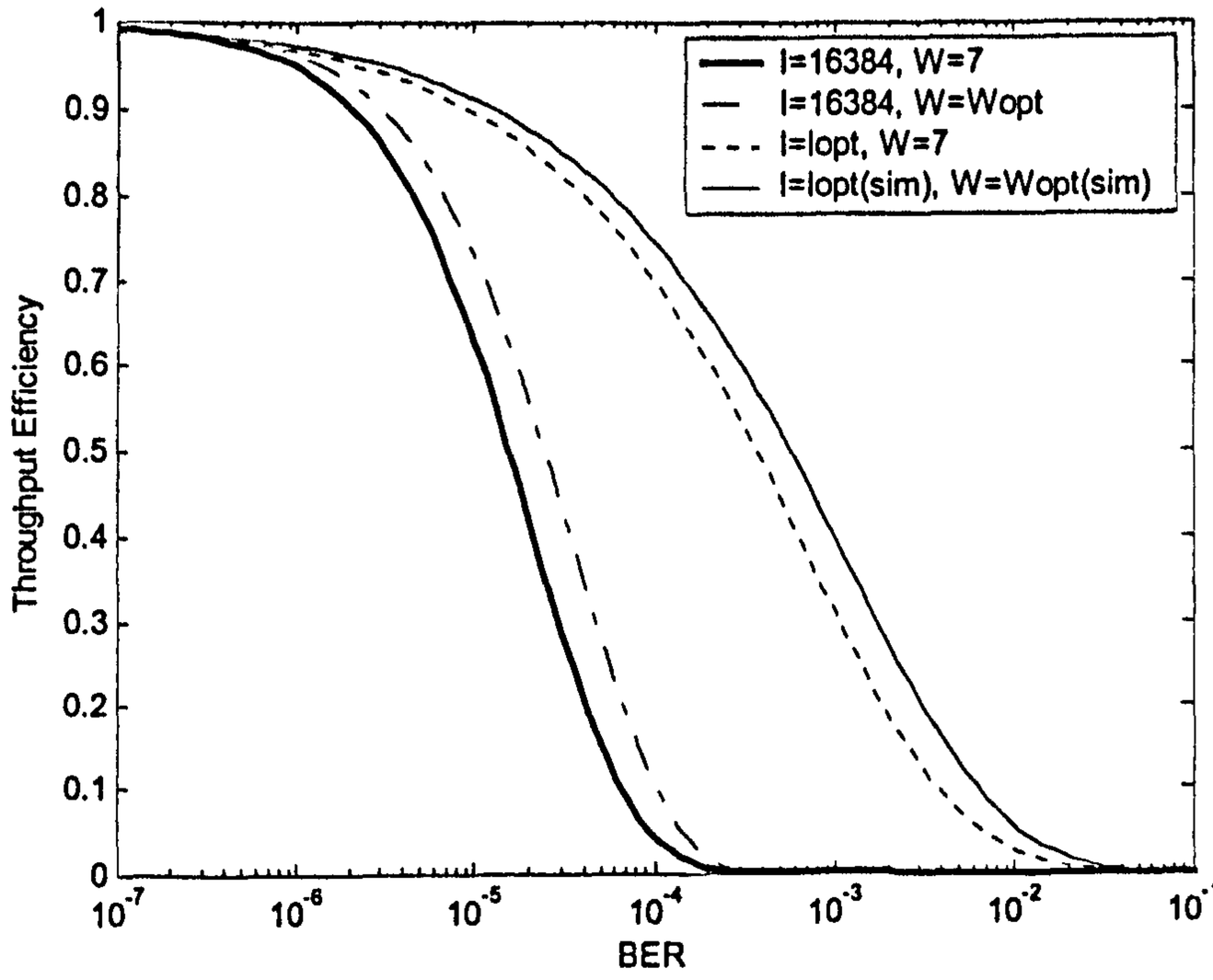

data rate = 115.2 kbits/s
max ta time = 500 ms
min ta time = 0.1 ms
overhead = 48 bits

Figure 6.13 Throughput efficiency versus link BER for 115.2 kbits/s link with maximum and optimum packet and window sizes

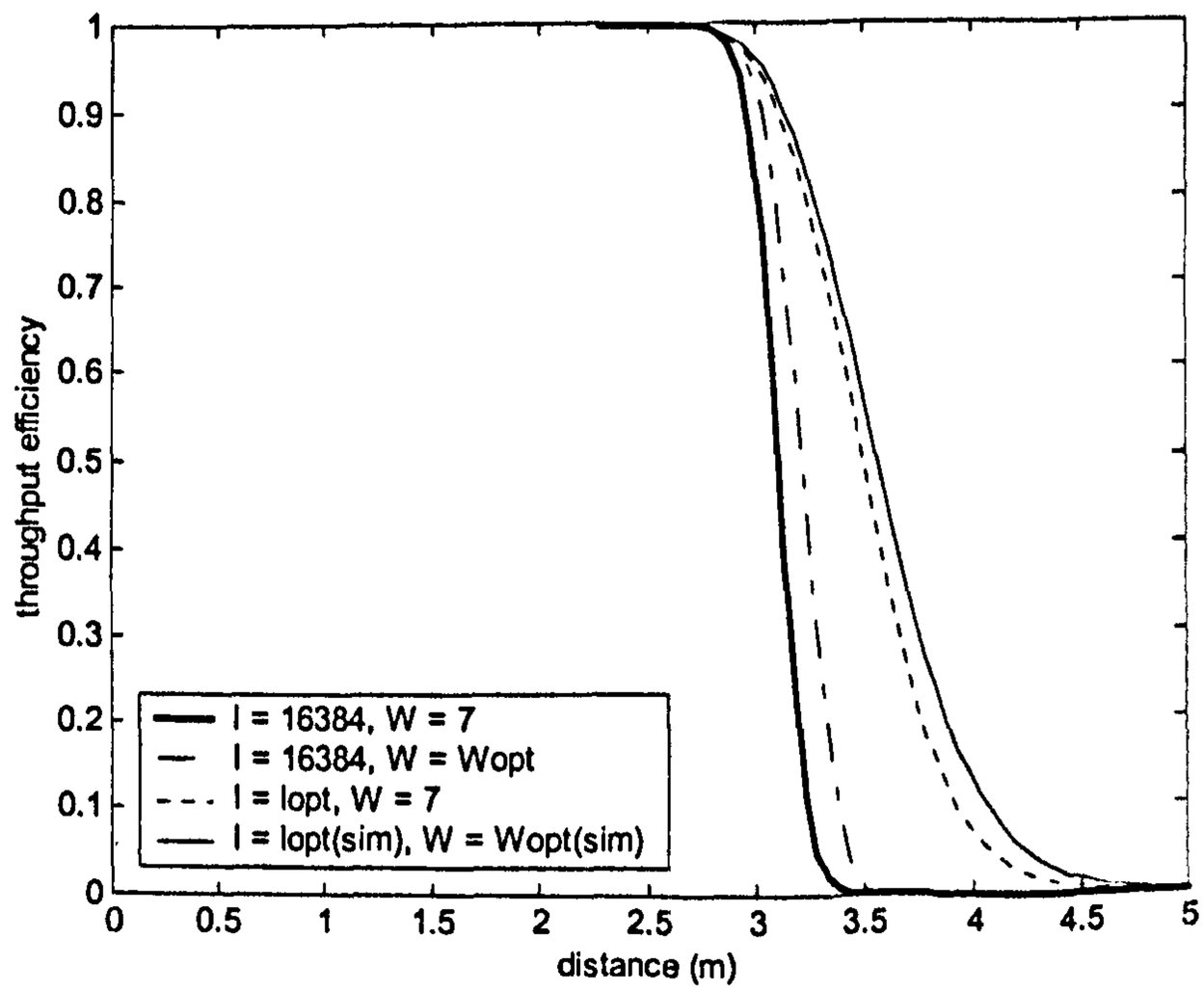

data rate = 115.2 kbits/s
max ta time = 500 ms
transmitter power = 109 mW/Sr
min ta time = 0.1 ms
overhead = 48 bits
bandwidth = 250 KHz

Figure 6.14 Throughput efficiency versus link distance for 115.2 kbits/s 3/16 RZI link with maximum and optimum packet and window sizes

6.2.2 IrDA FIR 4 Mbits/s Analysis

Figure 6.15a shows throughput efficiency versus packet size for the 4 Mbits/s link with the maximum window size of 7 frames and BER of 10^{-9}. It can be seen that at this higher data rate, the minimum turn-around time has a greater significance. This is because the link is turned round much more frequently than for the 115.2 kbits/s link. It can be seen that all 7 packets of the window are transmitted within the maximum turn-around time of 500ms at the maximum packet size of 16384 bits. Figure 6.15b shows throughput efficiency versus packets size for the same configuration but with a BER of 10^{-5}. It can be seen that the greater effect of the minimum turn-around time causes a greater degradation of throughput when packet errors arise.

Figure 6.16a shows throughput efficiency versus window size with packet size of 16384 bits for the 4 Mbits/s link. The analysis here extends the window size beyond the maximum 7 frames to 100 frames to examine if an extension of the maximum window size would be beneficial. It can be seen that if a large minimum turn-around delay is used, the throughput can benefit from a window size greater than 7 frames. Figure 6.16b shows the same configuration but with a BER of 10^{-5}. Here the throughput falls with greater window size as a larger average number of frames require re-transmission from a frame error. However for a large minimum turn-around delay, the throughput can be seen to initially rise as the larger window size reduces the relative acknowledgement delay.

Figure 6.17 shows the optimum packet size versus link BER for the 4 Mbits/s link using the maximum window size of 7 frames. It can be seen that the optimum packet size for good BER is generally much larger than the maximum specification of 16384 bits. Figure 6.18 shows optimum window size versus BER for the 4 Mbits/s link using the maximum packet size of 16384 bits. It can be seen that a window size greater than the maximum specification of 7 frames would improve throughput at low BER values.

Figure 6.19 shows the simultaneously optimised packet size versus BER for the 4 Mbits/s link. The plots for all minimum turn-around time values almost exactly overlie at the data rate and so only a single plot is drawn. Figure 6.20 shows the simultaneously optimised window size versus BER for the 4 Mbits/s link. For a small minimum turn-around time, the window size can be made small and effectively constant, but varies with BER for a large turn-around time and would require an extension of maximum window to 127 frames.

Figure 6.21 shows throughput efficiency versus BER using maximum, optimum and simultaneous optimum packet sizes and window sizes for the 4 Mbits/s link with minimum turn-around delay of 0.1 ms. As the optimum window size is effectively 7 frames, the optimum packet size with fixed window size and simultaneously optimised packet and window size produce nearly identical performance.

Figure 6.22 shows throughput efficiency versus link distance for the 4 Mbits/s 4 PPM link using transmitter power of 109 mW/Sr and a receiver bandwidth of 6.1 MHz. In comparison with the 115.2 kbits/s link, the link range using the maximum packet and window sizes is significantly reduced, from the increases bandwidth requirement, and the range extension from optimisation is reduced to approximately 0.4 m.

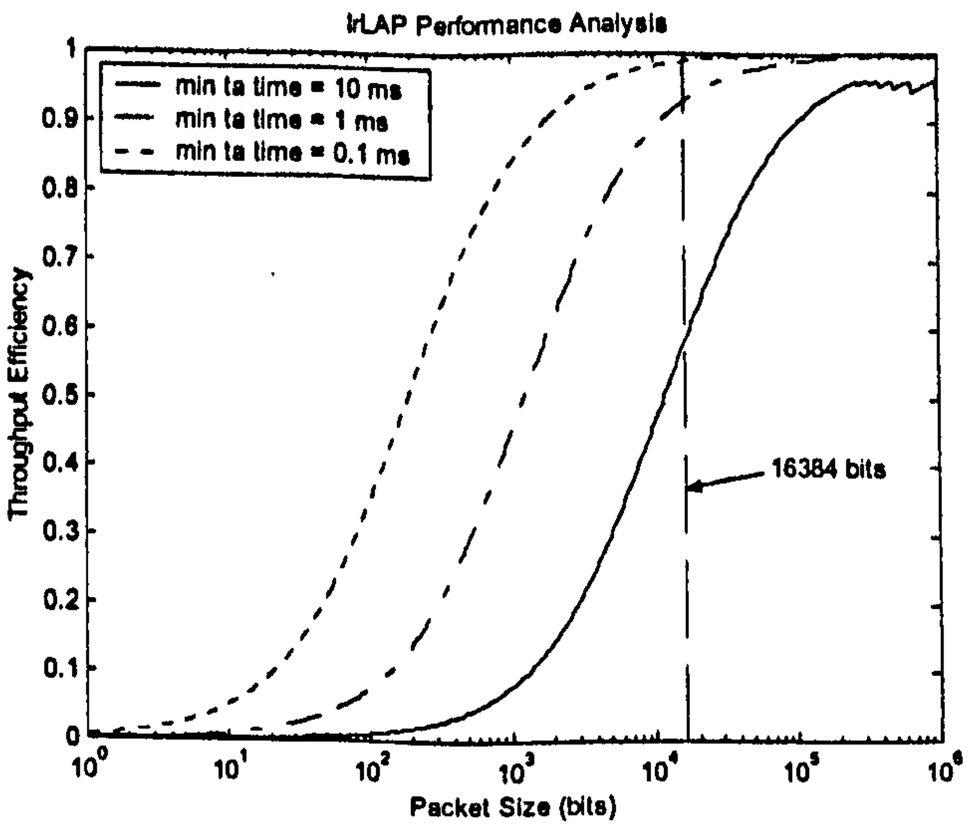

a) BER = 10^{-9}

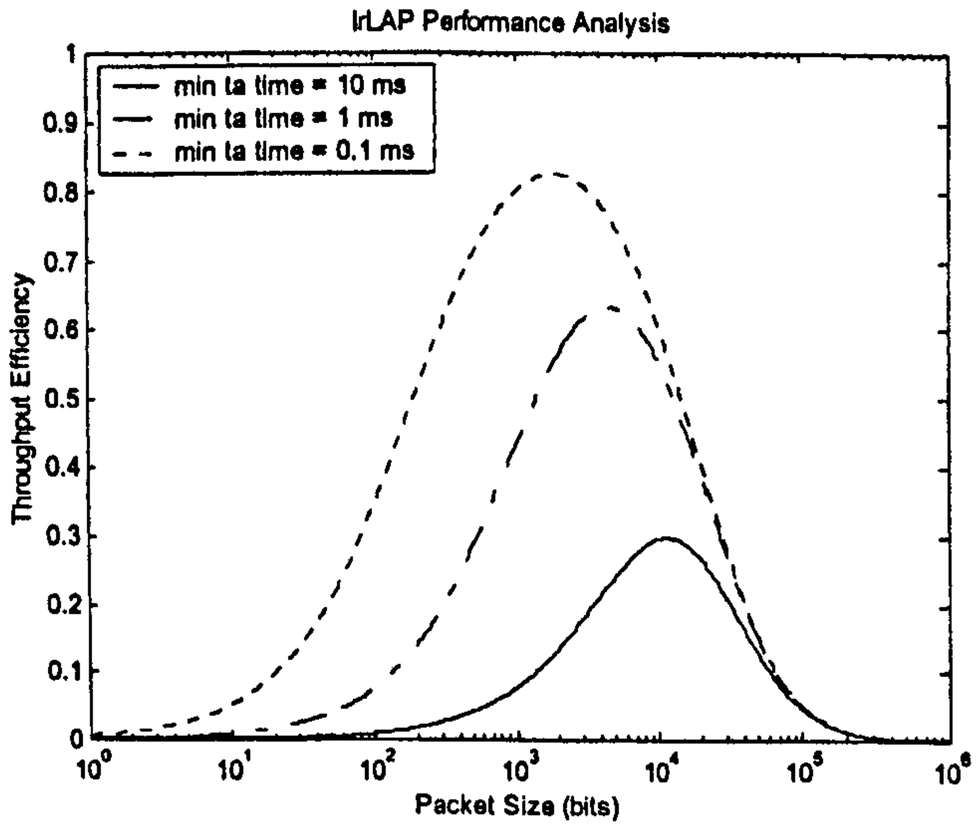

b) BER = 10^{-5}

data rate = 4 Mbits/s
max ta time = 500 ms
window size = 7 frames
BER = 10^{-9}

Figure 6.15 Throughput versus packet size for 4 Mbits/s link

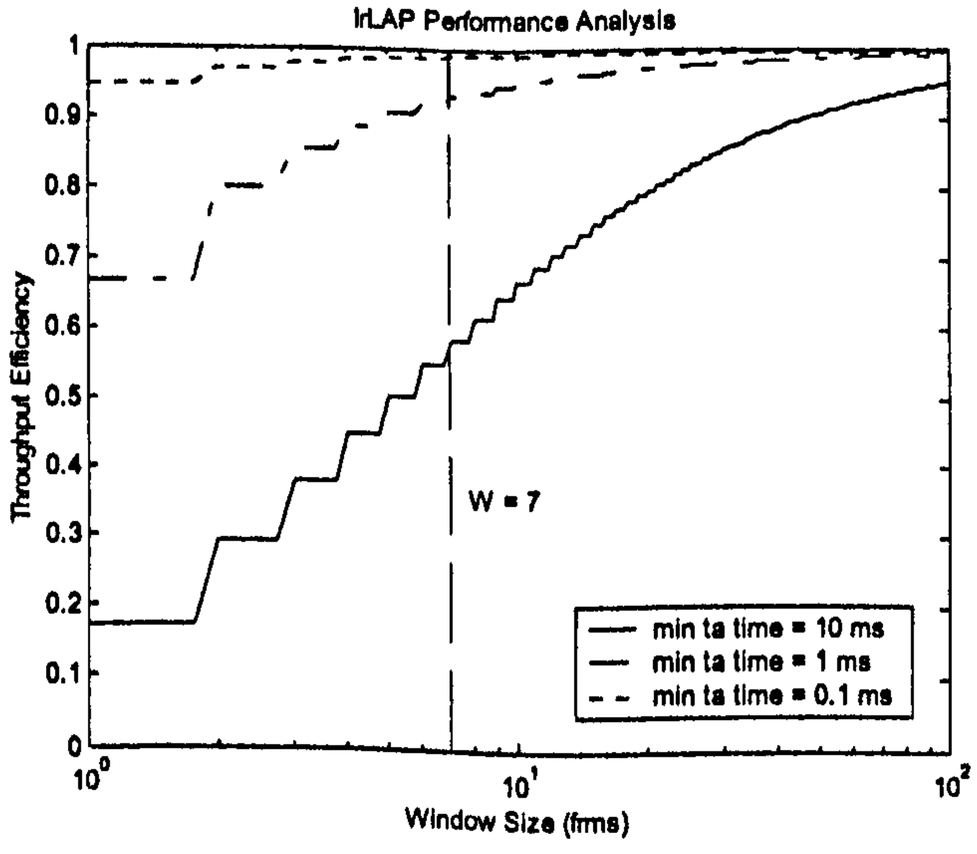

a) BER = 10^{-9}

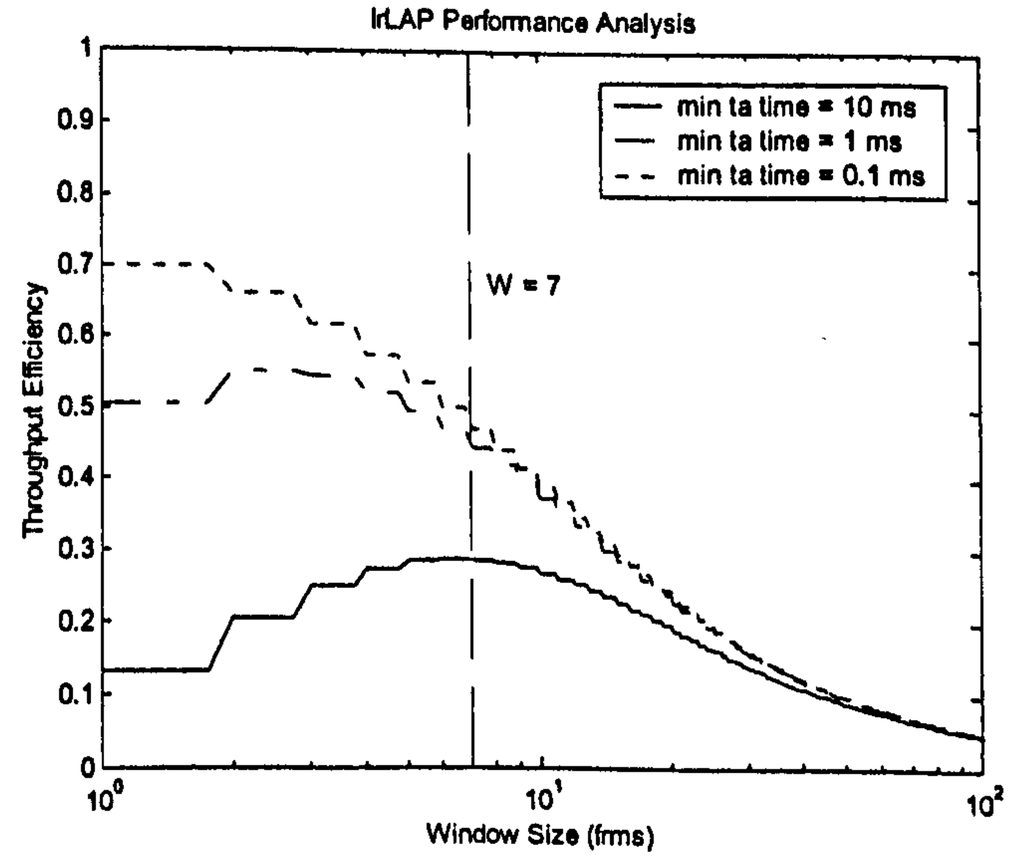

b) BER = 10^{-5}

data rate = 4 Mbits/s
max ta time = 500 ms
window size = 7 frames
packet size = 16384 bits

Figure 6.16 Throughput versus window size for 4 Mbits/s link

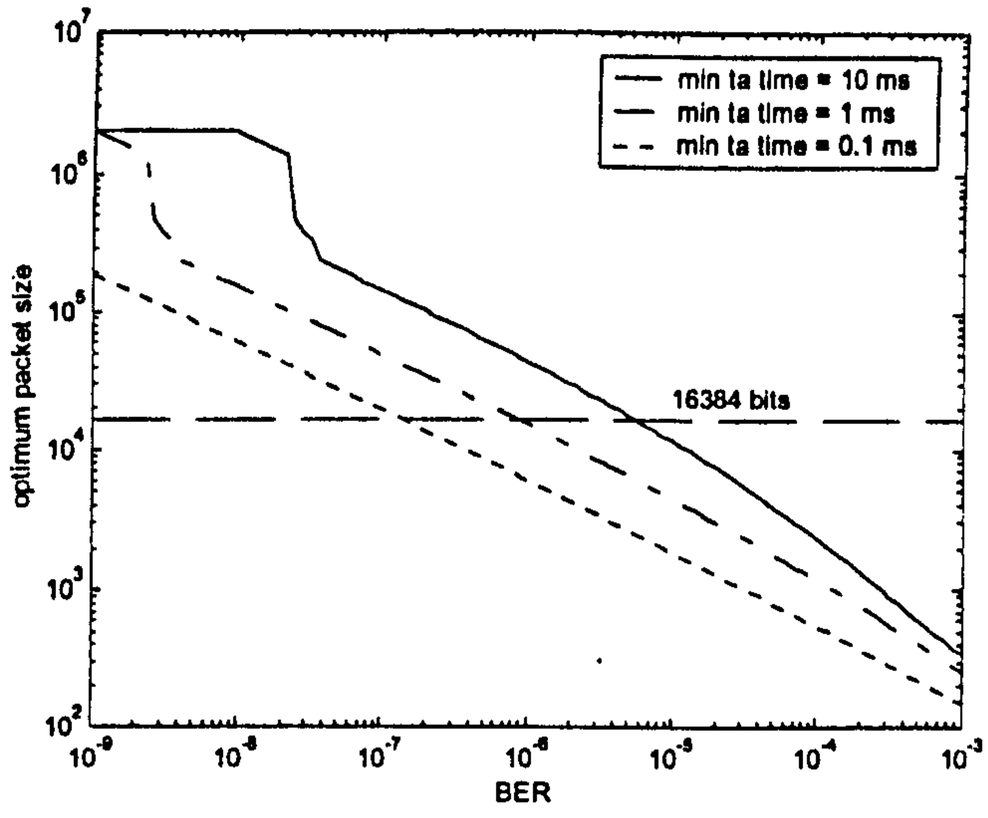

data rate = 4 Mbits/s window size = 7 frames
max ta time = 500 ms

Figure 6.17 Optimum packet size versus link BER for 4 Mbits/s link

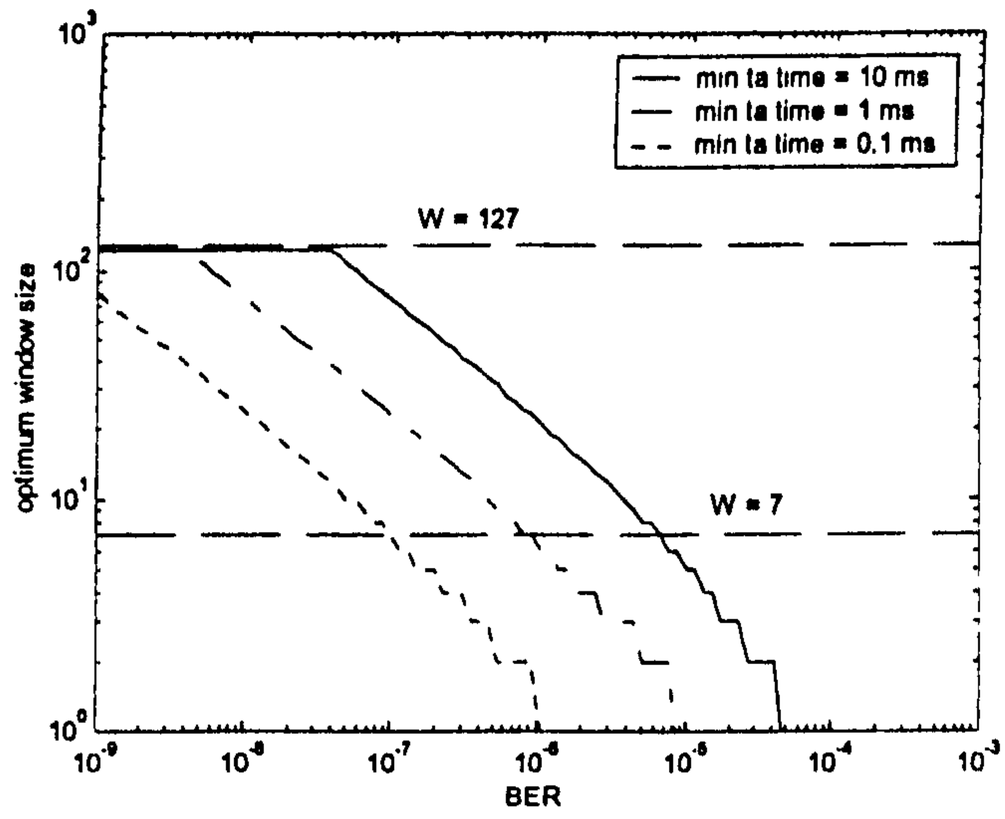

data rate = 4 Mbits/s packet size = 16384 bits
max ta time = 500 ms

Figure 6.18 Optimum window size versus link BER for 4 Mbits/s link

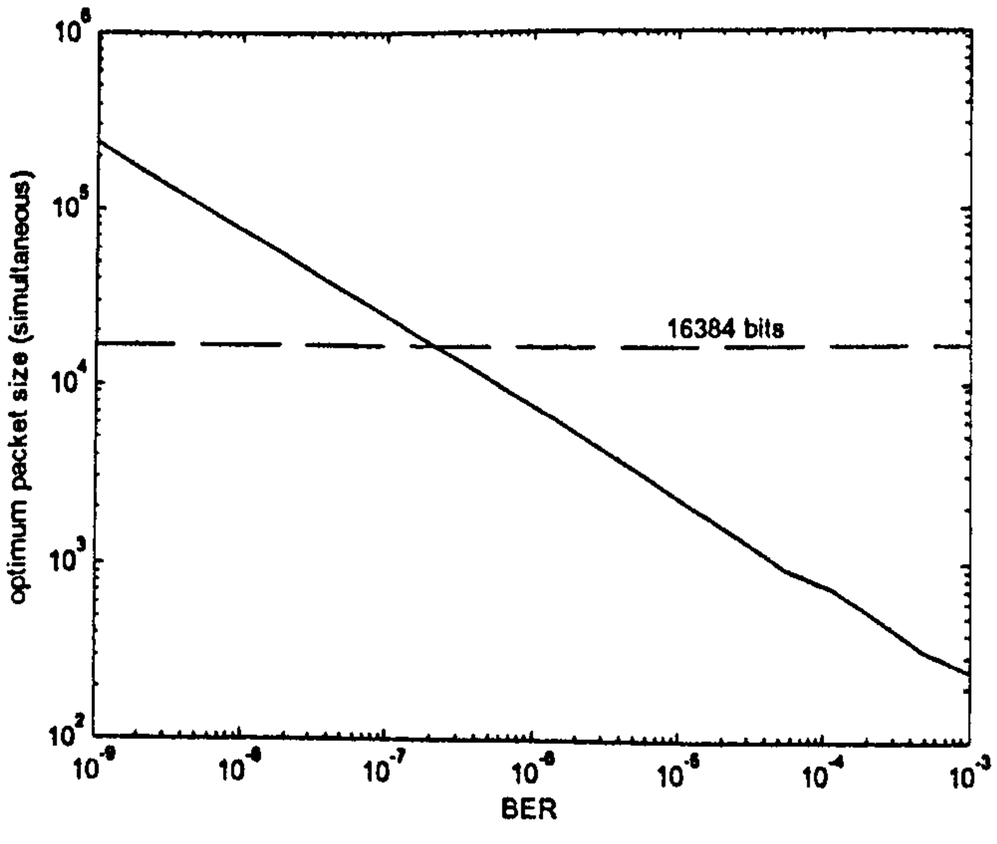

data rate = 4 Mbits/s window size = optimum
max ta time = 500 ms

Figure 6.19 Simultaneous optimum packet size versus link BER for 4 Mbits/s link

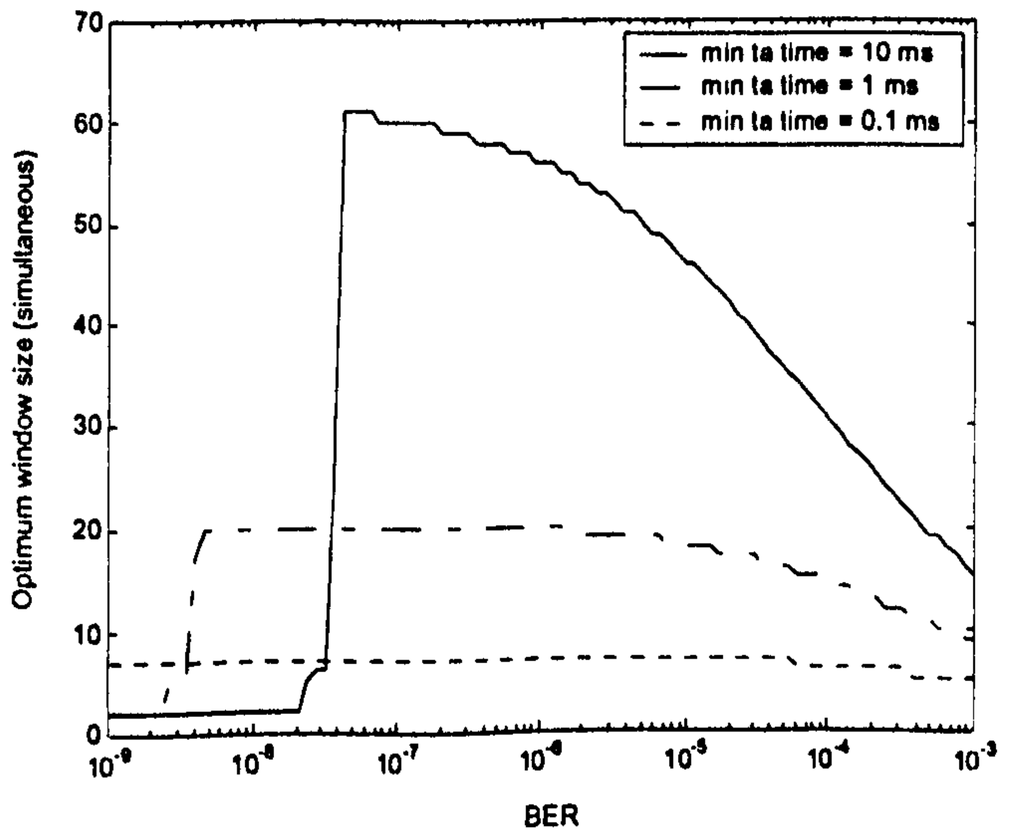

data rate = 4 Mbits/s packet size = optimum
max ta time = 500 ms

Figure 6.20 Simultaneous optimum window size versus link BER for 4 Mbits/s link

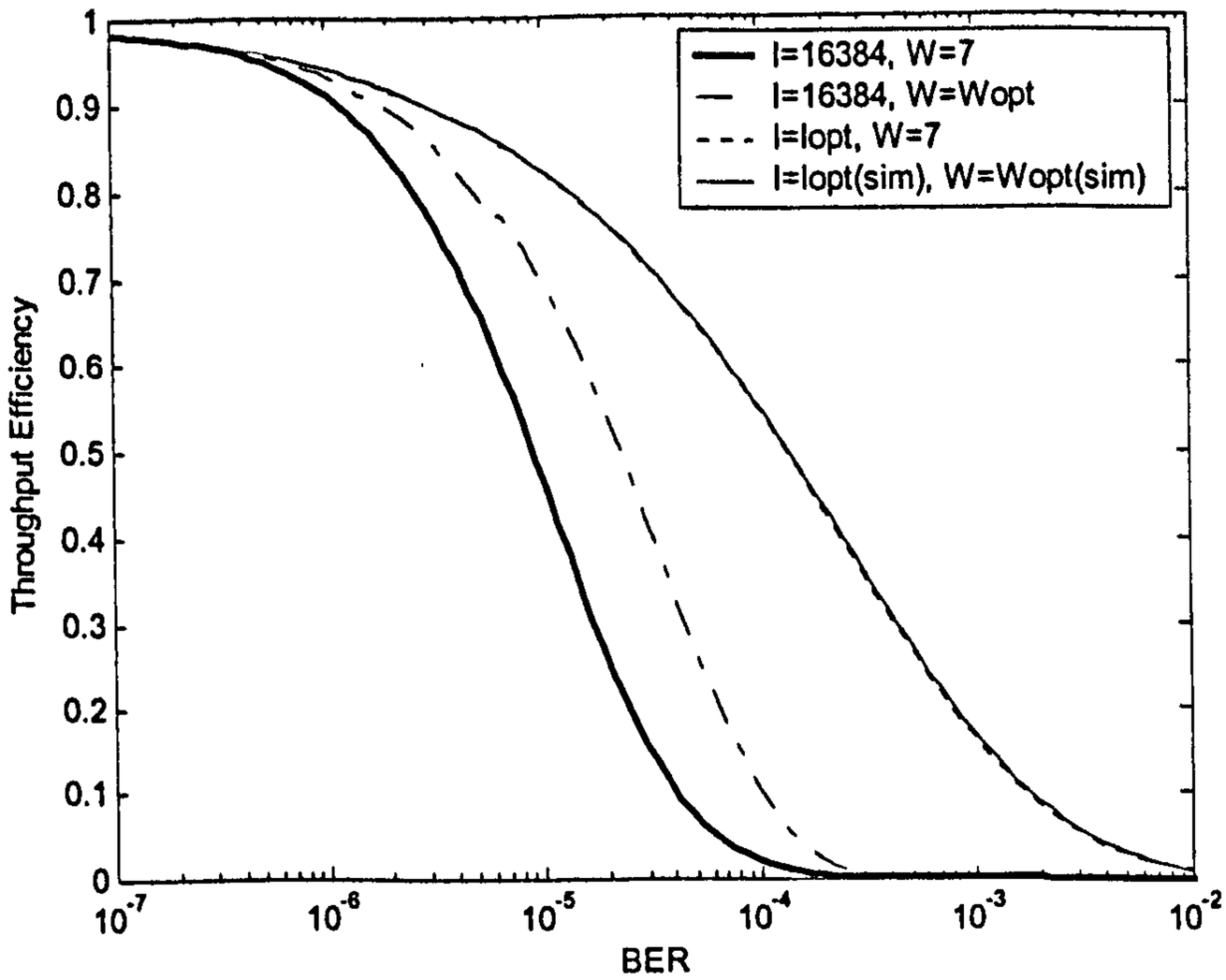

data rate = 115.2 kbits/s
max ta time = 500 ms
min ta time = 0.1 ms
overhead = 64 bits

Figure 6.21 Throughput efficiency versus link BER for 4 Mbits/s link with maximum and optimum packet window sizes

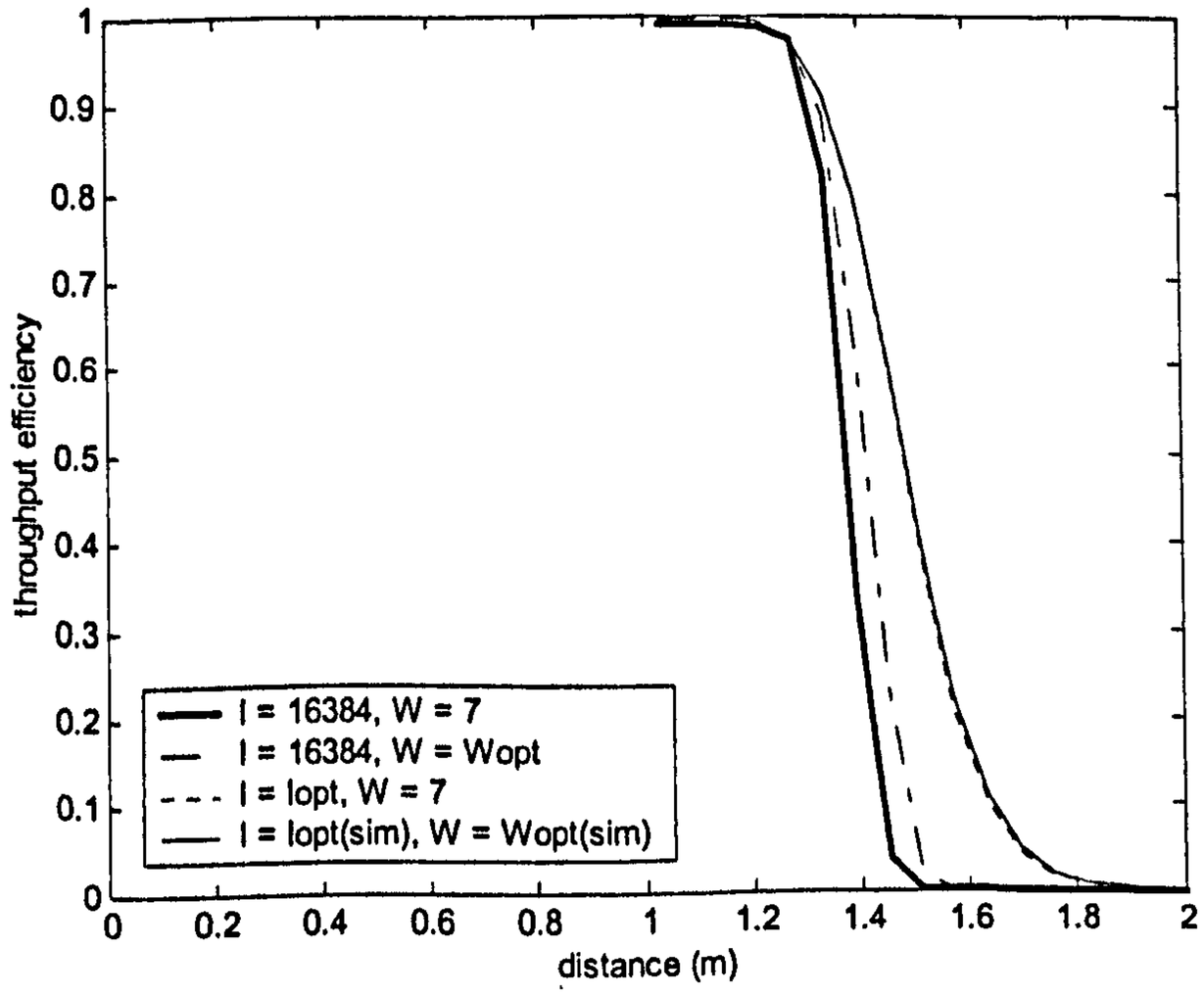

data rate = 115.2 kbits/s
max ta time = 500 ms
transmitter power = 109 mW/Sr
min ta time = 0.1 ms
overhead = 64 bits
bandwidth = 6.1 MHz

Figure 6.22 Throughput efficiency versus link distance for 4 Mbits/s 4PPM link with maximum and optimum packet and window sizes

6.2.3 IrDA VFIR 16 Mbits/s Analysis

It can be seen from the analysis of the 4 Mbits/s link that as the data rate increases, the effect of the minimum turn-around delay is increased as the link is turned around much more frequently. For this very reason when designing the 16 Mbits/s VFIR link, IrDA proposed to extend the maximum window size from 7 to 127 frames. This reduces the effect of the minimum turn-around delay. However when the BER becomes significant, the greater window size can be a problem since there are more packets that may require re-transmitting when a packet error occurs. Figure 6.23a shows the throughput versus packet size for the 16 Mbits/s link with window size of 127 frames and BER of 10^{-9}. It can be seen that having increased the maximum window size from 7 to 127 frames, the effect of the minimum turn-around delay is reduced in comparison to the 4 Mbits/s link. Figure 6.23b shows the same configuration but with a BER of 10^{-5}. It can be seen here that the effect of the larger maximum window size causes the performance to be more sensitive to packet errors causing a much reduced maximum throughput with lower values for optimum packet size.

Figure 6.24a shows throughput versus window size for the 16 Mbits/s link with maximum packet size of 16384 bits, and with a BER of 10^{-9}. It can be seen that for a low minimum turn-around time (< 0.1 ms), the throughput is near its maximum and effectively independent of window size. However for a large minimum turn-around time the throughput is significantly reduced for a small window size as the frequency of turn-around delay implementation is large. Figure 6.24b shows the same configuration but with BER of 10^{-5}. The throughput falls off significantly with window size as the average re-transmission window size increases.

Figure 6.25 shows the optimum packet size versus BER for the 16 Mbits/s link with a window size of 127 frames. In comparison with the 4 Mbits/s link, a lower optimum packet size is obtained for the same BER value. Figure 6.26 show the optimum window size versus BER for the 16 Mbits/s with a packet size of 16384 bits. It can be seen that for a large minimum turn-around time, a window size greater than the maximum 127 for low BER values could be beneficial.

Figure 6.27 shows the simultaneous optimum packet size for the 16 Mbits/s link. As with the 4 Mbits link, the optimum packet size for each minimum turn-around time coincide, therefore only one plot is produced. Figure 6.28 shows the simultaneous optimum window size for the 16 Mbits/s link. It can be seen that for a small minimum turn-around delay, the optimum window size is small and effectively independent of BER. Therefore for a small minimum turn-around delay, optimisation can be achieved by keeping the window size constant and adjusting the data packet size only. For larger minimum turn-around delays, the window size reduces with increasing BER and therefore would need to be simultaneously adjusted with the data packet size for optimisation.

Figure 6.29 shows throughput efficiency versus BER for the 16 Mbits/s link with maximum, optimum and simultaneous optimum packet size and window size. It can be seen that using the simultaneous optimum packet and window size provides a significant improvement over using maximum and single optimised window and packet sizes. Figure 6.30 shows throughput efficiency versus link distance for the 16 Mbits/s link using a transmitter power of 109 mW/Sr and a receiver bandwidth of 14.5 MHz. Because of the low signal-to-noise ratio achieved with the higher bandwidth, there is only a minimal improvement in effective range from optimisation.

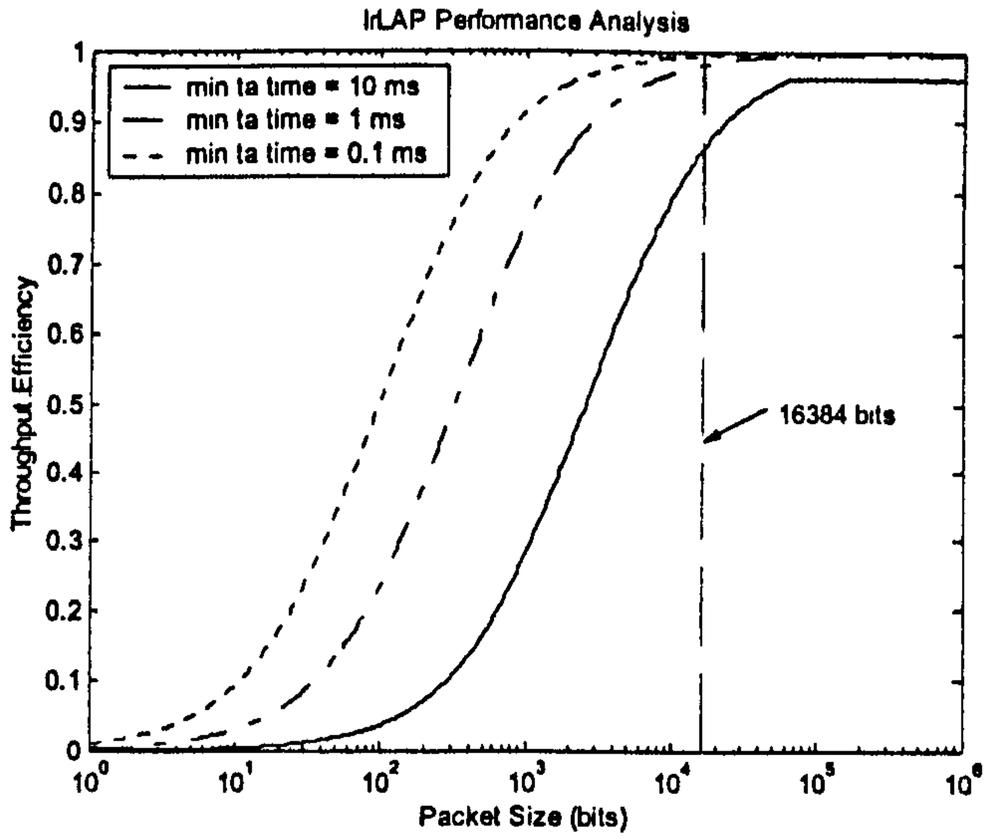

a) BER = 10^{-9}

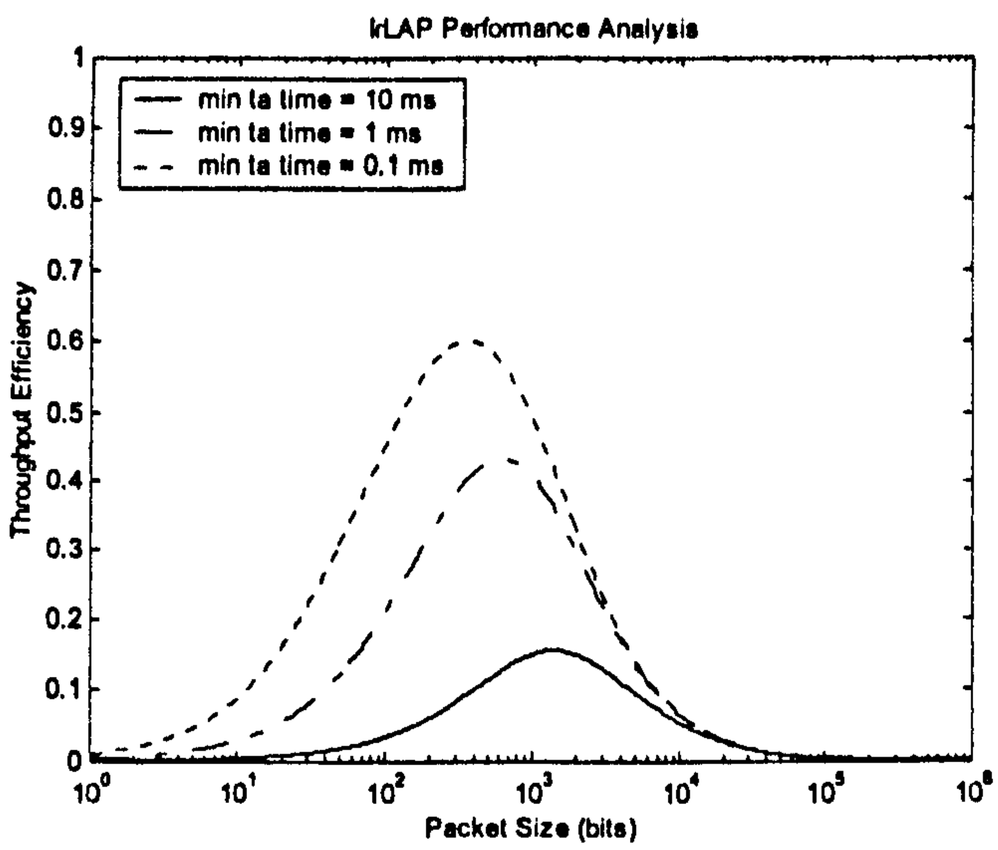

a) BER = 10^{-5}

data rate = 16 Mbits/s
max ta time = 500 ms

window size = 127 frames

Figure 6.23 Throughput versus packet size for 16 Mbits/s link

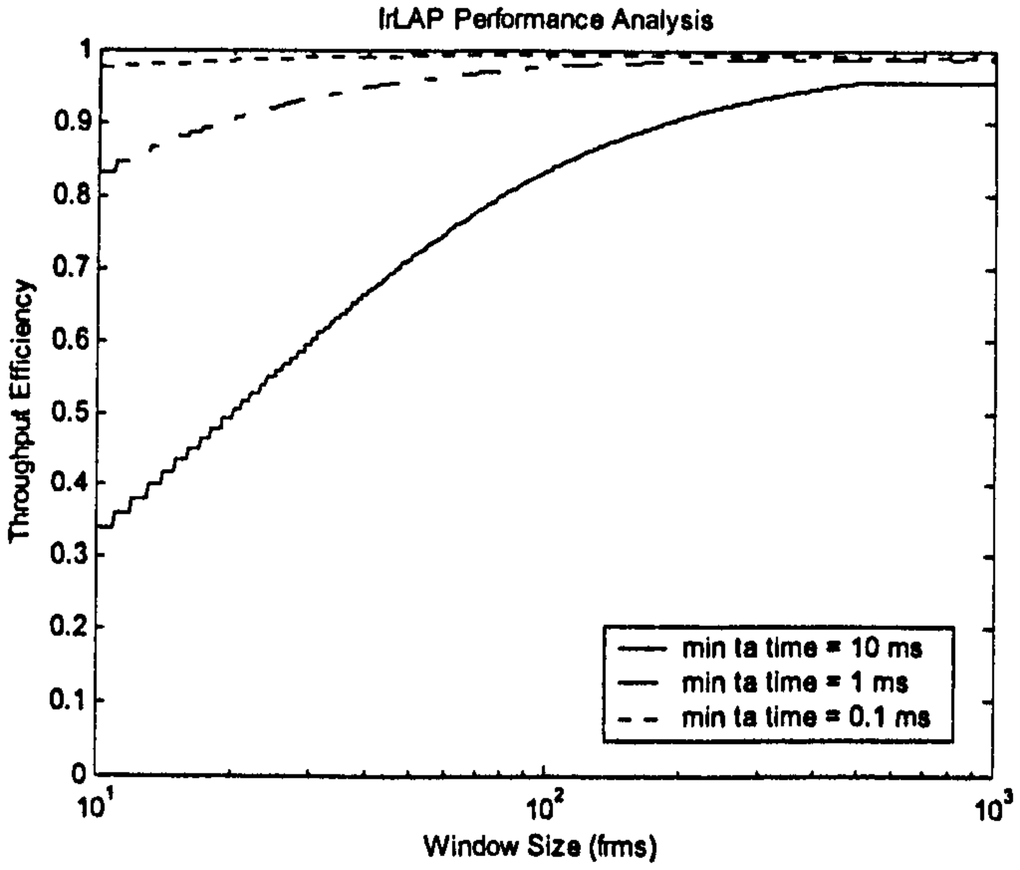

a) BER = 10^{-9}

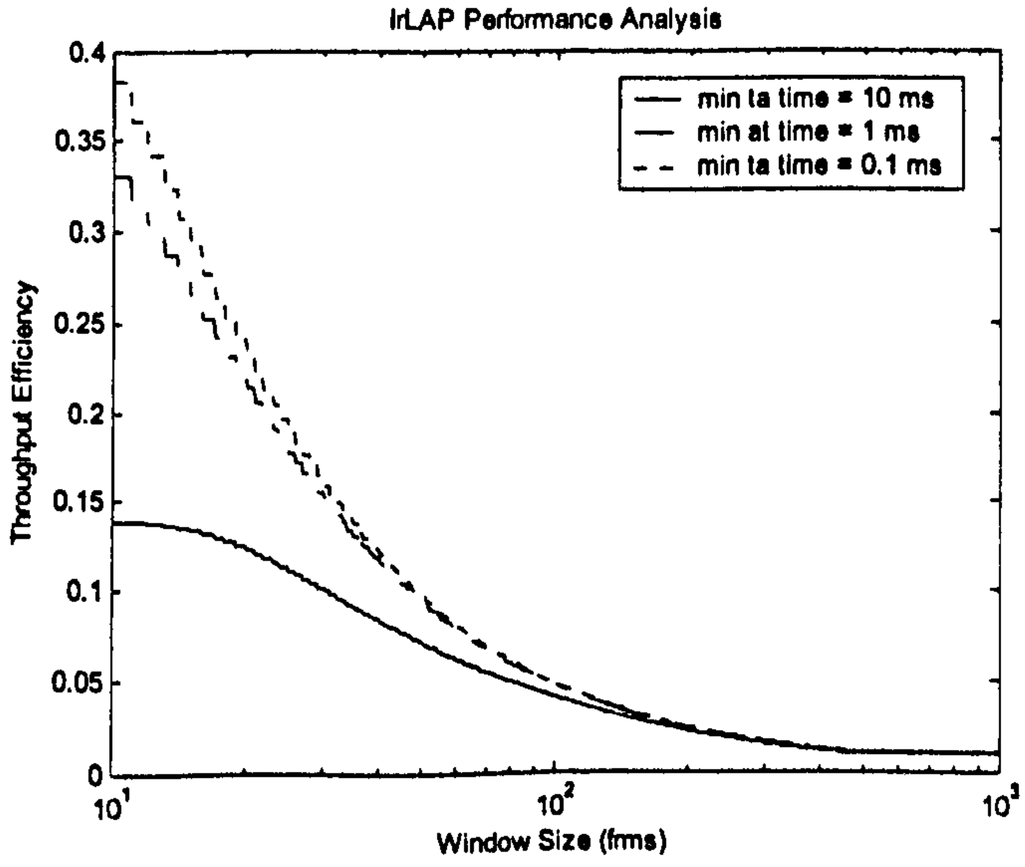

b) BER = 10^{-5}

data rate = 16 Mbits/s
max ta time = 500 ms

packet size = 16384 bits

Figure 6.24 Throughput versus window size for 16 Mbits/s link

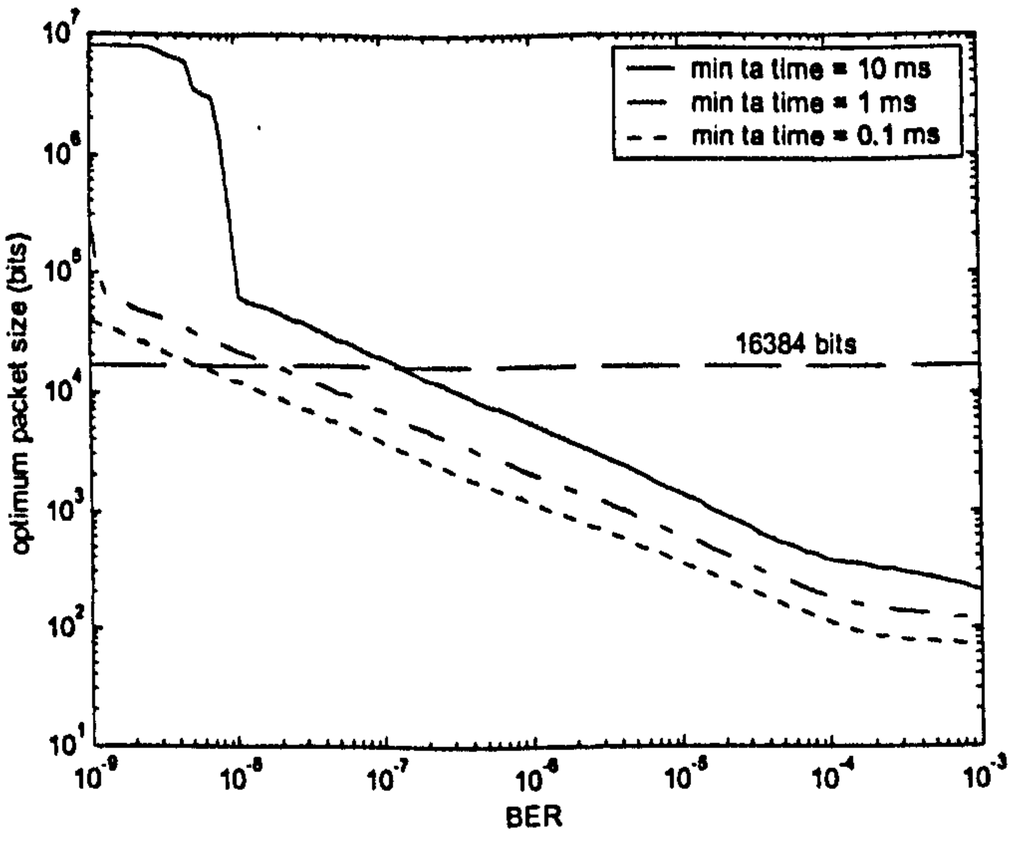

data rate = 16 Mbits/s window size = 127 frames
max ta time = 500 ms

Figure 6.25 Optimum packet size versus link BER for 16 Mbits/s link

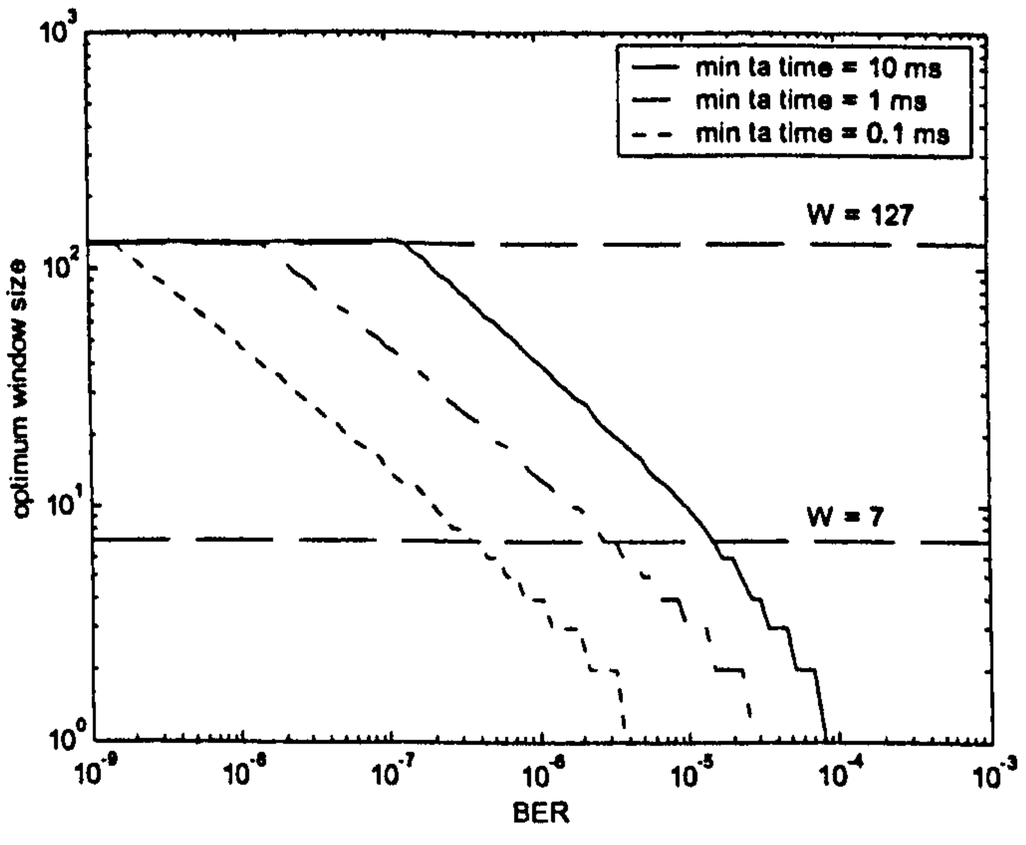

data rate = 16 Mbits/s packet size = 16384 bits
max ta time = 500 ms

Figure 6.26 Optimum window size versus BER for 16 Mbits/s

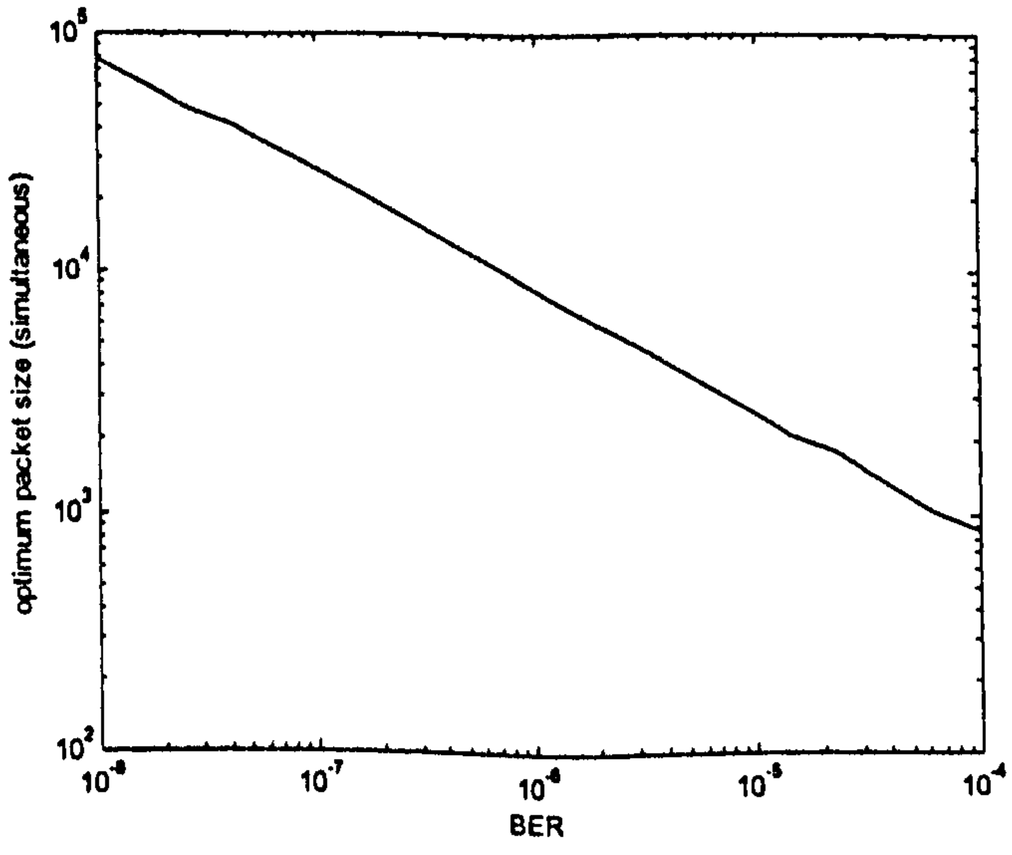

data rate = 16 Mbits/s window size = optimum
max ta time = 500 ms

Figure 6.27 Simultaneous optimum packet size versus link BER for 16 Mbits/s link

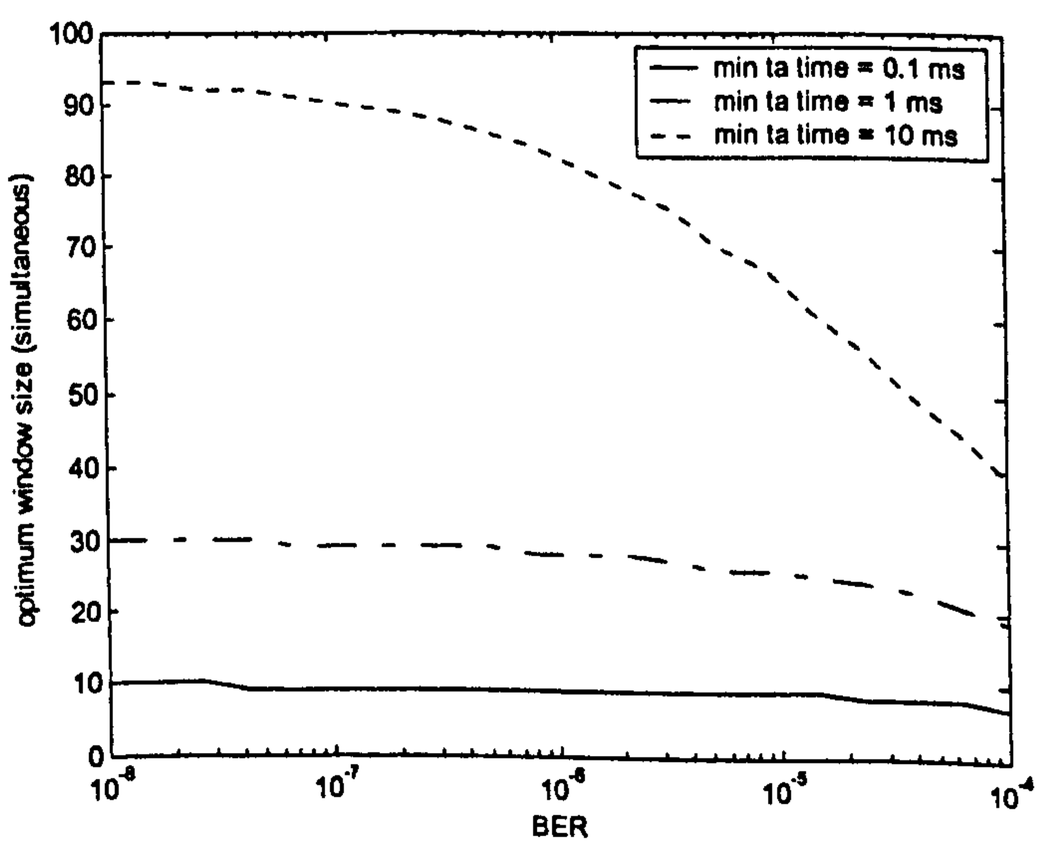

data rate = 16 Mbits/s packet size = optimum
max ta time = 500 ms

Figure 6.28 Simultaneous optimum window size versus BER for 16 Mbits/s link

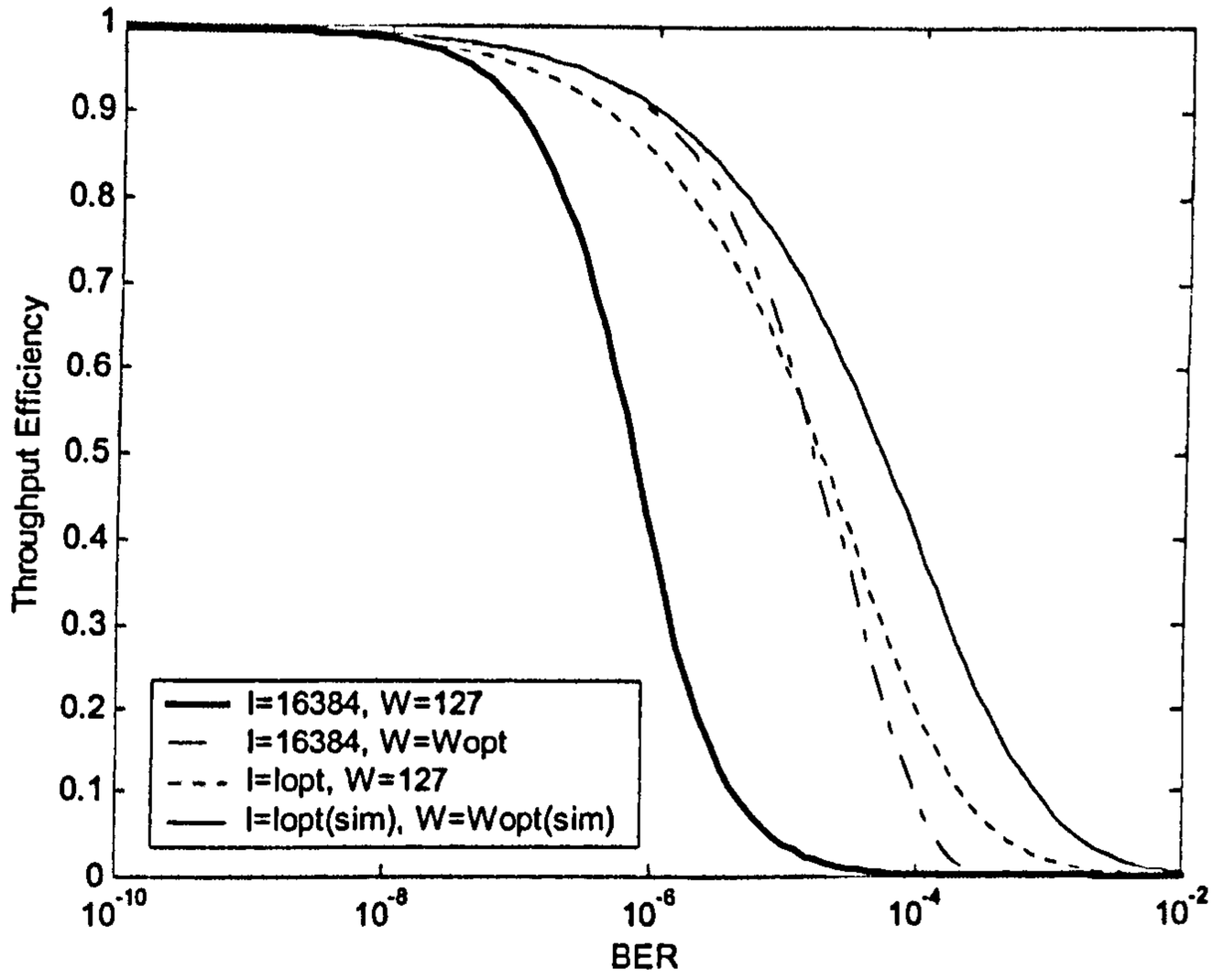

data rate = 16 Mbits/s
max ta time = 500 ms
min ta time = 0.1 ms
overhead = 72 bits

Figure 6.29 Throughput Efficiency versus link BER for 16 Mbits/s link with maximum and optimum packet and window sizes

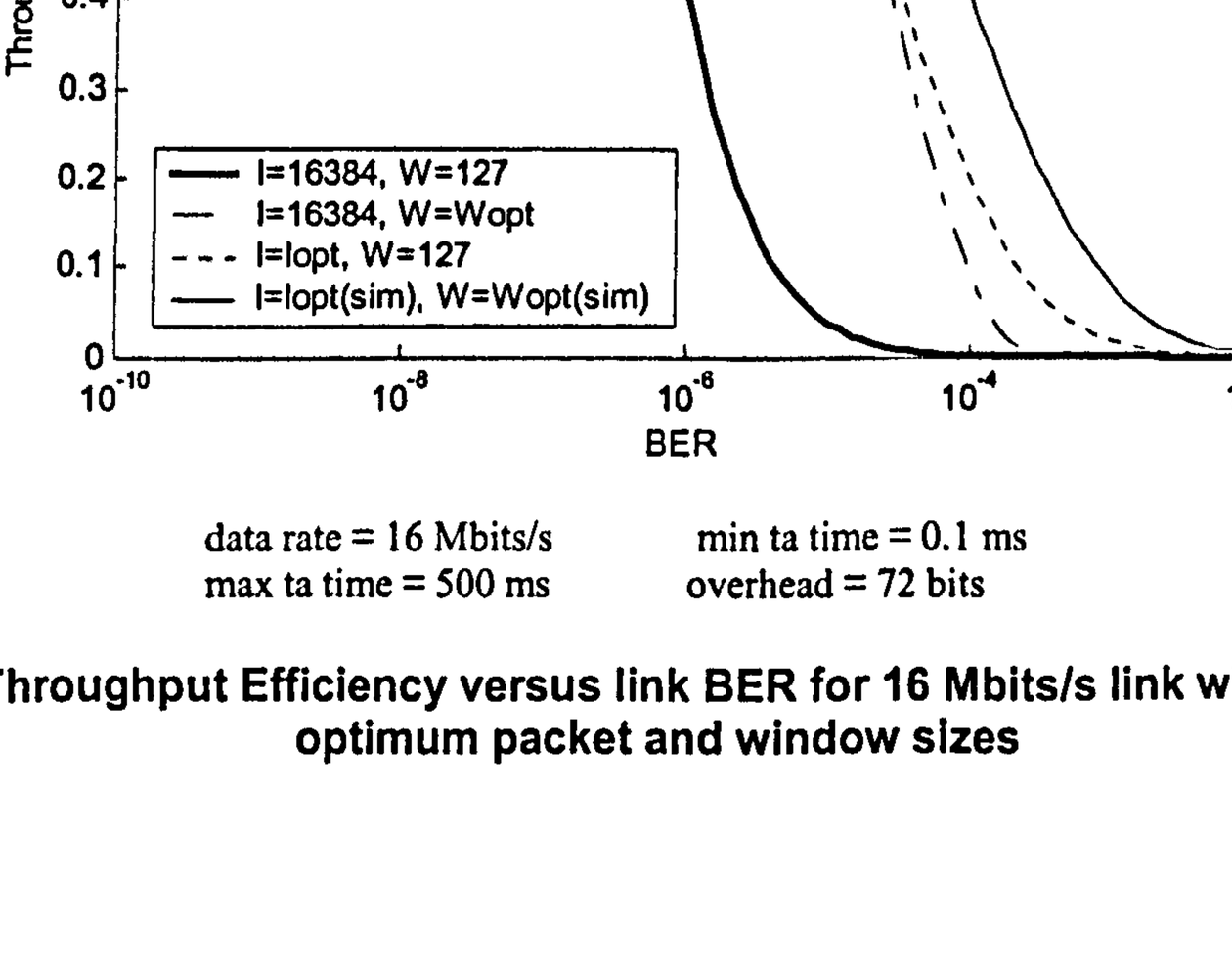

data rate = 16 Mbits/s
max ta time = 500 ms
transmitter power = 109 mW/Sr
min ta time = 0.1 ms
overhead = 72 bits
bandwidth = 14.5 MHz

Figure 6.30 Throughput Efficiency versus link distance for 16 Mbits/s HHH link with maximum and optimum packet and window sizes

The following general conclusions can therefore be made about the performance of the IrDA 1.x protocol. The minimum turn-around time is always significant as it reduces the maximum throughput. The effect increases with higher data rates as the link is reversed more frequently. The minimum turn-around delay is used to cover receiver latency. This is a physical characteristic of the receiver manufacture. Higher quality receiver devices will can have lower latency ratings but will cost more. The link throughput increases with data packet size as the relative overhead from the acknowledgement delay and packet headers are reduced. Higher data rate links (4 Mbits/s and above) could benefit from a larger packet data size than the specified maximum of 16384 bits, provided the link BER is good. The larger the packet, the more susceptible it becomes to bit errors. Therefore if the link has a poor BER value, the throughput for increasing packet sizes will increase to a maximum and then decrease as packet errors (and hence re-transmissions) increase. There is therefore an optimum packet size to achieve the maximum throughput for a particular BER value and other link parameter settings. In general for the maximum packet size of 16384 bits, the throughput will fall off quite sharply somewhere around a BER of 10^{-6}.

If the link has a small minimum turn-around delay (≤ 0.1 ms), the throughput performance can be optimised by making the window size small (equation 6.42) and constant (no requirement for 127 frame extension) and the frame size varied with the BER (according to equation 6.43) with the packet size limit of 16384 bits removed. This however will require segmentation and re-assembly functions for the data packets and a BER derivation mechanism from the number of discarded frames. If the minimum turn-around delay is large, the window size must also be adjusted in relation to the BER, and for the 115.2 kbits/s and 4 Mbits/s links, the maximum window extended to 127 frames. It should also be noted that increasing the packet size beyond the maximum 16384 bits may have implications for the effectiveness of the 32 bit CRC in detecting frame errors (Fiorini et al., 1994).

6.3 IrDA 1.x Simulation Model Results

The following results are produced from the IrDA 1.x OPNET simulation model described in Appendix A.

6.3.1 IrDA 1.x Delay Results

Figure 6.31 shows the simulation packet delay statistics output for a 4Mbits/s link with BER = 10^{-8}. These are vector output statistics recorded as a time-value pair for each data packet successfully received at the secondary. Subplot (a) shows the full scale of the simulation output for 100 seconds simulation time. The 'spikes' are re-transmission delays due to packet errors (relatively few for BER = 10^{-8}). Subplot (b) is a zoom-in to plot (a) for simulation time from 0 to 1 second. The periodic spikes here are from the turn-around delay implemented after each window transmission. The lower limit to the delay is the transmission delay of each packet.

Figure 6.32 shows the packet delay (a) and average packet delay (b) for a 4 Mbits/s link with a BER of 10^{-5}. It can be seen that the frequency and size of the packet delays are much greater for this error rate. The average packet delay plot demonstrates the choice of a suitable simulation time to obtain a stable average result. For this BER (10^{-5}), a simulation time in excess of 40 seconds is required.

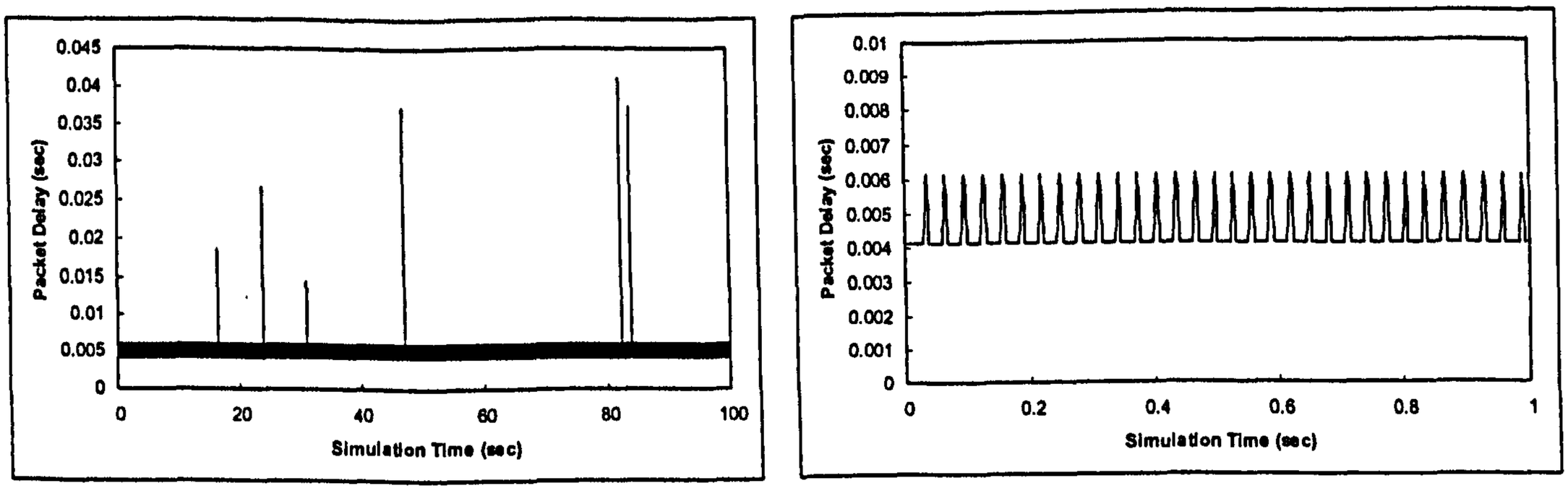

(a) 0 – 100 sec (b) 0 – 1 sec

Figure 6.31 Packet delay versus simulation time for 4 Mbits/s link with BER = $1e^{-8}$

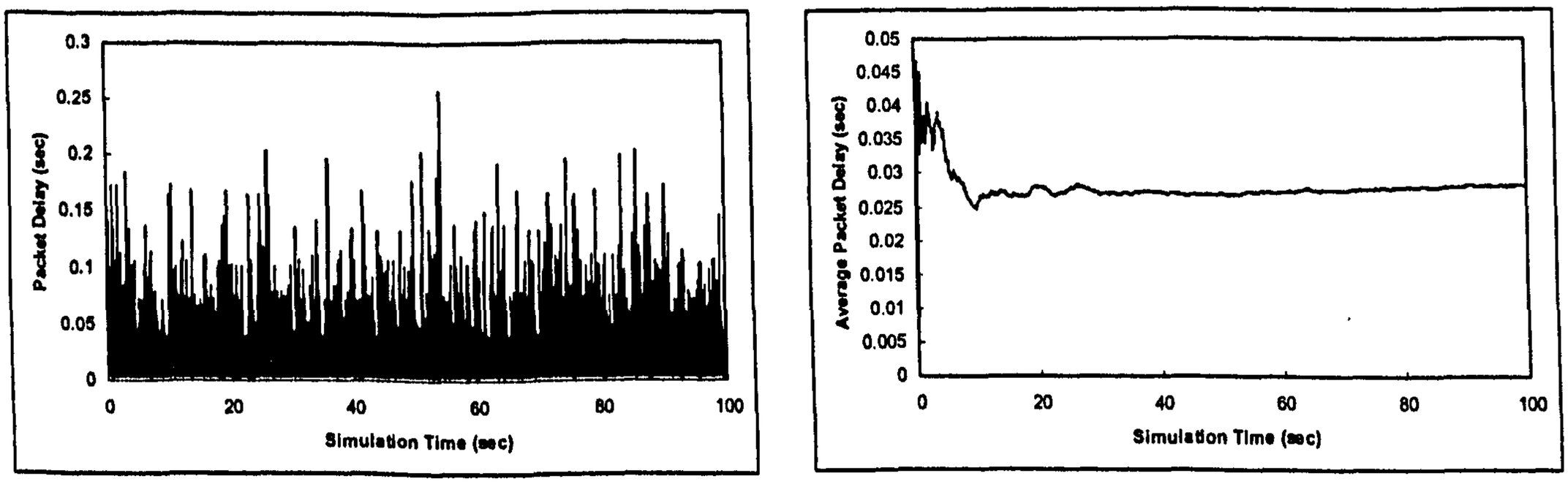

(a) (b)

Figure 6.32 Packet delay (a) and average packet delay (b) for 4 Mbits/s with BER = 10^{-5}

6.3.2 IrDA 1.x Non-saturation Results

Non-saturation results are produced from the IrDA 1.x advanced simulation model (see Appendix A). Here data packets are sent to the IrLAP input stream at random intervals using a Poisson distribution with a specified mean service rate. Figure 6.33 shows throughput efficiency versus mean service rate for the 4 Mbits/s link. The throughput increases linearly with service rate until the saturation point is reached, and then maintains the throughput at the saturation throughput level for the specific BER. This is from re-transmissions (from frame errors) temporally halting the removal of packets from the input stream allowing a queue to build.

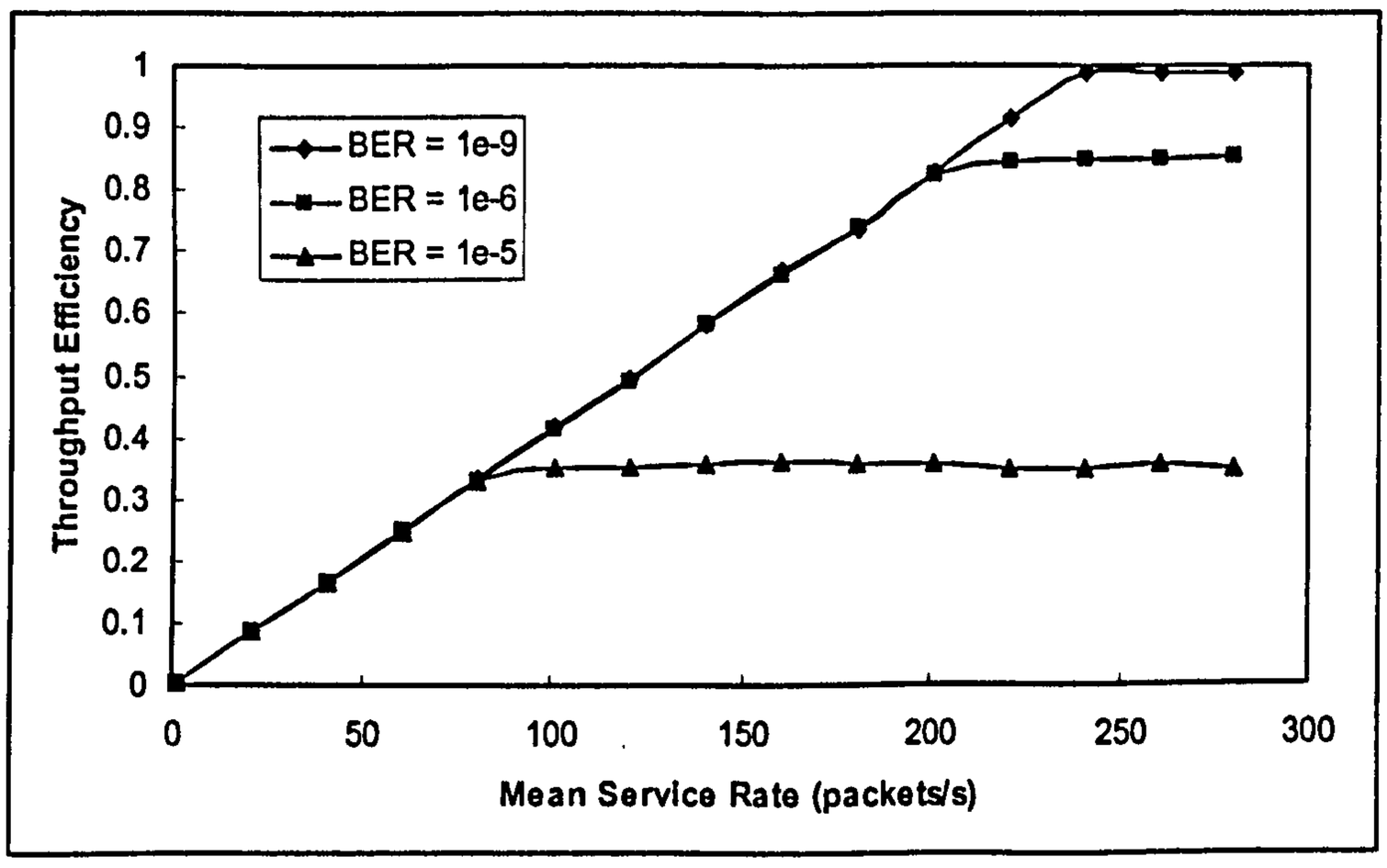

data rate = 4 Mbits/s	window size = 7 frames
max ta time = 500 ms	packet size = 16384 bits
min ta time = 0.1 ms	simulation time = 200 s

Figure 6.33 Simulation throughput efficiency versus mean service rate

6.4 Chapter Summary

This chapter has presented an analytical model for the saturation throughput performance of the IrDA 1.x IrLAP data link protocol in relation to the link data rate, BER and IrLAP parameter settings. The model uses window position dependent frame transmission probabilities and a Markov chain analysis for the probability of frame window position. Optimisation of the data packet size and transmission window size are provided through numerical differentiation and successive approximation algorithms. Graphical results are presented for throughput versus data packet size and window size using fixed and optimised values for 115.2 kbits/s, 4 Mbits/s and 16 Mbits/s data rates. Plots are presented for optimised throughput Vs BER and link distance with the same data rates. Simulation model results are used for validation of the analytical model and to provide results for non-saturation throughput and delay. The following chapter presents an analytical model for saturation condition utilisation and delay of the IrDA AIr MAC protocol using Markov analysis of the linear collision avoidance backoff procedure.

7. AIr MAC Protocol Performance Modelling

This chapter presents an analytical model of the AIr MAC protocol to provide saturation condition utilisation and delay in reservation mode (i.e. using RTS/ CTS media reservation). The model provides utilisation in relation to the network size and the CAS (Collision Avoidance Slot) window size and investigates the effectiveness of the linear CAS back-off process using a Markov analysis of the contention back-off process. Simulation results are provided for validation of the analytical model and non-reservation mode utilisation and delay.

7.1 AIr MAC Analytical Model

Saturation condition utilisation is found by determining the average transmission slot time in which a known amount of data is transmitted. The transmission slot time includes the contention delay time, time taken for collisions of RTS transmissions and the successful data burst transmission time. The average delay is given by the average reservation time multiplied by the average number of reservations required for successful burst transmission by a station. A Markov model of the linear CAS window back-off process is used to determine the probability of transmission within a particular time slot. The model is a development of a model developed by Bianchi (2000) for the 802.11 MAC DCF protocol where an exponential back-off procedure is used.

7.1.1 Model Parameters and Assumptions

A saturation condition is assumed in which a 'chain' of data packets is continuously available for transmission. The propagation delay is assumed to be negligible. We also assume an error-free medium and all devices within range (i.e. no hidden nodes). The input parameters used in the model are given in Table 7.1. Fixed system constants used are given in table 7.2.

Parameter	Description	Unit
L	packet data size	bits
n	network size	stations
N_b	burst size	frames
W	(initial) CAS window size	slots
m	+/- CAS adjustment factor	slots
RR	main body repetition rate	-

Table 7.1 AIr MAC analysis input parameters

Parameter	Description	Value
C	base data rate	4 Mbits/s
σ	single CA slot duration	800 µs
T_{EXIT}	EXIT1 timer duration	632 µs
$T_{WF\text{-}CTS}$	Wait-For-CTS timer duration	556 µs
T_{ta}	turn-around time	200 µs
H_{Data}	DATA frame overhead	72 bits
H_{RTS}	RTS frame overhead	48 bits
H_F	Frame Header (PA + Sync)	416 bits
H_R	Robust Header	32 bits

Table 7.2 AIr MAC analysis system constants

The AIr MAC frame composition is shown in Figure 7.1 .

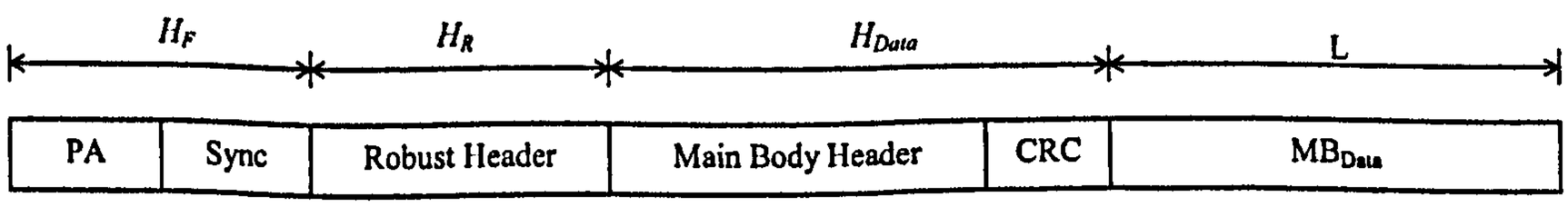

Figure 7.1 AIr MAC frame composition

7.1.2 Utilisation Calculation

To determine the utilisation we need to define a period called the *transmission slot* which is the time taken for the reservation and the total contention time in establishing the reservation. The utilisation can then be given by:

$$S = \frac{E[Data]}{E[Ls]} \tag{7.1}$$

where $E[Data]$ is the average data size (in seconds) transmitted in a transmission slot and $E[Ls]$ is the average length of a transmission slot. These are given by:

$$E[Data] = P_S P_{tr} N_b L \tag{7.2}$$

$$E[Ls] = (1 - P_{tr})\sigma + P_{tr} P_S T_S + P_{tr}(1 - P_S) T_C \tag{7.3}$$

where P_{tr} is the probability of transmitting at least 1 frame in a particular time slot, given by:

$$P_{tr} = 1 - (1 - \tau)^n \tag{7.4}$$

where n is the number of contending stations in the network and τ is the probability that the station transmits after a randomly chosen set of CA slots. The probability of collision p is related to τ by:

$$p = 1 - (1 - \tau)^{n-1} \tag{7.5}$$

The key approximation in the model is that the probability of collision p is independent of the station state. This becomes more accurate with higher W and n. P_S is the probability of a transmission being successful (i.e. collision free) given by:

$$P_S = \frac{n\tau(1-\tau)^{n-1}}{P_{tr}} \tag{7.6}$$

T_S is the time taken on the network (sensed busy) when a successful reservation has been made, and T_C is time taken when a collision occurs. These are as defined in Figure 7.2.

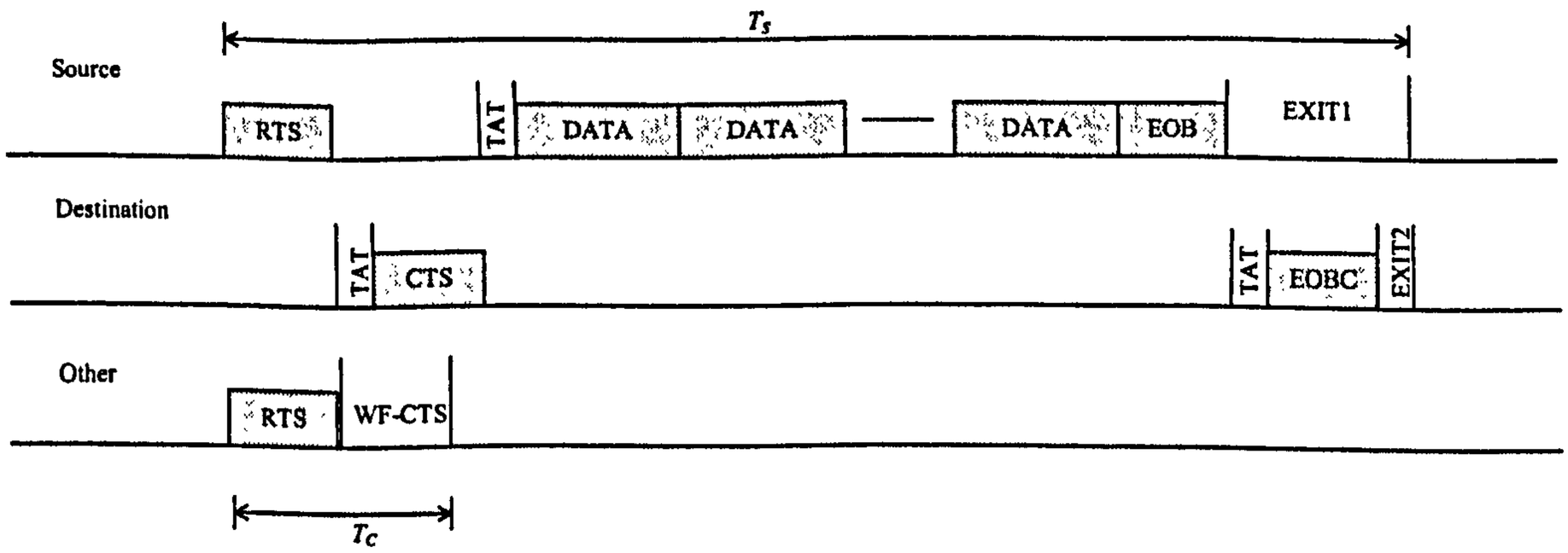

Figure 7.2 Air MAC transmission slot time

T_S and T_C are therefore given by:

$$T_S = T_{RTS} + T_{ta} + T_{CTS} + T_{ta} + N_b T_{Data} + T_{EOB} + T_{EXIT} \tag{7.7}$$

$$T_C = T_{RTS} + T_{WF-CTS} \tag{7.8}$$

The time T_C is the time for the RTS transmission and then the time for the wait-for-CTS timer. As the RTS packets collide, the CTS will not be returned and so the sending station will wait for the Wait-For-CTS timer to expire before attempting the reservation again.

The frame transmission times are given by:

$$T_{RTS} = \frac{H_F + 16H_R + RRH_{RTS}}{C} \tag{7.9}$$

$$T_{CTS} = \frac{H_F + 16H_R}{C} \tag{7.10}$$

$$T_{Data} = \frac{H_F + 16H_R + RR(L + H_{Data})}{C} \tag{7.11}$$

$$T_{EOB} = \frac{H_F + 16H_R}{C} \tag{7.12}$$

7.1.3 Average Burst Delay

The average burst delay, denoted δ, is the average time taken from the time the packet chain becomes the head of the station queue to the time of reception of the EOBC confirmation from the receiving station. This is given as:

$$\delta = E[X] \cdot E[Ls] \tag{7.13}$$

where *E[Ls]* is the average length of a transmission slot time (as given in 7.3) and $E[X]$ is the average number of transmission slot times required for successful transmission. As τ is the probability of transmitting in a time slot, $E[X]$ is given by:

$$E[X] = \frac{1}{\tau(1-\tau)^{n-1}} \tag{7.14}$$

and $E[Ls]$ is a given in (7.3).

Using the definitions for P_s and P_{tr} provided in 7.4 and 7.6 and substituting into 7.14, $E[X]$ can be re-written as:

$$E[X] = \frac{n}{P_s P_{tr}} \tag{7.15}$$

The average burst delay can then be written as:

$$\delta = \frac{n(1-P_{tr})}{P_S P_{tr}}\sigma + nT_s + \frac{n(1-P_s)}{P_s}T_C \tag{7.16}$$

If the CA slot duration σ is small in relation to the data burst transmission time, and the probability of frame collision is very small, the delay can be written to a good approximation as:

$$\delta \approx nT_s \tag{7.17}$$

In other words the average delay is the total time for all n stations in the network to successfully make one reservation and transmit a data burst.

7.1.4 Markov Model of Collision Avoidance Back-off Mechanism

We assume that a collision avoidance window linear back-off mechanism is employed in the AIr protocol as described in section 3.2.3. If an RTS frame collision occurs, the CA window size increases by a slots. This continues up to the maximum CA window size. If the frame transmission is successful, the CA window size is reduced by a, down to the minimum CA window size.

The crucial assumption made for the model is that an RTS frame collision occurs with a constant and independent probability p (and hence frame transmission success probability 1- p). This becomes more accurate with larger network size n and maximum CA window size.

Let $W = W_0$ be the minimum (and initial) CAS window size. Let m be the 'maximum window back-off stage' such that:

$$W_{\max} = W + am \tag{7.18}$$

where a is the +/- CAS adjustment value. In general therefore we have:

$$W_i = W + ai \quad i \in (0, m) \tag{7.19}$$

where i is the 'window back-off stage'. Let $k \in (0, W_i\text{-}1)$ be the collision avoidance slot number chosen randomly with probability $1/W_i$.

The process can be described as a Markov chain consisting of state set S(i, k) as illustrated in Figure 7.3. A frame transmission collision causes a transition from state S(i, 0) to S(i+1, k) for $i \in (0, m\text{-}1)$ with probability p/W_{i+1} and to S(m, k) for $i = m$ with probability p/W_m . A successful frame transmission causes a transition from state S(i, 0) to S(i-1, k) for $i \in (1, m)$ with probability $(1\text{-}p)/W_{i-1}$ and to S(0, k) for $i = 0$, with probability $(1\text{-}p)/W_0$. The CA timer counts down from state S(i, k) to S(i, k-1) with probability 1, down to S(i, 0) before the next RTS frame transmission attempt.

The only non-zero transition probabilities are therefore:

$$\begin{aligned}
&P\{i+1,k \mid i,0\} = p/W_{i+1} \quad k \in (0,W_i - 1) \quad i \in (0,m-1)\\
&P\{m,k \mid m,0\} = p/W_m \quad k \in (0,W_m - 1) \quad i = m\\
&P\{i-1,k \mid i,0\} = (1-p)/W_{i-1} \quad k \in (0,W_i - 1) \quad i \in (1,m)\\
&P\{0,k \mid 0,0\} = (1-p)/W_0 \quad k \in (0,W_0 - 1) \quad i = 0\\
&P\{i,k-1 \mid i,k\} = 1 \quad k \in (0,W_i - 1) \quad i \in (0,m)
\end{aligned} \tag{7.20}$$

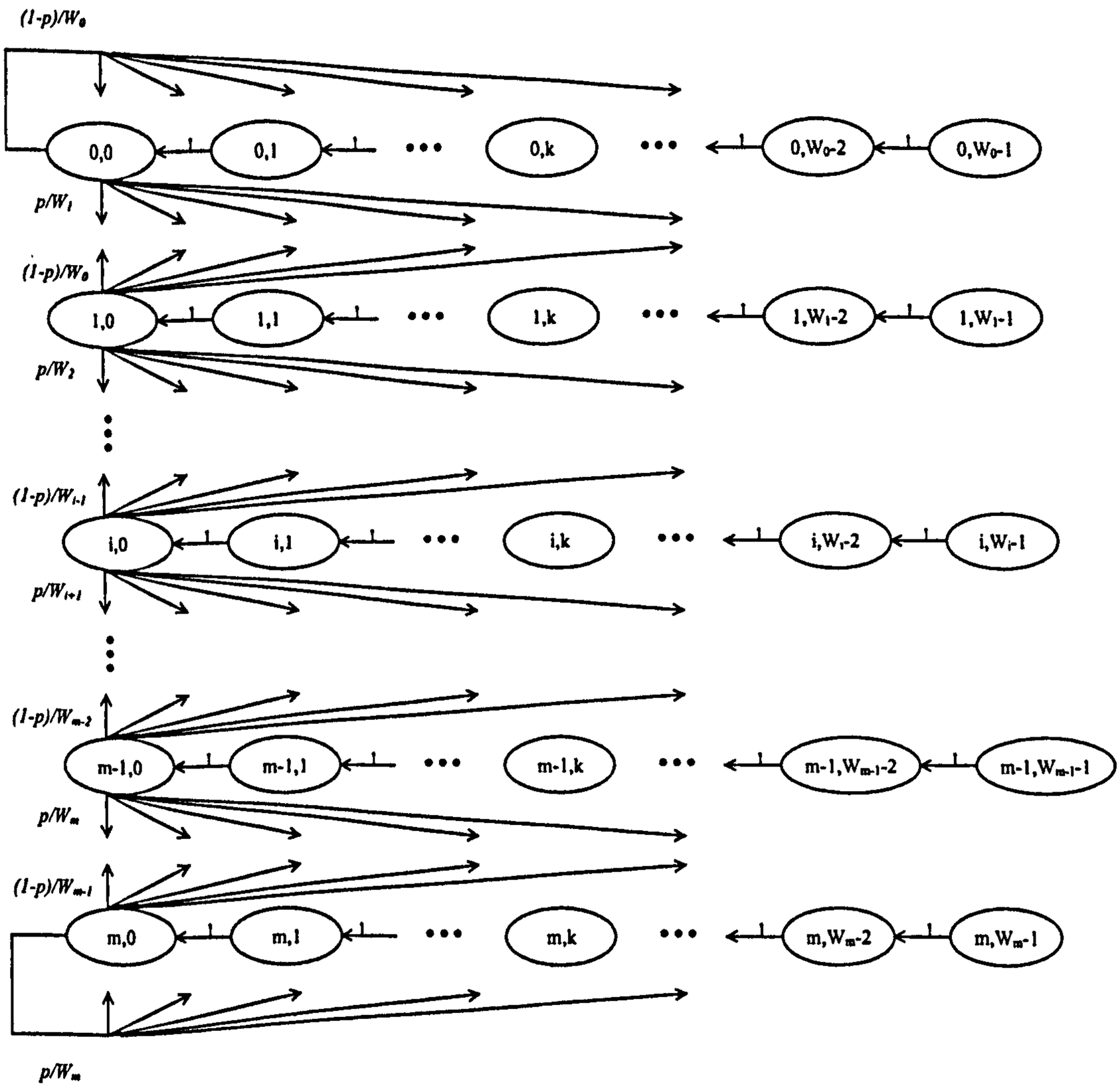

Figure 7.3 CAS window size back-off process state transition diagram

The transition matrix R for the states S(i,0) can therefore be given as:

$$R = \begin{array}{c|ccccccc} & 0 & 1 & \cdots & i & \cdots & m-1 & m \\ \hline 0 & 1-p & 1-p & 0 & 0 & 0 & 0 & 0 \\ 1 & p & 0 & 1-p & 0 & 0 & 0 & 0 \\ \vdots & 0 & p & 0 & 1-p & 0 & 0 & 0 \\ i & 0 & 0 & p & 0 & 1-p & 0 & 0 \\ \vdots & 0 & 0 & 0 & p & 0 & 1-p & 0 \\ m-1 & 0 & 0 & 0 & 0 & p & 0 & 1-p \\ m & 0 & 0 & 0 & 0 & 0 & p & p \end{array} \qquad (7.21)$$

Let $\phi(i,k)$ be the limiting distribution for the Markov chain. From the equality $\phi(i,k)\cdot R=\phi(i,k)$, (see Appendix B), we obtain that:

$$\begin{aligned}
&(1-p)\phi(0,0)+(1-p)\phi(1,0)=\phi(0,0)\\
&p\phi(i-1,0)+(1-p)\phi(i+1,0)=\phi(i,0) \qquad i\in(1,m-1) \qquad (7.22)\\
&p\phi(m-1,0)+p\phi(m,0)=\phi(m,0)
\end{aligned}$$

From which we get:

$$\phi(i,0)=\left[\frac{p}{(1-p)}\right]^{i}\phi(0,0) \qquad i\in(0,m) \qquad (7.23)$$

It can be shown that the general probability $\phi(i, k)$ is related to $\phi(i, 0)$ by:

$$\phi(i,k)=\frac{W_i-k}{W_i}\phi(i,0) \qquad (7.24)$$

From the Markov normalisation condition we have

$$\sum_{i=0}^{m}\sum_{k=0}^{W_i-1}\phi(i,k)=1 \qquad (7.25)$$

$$\Rightarrow\sum_{i=0}^{m}\phi(i,0)\sum_{k=0}^{W_i-1}\frac{W_i-k}{W_i}=1 \qquad (7.26)$$

$$\Rightarrow\sum_{i=0}^{m}\phi(i,0)\frac{W_i+1}{2}=1 \qquad (7.27)$$

From this we get

$$\phi(0,0) = \frac{2}{\sum_{i=0}^{m}\left\{\left[\frac{p}{(1-p)}\right]^{i}(W+ai+1)\right\}} \tag{7.28}$$

By using $\Phi = p / (1 - p)$, this can be simplified to

$$\phi(0,0) = 2/\left\{(W+1)\left[\frac{1-\Phi^{m+1}}{1-\Phi}\right]+a\left[\frac{(\Phi m+\Phi-m-2)\Phi^{m+1}+\Phi}{(1-\Phi)^{2}}\right]\right\} \tag{7.29}$$

As transmission takes place when the CA counter reaches zero, this occurs in state (i, 0) i $\in$ (0, m), the probability τ of transmitting within a particular time slot is then given by:

$$\tau = \sum_{i=0}^{m}\phi(i,0) = \sum_{i=0}^{m}\left[\frac{p}{(1-p)}\right]^{i}\phi(0,0) \tag{7.30}$$

which can then be written as:

$$\tau = \frac{2(1-\Phi^{m+1})}{(W+1)(1-\Phi^{m+1})+a\left[\frac{(m\Phi+\Phi-m-2)\Phi^{m+1}+\Phi}{(1-\Phi)}\right]} \tag{7.31}$$

Note that if we have no CAS back-off and hence a = 0, τ reduces to the simple expression:

$$\tau = \frac{2}{W+1} \tag{7.32}$$

Note also that if p = 1/2, then Φ = 1 and the expression for τ in (7.32) can not be resolved. This is addressed by using (7.29) and (7.31) giving:

$$\tau = \frac{2}{W + am/2 + 1} \quad p = 1/2 \tag{7.33}$$

This gives a non-linear systems in p and τ which can be solved using a numerical successive approximation techniques. As p and τ are probabilities in the range [0 1], a very accurate numerical solution can be found through successive approximation.

In summary, the AIr MAC utilisation and delay are given by:

Utilisation

$$S = \frac{P_S P_{tr} N_b L}{(1-P_{tr})\sigma + P_{tr} P_S T_S + P_{tr}(1-P_S) T_C}$$

Delay

$$\delta = \frac{n \cdot [(1-P_{tr})\sigma + P_{tr} P_S T_S + P_{tr}(1-P_S) T_C]}{P_S P_{tr}}$$

Probability of transmission success

$$P_S = \frac{n\tau(1-\tau)^{n-1}}{P_{tr}}$$

Probability of transmission

$$P_{tr} = 1-(1-\tau)^n$$

Successful transmission network time

$$T_S = T_{RTS} + T_{ta} + T_{CTS} + T_{ta} + N_b T_{Data} + T_{EOB} + T_{EXIT}$$

Collision transmission network time

$$T_C = T_{RTS} + T_{WF-CTS}$$

Probability of transmission within a transmission slot

$$\tau = \frac{2(1-\Phi^{m+1})}{(W+1)(1-\Phi^{m+1}) + a\left[\frac{(m\Phi+\Phi-m-2)\Phi^{m+1}+\Phi}{(1-\Phi)}\right]} \qquad p \neq 1/2 \qquad \Phi = \frac{p}{1-p}$$

$$\tau = \frac{2}{W + ma/2 + 1} \qquad p = 1/2$$

Probability of transmission collision

$$p = 1-(1-\tau)^{n-1}$$

solve numerically p and τ

These expressions therefore provide the AIr MAC protocol saturation condition utilisation and delay in relation to the network size, minimum and maximum CAS window size, CAS window adjustment step, CA slot size, data packet size, data burst size, frame overhead sizes and protocol timer durations.

7.2 AIr MAC Performance Results

The following performance results are produced from the AIr MAC utilisation and delay expressions derived. Results are produced for both a fixed CAS window size and utilising the linear CAS window back-off process.

7.2.1 AIr MAC Reserved Mode Analysis

Figure 7.4 show throughput against CAS window size (fixed) for various network sizes. It can be seen that there is an interaction between the CAS window size and the number of nodes in the network. A small CAS window size in relation to the network will mean a high probability of collisions (i.e. stations choosing the same CAS slot value) which will affect the network utilisation. If a collision occurs, then it is the next highest non-colliding slot time that will succeed. A large CAS window value in relation to the network size will mean a low probability of collision. However the large number of empty CAS slots before transmission will cause an excessive time overhead in establishing a reservation which will affect the utilisation. Therefore there is an optimum CAS window size for a particular network size which will minimise both the probability of collision and contention overhead.

Figure 7.5 shows the average burst delay against CAS window size for the same network sizes. If the CAS window size is small in comparison with the network size the average burst delay falls sharply as the probability of collision becomes very small. For window sizes comparable or larger than the network size, the delay remains constant with the window size until the CAS window causes an excessive contention delay.

Figure 7.6 shows utilisation against number of network nodes for various CAS window sizes. This again shows an optimum network size for a particular CAS window value. However it can also be seen that a CAS window value of around 32 slots will provide an approximate constant throughput for a network size above 5 nodes and only slightly reduced below.

Figure 7.7 shows the average burst delay against number of network nodes for the same window sizes. It is seen that for large window sizes the delay is linear with n and agrees with the approximation in (7.18). However for a small window size the delay increases non-linearly with n as the average collision time component becomes dominant (equation 7.17).

In Figure 7.8 shows the utilisation versus number of network nodes using the CAS window back-off process with an adjustment of ± 4 slots. This produces the result that with the initial CAS window size as small as possible, the throughput becomes effectively independent of network size. Figure 7.9 show the average burst delay for versus network size using the CAS window adjustment. The delay is linear with n but with a higher average contention delay than for the fixed CAS value. These results show that the ± 4 CAS window back-off algorithm works very well at maximising the throughput for all network sizes. If a simpler low-cost system using a static CAS window size is required, a window size of 32 slots is shown to produce good results for large networks, while a window size of 8 is effective for small networks.

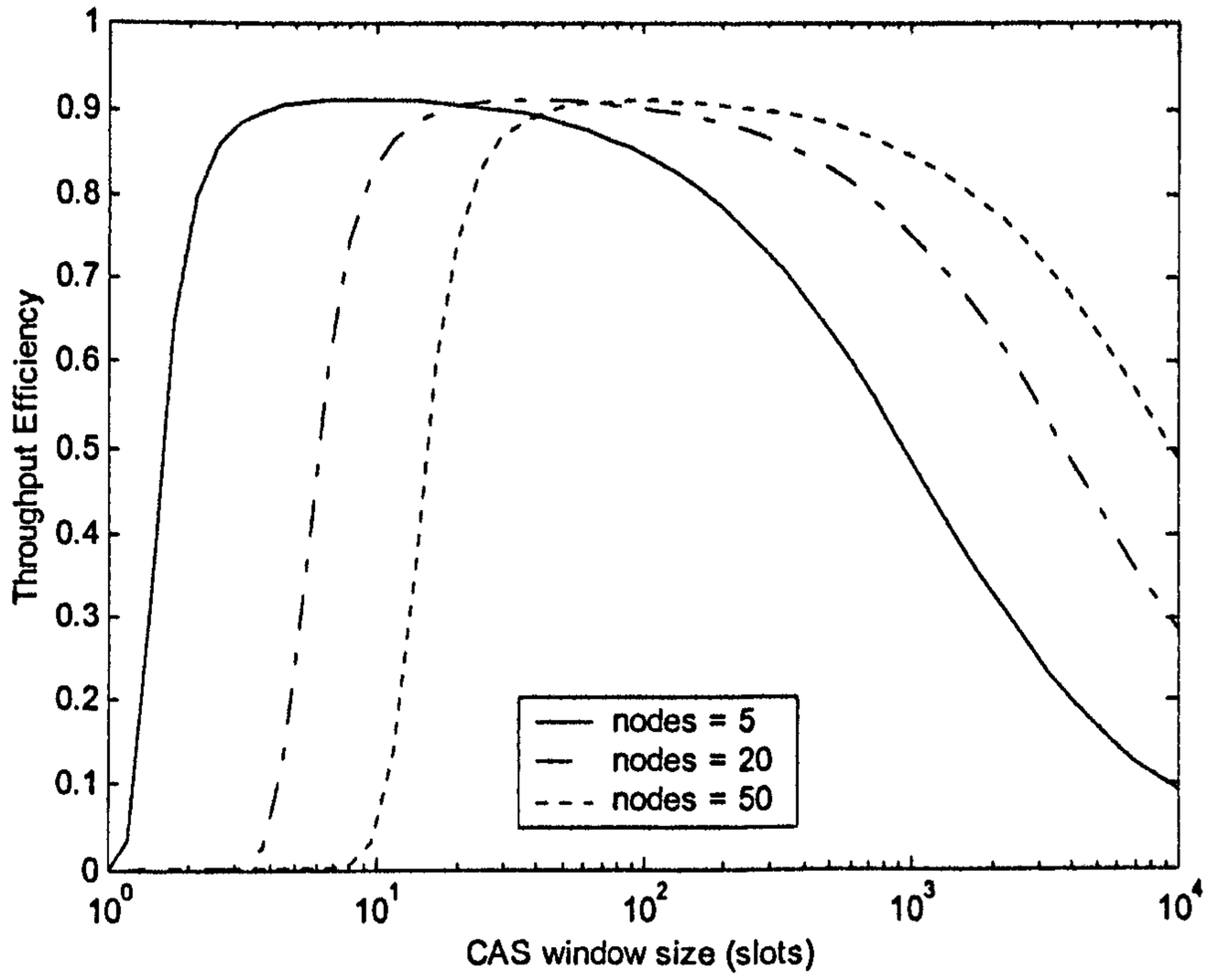

data rate = 4 Mbits/s repetition rate = 1
burst size = 20 frames packet size = 16384 bits

Figure 7.4 Throughput versus CAS window size

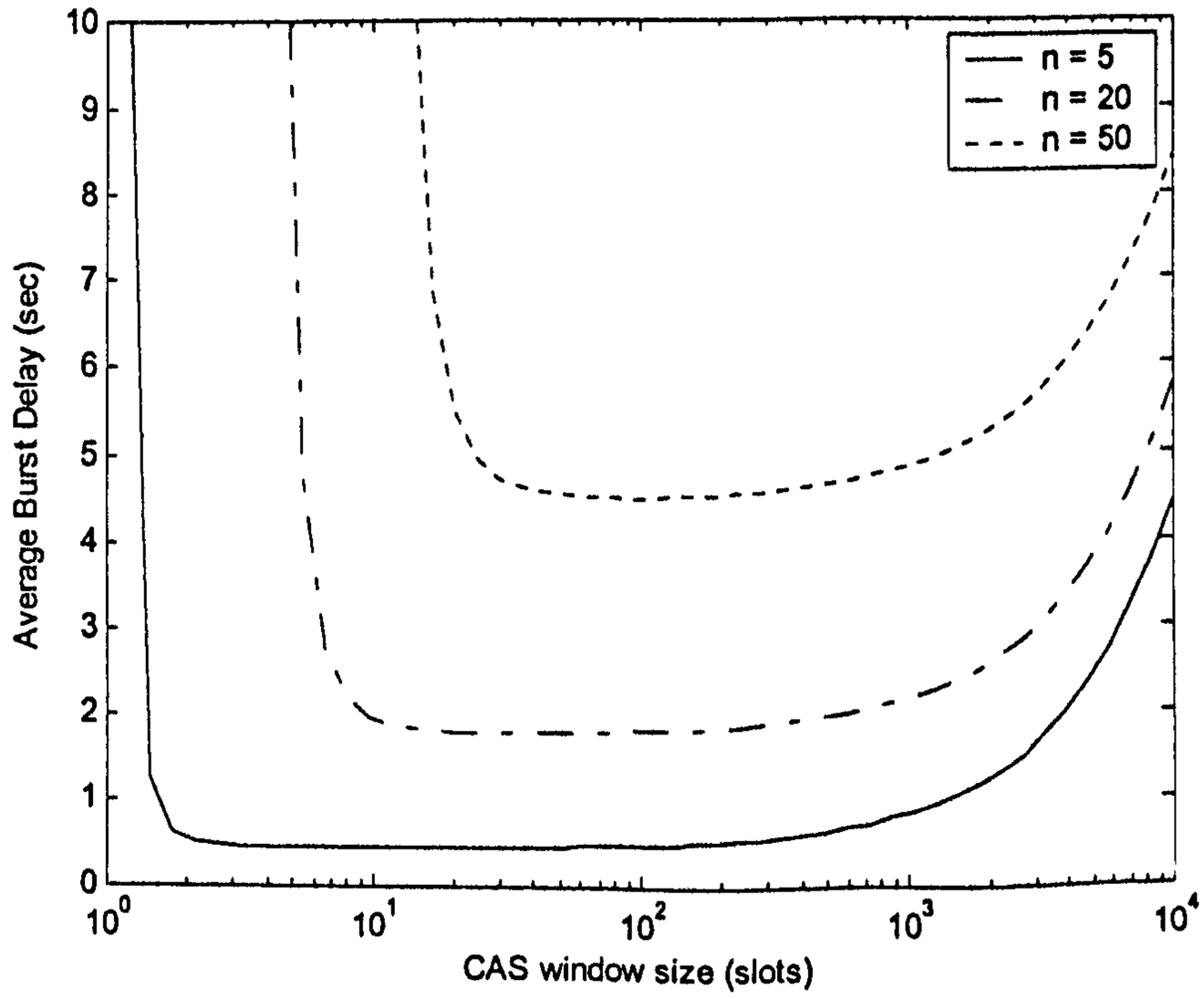

data rate = 4 Mbits/s repetition rate = 1
burst size = 20 frames packet size = 16384 bits

Figure 7.5 Average burst delay versus CAS window size

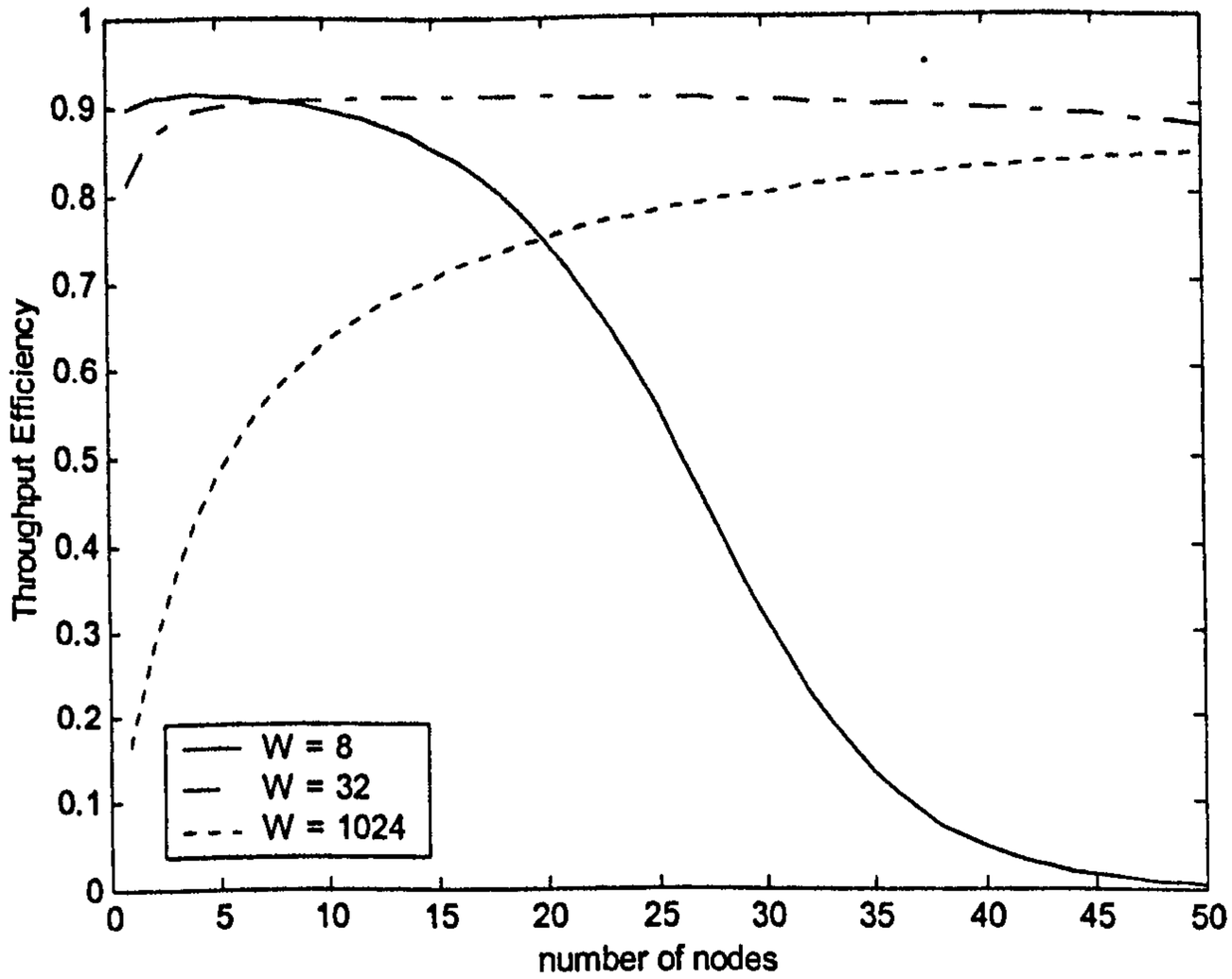

data rate = 4 Mbits/s repetition rate = 1
burst size = 20 frames packet size = 16384 bits

Figure 7.6 Throughput versus number of nodes and CAS window size

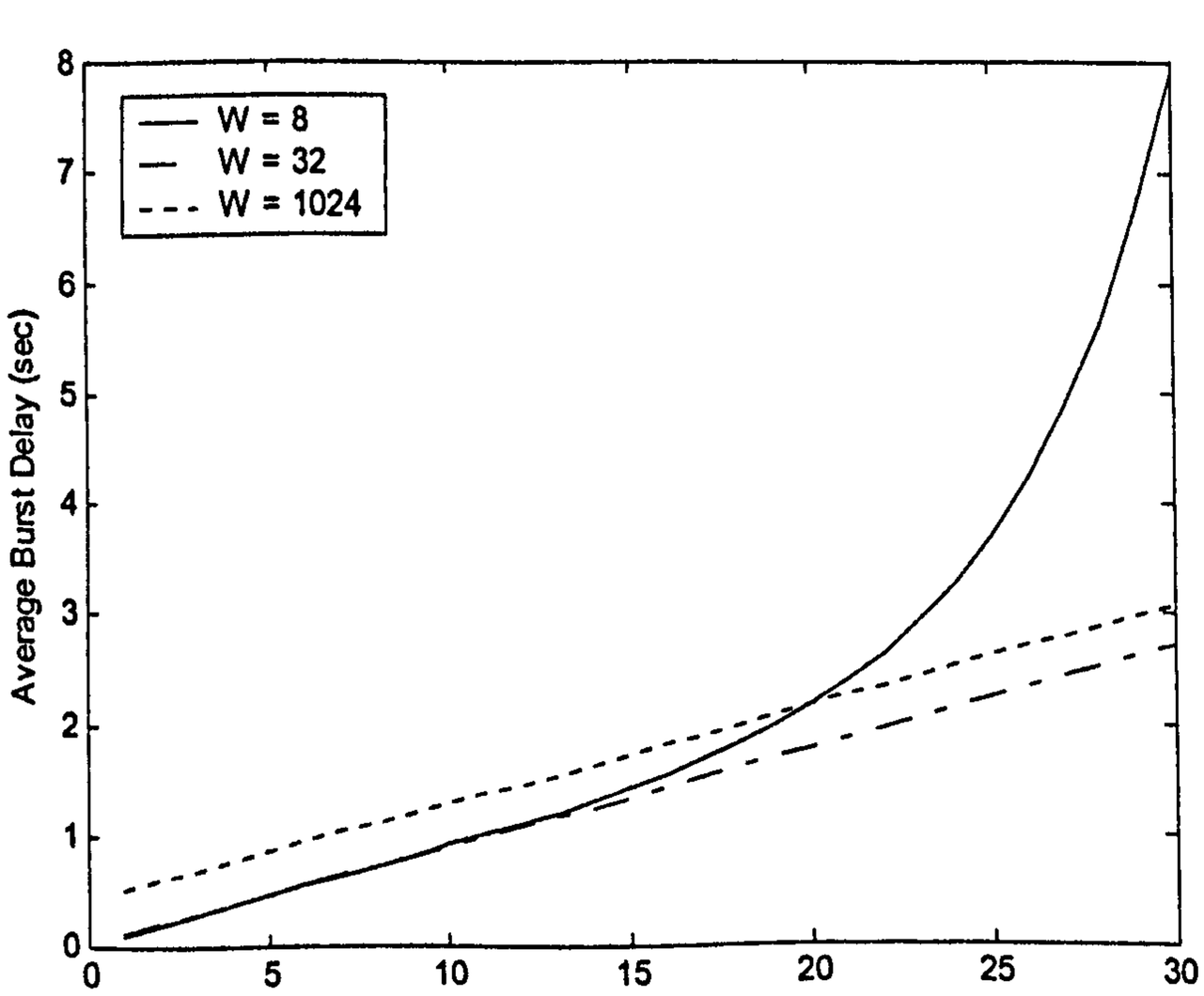

data rate = 4 Mbits/s repetition rate = 1
burst size = 20 frames packet size = 16384 bits

Figure 7.7 Average burst delay versus number of nodes and CAS window size

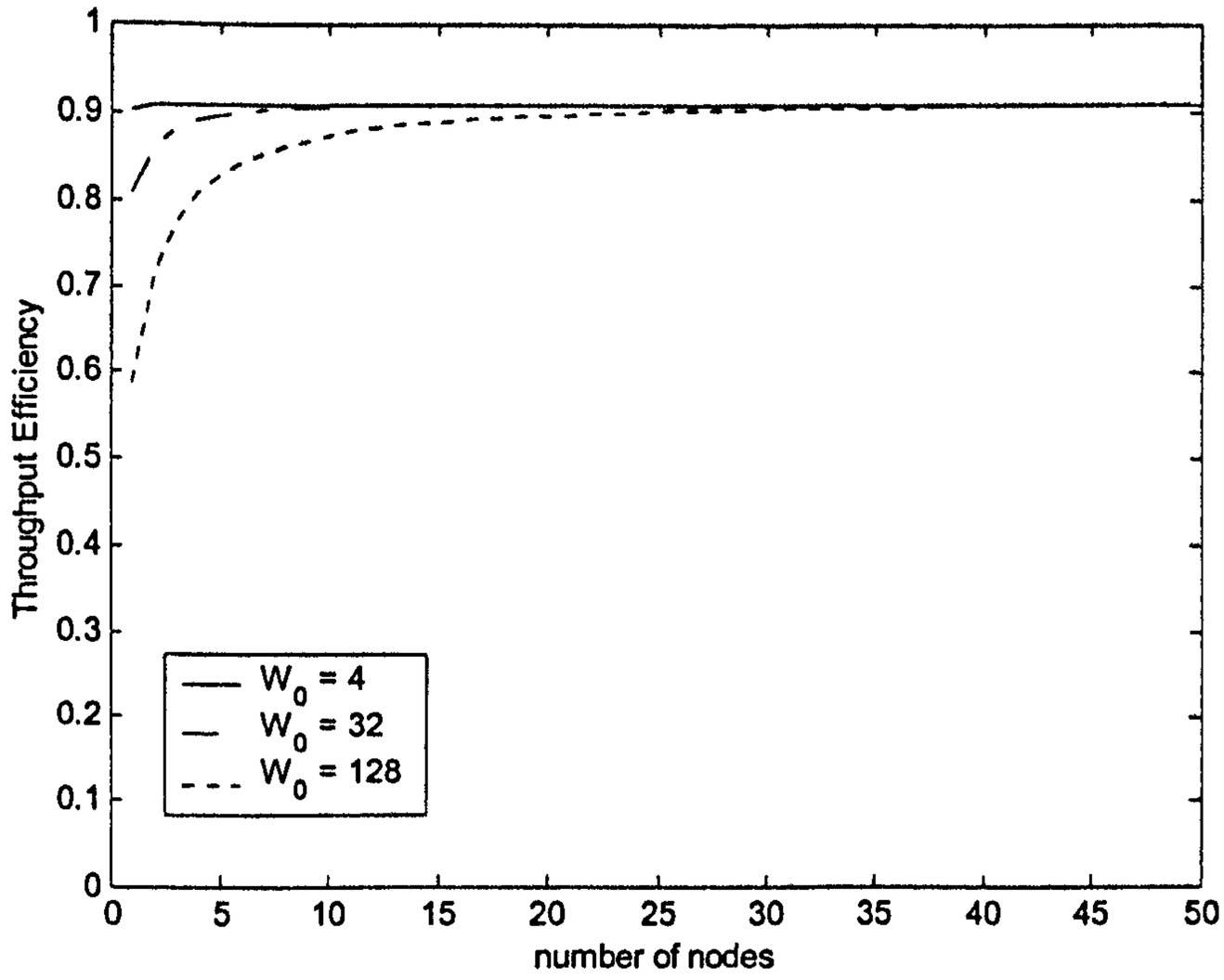

data rate = 4 Mbits/s repetition rate = 1
burst size = 20 frames packet size = 16384 bits

Figure 7.8 Throughput versus number of nodes for ± 4 CAS window back-off

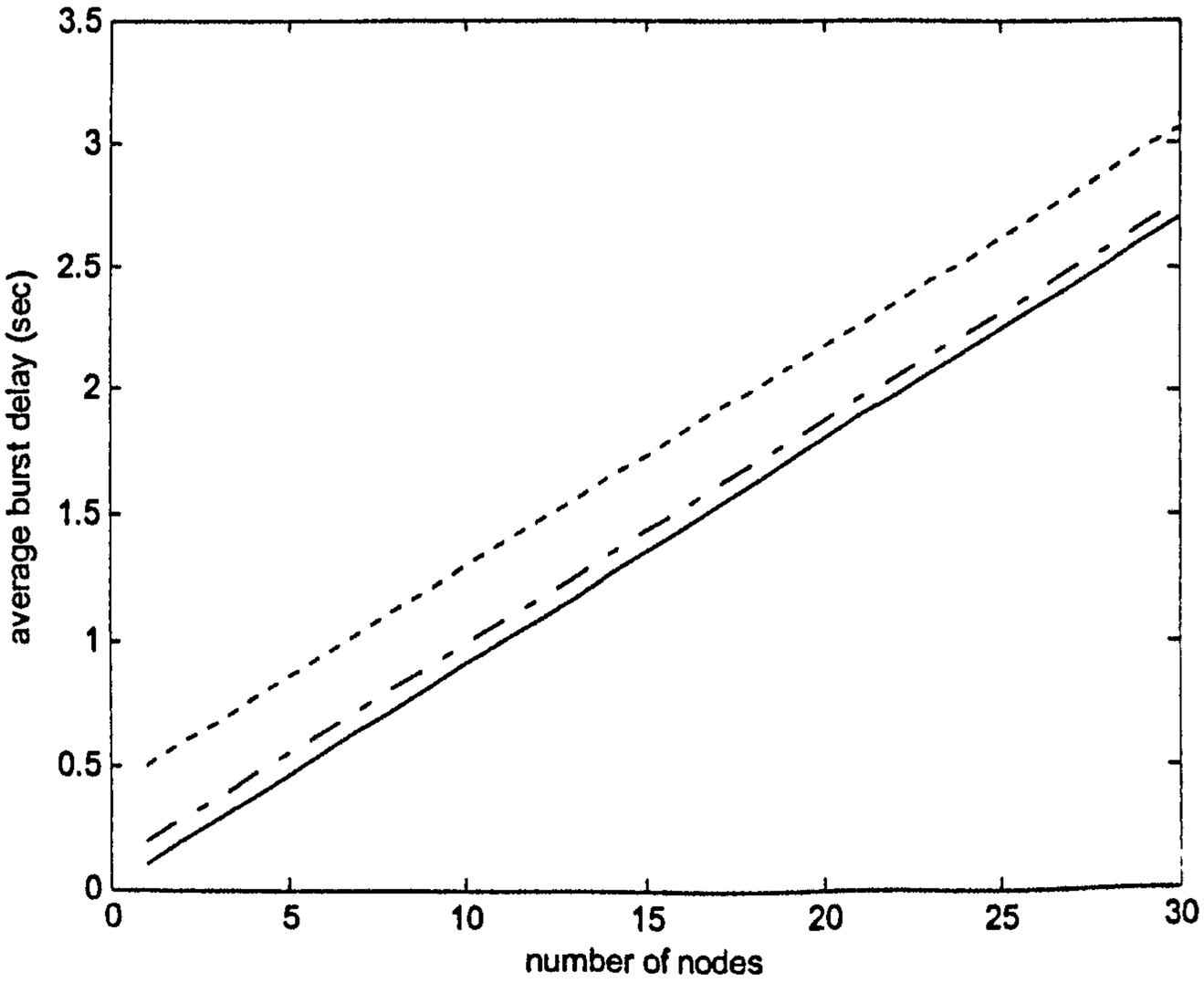

data rate = 4 Mbits/s repetition rate = 1
burst size = 20 frames packet size = 16384 bits

Figure 7.9 Average burst delay versus number of nodes for ± 4 CAS window back-off

7.2.2 Validation of AIr MAC Analysis results

Figures 7.10 to 7.13 show simulation and analytical utilisation and delay results for validation of the results from the AIr MAC analytical model. The results are produced from the AIr network OPNET simulation model described in Appendix A. These show a good correlation between the simulation and analytical results demonstrating a good accuracy of the analytical model.

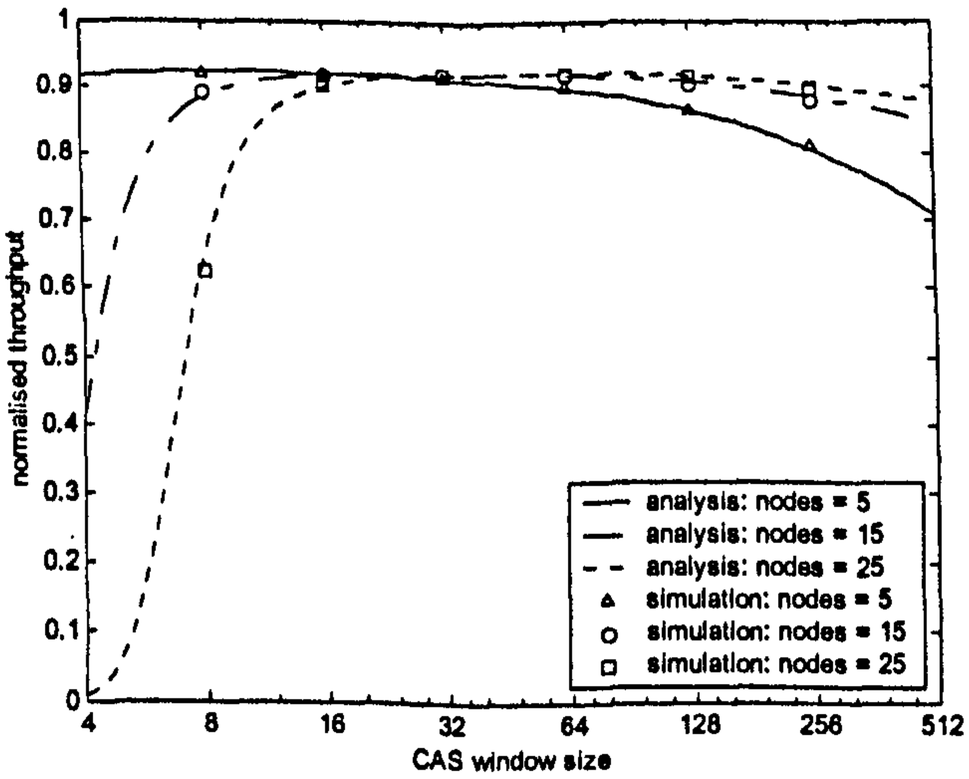

Figure 7.10 Simulation and analysis throughput versus CAS window size

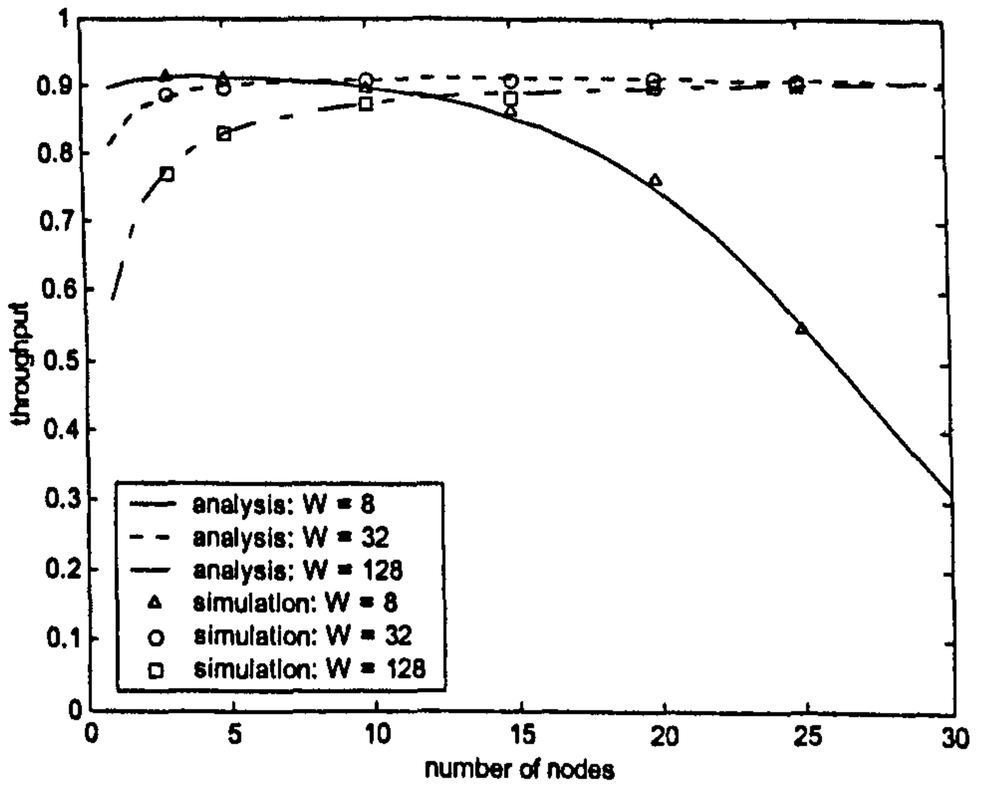

Figure 7.11 Simulation and analysis throughput versus network size

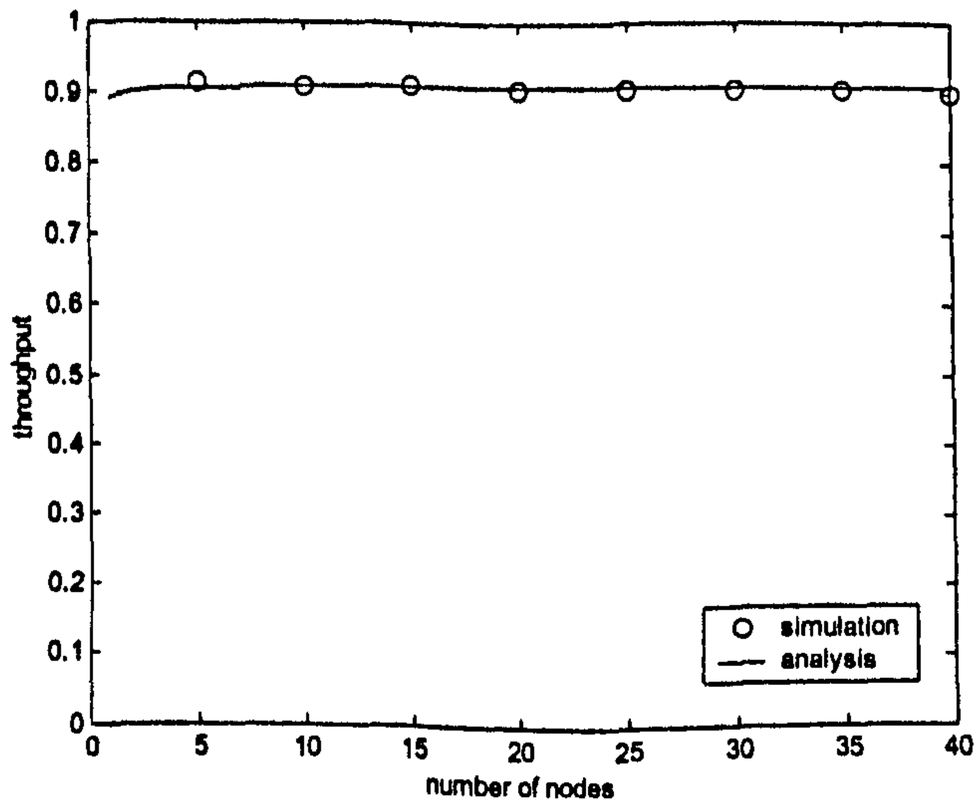

Figure 7.12 Simulation and analysis throughput versus network size with CAS back-off

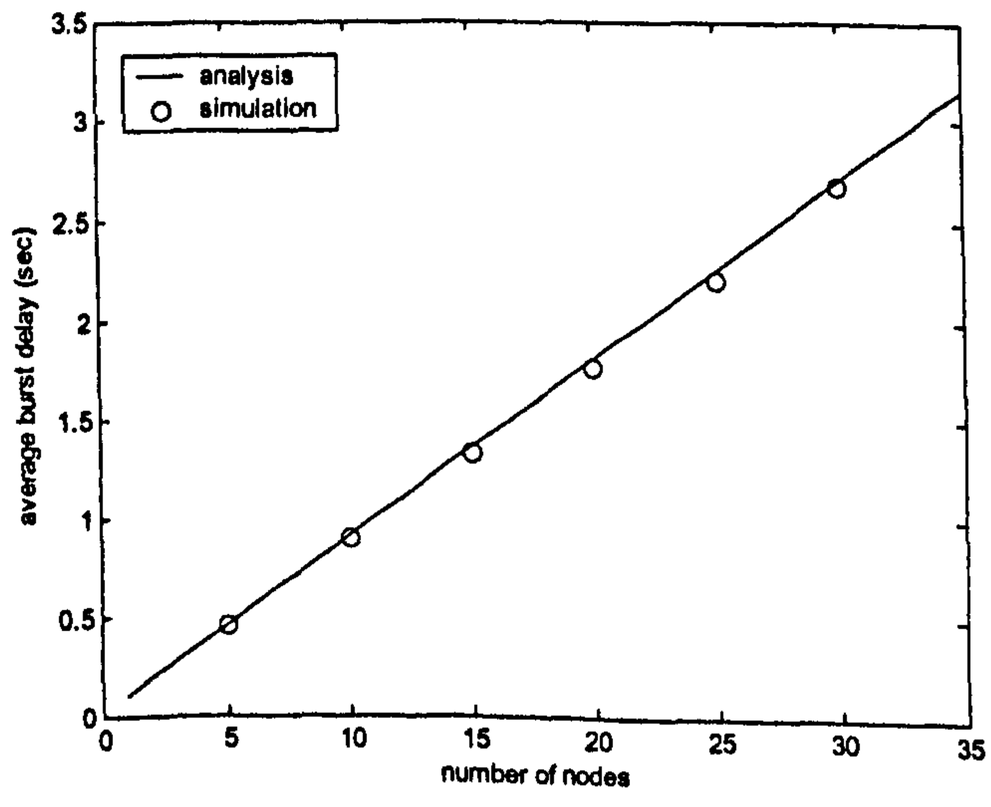

Figure 7.13 Simulation and analysis delay versus network size with CAS back-off

7.2.3 AIr MAC Unreserved Simulation Results

In the Unreserved mode, a UDATA frame is transmitted after winning contention for the medium. There is no acknowledgement from the receiving station so the transmitting station does not know if a collision has occurred. As such the CAS window back-off process is not possible in this mode. If a collision occurs, the other stations in the network will not be aware that any transmission has been made and will continue to contend for the medium. The two or more transmitting devices who collided (choose the same CAS slot time) will continue contending for the medium when the frame transmission has completed. This puts these stations out of synchronisation with the other contending stations as the UDATA frame transmission time is greater than a slot time duration. Collisions can then occur when transmissions times partially overlap. Synchronisation only occurs following a successful transmission. In this case stations hearing the start of transmission will pause the CA timer, and restart the timer when reception of the frame has completed. Figure 7.14 shows throughput versus CAS window size for networks sizes of 5, 10 and 20 stations in unreserved mode. The throughput initial rises with the CAS window size as the probability of collision decreases then fall . The maximum utilisation achieved for the 5 station network in only approximately 50%. Figure 7.15 shows the average packet delay versus CAS window size for the unreserved mode. These demonstrate that the unreserved mode is both unreliable (no acknowledgement) and inefficient. The CAS window size would need to be carefully set for a particular network size to optimise the utilisation.

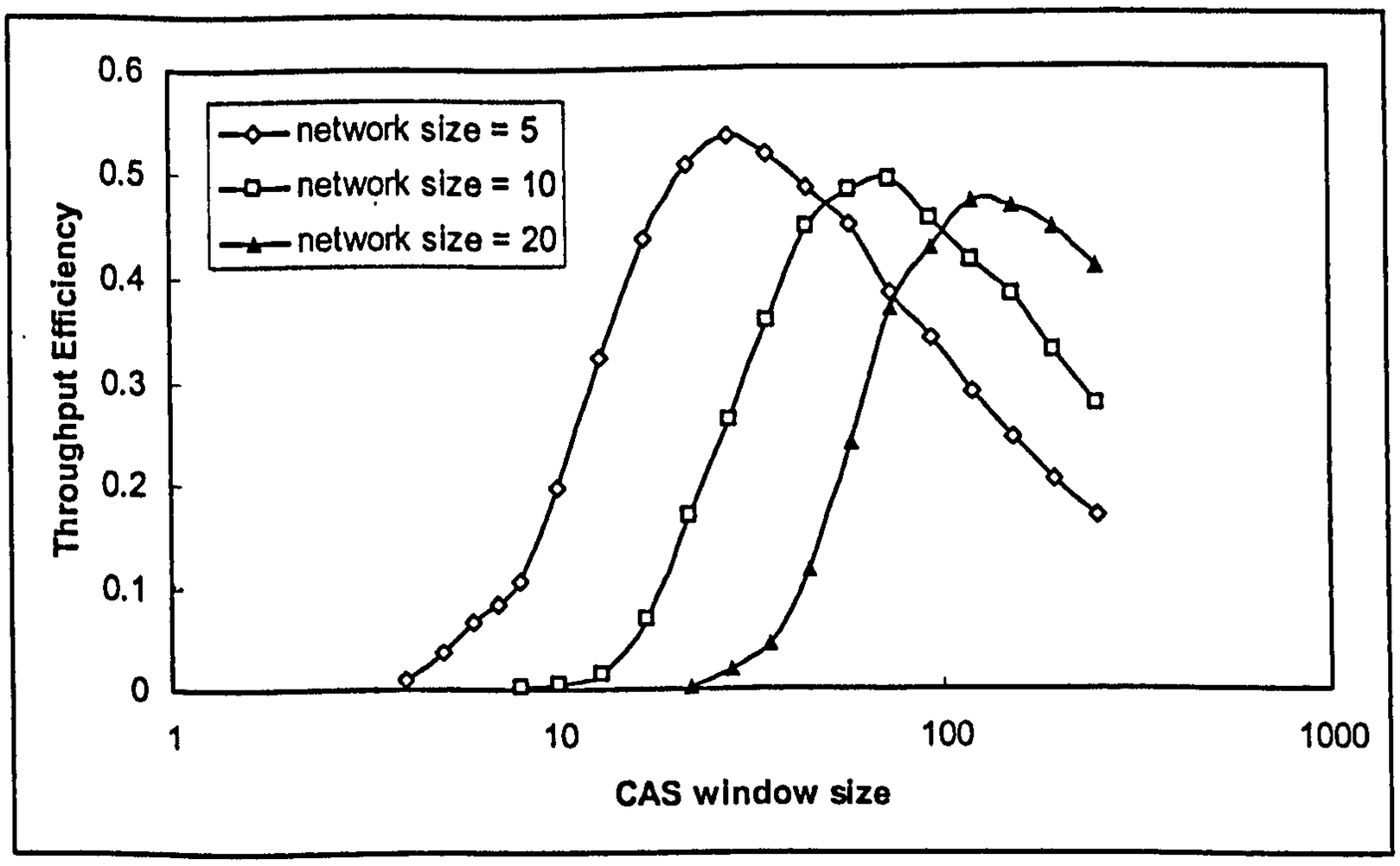

Figure 7.14 Simulation of unreserved throughput versus CAS window size

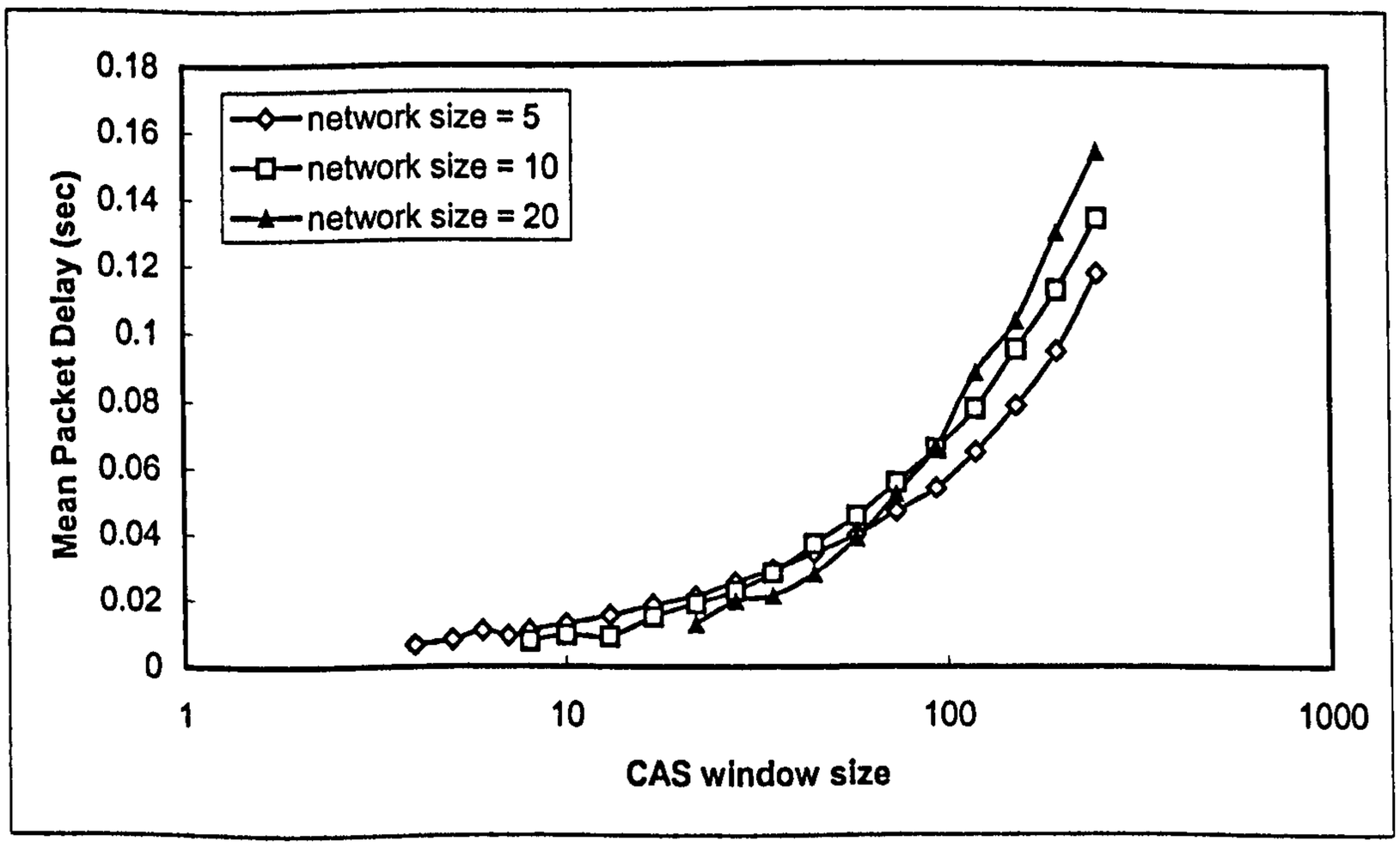

Figure 7.15 Simulation of unreserved packet delay versus CAS window size

7.3 Chapter Summary

This chapter has presented an analytical model of the AIr MAC protocol to provide reservation mode saturation utilisation and delay in relation to the network size (number of contending devices), contention window size and other MAC parameters. The analysis also examines the contention window back-off process using a Markov model of the process and concludes that the process is very effective at optimising utilisation for all network sizes. Analytical results are validated by results from an OPNET simulation model of the AIr protocol. The simulation model is also used to produce unreserved mode utilisation and delay results in relation to network size and contention window size.

8. CONCLUSIONS AND FURTHER WORK

8.1 Summary of Thesis

An analysis of the IR wireless physical layer has provided expressions for link bit-error-rate (BER) in relation to transmitter characteristics (output radiant intensity, radiation lobe), receiver characteristics (area, responsivity, field-of-view, bandwidth), link distance and geometry, line modulation / encoding scheme, and ambient light power level. The effect on the link BER of third IR wireless user interference and resultant directional and spatial asymmetry have also been examined. This indicates the minimum separation distance for independent links without cross-interference.

An analytical model of the IrDA 1.x IrLAP protocol has been presented which provides saturation condition throughput in relation to link data rate, BER and link parameter settings of data packet size, transmission window size, minimum turn-around delay, and maximum turn-around time. Numerical values have been provided for simultaneous optimisation of data packet size and transmission window size for maximum throughput. Linking of the physical layer BER to throughput analysis provides the effective range of links and range increase with optimisation. Results from a simulation model of the IrDA 1.x protocol validate the analytical model results and analyse non-saturation IrLAP throughput and delay.

An analytical model of the IrDA AIr (Advanced Infrared) MAC protocol has been presented and provides saturation condition utilisation and delay in relation to the network size (number of contending devices), contention window size and parameter settings of data packet size, transmission burst size and contention time slot size. The effectiveness of the proposed contention window back-off process has been examined using Markov analysis. Results from a simulation model of the AIr MAC process validate the analytical model and analyse non-reservation utilisation and delay.

The main contributions to knowledge from this thesis are:

1. Derivation of expressions for accurate calculation of IrDA 1.x IrLAP link saturation throughput from link BER, data rate and protocol settings.
2. Simultaneous optimisation values for data packet size and transmission window size.
3. Derivation of expressions for utilisation of and delay of the IrDA AIr MAC protocol and analysis of the effectiveness of the contention window back-off procedure.
4. Derivation of expressions for IrDA based physical layer BER in relation to transceiver characteristics, link geometry, line encoding schemes, ambient light levels and the presence of a third user interferer.
5. Indication of minimum independent link separation through asymmetry analysis.
6. Linking of IR physical layer properties derived BER to IrLAP layer throughput.

8.2 IrDA 1.x Analysis Conclusions

Minimum Turnaround Delay. The Minimum Turnaround Delay required each time control of the link is passed from one station to the other has been shown to be a critical factor in the link performance. The effect becomes more significant with higher data rates as the link is turned around (after the maximum window of frames has been transmitted) much more frequently. The delay required must cover the latency period of the receiver. Receivers can have very low latencies but at a higher manufacturing cost. There is thus a trade-off between cost and higher throughput efficiency through lower minimum turn-around delay. A low turn-around delay will also allow a constant and small window size to be used in the simultaneous optimisation of the packet and window size with a varying packet size optimising throughput.

Packet Data Size. The performance of an IrLAP link will generally improve with an increased packet size as a) the relative contribution of the frame overhead is reduced and b) the frequency of the minimum turn-around delay implementation is reduced. However a larger packet size becomes more susceptible to bit errors. There is therefore a trade-off between packet size and reduced throughput through the packet error probability which results in an optimum packet size for a particular link BER. It has been shown that with a low BER in certain configurations, the optimum packet size is in

excess of the maximum specified 16384 bits (2 Kbytes). The maximum data packet size may therefore need to be extended but may still be limited by the maximum size that can be protected by the CRC. Using a variable packet size may also require packet segmentation and reassemble functions at higher protocol levels.

Transmission Window Size. As with the data packet size there is a trade-off between transmission window size and the number of frame re-transmissions due to errors. If frame errors occur for a large window size then, as the re-transmission starts with the first frame error in the window, a large number of frame re-transmissions may be required. The larger the link BER value, the greater the probability will be of a frame error occurring near the beginning of the window requiring most of the window to be re-transmitted. As with the data packet size there is therefore an optimum transmission window size for a particular BER.

Optimisation of Performance. It has been shown that using simultaneous optimisation of the data packet size and window size optimises the link performance in relation to the link BER. If the minimum turn-around delay is made small ($\leq$ 0.1 ms) the optimised window size can be made independent of BER and small (< 7 frames) such that the 127 frame extension may not be required. Optimisation is then provided through setting the optimum data packet size in relation to the BER. This may be physically implemented by inference of the BER from the current frame size and frame drop rate. In relation to the link distance, optimisation provides a more gradual fall-off in throughput with increasing link distance and increases the link cut-off range.

F-timer duration. The analysis of the IrLAP protocol has shown that the F-timer duration is of significance. If the P-bit frame or returned F-bit frame from the secondary is lost, the primary must wait for the expiration of the F-timer before sending an S-frame to re-poll the secondary. This delay can significantly affect the link throughput. The F-timer duration should therefore be set to the minimum required to receive the F-bit frame from the secondary for the particular application envisioned.

8.3 IR Physical Layer Conclusions

Optical Power Output: The electrical signal-to-noise ratio (SNR) increases with the square of the received optical power. Therefore increasing the LED optical power output can greatly increase the SNR and hence performance of the link. However there are limits on the optical output. Power efficiency must be maintained in order to preserve the battery life of portable IR devices. There is also a output power regulation for eye-safety limiting the maximum output intensity to 500 mW/Sr. Output power should therefore be minimised while maintaining the required link quality.

Ambient Light: The dominant source of noise in an IR receiver is shot noise induced by background ambient light (from both sunlight and artificial sources) in the receiver. The induced shot noise is a white Gaussian random fluctuation of the photodetector current about its mean value. An optical filter can reduce the level of ambient light outside of the signal wavelength band, but ambient sources can have a high infrared content within the band. High quality optical filters can have a very narrow pass-band with high attenuation outside the band, but with greater expense. An input electrical high pass filter in the receiver can also reduce the dc and low frequency components from the noise signal.

Receiver Bandwidth. A critical factor at the physical layer is the bandwidth of the receiver. As the receiver noise is dominated by a white Gaussian component induced from incident ambient light levels, the total receiver noise power increases with the receiver bandwidth. The bandwidth needs approximately to be equal to the line data rate in Hertz so higher data rates require a higher bandwidth causing a lower SNR and hence higher BER for the same transmitter power. Analysis of the IR physical layer has shown that there is a sharp 'cut-off' of performance at a critical link distance. Increasing the bandwidth decreases the cut-off distance.

Link Asymmetries. It has been demonstrated that link directional and spatial asymmetry can occur in the presence of a third user interferer. For IrDA 1.x links, there is no inherent mechanism to detect a third user interferer so the approach of the interferer will degrade the BER and hence IrLAP level throughput in the direction of

approach. The use of narrow angle transceivers can reduce the spatial asymmetry effects. Using narrow angle transceivers with the minimum IrDA physical layer specification allows multiple IR wireless links to be operating in very close proximity (< 0.5 m) without cross interference.

8.4 AIr Analysis Conclusions

Collision Avoidance Window Size. It has been shown that the size of the CAS window (the range from which a random number of CA slots is chosen) is significant in the performance of the AIr network. If the CAS window is small in relation to the network size (number of stations) then there is a high probability of collision. If a collision occurs (when two or more stations chose the same lowest CAS value – assuming saturated conditions), it is the next highest non-coinciding chosen slot that will succeed. If the CAS window is large in relation to the network size then collisions are less probable but the extra CAS slots provide an excessive time overhead which affects the utilisation. Using a dynamic CAS window back-off process can be very effective in dealing with this. However the CAS back-off can only be used where an acknowledgement is returned from the destination station (e.g. the RTS/CTS exchange). A collision is then detected by the acknowledgement timer expiring. For the unreserved data exchange where there is no recipient acknowledgement (i.e. transmitting UDATA frames) there is no way of determining if a collision has occurred. A fixed CAS value must be used in such situations. For a low-cost reservation system with a fixed CAS window, a value of 32 slots has been shown to provide good utilisation for large networks (above 5 devices) and a value of 8 slots to provide good utilisation for small network sizes.

Dynamic CAS Window Back-off Process. It has been shown that using the proposed dynamic CAS window back-off process with an adjustment of ±4 slots is very effective in optimising the CAS window size and effectively produces a throughput independent of network size. The process parameters that may affect performance are the upper and lower limits placed on the adjustments. For example for a network of just 3 stations, the default lower limit of 8 slots may need to be reduced to remove an excessive overhead. As stated above, the process cannot be used in the unreserved mode.

Collision Avoidance Slot Size. A default CA slot time of 800 μs is used in the AIr specification. This was chosen to be sufficiently large to cover the time for an RTS transmission and the beginning of a CTS reply. This prevents overlapping of reservation attempts and covers the 'hidden node' problem. However in certain situations this time can cause an excessive overhead that can affect performance. When using the unreserved mode, a single frame only is transmitted for each contention and a fixed CAS window size must be used. The relative time overhead can severely impair the performance. As there is no CTS reply in this situation, the CA slot time could be reduced to cover the PA and Sync portions of the transmitted UDATA frame only (e.g. 200 μs).

Reservation Burst Size. It can be seen that due to the time overheads of collision avoidance, reservation establishment and frame overheads, the efficiency the AIr network improves with greater burst size (packets per burst). However the burst size may be limited by the requirements of upper layer protocols.

8.5 Suggestions for Further Research

The following presents suggestion for further research related to the performance modelling and optimisation of IR wireless systems and protocols.

8.5.1 Further IrDA Protocol Research

Dynamic Adjustment of IrLAP parameters: It has been shown in the IrDA 1.x protocol analysis that the IrLAP parameters of packet size and transmission window size have optimum values for link throughput in relation to the link quality (BER). A dynamic adjustment of these parameters could help stabilise the link performance in varying noise level environments. The adjustments would need to be based on the number of required packet re-transmissions indicated by the returned Nr field. A packet size adjustment may require data packet segmentation and re-assembly functions for packets from upper protocol levels which can increase the complexity of the protocol. The exact nature of the adjustment algorithms for optimum performance (e.g. linear or

exponential, parameters) can be determined experimentally. Simulation modelling of the protocols can be useful for these experimental processes.

Modelling High Speed Extensions: In addition to the proposed 16 Mbits/s high speed IrDA extension, it may be feasible to extend to even higher data rates such as 100 Mbits/s, which could facilitate interfacing to existing LAN architectures (e.g. 100 Mbits/s Ethernet). The possible implications of operating at such data rates would need to be examined. For example it can be seen from the IrDA analysis that very low minimum turn-around delay and a high receiver bandwidth would be required. For such high speeds, propagation delay may also begin to be a factor needing consideration.

Varying Noise: In the analysis of the IrDA protocol it has been assumed that the devices used in the link are static and that the link noise level (BER) is constant. However in reality the link noise level may vary during course of data transfer. This may be due to some physical movement of the devices involved or varying ambient light levels due to some external variance (e.g. turning on/off of lights, movement of people). An example of a movement of devices could be the natural 'sway' of hand movement when using a hand-held computing device transmitting to fixed device. Simulation modelling can be very useful for performance modelling of these condition as the response to a time varying input can be simulated. However it may be difficult to accurately simulate the varying input itself. Normally some mathematical distribution of values is required.

Modelling LAN Interface: It may be possible using simulation to model the interaction of the IrLAP layer with an interface to a LAN network such as Ethernet using an IrLAN protocol model in combination with other upper IrDA protocol layers such as IrLMP and Tiny TP.

Physical System Experiments: It would be useful to obtain experimental results of IrLAP performance against physical layer measurements (link distance, ambient light levels, transceiver characteristics etc.) to compare with the performance results obtained in this thesis.

8.5.2 Further AIr Protocol Research

Link level and link quality performance. In the performance modelling of the AIr protocol so far carried out, the medium is assumed error free and that all stations can receive transmissions from all other stations in the network. The performance has been solely based on the media access feature of collision avoidance and media reservation. Further research can be carried out by examining the effects of physical layer characteristics and link noise on AIr performance. Rather than the BER of the medium the PPM chip-error-probability (chip = single PPM slot) should be used to determine the error allocation for variable repetition PPM encoded AIr packet segments. At the MAC layer, this will allow the effects of hidden nodes and of packets lost due to errors in addition to packet collisions to be examined. At the AIr LC data link layer, the throughput of the balanced HDLC based procedures can be examined in a similar manner to the analysis of the IrLAP protocol.

APPENDIX A OPNET SIMULATION MODELS

A.1 The OPNET Modeler package

OPNET Modeler is a communication networks modelling and simulation software package from OPNET Technologies (formerly MIL3 Inc). OPNET Modeler uses a set of graphical hierarchical domains which reflect the structure of actual networking systems, namely the Network domain, the Node domain, and the Process domain, to produce a C/C++ coded simulation model of the communications network or system.

The Network domain consists of network node objects (workstations, routers etc.) and network links (e.g. Ethernet lines). Sub-networks can also be used to represent an entire network topology. Long distance networks can also be represented against a geographical map. Data packets are transferred between nodes on the network level. The transmission of packets across network links is controlled by pipeline-stage C/C++ coded routines. The complexity of these depends on the link type (e.g. point-to-point, multiple access, wireless). The main functions include the assignment of transmission and propagation delays to the packet, and the assignment of bit errors. The latter are assigned randomly based on the link bit-error-rate ('ber') parameter value and the packet size. There is then an error threshold at the receiver that determines the packets acceptability. Rejected packets are simply discarded and do not reach their destination. This simulates the action of the CRC process used in most communications systems.

Each node object in the network domain represents a node model in the Node domain. The Node domain consists of connected process modules and link receiver and transmitter modules. Some process modules are pre-built (e.g. queue modules and ideal data source modules). The principal means of communication between processes in a node is through data packets and Interface Control Information packets (ICIs), both of which are actually C data structures. Each process module (not including pre-built modules) in the node domain represents a process model in the Process domain. A process model is represented as a finite state machine (FSM). Each state in the model has an Enter and Exit execution block where C/C++ coded procedures are entered.

Transitions between states have associated condition macros. The flow of control in the process is determined by interrupt events. Theses typically constitute packet arrivals or timer expirations. These are identified by an interrupt type and user defined code using symbolic constants. There are two types of state used; the forced state and the un-forced state. The process will remain in the unforced state until the next interrupt event occurs after which it will move to the next state determined by the state-flow diagram. The process will move immediately from a forced state once the executive blocks have been processed. Thus only the un-forced states actually model true states of the system, while forced states are used to model transitionary processes.

The code blocks in the process domain employ an extensive library of proprietary C functions (known as Kernel Procedures – KPs) that implement OPNET specific procedures, in addition to standard C/C++ functions and syntax. The process is compiled using a standard C/C++ compiler and becomes an 'object' used in the simulation. When compiling, OPNET uses the code in the execution blocks with its own header information and structure to create a single C/C++ code file for the process object. Objects in each domain in the hierarchy can have a set of attributes that can be modified to control the behaviour of the object. These can be set at the object level or promoted to higher levels. Figure A.1 demonstrates the model hierarchy from an example Ethernet model.

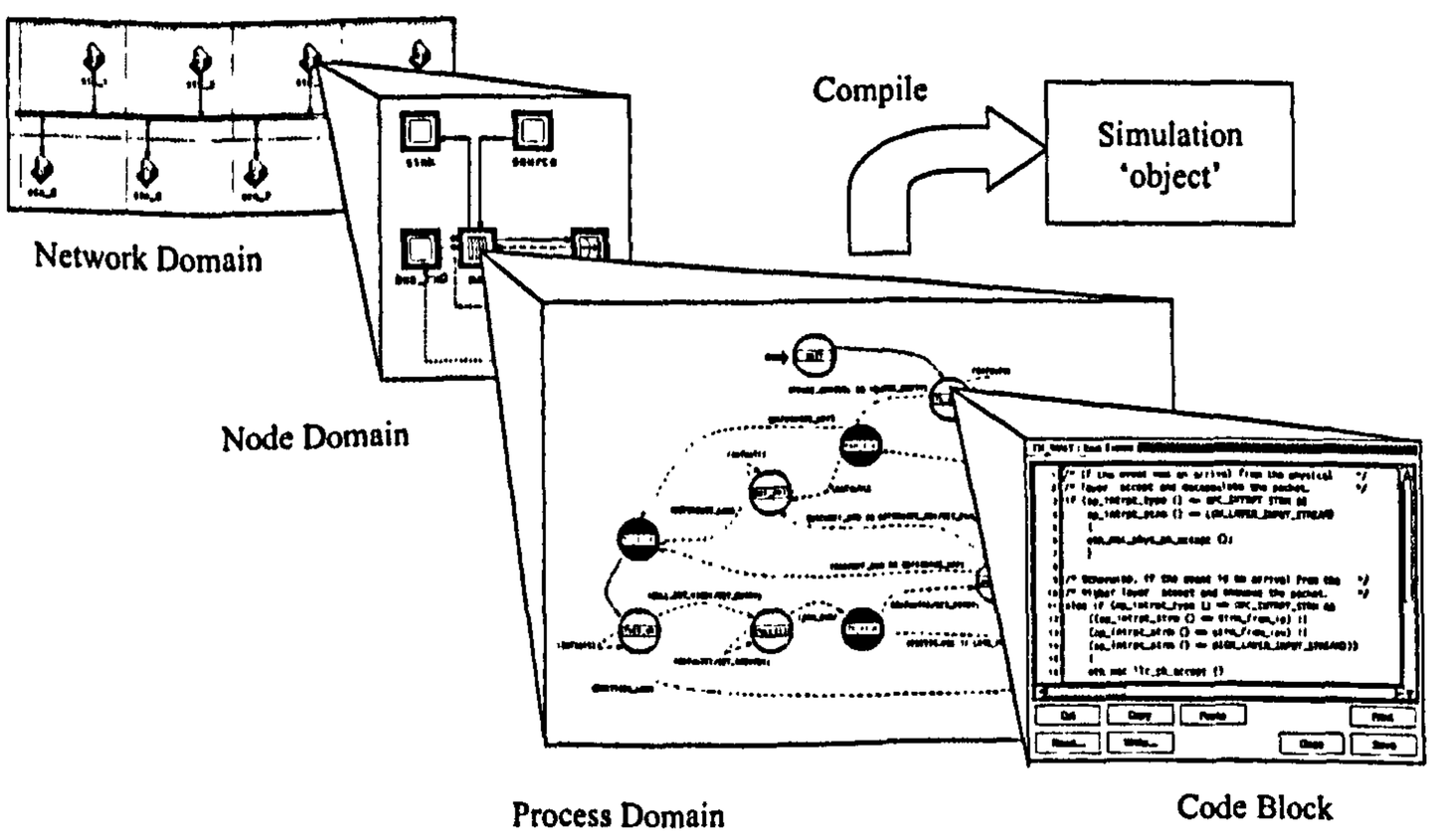

Figure A.1 OPNET modelling hierarchy - Ethernet model example

Simulation takes place in a simulation kernel where the process objects are 'linked' in accordance with the hierarchical structure of the network. The simulation is then event driven where an event is a process interrupt and each event has a simulation time tag association. There are two types of statistics that can be obtained from a simulation. Vector statistics are recorded as a time-value pair and are recorded from individual events during a simulation run. It can therefore be seen how a single statistic varies during the course of the simulation. The other type of statistic are Scalar statistics which are single values collected at the end of a simulation run. A set of simulation runs can then be used to see how a performance measure (e.g. average throughput) varies against some system parameter.

User models can be developed from the beginning but OPNET comes with a substantial model library of standard network systems and protocols. These can be used as they stand or copied and modified for the users particular requirements. An issue in running a simulation is how long (in simulation time) to run the simulation. This depends on the objective of running the simulation, but if some average value of a performance measure is required (e.g. average throughput) for a scalar statistic then the simulation needs to be long enough to 'smooth out' the average value. The collection of the value intended for the end-of-simulation scalar statistic as a vector statistic during the simulation can help determine an effective simulation time. The actual time (clock time) that a simulation takes to complete depends on the processor speed of the host computer and the complexity of the model. Although processes in each node may run concurrently in simulation time, each event will still need to be processed sequentially in the host processor (Barker and Boucouvalas, 2000a).

A.2 The IrDA 1.x OPNET Simulation Model

The following presents details of the IrDA 1.x OPNET simulation model. The model is primarily concerned with modelling the IrLAP process in the information exchange mode. The IrLMP and higher layers of the protocol are not considered in the model.

A.2.1 IrDA Model Network Level

Figure A.2 shows the network level for IrDA 1.x model. The 'network' consists of two desktop computer nodes acting as Primary and Secondary devices, connected by a pair of uni-directional point-to-point links.

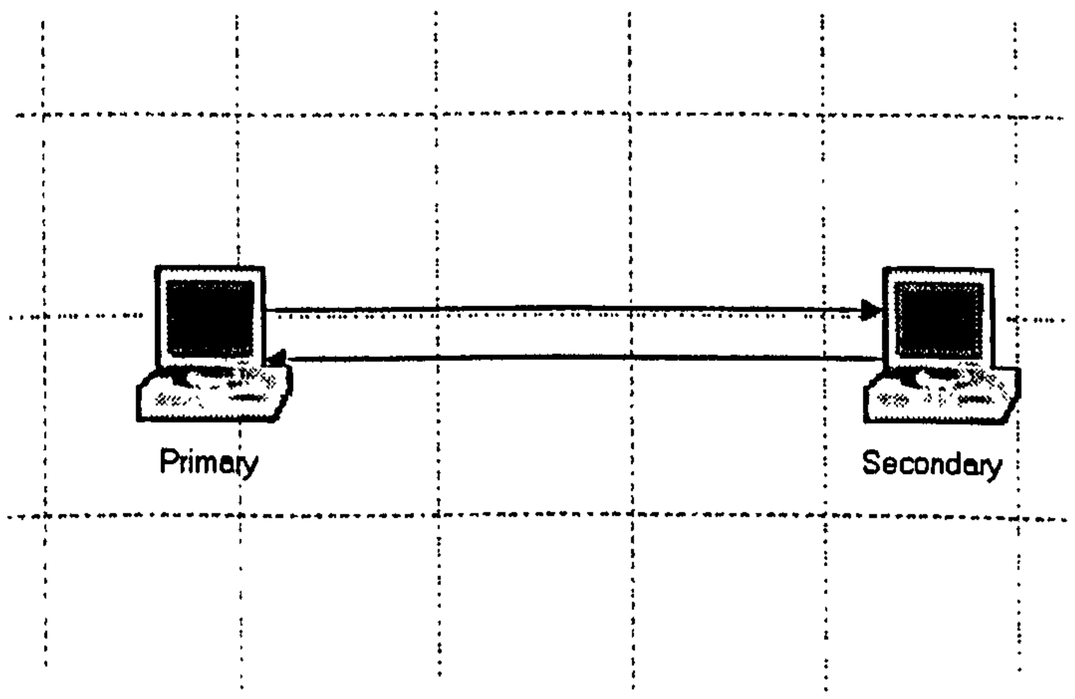

Figure A.2 IrDA 1.x network level model

Although we are modelling an IR wireless system, we are primarily interested in the IrLAP layer performance. The effects of physical layer properties are not considered in the present model. The model simply uses fixed links with user specified 'ber' attributes. These can be set individually for the link in each direction. The link data rates are set by those of the transceivers in the node models.

A.2.2 IrDA Model Packet Format

Only S-frame and I-frame packet format are used. These constitute C data structures that model the contents and size of the individual packet fields. The formats for the standard IrLAP packets are as given in Tables A.1 and A.2:

Name	Type	Size (bits)
BOF	int	8
Address	int	8
Type	int	2
Nr	int	3
P/F	int	1
FCS	int	16
EOF	int	8

Table A.1 IrDA S-frame packet format model

Name	Type	Size (bits)
BOF	int	8
Address	int	8
Type	int	1
Nr	int	3
P/F	int	1
Ns	int	3
Information	Packet	inherited
FCS	int	16
EOF	int	8

Table A.2 IrDA I-frame packet format model

The sizes (in bits) of the individual fields make the total modelled packet size. This is used in calculating the packet transmission time. The value of each field can be set and read from within a process by suitable KPs.

A.2.3 IrLAP Basic Model

The basic model considers saturation traffic from the primary to the secondary only with the secondary returning S-frames only. This is used to validate the throughput and delay results from the IrLAP analytical model. There is no requirement for the P-timer in the primary model as data packets are continually available. The secondary is reduced

in complexity to simply return S-frames and record statistics of correctly received I-frames (Barker and Boucouvalas, 1998d).

A.2.3.1 IrDA Basic Model Node Level

Figure A.3a shows the node level for the IrDA Basic primary station model. This consists of point-to-point transmitter (xmt) and receiver (rcv) modules, and an IrLAP (irlap) process module. Data packets are created internally within the irlap process. Packet streams connect the IrLAP process with the transmitter and receiver. There is also a statistic stream (dashed line) from the transmitter to the IrLAP process. This is used to indicate the completion of a frame transmission on the physical link. Figure A.3b shows the secondary node model. This is similar to the primary except there is no statistic link from transmitter as only S-frames are returned.

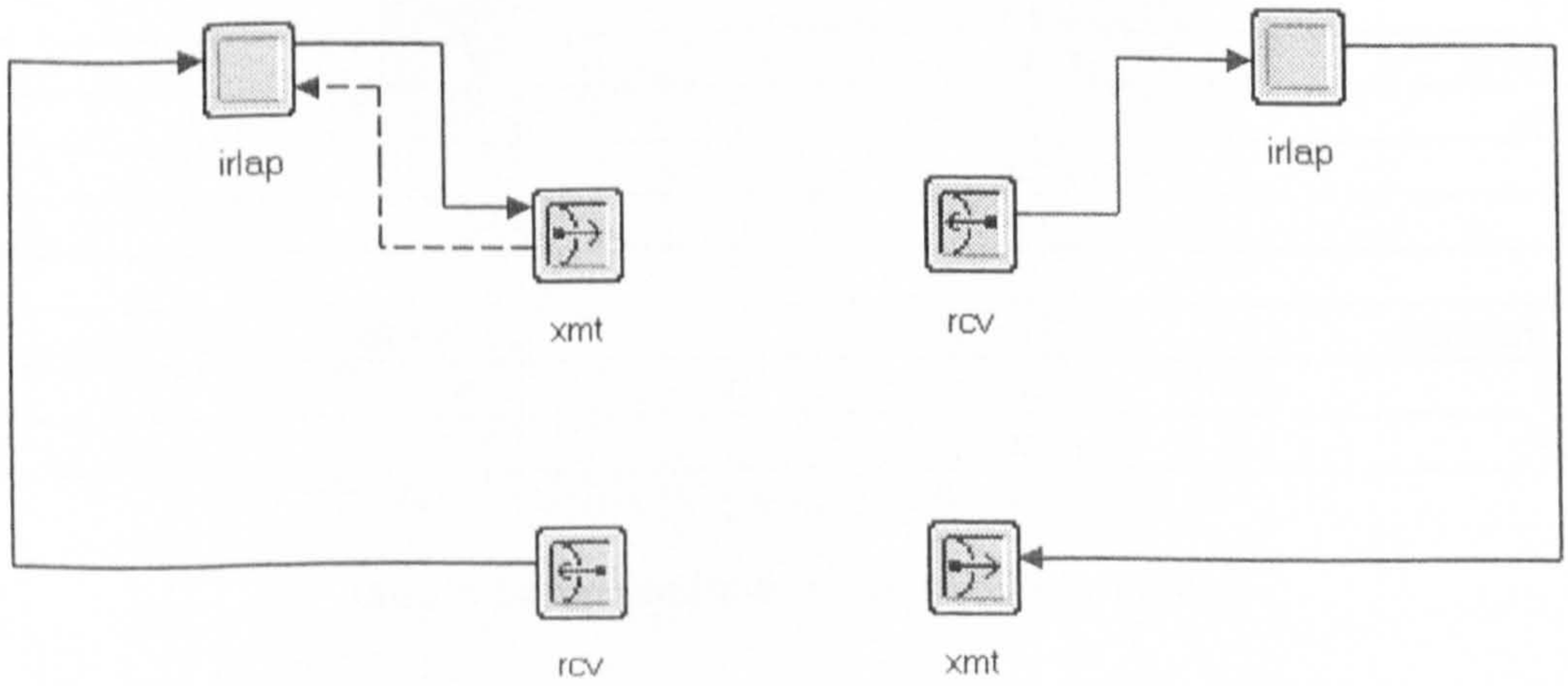

a) primary b) secondary

Figure A.3 IrDA Basic model node models

A.2.3.2 IrLAP Basic model process level

Figure A.4 shows the process finite state machine for the IrLAP Basic model primary station process model. There are 5 states: initialisation (INIT), transmit (XMIT), receive (RECV), re-transmit (REXMIT) and turn-around delay (TA_DEL). The INIT state is forced with the remaining states unforced.

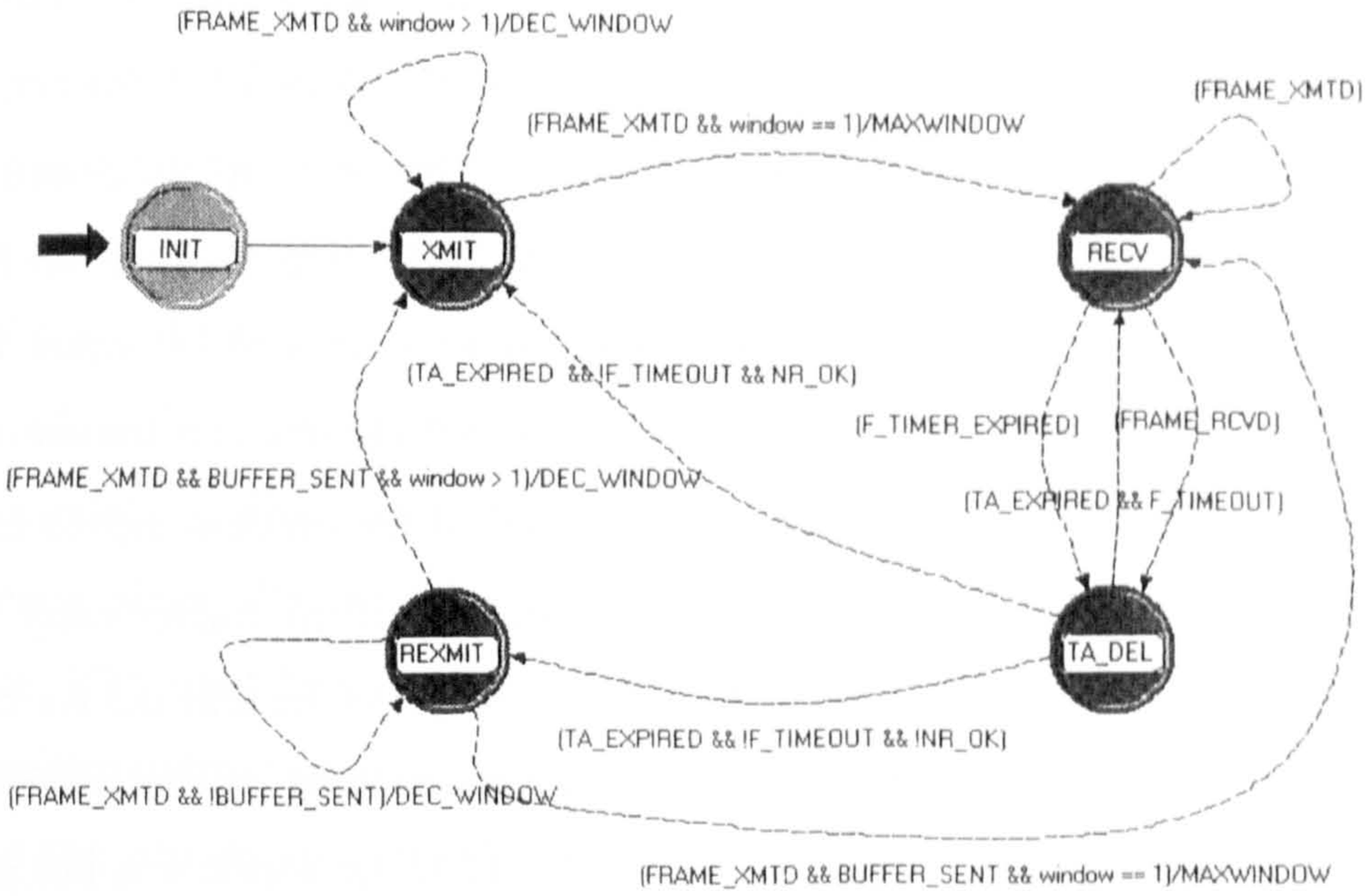

Figure A.4 IrLAP Basic model primary station process model FSM

The process operates as follows. The initialisation (INIT) state reads the process input attributes and initialises variables. Procedures for the transmission of I-frames are contained in the enter execution block of the transmission (XMIT) state. For each frame, a data packet is created and a buffer copy with the current Vs value made. The packet is then inserted into an I-frame packet and transmitted with the Nr field set to the current Vs value. The Vs variable is incremented (with modulus). The process then waits for completion of frame transmission as indicated by the statistic interrupt from the transmitter module. If the window value is greater than 1, the frame is transmitted with the P-bit unset. On completion of transmission the window value is decremented (DEC_WINDOW) and the process returns to the XMIT state. Note that the DEC_WINDOW operation is performed as an execution statement after the transition condition is evaluated. This is because the action changes the value that is being evaluated. If the window is equal to 1, the frame is transmitted with the P-bit set, the window returned to the maximum value (MAX_WINDOW) upon frame transmission, and the f-timer started (scheduled self-interrupt).

The process then moves to the receive (RECV) state. Here the process waits for either a frame reception interrupt from the receiver input stream or expiration of the f-timer. If a frame is received, the f-timer is stopped. The Nr value is extracted from the frame and the frame destroyed. The process then moves to the TA_DEL state to wait the turn-around delay. On completion of the turn-around delay, if the received Nr value is as expected (Nr == Vs) the process returns to the XMIT state and commences transmitting a new window of I-frames. If Nr is not as expected (Nr ≠ Vs) the process moves to the re-transmission (REXMIT) state. Here a copy packet is made of the buffer copy with index Rs. This is transmitted in an I-frame with the Nr field set to Rs and the Rs index incremented (with modulus). On completion of frame transmission, if the buffer has been transmitted (Rs == Vs) the process moves to the XMIT if the window is not equal to 1, to transmit new I-frames to fill the window. If the window is 1, the process moves to the RECV state, starts the f-timer and resets the window to maximum. If the buffer is not transmitted (Rs ≠ Vs) the process returns to the REXMIT state to continue re-transmission. If the f-timer expires (self interrupt) when in the RECV state an f-timer-expired flag is set and the process moves to the TA_DEL to wait the turn-around delay. After this delay, an S-frame is transmitted and the process returns to the RECV state. On completion of transmission, the f-timer is restarted.

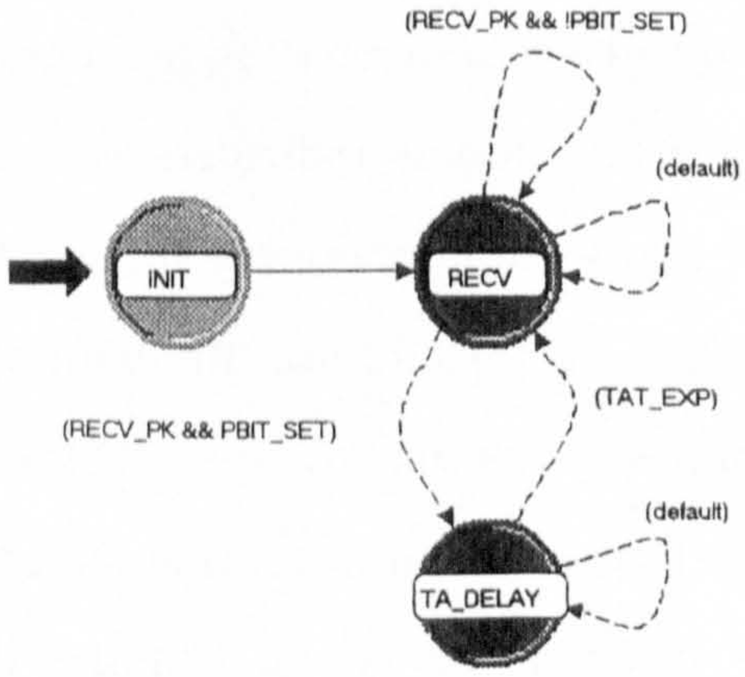

Figure A.5 IrLAP Basic model secondary station process model FSM

The process model for the secondary station in the basic IrDA model is much simpler as it just receives I-frames from the secondary, records statistics and returns an S-frame acknowledgement after receiving the P-bit and completion of a turn-around delay. There is therefore just a RECV state and a TA_DEL state. On receiving an I-frame in the RECV state, the Ns, Nr and P-bit field values and the Information field data packet are extracted. If the Ns value is equal to the current Vr value, the Vr value is incremented (with modulus). The size of the data packet (in bits) is recorded and with the time difference since the previous packet arrival provides the instantaneous throughput statistic. The total bits received divided by the current simulation time provides the average throughput statistic. If the P-bit is set, the process moves to the TA_DEL state to wait the turn-around delay. On completion of the delay, an S-frame is transmitted with the current Vr value in the Nr field.

A.2.3.3 IrDA Basic Model simulation Execution

Model attributes can be set at the appropriate model level or promoted to the simulation configuration level where multiple value sets can be assigned if required for a scalar output set (e.g. throughput versus packet size). The following provides the simulation attributes for the IrDA basic model.

Attribute Name	Type	Units
Primary.irlap.Diagnostic	Boolean	-
Primary.irlap.Max Ta Time	double	seconds
Primary.irlap.Min Ta Time	double	seconds
Primary.irlap.Packet Size	double	bits
Primary.irlap.Window Size	int	frames
Primary.rcv.data rate	double	bits / second
Primary.xmt.data rate	double	bits / second
Primary -> Secondary.ber	double	errors / bit
Secondary -> Primary.ber	double	errors / bit

Table A.3 IrDA basic model simulation attributes

The 'Diagnostic' attribute is used to switch on / off a diagnostic text output to the console window. This provides details of the IrLAP procedure execution events. This is very useful in debugging the process while in development but can slow down the execution if not required. The following shows an example diagnostic output from the Primary node for a simulation run. The Figure before each event is the simulation time.

The figures in the I-frame transmission output are the Ns, Nr, P/F bit and data packet id respectively. The figure for the received S-frame is the returned Nr value. It can be seen that following the first transmission window shown, the I-frame [4, 0, 1 (6432)] which carries the P-bit is lost. The F-timer therefore expires. The frame (6432) is re-transmitted at the start of the next transmission window.

```
D:\OPNET\8.1.A\sys\pc_intel_win32\bin\op_runsim.exe
(493.162000) Primary: TA Delay Implemented
(493.162000) Primary: Transmitting I-frame [2, 0, 0, (6428)]
(493.304639) Primary: Transmitting I-frame [3, 0, 0, (6430)]
(493.447278) Primary: Transmitting I-frame [4, 0, 1, (6432)]
(494.018833) Primary: F-timer expired
(494.019833) Primary: TA Delay Implemented
(494.019833) Primary: Transmitting S-frame
(494.021667) Primary: S-frame received [4]
(494.022667) Primary: TA Delay Implemented
(494.022667) Primary: Retransmitting I-frame [4, 0, 0, (6432)]
(494.165306) Primary: Transmitting I-frame [5, 0, 0, (6437)]
(494.307944) Primary: Transmitting I-frame [6, 0, 1, (6439)]
(494.452000) Primary: S-frame received [7]
(494.453000) Primary: TA Delay Implemented
(494.453000) Primary: Transmitting I-frame [7, 0, 0, (6442)]
(494.595639) Primary: Transmitting I-frame [0, 0, 0, (6444)]
(494.738278) Primary: Transmitting I-frame [1, 0, 1, (6446)]
(494.882333) Primary: S-frame received [2]
(494.883333) Primary: TA Delay Implemented
(494.883333) Primary: Transmitting I-frame [2, 0, 0, (6449)]
(495.025972) Primary: Transmitting I-frame [3, 0, 0, (6451)]
(495.168611) Primary: Transmitting I-frame [4, 0, 1, (6453)]
(495.312667) Primary: S-frame received [5]
(495.313667) Primary: TA Delay Implemented
(495.313667) Primary: Transmitting I-frame [5, 0, 0, (6456)]
```

Figure A.6 Primary station example diagnostic output

At the secondary irlap process, the throughput and delay statistics are recorded (as time-value pairs) for each correctly received packet. Delay is read from the creation time stamp of each packet. At the termination of the simulation, the average throughput and average delay are recorded together with the link BER value and parameter setting as a scalar statistics set.

A.2.4 IrLAP Advanced Model

The advanced model does not assume a saturated data condition but instead accepts data requests from a packet source process. The secondary also has a full IrLAP information transfer procedure and can return its own I-frame data packets, if available, in addition to returning S-frame acknowledgements.

A.2.4.1 IrLAP Advanced Model Node Level

The node levels for the advanced model differ from the basic model in that source and sink process modules are connected to the IrLAP process. For the IrDA model a constant packet size is used with random delivery times.

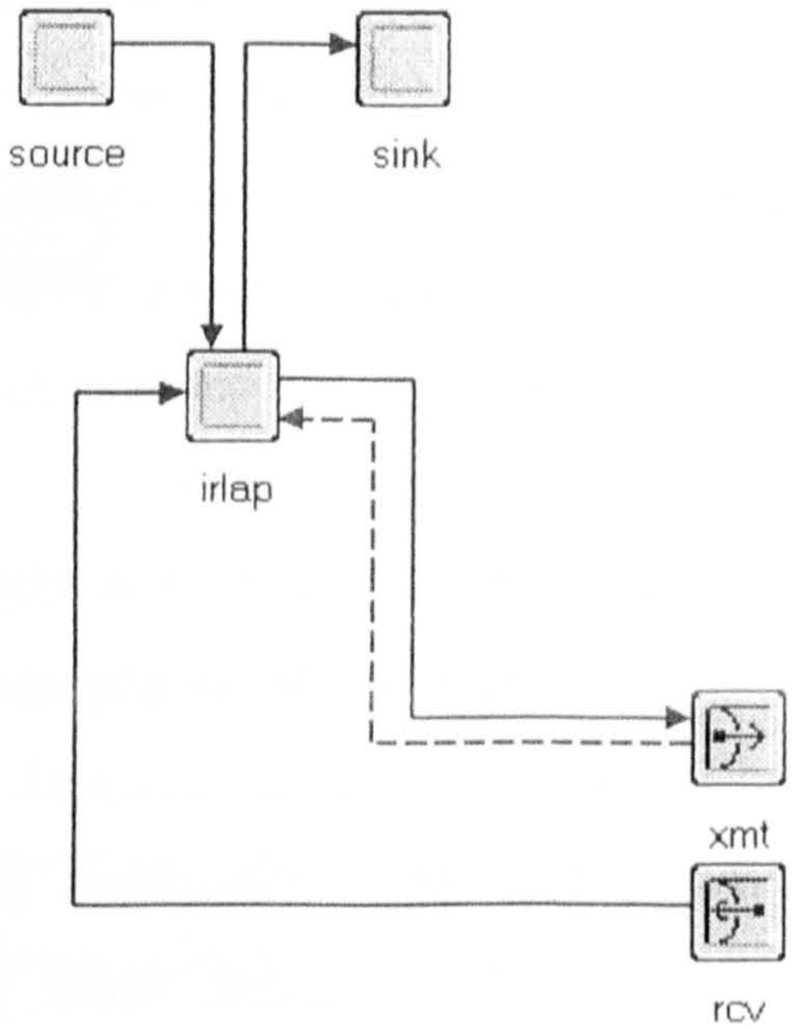

Figure A.7 IrDA Advanced model primary station node model

A.2.4.2 IrDA Source and Sink Models

The source model process uses a Poisson distribution to schedule packet transmissions to the irlap process at random intervals with the specified mean interarrival time. Attributes also specify the packet size and send-data enabled / disabled condition. The sink process receives correctly received packets from the irlap process, records statistics and destroys the packets. Throughput and Delay vector statistics are recorded for each packet arrival during the simulation run. At the termination of the simulation, average throughput and delay together with irlap and source parameter values from the transmitting node are printed to the terminal output and recorded as scalar statistics.

A.2.4.3 IrLAP Primary Station Advanced Process Model

The advanced IrLAP primary station model is similar to the basic model except that the process waits in the XMIT state for a data packet request (REQ stream interrupt) from the packet source process unless there are packets queued in the request stream waiting

transmission. If packets are waiting transmission, a frame transmission is in progress or the process is not in the XMIT state, the REQ stream interrupt is disabled. Thus, any arriving packets in the REQ stream are queued in the stream without an interrupt. The P-timer is also used in the process. It is started (scheduled self-interrupt) on entering the XMIT state from any other state. The duration is set to be slightly longer than the maximum time to transmit (N – 1) sequential I-frames. If the Nth frame (frame to the P-bit set) arrives before expiration of the timer, the timer is stopped. If the P-timer expires, an S-frame is transmitted with the current Vr value in the NR field to poll the secondary. If data packets are queued in the REQ stream, the process will sequentially transmit the packets as with the basic model until the queue is empty.

I-frame arrivals in the RECV state from the secondary if in sequence (Ns == Vr) have the data packet extracted and passed to an external 'sink' process where statistics are collected. The Vr variable is then incremented (with modulus). If the I-frame is not in sequence, the data packet is discarded. Other procedures (F-timer expiration, re-transmission) are as the basic model. The advanced model primary and secondary IrLAP finite-state diagrams are illustrated in Figures A.8 and A.9.

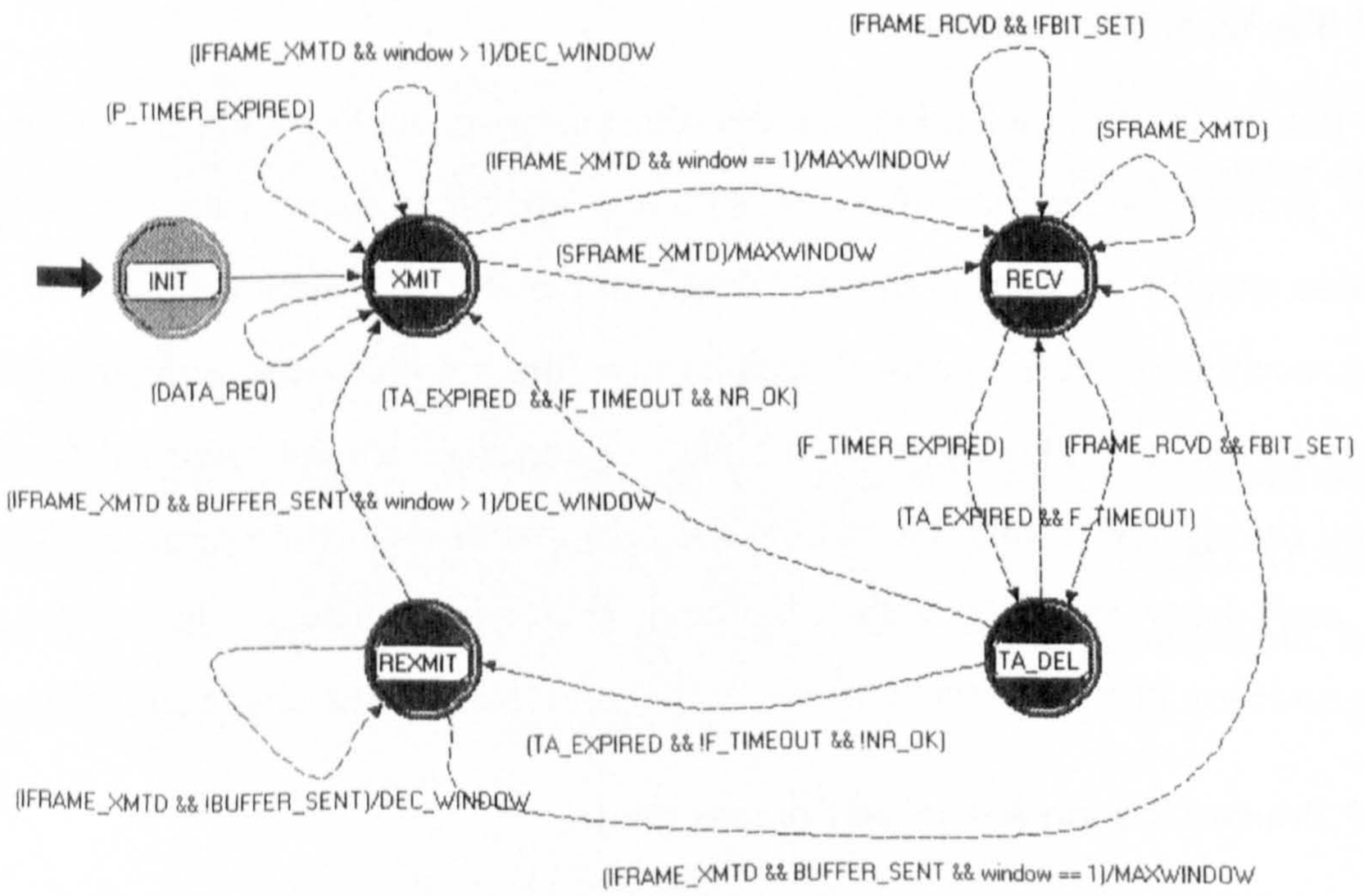

Figure A.8 IrLAP advanced model primary station process model FSM

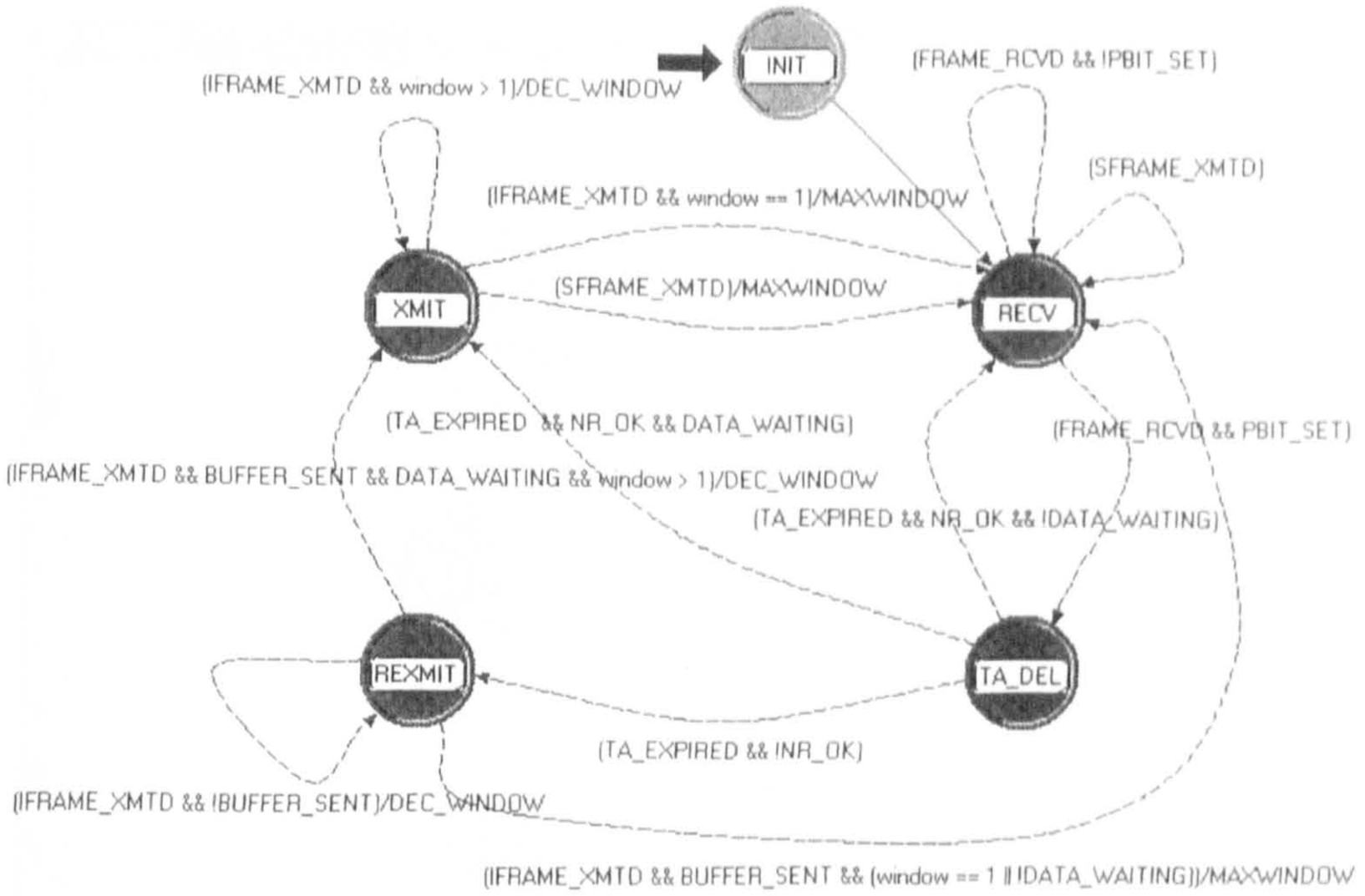

Figure A.9 IrLAP advanced model secondary station process model FSM

The secondary advanced model operates as the primary except that it will not wait in the XMIT state for packet arrivals in REQ steam. It will only transmit data packets if they are waiting transmission (queued in the REQ stream). If the queue is empty, the process will return the RECV state to wait I-frame arrivals from the primary. If the queue becomes empty following packet extraction from the REQ stream, the I-frame is sent with the P-bit set regardless of remaining frame slots in the window. The secondary also does not hold P or F timers.

A.2.4.4 Advanced Model Simulation Execution

The behaviour of the advanced simulation model depend on the link BER, IrLAP process parameters and the new parameter of the source packet service time. For large service time values, the throughput will be reduced as the process is not at saturation level. Beyond a certain value, the packets will queue in the input stream to the IrLAP process and the throughput will be that of the saturation condition. The saturation point will depend on the link BER. If packet errors occur, requiring re-transmissions, new packet arrivals will queue up during the re-transmission period.

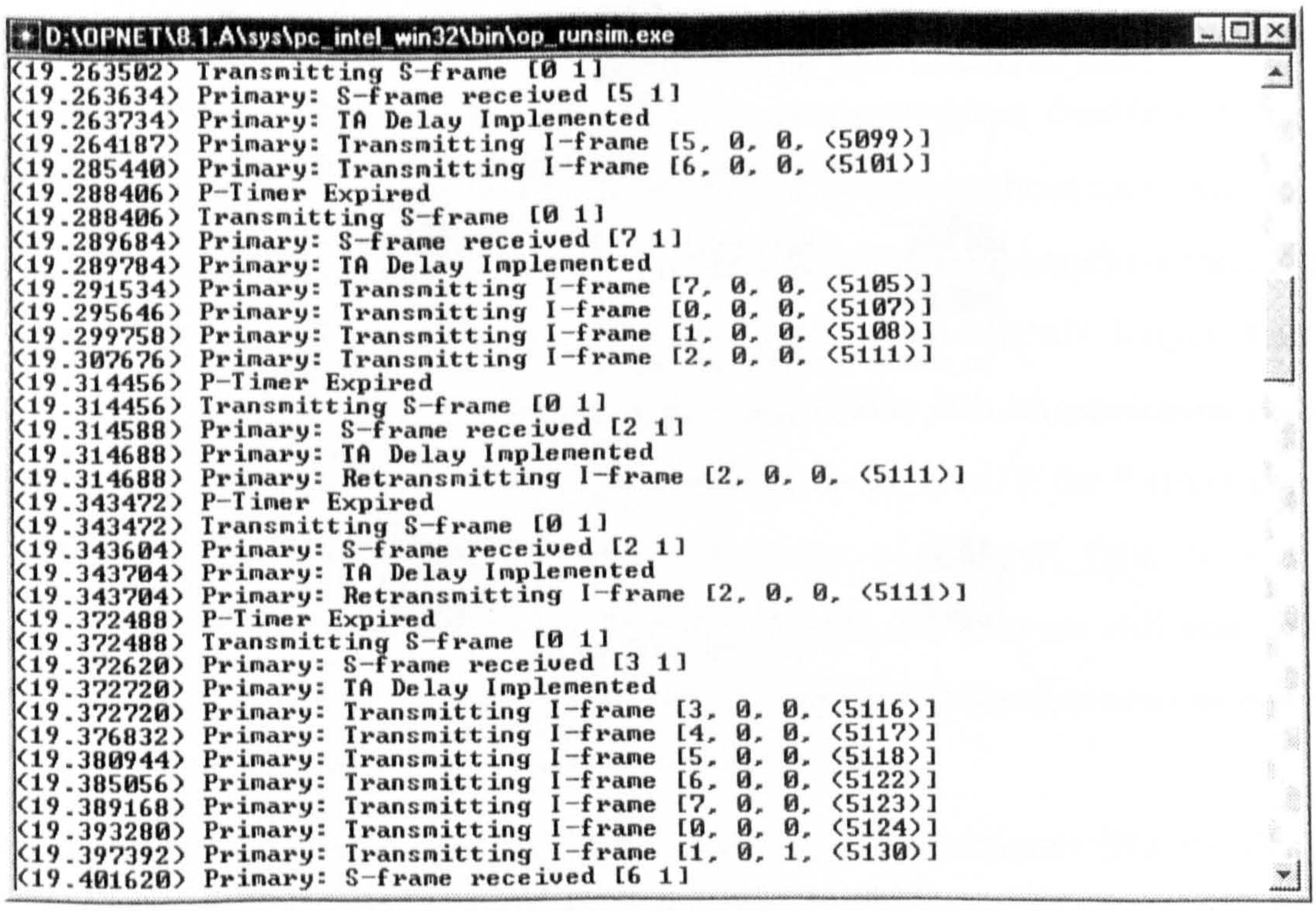

Figure A.10 Non-saturation advanced IrDA model diagnostic output

A.3 AIr OPNET Model

The following presents a description of the AIr OPNET simulation model. The basis of the model is principally to simulate the behaviour of the AIr MAC process. As such we are interested in how the media reservation process and packet collisions affect the performance rather than the effect of bit errors (Barker and Boucouvalas, 2000b; Barker et al., 2002).

A.3.1 AIr Model Network Level

Figure A.11 shows a 5-station scenario network level for the AIr OPNET model. In addition to the AIr node stations there is a monitor station the records statistics on network traffic. Other network scenario models were produced for different network sizes (e.g. 10, 15, 20 stations etc.).

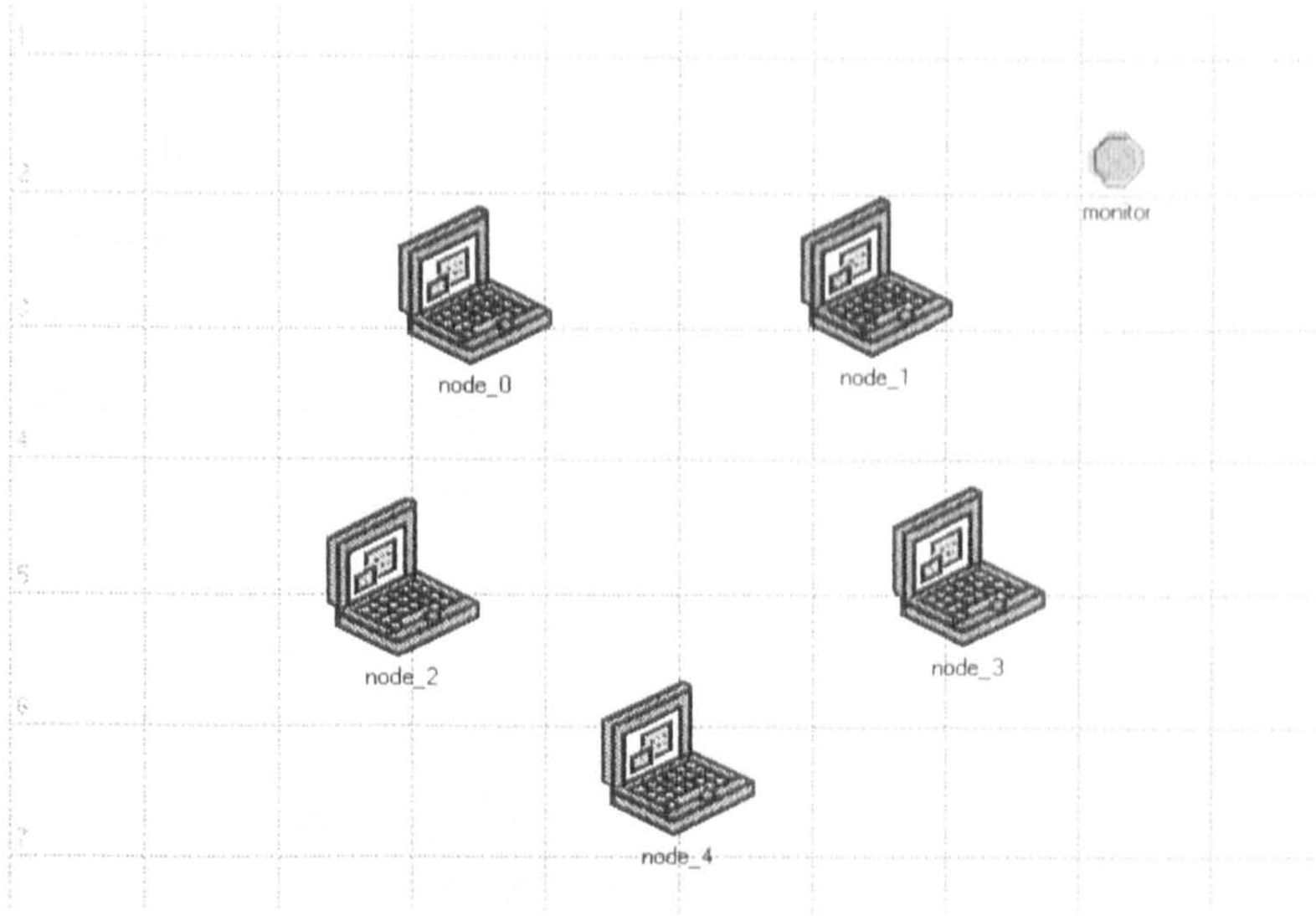

Figure A.11 AIr model 5-station network level

The model is actually implemented as a 'radio' wireless network with certain modifications to the pipeline stages to model the behaviour of the AIr IR wireless physical layer. Infrared as a wireless medium is not as yet supported by OPNET Modeler, but as we are primarily concerned with the AIr MAC protocol behaviour, the radio medium can be used with some modifications. The principal change was to have nodes unable to 'hear' their own transmissions while ensuring that packet collisions would cause appropriate errors in the relevant packets. With the 'radio' medium the BER is not specified as an attribute as is the case with wired network links but is determined from link distances and transmitter, receiver and antenna model attributes. With a multiple access medium such as the 'radio' medium, a transmitted packet is duplicated and sent to each receiver on the network. Pipeline stages are used for each destination to determine a packets error and acceptability. In the current model we are primarily considering an error free situation with no 'hidden nodes' so the network model was modified to remove all packet errors. However future modifications to the model could easily be made if a single BER value for the network was required or errors to be calculated form link geometry and transceiver characteristics.

A.3.2 AIr Station Node Model

Figure A.12 shows the AIr station node model. This consists of 'radio' transceiver modules, an AIR_PHY physical layer interface module, the AIr MAC process module and the AIr LM module. The LM module acts as a data source / sink and management client to the MAC layer in this model. The LC process was not included in the current model.

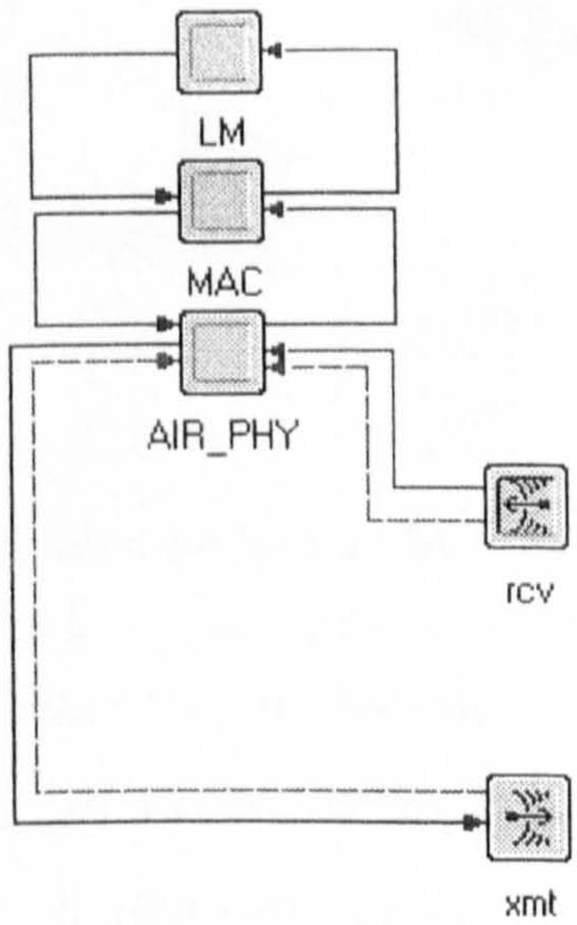

Figure A.12 AIr station node model

A.3.3. AIr LM Process Model

Figure A.13 shows the AIr LM process FSM. The process here acts as a reservation client to the AIr MAC process and as a data source and sink. The procedures for interfacing with the MAC is not fully developed in the LM draft specification document and as such the process here is some what different from that in the LM specification.

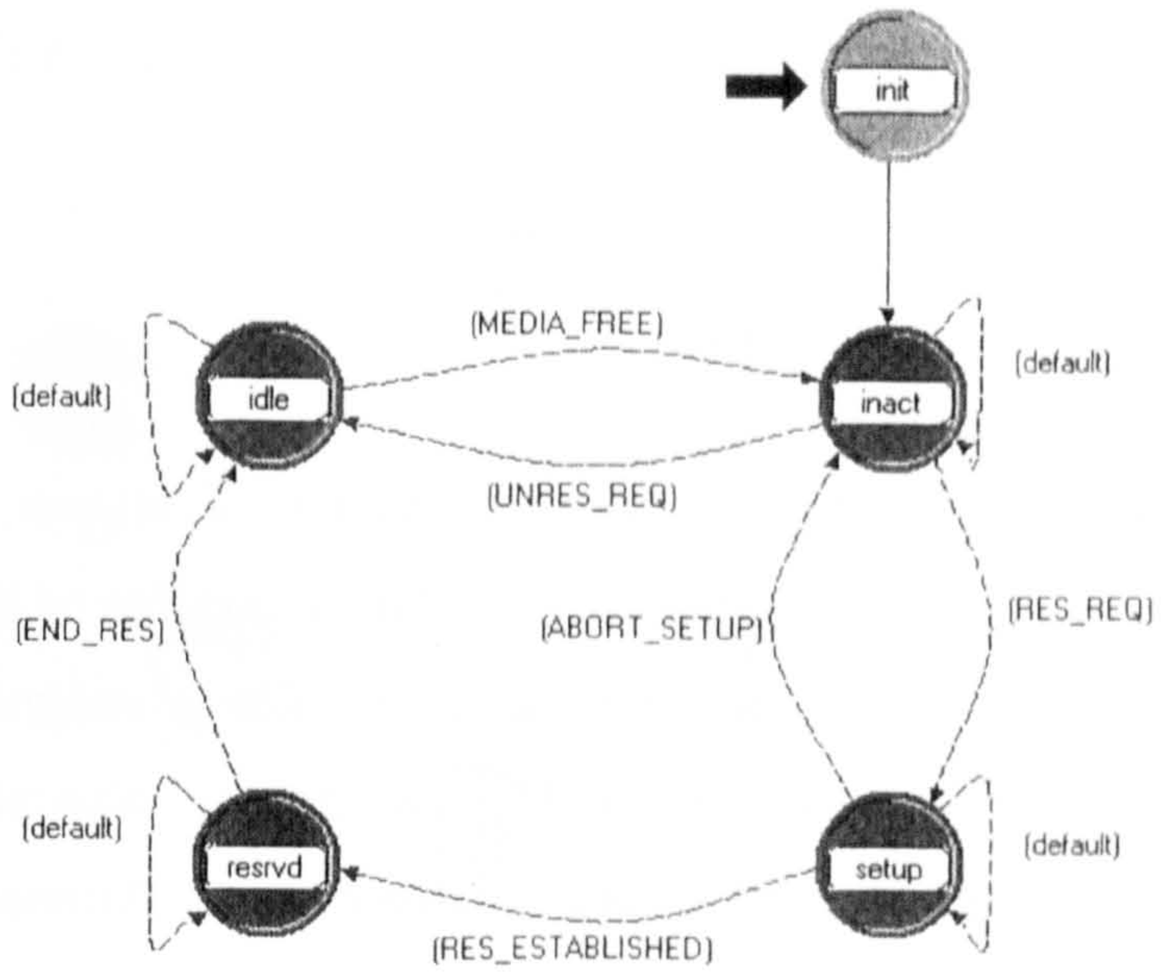

Figure A.13 AIr LM process model FSM

Of particular importance is the responsibility of the LM to generate the CAS values for the MAC. The model uses a set of input attribute values to control the CAS algorithm. These are: minimum CAS window, maximum CAS window, CAS window increase value, CAS window decrease value. A retry limit of 5 is used in the model and so the CAS value vector (array) has 5 values. The CAS window for the kth element in the array (0 to 4) is:

cas_window[k] = *min*(max_cas_window, init_cas_window + k*cas_window_increase)

The CAS values are then created by:

cas[k] = *floor*(*op_dist_uniform*(cas_window[k]))

where *op_dist_uniform* is an Opnet procedure that returns a random value from a uniform distribution between 0 and the given argument value. When the reservation has completed, the retry count is returned to the LM. This is used to adjust the initial CAS window by:

```
init_cas_window = max(min_cas_window, cas_window[retry_count] - cas_window_decrease)
```

If the retry limit is reached and hence the MAC process returns a failed reservation, the initial CAS window value becomes:

```
init_cas_window = cas_window[retry_limit]
```

The station destination address for each reservation is chosen randomly from the network size detected, ignoring the nodes own address and that of the monitor station. A nodes devices address is taken from the 'object id' that is assigned by the simulation kernel to every object in the simulation. The LM process also acts as a data sink to received packets and collects performance statistics. The statistics collected here, as opposed to those at the monitor node, are for end-to-end performance above the MAC layer.

A.3.4 AIr MAC Process Model

Figure A.14 shows the process level FSM for the AIr MAC protocol. The FSM is closely based on that laid out in the specification. However procedures for DATA and UDATA data frames only have been implemented. The procedure for transmitting DATA frames can be summarised as follows. After initialisation in the INIT state where process attribute values are read, the process moves to the IDLE state. A setup-reservation-request primitive is passed from the LM to the MAC and consists of a 'chain' of data packets together with an ICI containing parameter values for the reservation. This includes the array of CAS values created by the LM. Each data packet in the chain also has its own ICI containing parameter values relevant to the packet. The packet chain consists of an empty 'holder' packet with the data packets inserted as numbered fields. The CA (collision avoidance) timer is started (scheduled self-interrupt) using the 1st value in the CAS array. The process then moves to the CONTEND state. The process then proceeds as defined in chapter 4.

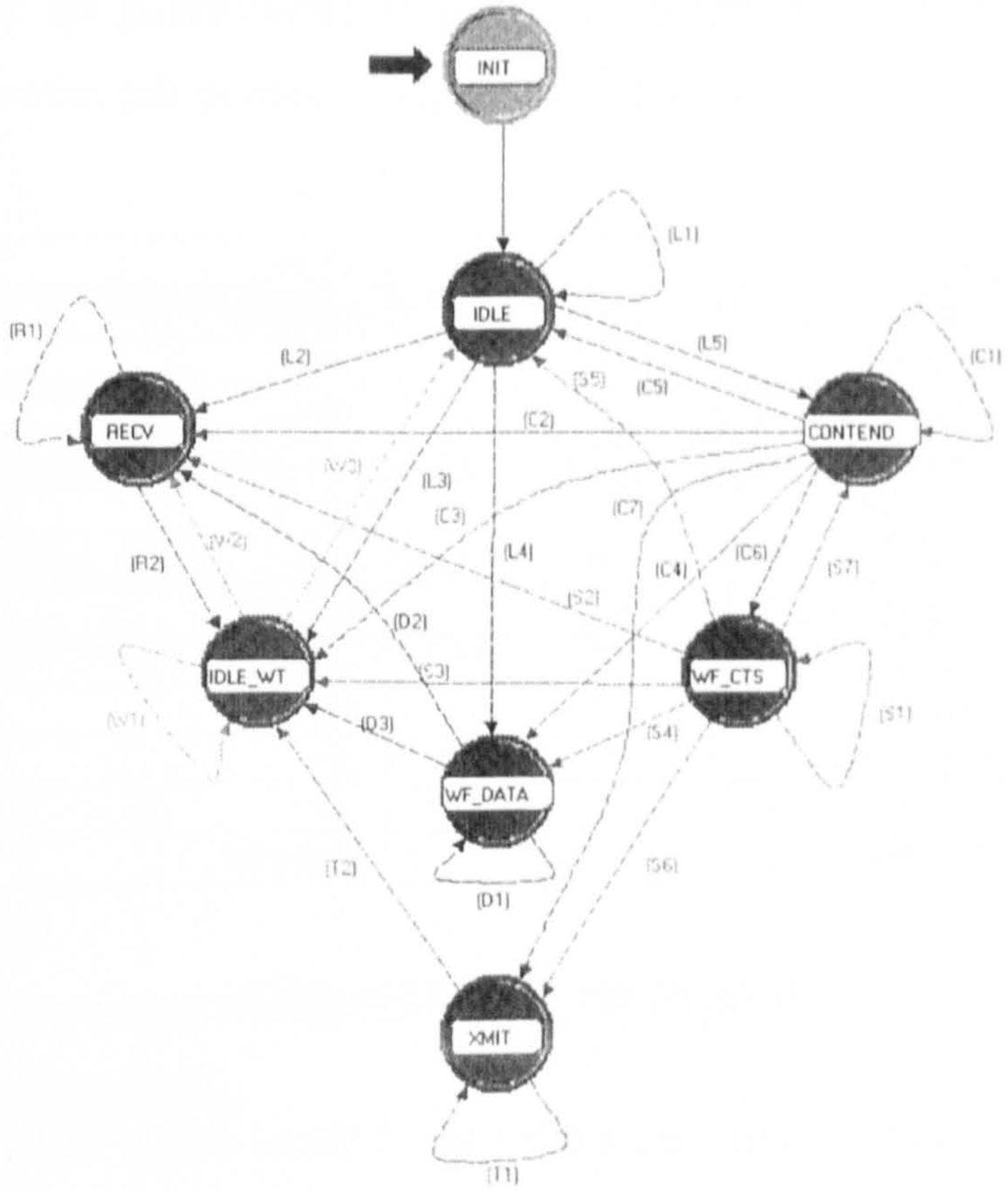

Figure A.14 AIr MAC process model FSM

A.3.5 The AIr Physical Layer Interface Process Model

The individual components of the AIr MAC frame (i.e. Preamble, Sync, Robust Header, and Main Body fields) are transmitted as separate packets on the medium. This is because the arrival of each frame portion triggers a separate event in the process. The size of the main body packet is multiplied by the RR value for the frame before transmission.

A.3.6 The AIr Monitor Node and Process Models

The monitor node consists of a single receiver and a monitor process module. The monitor process accepts only main body packets from data carrying frames. These are used to the measure the throughput on the network. As the IrDA sink process, instantaneous and average throughput are recorded. Required attribute values from other nodes are also recorded for scalar statistics.

A.3.7 AIr Model Attributes and Statistics

The following table provides the attribute set for each node in the network.

Attribute	Type
Phy.diagnostic	Boolean
LM.burst size	int
LM.min CAS window	int
LM.max CAS window	int
LM.packet size	int
LM.repetition rate	int
LM.reservation time	double
LM.send data	Boolean
LM.diagnostic	Boolean
LM.up CAS adjust	int
LM.down CAS adjust	int
MAC.diagnostic	Boolean

Table A.4 AIr node attribute list

The attributes representing system parameters are defined at the LM process. Optional diagnostic output is used here as with the IrDA model. For the AIr model the name of each node is appended to the front of each output string to the determine the diagnostic origin. An example diagnostic output from the AIr MAC OPNET model is shown in Figure A.15.

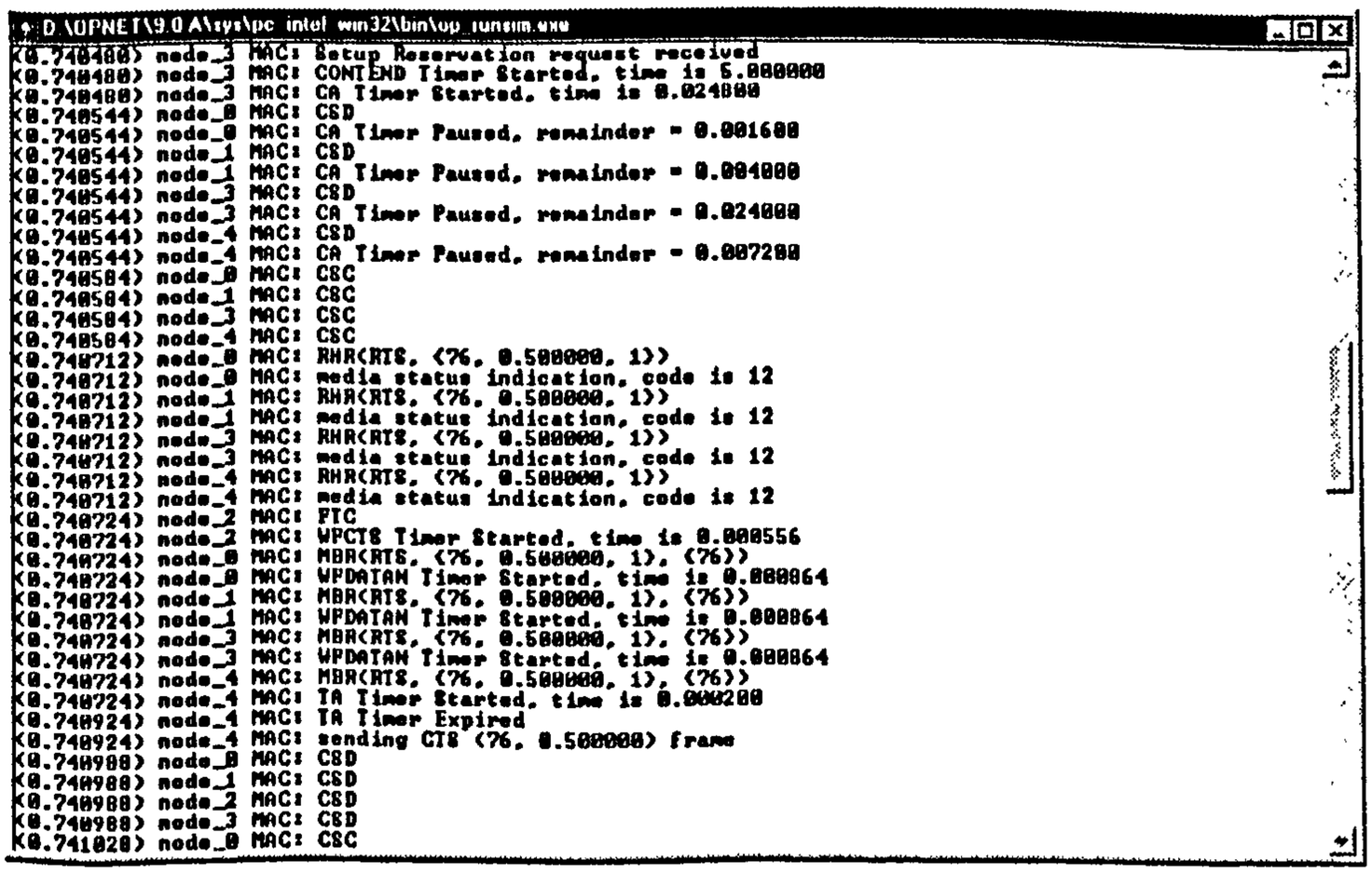

Figure A.15 Example AIR OPNET MAC model diagnostic output

APPENDIX B Limiting Distribution of a Markov Chain

A Markov chain is a discrete time, discrete state process in which the future behaviour of the process is dependent only on the current state and not its state history. If the probability of transition between states is known (may be zero for some transitions), a state transition matrix P can be formed consisting of transition probabilities p_{ij} (the probability of transition from state i to state j), defined as:

$$p_{ij} = \mathbf{P}(X_{n+1} = j \mid X_n = i) \tag{B.1}$$

where X_n is the process state at discrete time n. This is the '1-step' transition probability. For n steps $p_{ij}(n)$ is defined as:

$$p_{ij}(n) = \mathbf{P}(X_{m+n} = j \mid X_m = i) \tag{B.2}$$

Using the theorem of total probabilities gives:

$$p_{ij}(m+n) = \sum_k p_{ik}(m) p_{kj}(n) \tag{B.3}$$

Letting $P(n)$ be the transition probability matrix for n steps, consisting of elements $p_{ij}(n)$ from (B.3) we get:

$$P(n) = P^n \tag{B.4}$$

It is a property of finite state Markov chains that as $n \to \infty$, all rows of the matrix P^n converge towards a common limit.

The limiting distribution for the Markov chain is the vector of probabilities v_j such that:

$$v_j = \lim_{n\to\infty} p_j(n)$$

Applying the normalisation condition gives:

$$\sum_j v_j = 1$$

i.e. the sum of all state probabilities in v is 1.

The limiting distribution vector v is therefore found from:

$$v = v.P$$

In other words, v is a vector such that v times (using matrix multiplication) the one-step probability matrix P results in same vector v. This provides a set of simultaneous equations, which together with the normalisation condition, provide a solution for v.

Appendix C Gaussian Tail Integral, Q – function

The function $Q(z)$, defined in (C.1), provides the area under the tail of a Gaussian curve from the point z forward (shaded area Figure C.1). It therefore provides the probability that a random outcome with a Gaussian distribution, with mean value μ and standard deviation σ exceeds the value $(\mu + \sigma z)$.

$$Q(z) = \frac{1}{\sqrt{2\pi}} \int_{z}^{\infty} e^{-y^2/2} dy \qquad \text{(C.1)}$$

This can also be determined from the *erfc* function (conjugate error function - commonly included in the maths library of programming languages).

$$Q(z) = \frac{1}{2} erfc\left(\frac{z}{\sqrt{2}}\right) \qquad \text{(C.2)}$$

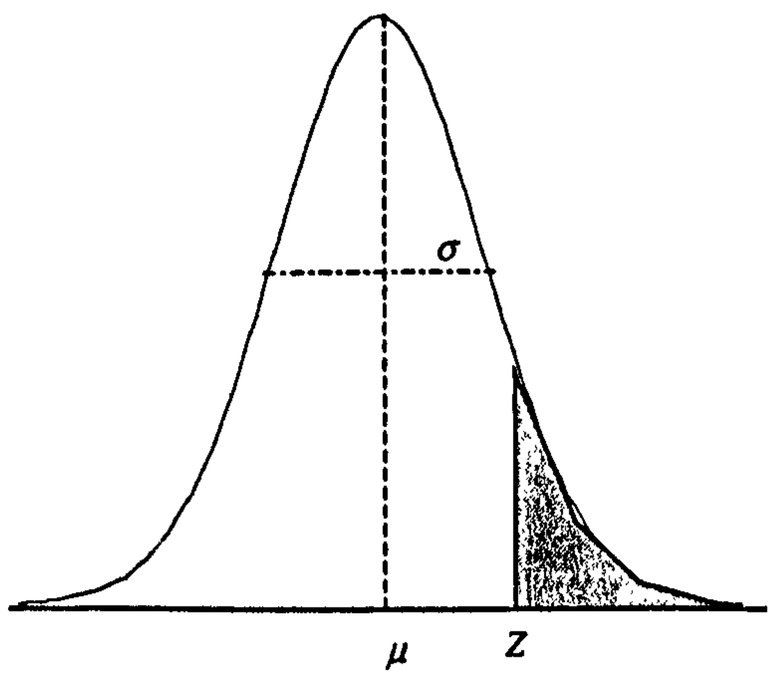

Figure C.1 Area under Gaussian curve tail

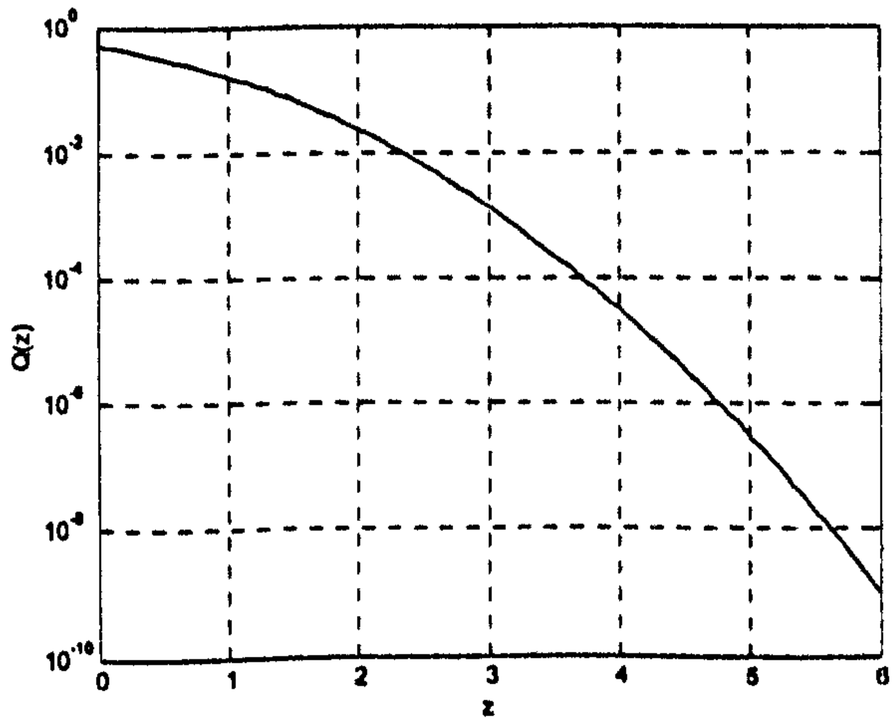

Figure C.2 Plot of *Q*(z) versus *z*

References

[1] AGILENT, 2000. IrDA Data Link Design Guide. Agilent Technologies

[2] AIMES, G. T. AND LAZOWSKA, E. D., 1979. The Behaviour of Ethernet-Like Computer Communications Networks. *In: ACM SIGCOM 7th International Symposium on Operating System Principles, Asilomar, CA, 1979,* 66 - 81.

[3] ALDIBBIAT, N. M., GHASSEMLOOY, Z. AND MCLAUGHLIN, R., 2001. Performance of Dual Header-Pulse Interval Modulation (DH-PIM) for Optical Wireless Communications Systems. *Proceedings of the SPIE,* 4214(February 2001), 144 -152.

[4] ALVAREZ, J. R. V., HERNANDEZ, F. J. L., GALDON, A. S., JIMENEZ, R. P. AND BORGES, J. A. R., 1999. Infrared Wireless DSSS System for Indoor Data Communication Links. *Proceedings of the SPIE - The International Society for Optical Engineering,* 3850, 92 - 99.

[5] ANANTH, R., NOLL, M. AND PHANG, K., 1997. Low-Voltage Infrared Transceiver Design. *Communications Systems Design,* (October 1997), 52 - 61.

[6] AUDEH, M. D. AND KAHN, J. M., 1995. Performance Evaluation of Baseband OOK for Wireless Indoor Infrared LAN's Operating at 100 Mb/s. *IEEE Transactions on Communications,* 43(6), 2085 - 2094.

[7] AUDEH, M. D., KAHN, J. M. AND BARRY, J. R., 1996. Performance of Pulse-Position Modulation on Measured Non_Directed Indoor Infrared Channels. *IEEE Transactions on Communications,* 44(6), 654 - 659.

[8] BAKALIDIS, G. N., GLAVAS, E. AND TSALIDES, P., 1996. Optical Power Distribution in Wireless Infrared LANs. *IEE Proceedings Communications,* 143(2), 93 - 97.

[9] BARKER, P. AND BOUCOUVALAS, A. C., 1998a. IrLAP Protocol Performance Analysis of IrDA Wireless Communications. *Electronics Letters,* 34(25), 2380 - 2381.

[10] BARKER, P. AND BOUCOUVALAS, A. C., 1998b. Performance Analysis of the IrDA Protocol in Wireless Communications. *In: First International Symposium on Communications Systems & Digital Signal Processing, Sheffield Hallam University - UK, 6-8 April 1998*, Sheffield Hallam University Press, 6 - 10.

[11] BARKER, P. AND BOUCOUVALAS, A. C., 1998c. Performance Modelling of the IrDA Protocol for Infrared Wireless Communications. *IEEE Communications Magazine,* 36(12), 113 - 117.

[12] BARKER, P. AND BOUCOUVALAS, A. C., 1998d. A Simulation Model of the IrDA Infrared Communications Protocol. *In: First International Symposium on*

Communications & Digital Signal Processing, Sheffield Hallam University - UK, 6-8 April 1998, Sheffield Hallam University Press, 2 - 6.

[13] BARKER, P. AND BOUCOUVALAS, A. C., 2000a. Modelling of the IrDA and AIr Wireless Infrared Communications Protocols. *In: 1st Annual PostGraduate Symposium on the Convergence of Telecommunications, Networking and Broadcasting (PGNET 2000), Liverpool John Moores University, 19 - 20 June 2000*, 137 - 142.

[14] BARKER, P. AND BOUCOUVALAS, A. C., 2000b. A Simulation Model of the Advanced Infrared (AIr) MAC protocol using OPNET. *In: 2nd International Symposium on Communication Systems, Networks and Digital Signal Processing (CSNDSP 2000), Bournemouth University, 18 - 20 July 2000*, 153 - 156.

[15] BARKER, P. AND BOUCOUVALAS, A. C., 2002a. Directional and Spatial Asymmetry in IrDA 4PPM Infrared Wireless Links with Third User Interference. *In: 3rd Annual PostGraduate Symposium on the Convergence of Telecommunications, Networking and Broadcasting (PGNET 2002), Liverpool John Moores University, 17 - 18 June 2002*, 353 - 358.

[16] BARKER, P. AND BOUCOUVALAS, A. C., 2002b. Interference Induced Asymmetry in IrDA 4PPM Infrared Wireless Links. *In: 3rd International Symposium on Communication Systems, Networks and Digital Signal Processing (CSNDSP '02), University of Staffordshire, 15 - 17 July 2002*, 479 - 482.

[17] BARKER, P., BOUCOUVALAS, A. C. AND VITSAS, V., 2000. Performance Modelling of the IrDA Infrared Wireless Communications Protocol. *International Journal of Communications Systems,* 13(7-8), 589 - 604.

[18] BARKER, P., VITSAS, V. AND BOUCOUVALAS, A. C., 2002. Simulation Analysis of the advanced infrared (AIr) MAC wireless communications protocol. *IEE Proceedings Circuits, Devices and Systems,* 149(3), 193 - 197.

[19] BARRY, J. R., 1994. *Wireless Infrared Communications,* ed. Kluwer.

[20] BARRY, J. R. AND KAHN, J. M., 1995. Link Design for Non-Directed Wireless Infrared Communication. *Applied Optics,* 34(19), 3764 - 3776.

[21] BARRY, J. R., KAHN, J. M., LEE, A. E. AND MESSERSCHMITT, D. G., 1991a. High Speed Nondirective Optical Communication for Wireless Networks. *IEEE Network Magazine,* November 1991, 44 - 53.

[22] BARRY, J. R., KAHN, J. M., LEE, E. A. AND MESSERSCHMITT, D. G., 1991b. Simulation of Multipath Impulse Response for Indoor Diffuse Optical Channels. *In: IEEE workshop on wireless local area networks, Worcester MA, May 1991*, 81 - 87.

[23] BEALE, M., 1999. Optimizing the High-Speed IrDA Extensions. *Electronic Engineer,* (August 1999).

[24] BEALE, M., 2000. Understanding the High-Speed Extensions to IrDA. *In: IIC International Conference and Exhibition, Taipei, Taiwan, 3-4 May , 2000,* 67 - 70.

[25] BI, Q., ZYSMAN, G. I. AND MENKES, H., 2001. Wireless Mobile Communications at the Start of the 21st Century. *IEEE Communications Magazine,* 39(1), 110 - 116.

[26] BIANCHI, G., 1998. IEEE 802.11 - Saturation Throughput Analysis. *IEEE Communications Letters,* 2(12), 318 - 320.

[27] BIANCHI, G., 2000. Performance Analysis of the IEEE 802.11 Distributed Coordination Function. *IEEE Journal on Selected Areas in Communications,* 18(3), 535 - 547.

[28] BIANCHI, G., FRATTA, L. AND OLIVERI, M., 1996. Performance Evaluation and Enhancement of CSMA/CA MAC Protocol for 802.11 Wireless LANs. *In: 7th International Symposium on Personal, Indoor & Mobile Radio Communications (PIMRC '96), Taiwan, 15 -1 8 Oct 1996,* 392 - 396.

[29] BOUCOUVALAS, A. C., 1996. Indoor Ambient Light Noise and its Effect on Wireless Optical Links. *IEE Proceedings on Optoelectronics,* 143(6), 334 - 338.

[30] BOUCOUVALAS, A. C. AND BARKER, P., 2000. Asymmetry in Optical Wireless Links. *IEE Proceedings in Optoelectronics,* 147(4), 315 - 321.

[31] BOUCOUVALAS, A. C., JERRAMS-SMITH, J. AND HEATHCOTE, D., 1996. Interference Induced IR Link Spatial Asymmetries. *In: Third Communication Networks Symposium, Manchester Metropolitan University, 8 -9 July 1996,* 214 -219.

[32] BOUCOUVALAS, A. C. AND VITSAS, V., 2001. Optimum Window and Frame Size for IrDA Links. *Electronics Letters,* 37(3), 194 - 196.

[33] BREWSTER, R. L. AND GLASS, A. M., 1987. Throughput Analysis of Non-persistent and Slotted Non-persistent CSMA/CA Protocols. *In: 4th International Conference on Land Mobile Radio, Coventry, UK, 1997,* 231 - 236.

[34] BUCHANAN, W., 1996. *Applied Data Communications and Networks,* ed. Oxford: Chapman & Hall.

[35] BURAKOWSKI, W., BURSZTYNOWSKI, D. AND LUBACZ, J., 1986. Protocol HDLC-ABM: Traffic Considerations Given Error Dependent Channel. *In:* Kuhn, P. Ed, North-Holland: Elsevier Science Publishers, 549 - 554.

[36] BUX, W. AND KUMMERLE, K., 1980. Balanced HDLC Procedures: A Performance Analysis. *IEEE Transactions On Communications,* com-28(11), 1889 - 1898.

[37] CARLSON, D. E., 1980. Bit-Oriented Data Link Control Procedures. *IEEE Transactions on Communications,* COM-28(4), 455 - 467.

[38] CARRUTHERS, J. B. AND KAHN, J. M., 1997. Modeling of Nondirected Wireless Infrared Channels. *IEEE-Transactions-on-Communications.,* 45(10), 1260 - 1268.

[39] CHAN, H.-H., ELMIRGHANI, J. M. H. AND CRYAN, R. A., 1996. Performance Analysis of Indoor Infrared Wireless Networks Utilising PPM CDMA. *In: IEEE International Conference on Communications. Converging Technologies for Tomorrow's Applications. ICC '96, Dallas, TX, USA, 23 - 27 June 1996*, IEEE, 1467 - 1471.

[40] CHAN, W. C., 2000. *Performance Analysis Of Telecommunications and Local Area Networks,* ed. Kluwer.

[41] CHHAYA, H. S. AND GUPTA, S., 1997. Performance Modeling of Asynchronous Data Transfer Methods of IEEE 802.11 MAC Protocol. *Wireless Networks,* 3(3), 217 - 234.

[42] CHOW, F. M. AND KAHN, J. M., 1999. Effect of Non-reciprocity on Infrared Wireless Local-Area Networks. *In: IEEE Global Communications (GLOBECOM '99), Rio de Janero, Brazil, 5 - 9 Dec 1999,* 330 - 338.

[43] CHU, T. S. AND GANS, M. J., 1987. High Speed Infrared Local Wireless Communication. *IEEE Communications Magazine,* 25(8), 4 - 10.

[44] CROW, B., WIDJAJA, I., KIM, J. G. AND SAKAI, P., 1996. Performance of IEEE 802.11 Wireless Local Area Networks. *Proceedings of the SPIE,* 2917, 480 -491.

[45] CROW, B. P., WIDJAJA, I., KIM, J. G. AND SAKAI, P. T., 1997. IEEE 802.11 Wireless Local Area Networks. *IEEE Communications Magazine,* 35(9), 116 - 126.

[46] DESIMONE, A. AND NANDA, S., 1995. Wireless Data: Systems, Standards, Services. *Wireless Networks,* 1(3), 241 - 253.

[47] DJAHANI, P. AND KAHN, J. M., 2000. Analysis of Infrared Wireless Links Employing Multi-beam Transmitters and Imaging Diversity Receivers. *IEEE Transactions on Communications,* 24(12), 2077 - 2088.

[48] ELMIRGHANI, J. M. H. AND CRYAN, R. A., 1994. Indoor Infrared Wireless Networks Utilising PPM CDMA. *In:* Ng-CS AND Yeo-TS Eds. *Singapore ICCS '94. Conference Proceedings, Singapore, 1994*, IEEE, 334 - 337.

[49] FIORINI, D., CHIANI, M., TRALLI, V. AND SALATI, C., 1994. Can We Trust in HDLC. *ACM SIGCOMM - Computer Communications Review,* 24(5), 61 - 80.

[50] FLOREZ, S. A. J., HDEZ, F. J. L., GALDON, A. S. AND ALVAREZ, J. R. V., 1997. Infrared Wireless Indoor Channels Characterisation in Asymmetrical Rooms. *In: 1997 SBMO/IEEE MTT-S International Microwave and Optoelectronics Conference. 'Linking to the Next Generation'. Natal, Brazil, 11 - 14 Aug 1997*, IEEE, 492 - 497.

[51] GAGLIARDI, R. M. AND SHERMAN, K., 1995. *Optical Communications*, 2nd ed. Wiley.

[52] GAMEIRO, A. AND ALVES, R., 1999. Coding Techniques for Wireless Infrared Communications. *Proceedings of the SPIE - The International Society for Optical Engineering.*, 3532, 70 -81.

[53] GARCIA-ZAMBRANA, A. AND PUERTA-NOTARIO, A., 1999. RZ-Gaussian Pulses Reduce the Receiver Complexity in Wireless Infrared Links at High Bit Rates. *Electronics-Letters*, 35(13), 1059 - 1061.

[54] GEORGES, J. AND WYBAUX, D., 1981. A Simulation Study of the Performances of HDLC Controlled Links. *Performance Evaluation*, (1), 126 - 138.

[55] GEORGHIADES, C. N., 1994. Modulation and Encoding for Throughput-Efficient Optical Systems. *IEEE Transactions on Information Theory*, 40(5), 1313 - 1326.

[56] GERALD, C. F. AND WHEATLEY, P. O., 1999. *Applied Numerical Analysis*, 6th ed. MA: Addison-Wesely.

[57] GFELLER, F. AND HIRT, W., 1998. A Robust Wireless Infrared System with Channel Reciprocity. *IEEE Communications Magazine*, 36(12), 100 - 106.

[58] GFELLER, F., HIRT, W., DE-LANGE, M. AND WEISS, B., 1996. Wireless Infrared Transmission: How to Reach all Office Space. *In: 1996 IEEE 46th Vehicular Technology Conference. Mobile Technology for the Human Race, Atlanta, GA, USA, 28 Apr - 1 May 1996*, IEEE, 1535 - 1539.

[59] GFELLER, F. R. AND BAPST, U., 1979. Wireless Communication via Diffuse Infrared Radiation. *Proceedings of the IEEE*, 67(11), 1474 - 1486.

[60] GHASSEMLOOY, Z., HAYES, A. R. AND SEED, N. L., 2001. The Effect of Multipath Propagation on the Performance of DPIM on Diffuse Optical Wireless Communications. *In: IASTED conference on wireless and optical communications, Canada, June 27 - 29 2001*, 166 - 172.

[61] GHASSEMLOOY, Z., HAYES, A. R., SEED, N. L. AND KALUARACHCHI, E. D., 1998. Digital Pulse Interval Modulation for Optical Communications. *IEEE Communications Magazine*, 36(12), 95 - 99.

[62] GLASS, A. M., BREWSTER, R. L. AND ABDULAZIZ, N. K., 1988. Modelling of CSMA/CA Protocol by Simulation. *Electronics Letters*, 24(11), 692 - 694.

[63] GUMMALLA, A. C. V. AND O'LIMB, J., 2000. Wireless Medium Access Control Protocols. *IEEE Communications Surveys*, 2 - 15.

[64] HARRISON, P. G. AND PATEL, N. M., 1993. *Performance Modelling of Communication Networks and Computer Architecture,* ed. Addison-Wesley.

[65] HAYES, A. R., GHASSEMLOOY, Z. AND SEED, N. L., 1999. Optical Wireless Communication using Digital Pulse Interval Modulation. *Proceedings of the SPIE - The International Society for Optical Engineering,* 3532, 61 - 69.

[66] HEATLY, D. J. T., WISELY, D. R., NEILD, I. AND COCHRANE, P., 1998. Optical Wireless: The Story So Far. *IEEE Communications Magazine,* 36(12), 72 - 82.

[67] HIGGINBOTTOM, G. N., 1998. *Performance Evaluation of Communication Networks,* ed. Norwood, MA: Artech House.

[68] HIRT, W., HASSNER, M. AND HEISE, N., 2001. IrDA-VFIr (16 Mb/s): Modulation Code and System Design. *IEEE Personal Communications,* 1(1), 58 - 71.

[69] IEC, 1993. IEC 825-1 Safety of Laser Products - Part 1: Equipment classification, requirements, and user's guide.

[70] IEEE, 1997. Wireless LAN Medium Access Control (MAC) and Physical Layer Specification 802.11. IEEE

[71] IRDA, 1995a. IrCOMM: Serial and Parallel Port Emulation over IR - Version 1.0. Infrared Data Association

[72] IRDA, 1995b. Serial Infrared Physical Layer link Specification - Version 1.1. Infrared Data Association

[73] IRDA, 1995c. Tiny TP: A Flow-Control Mechanism for use with IrLMP - Version 1.0. Infrared Data Association

[74] IRDA, 1996a. Link Management Protocol (IrLMP) - Version 1.1. Infrared Data Association

[75] IRDA, 1996b. Serial Infrared Link Access Protocol (IrLAP) - Version 1.1. Infrared Data Association

[76] IRDA, 1997a. IrLAN: Access Extensions for Link Management Protocol - Version 1.0. Infrared Data Association

[77] IRDA, 1997b. IrOBEX: IrDA Object Exchange Protocol - Version 1.0. Infrared Data Association

[78] IRDA, 1999a. Advanced Infrared (AIr) MAC Draft Protocol Specification - Version 0.3. Infrared Data Association

[79] IRDA, 1999b. Advanced Infrared Logical Link Control (AIrLC) Specification - Version 0.1. Infrared Data Association

[80] IRDA, 1999c. AIr Link Manager Draft Specification - Version 0.3. Infrared Data Association

[81] JUNGNICKEL, V., POHL, V., NONNING, S. AND VON HELMHOLT, C., 2002. A Physical Model of the Wireless Infrared Communication Channel. *IEEE Journal on Selected Areas in Communications,* 30(3), 631 - 640.

[82] KAHN, J. M. AND BARRY, J. R., 1997. Wireless Infrared Communications. *Proceedings of the IEEE,* 85(2), 265 - 298.

[83] KAHN, J. M., YOU, R., DJAHANI, P., WEISBIN, A. G., TEIK, B. K. AND TANG, A., 1998. Imaging Diversity Receivers for High Speed Infrared Wireless Communications. *IEEE Communications Magazine,* 36(12), 88 - 94.

[84] KUROSE, J. F. AND ROSS, K. W., 2001. *Computer Networking: A Top-Down Approach Featuring the Internet,* ed. Boston, MA: Addison-Wesley.

[85] LABETOULLE, J. AND PUJOLLE, G., 1981. HDLC Throughput and Response Time for Bi-Directional Data Flow with Non-uniform Frame Sizes. *IEEE Transactions on Computers,* C-30(6), 405 - 413.

[86] LARUE, W. W. AND FROST, V. S., 1990. A Technique for Extrapolating the End-to-End Performance of HDLC Links for a Range of Lost Packet Rates. *IEEE Transactions on Communications,* 38(4), 461 - 466.

[87] LEE, D. C. M., KAHN, J. M. AND AUDEH, M. D., 1997. Trellis-Coded Pulse-Position Modulation for Indoor Wireless Infrared Communications. *IEEE Transactions on Communications,* 45(9), 1080 -1087.

[88] MARSAN, M. A., BARBETTA, L. AND NERI, F., 1989. A Petri Net Simulation Model of HDLC. *In: 4th IEEE Region 10 Conference (Tencon '89), Bombay, India, 22 - 24 November 1989,* 240 - 247.

[89] MASUNAGA, Y., 1978. A Probabilistic Automaton Model of the NRM, HDX HDLC Procedure. *Computer Networks,* (2), 442 - 453.

[90] MATSUO, M., OHTSUKI, T. AND SASASE, I., 1998. Rate-Adaptive Indoor Infrared Wireless Communication Systems using Punctured Convolutional Codes and Adaptive PPM. *In: Ninth IEEE International Symposium on Personal, Indoor and Mobile Radio Communications (PIMRC'98). Boston, MA, USA., 8 -11 Sept 1998,* IEEE, 693 - 697.

[91] METCALFE, R. M. AND BOGGS, D. R., 1976. Ethernet: Distributed Packet Switching for Local Computer Networks. *Communications of the ACM,* 19(7), 395 - 405.

[92] MILLAR, I., BEALE, M., DONOGHUE, B. J., LINDSTROM, K. W. AND WILLIAMS, S., 1998. The IrDA Standard for High-Speed Infrared Communications. *The Hewlett-Packard Journal,* 49(1), 10 - 26.

[93] MINAMI, T., YANO, K. AND TOUGUE, T., 1983. Optical Wireless Modem for Office Communication. *In: AFIPS National Computer Conference 1983, Anaheim, CA, USA, 1983,* 721 - 728.

[94] MOREIRA, A. C., VALADA, R. T. AND DE OLIVEIRA DUARTE, A. M., 1997. Optical Interference Produced by Artificial Light. *Wireless Networks,* 3, 131 - 140.

[95] MOREIRA, A. J. C., VALADAS, R. T. AND DE OLIVEIRA-DUARTE, A. M., 1996. Reducing the Effects of Artificial Light Interference in Wireless Infrared Transmission Systems. *In: IEE Colloquium on Optical Free Space Communication Links, IEE, Savoy Place, London, 1996,* 5/1 -10.

[96] NAKATA, Y., KASHIO, J., KOJIMA, T. AND NOGUCHI, T., 1984. In-House Wireless Communication Systems Using Infrared Radiation. *In: International Conference on Computer Communication, Australia, 1984,* 333 -337.

[97] NARASIMHAN, R., AUDEH, M. D. AND KAHN, J. M., 1996. Effect of Electronic-Ballast Fluorescent Lighting on Wireless Infrared Links. *IEE Proceedings Optoelectronics,* 43(6), 347 - 354.

[98] OTTE, R., DE JONG, L. P. AND VAN ROERMUND, A. H. M., 1999. *Low Power Wireless Infrared Communications,* ed. Kluwer.

[99] OZUGUR, T., 2000. *Advanced Infrared Local Area Networks*, Thesis (PhD), Georgia Institute of Technology.

[100] OZUGUR, T., COPELAND, J. A., NAGHSHINEH, M. AND KERMANI, P., 1999. Next-Generation Indoor Infrared LANs: Issues and Approaches. *IEEE Personal Communications,* 6(6), 6 - 19.

[101] OZUGUR, T., NAGHSHINEH, M., KERMANI, P., OLSEN, C. M., REZVANI, B. AND COPELAND, J. A., 1998. Performance Evaluation of L-PPM Links using Repetition Rate Encoding. *In: International symposium on Personal, Indoor and Moble Communications, PIMRC '98, Boston, MA, 8-11 Sept 1998,* 698 - 702.

[102] PETRILLA, J., 1998. Proposed Changes to the IrDA Serial Infrared Physical Layer Link Specification for VFIR. Infrared Data Association

[103] PHANG, K. AND JOHNS, D. A., 1999. A CMOS Optical Preamplifier for Wireless Infrared Communications. *IEEE Transactions on Circuits and Systems - II: Analog and Digital Signal Processing,* 46(7), 853 - 859.

[104] RAMIRO, J. AND ABDALLAH, C. T., 2002. Wireless Communications and Networking: An Overview. *IEEE Antenna's and Propagation Magazine,* 44(1), 185 - 193.

[105] SAMARAS, K., O'BRIEN, D. C. AND EDWARDS, D. J., 1998. Numerical Calculation of Channel Capacity for Wireless Infrared Multipath Channels. *Electronics Letters,* 34(15), 1462 - 1464.

[106] SAMARAS, M. AND STREET, A. M., 1997. BER Performance of Various Line Coding Schemes used in Wireless Infrared Channels in the Presence of Gaussian Noise and Intersymbol Interference. *In: Fourth Communications Networks Symposium, Manchester Metropolitan University, 7 - 8 July 1997,* 224 - 227.

[107] SCHWARTZ, M., 1987. *Telecommunications Networks: Protocols, Modelling and Analysis,* ed. Reading, MA: Addison Wesely.

[108] SEE, C. K., GHASSEMLOOY, Z. AND HOLDING, J. M., 2000. Hybrid PIM-CDMA for Optical Wireless Networks. *In: 1st Annual Postgraduate Symposium on the Convergence of Telecommunications, Networking and Broadcasting (PGNET 2000), Liverpool John Moores University, 19 - 20 June 2000,* 195 - 201.

[109] SHIN, D. H., CHANBUM, P. AND HONG-LEE, J., 1996. Performance of Code Division Multiple Access in Non-Directed Diffuse Optical Wireless Channels. *In: 1996 IEEE 46th Vehicular Technology Conference. Mobile Technology for the Human Race, Atlanta, GA, USA, 1996,* IEEE, 1381 - 1384.

[110] STALLINGS, W., 2000. *Local & Metropolitan Area Networks,* ed. New Jersey: Prentice hall.

[111] STREET, A. M., SAMARAS, K., O'BRIEN, D. C. AND EDWARDS, D. J., 1997. Indoor Optical Wireless Systems - A Review. *Optical and Quantum Electronics,* 29, 349 - 378.

[112] TAKAHASHI, O. AND TOUGE, T., 1985. Optical Wireless Network for Office Communication. *JARECT,* 20, 217 - 228.

[113] TANENBAUM, A. S., 2002. *Computer Networks,* 4th ed. New Jersey: Prentice Hall.

[114] TANG, A. P., KAHN, J. M. AND KEANG, P.-H., 1996. Wireless Infrared Communication Links using Multi-Beam Transmitters and Imaging Receivers. *In: 1995 IEEE International Conference on Communications. Converging Technologies for Tomorrow's Applications. ICC '96., Dallas, TX, USA, 23 - 27 June 1996,* IEEE, 180 - 186.

[115] VITSAS, V. AND BOUCOUVALAS, A. C., 2000. IrDA IrLAP Protocol Throughput Performance. *In: 2nd International Workshop on Networked Appliances, IWNA 2000, New Jersey, USA, Nov 30 - Dec 1 2000.*

[116] VITSAS, V. AND BOUCOUVALAS, A. C., 2001a. Performance Analysis of the AIr-MAC Optical Wireless Protocol. *In: International Conference on System Engineering , Communications and Information Technologies, ICSECIT 2001, Magallanes, Punta Arenas, Chile, April 16 -19 2001.*

[117] VITSAS, V. AND BOUCOUVALAS, A. C., 2001b. Simultaneous Optimisation of Window and Frame Size for IrDA IrLAP Links. *Electronics Letters,* 37(16), 1042 - 1043.

[118] VITSAS, V. AND BOUCOUVALAS, A. C., 2001c. Throughput Analysis of the IrDA IrLAP Optical Wireless Link Access Protocol. *In: 3rd conference on telecommunications, ConfTele 2001, Figueira da Foz, Portugal, April 23-24 2001,* 225 - 229.

[119] WILLIAMS, S., 2000. IrDA: Past, Present and Future. *IEEE Personal Communications,* 7(1), 11 - 19.

[120] YEH, K. W. AND WANG, L., 1996. An Introduction to the IrDA Standard and System Implementation. *Wireless Systems Design,* (May 1996), 657.

[121] YEN, C. S. AND CRAWFORD, R. D., 1985. The Use of Directed Optical Beams in Wireless Computer Communications. *In: IEEE GLOBECOME 1985, New Orleans, LA, 3 - 5 Dec 1985,* 1181 - 1184.